# SYNTHESIS, CHARACTERISATION AND BIOLOGICAL STUDIES ON SCHIFF BASE METAL COMPLEXES: CORROSION INHIBITION AND DYE ADSORBENT PROPERTIES OF SCHIFF BASES

Thesis submitted to the

# Bharathidasan University, Tiruchirappalli

in partial fulfilment to the requirements for the award of the degree of

# DOCTOR OF PHILOSOPHY IN CHEMISTRY

Submitted by

#### A. SHARMILA

(Ref. No: 16873 /Ph.D.K2/Chemistry/ Part- Time/October-2017/Date:20.09.2017)

*Under the guidance of* 

Dr. K. LAKSHMI PRABHA



# PG & RESEARCH DEPARTMENT OF CHEMISTRY GOVERNMENT ARTS COLLEGE

TIRUCHIRAPPALLI - 620 022 TAMIL NADU, INDIA.

**JUNE 2022** 

#### A.SHARMILA

Ph.D Part Time Research Scholar
PG and Research Department of Chemistry
Government Arts College
Tiruchirappalli – 620022
Tamilnadu, India.
E.mail:sharmipreethi@gmail.com



# **DECLARATION**

Thereby declare that the matter embodied in the thesis entitled "SYNTHESIS, CHARACTERISATION AND BIOLOGICAL STUDIES ON SCHIFF BASE METAL COMPLEXES: CORROSION INHIBITION AND DYE ADSORBENT PROPERTIES OF SCHIFF BASES" submitted to the Bharathidasan University, Tiruchirappalli in partial fulfillment of the requirements for the award of the degree of Doctor of Philosophy in Chemistry is a record of independent research work done by me under the guidance and supervision of Dr. K. LAKSHMI PRABHA, Assistant Professor, PG and Research Department of Chemistry, Government Arts College, Tiruchirappalli-620 022, that it has not been submitted for the award of any degree / Diploma / Associateship / Fellowship or similar title to any candidate of any University or Institute.

Place: Tiruchirappalli

Date: (A.SHARMILA)



# PG AND RESEARCH DEPARTMENT OF CHEMISTRY, GOVERNMENT ARTS COLLEGE, TIRUCHIRAPPALLI -620 022, TAMIL NADU, INDIA.

**Dr.K.Lakshmi Prabha**, *M.Sc.*, *M.Phil.*, *Ph.D.*, E-mail ID: lakshmiprabha21674@gmail.com *Assistant Professor of Chemistry*, Mobile: 9443764315

# **CERTIFICATE**

This certify that the thesis entitled "SYNTHESIS, CHARACTERISATION AND BIOLOGICAL STUDIES ON SCHIFF BASE METAL COMPLEXES: CORROSION INHIBITION AND DYE ADSORBENT PROPERTIES OF SCHIFF BASES" submitted by A.SHARMILA (Ref. No: 16873) /Ph.D.K2/Chemistry/ Part- Time/October-2017/Date:20.09.2017) to Bharathidasan University in partial fulfillment of the requirements for the award of the degree of **DOCTOR OF PHILOSOPHY IN CHEMISTRY** is a bonafide record of research work done by her under my guidance in the PG & Research Department of Chemistry, Government Arts College, Trichy-620 022, Tamil Nadu, India. The thesis has not previously formed the basis for the award of any degree or any other similar title. The thesis is the outcome of original research work done by the candidate under my overall supervision.

Place: Tiruchirappalli -22 Dr.K.Lakshmi Prabha

Date: (Research Supervisor)



# PG & RESEARCH DEPARTMENT OF CHEMISTRY GOVERNMENT ARTS COLLEGE TIRUCHIRAPPALLI – 620 022 TAMILNADU, INDIA.

# CERTIFICATE FOR PLAGIARISM CHECK

1.	Name of the Research Scholar	Ms. A. SHARMILA
2.	Course of Study	Ph.D. Chemistry
3.	Title of Thesis/Dissertation	Synthesis, Characterisation and Biological Studies on Schiff Base Metal Complexes: Corrosion Inhibition and Dye Adsorbent Properties of Schiff Bases
4.	Name of the Research Supervisor	Dr. K.LAKSHMI PRABHA
5.	Department / Institution / Research Centre	PG and Research Department of Chemistry, Government Arts College, Tiruchirappalli– 620 022.
6.	Acceptable Maximum Limit	10%
7.	Percentage of Similarity of Content Identified	
8.	Software Used	URKUND
9.	Date of Verification	

Report on Plagiarism check, item with % of similarity is attached

**Signature of the Candidate** 

**Signature of the Research Supervisor** 

# Curiginal

# **Document Information**

**Analyzed document** A. SHARMILA - Chemistry - Final Thesis.pdf (D138903946)

**Submitted** 2022-06-01T20:04:00.0000000

**Submitted by** Dr.S.Vanitha

**Submitter email** vanitha@bdu.ac.in

Similarity 5%

Analysis address navitha.bdu@analysis.urkund.com

### Sources included in the report

SA	Murugesan C.pdf Document Murugesan C.pdf (D53400465)	88	7
SA	<b>T_Thamarikannan_Chemistry.pdf</b> Document T_Thamarikannan_Chemistry.pdf (D34154455)		18
SA	JINCYE.M.COMBINED.pdf  Document JINCYE.M.COMBINED.pdf (D34261122)		:
SA	Synthesis, Spectral Characterization and Biological Evaluation Of Transition Metal Complexes of Macrocyclic Schiff's Base Ligands By Arvind Kumar Rajput , Dr. SP Sati, Chemistry, SC-15242.docx  Document Synthesis, Spectral Characterization and Biological Evaluation Of Transition Metal Complexes of Macrocyclic Schiff's Base Ligands By Arvind Kumar Rajput , Dr. SP Sati, Chemistry, SC-15242.docx (D35661545)	88	•
SA	sirumalar.docx Document sirumalar.docx (D135868385)		1
W	URL: https://hmdb.ca/metabolites/HMDB0036057 Fetched: 2020-12-06T16:57:00.2570000		
SA	Charles. A.pdf Document Charles. A.pdf (D120904688)	88	1
SA	RESHMA R PhD Thesis.pdf Document RESHMA R PhD Thesis.pdf (D110043038)		
W	URL: http://www.thegoodscentscompany.com/data/rw1279691.html Fetched: 2020-12-26T14:26:03.4870000	88	
SA	<b>08 R&amp; D.docx</b> Document 08 R& D.docx (D30369545)	88	
SA	Bharathidasan University, Tiruchirappally / Palanivelan_Thesis(Chemistry).pdf  Document Palanivelan_Thesis(Chemistry).pdf (D46014721)  Submitted by: bdulib@gmail.com  Receiver: bdulib.bdu@analysis.urkund.com	00	

# ACKNOWLEDGEMENT

At the outset, I bow before "Lord Almighty" the omnipotent, the most merciful and the passionate, for always giving me the inner strength to do the tasks which were tougher than the toughest. The almighty God has never set me alone in harsh situations, he is always there to bless me and sustain me to come victorious out of every situation. I feel special to get so many opportunities in my life by the universe and I am thankful to the God whom I have worshipped day and night, not to ask for success but to ask for the strength and mental calmness to go for the success with full determination. Thank you, God, for blessing me.

The journey of Ph.D has been an awesome and life changing experience for me. The completion of my work surely would not have been possible without the help, support, encouragement and guidance of many people. At the end of my thesis I would like to extend my sincere thanks to all those people who made this dissertation possible and an unforgettable experience for me.

First and Foremost, I convey my thankfulness and gratitude to my humble supervisor, **Dr.K.Lakshmi Prabha**, Assistant Professor, PG and Research Department of Chemistry, Government Arts College, Tiruchirappalli-620 022, for her patience, encouragement, keen supervision and valuable suggestions. It is her guidance par excellence that has been instrumental in the completion of this thesis. It has been an enriching experience to be in her supervision.

I would like to express my high esteem and sincere thanks to my Doctoral Committee Members **Dr.Shameela Rajam**, Associate Professor, Department of Chemistry, Bishop Heber College and **Dr.A.Sivarajan**, Assistant Professor and Head, PG and Research Department of Chemistry, Government Arts College, Trichirappalli-22, for supporting me to carry out my research work.

I pay my special thanks to **Dr.S.S.Rose Mary**, Principal, Government Arts College, Tiruchirappalli-620022, for providing the required facilities needed in my research work.

Special thanks and a deep sense of gratitude is expressed for **Dr.V.Sujatha**, Principal, Cauvery College for Women, Trichy for providing the facilities to do the Research work.

I feel immense pleasure in expressing my heartfelt thanks to **Dr.A.Sabastian**, Reader and Head of Chemistry (Retd), Urumu Dhanalakshmi College, Trichy and **Dr.B.R.Venkatraman** Associate Professor, PG & Research Department of Chemistry, Periyar E.V.R. College (Autonomous), Tiruchirappalli-620 023, for their constant support.

I extend my special thanks and appreciation to all the faculty members of the Chemistry Department, Cauvery College for Women especially **Dr.P.Amirtham**. They were always ready to help me whenever I needed them and gave their valuable advises which made my work easier. I also thank our Non-teaching faculties in this juncture for their support.

My lab mate **Ms.P.Thamizhini** who worked with me and boosted me with all ups and downs with smiling face and a fully cooperative and supporting attitude towards, I am always thankful to her.

I have no words to express my indebtedness to my friends, **Dr.G.Sivasankari** and **Dr.C.Rajarajeswari**, who always stood by my side in thick and thin and supported me at times of hopelessness. Thank you for your suggestions that helped me a lot to accomplish some of the toughest task of my thesis.

I owe my deepest gratitude to **Dr.S.Saranya** for always helping me in my Ph.D. work. She helped me in learning various research tools and supported me throughout my doctoral work.

Research is a mind-aching and body-wrenching journey which demands lots of love, affection, encouragement and above all prayers. Words fail and fingers tremble while expressing my gratitude, appreciation, indebtedness and a tribute to my spiritual teacher cum beloved mother Late **Mrs. Malliga Arulraj** for emotional support, love and prayers

that drove me such a long way in my life. May my Lord elevate the ranks of my beloved mother in the Heaven and prolong the shadow of motherly love and affection. Next to her are none but my Father, **Mr. A. Arulraj** and Uncle **Mr. P.Jothi** who left no stone unturned in bringing me up and were always there by my side at very crucial junctures of my life. It would not be an exaggeration if I call them the principal characters of my life. May God reward them in both the Worlds.

I am lucky enough to have a younger brother not less than the best friend, Mr.A.Manoj Keyean, who deserves special and profound gratitude for his constant advice, support, affection, encouragement, motivational and spiritual lessons and prayers. Thanks a lot dear for being the source of my inspiration. I render my special thanks to my sister-in-law, Mrs. D.Sureeya who always stood by me and strengthened my morale in all situations.

I would like to take a moment to thank a very important person in my life, the one who made things very easy just by his enthusiasm for me and my work, my husband Mr.S.M. Nanda Kumar. My husband always helped me to make tough decisions and this is just because of his stubbornness to see her wife get every success in life, that I am even writing this acknowledgments page for my thesis. Thank you dear for being there for me in every situation and for being my best friend throughout my life.

Finally, a praiseworthy mention goes to my kids. I am forever indebted to my daughters **S.N.Preethi** and **S.N Pooja** and my son **S.N.Shiva** for their unconditional love and endless prayers. No words can actually describe their everlasting love to me. I owe a lot to them, they encouraged and helped me at every walk of my life. Moreover, they acted as a technical assistant, chef, and a driver to me and they looked after me as a mother.

(A.SHARMILA)

# **CONTENTS**

Chapter No.	Title						
	LIST (	OF TABL	ÆS				
	LIST (	OF FIGU	RES				
	LIST OF SYMBOLS AND ABBREVIATIONS						
	ABST	RACT					
I			INTRODUCTION	1 - 55			
	1.1	Schiff b	pase ligands	4			
		1.1.1	Types of Schiff bases based on Chelating Property with Metal Ions	6			
		1.1.2	Biological Importance of Schiff Bases	12			
	1.2	Metallo	p-Elements in Biological Systems	14			
	1.3	Anti-Ba	acterial Activity	17			
		1.3.1	Bacteria	19			
	1.4	Anti-Fu	ingal Activity	20			
		1.4.1	Fungi	21			
	1.5	Antioxi	dant Activity	22			
	1.6	Anti-Di	iabetic Activity	23			
	1.7	Review	of the Ligands	23			
		1.7.1	Heterocyclic Compounds	23			
			1.7.1.1 Pyrrole	24			
			1.7.1.2 Pyridine	26			
			1.7.1.3 Indole	27			
		1.7.2	2-(Methylthio)aniline	28			
	1.8	Metallo	o-Elements under Investigation	28			
		1.8.1	Coordination Chemistry of Copper	28			
		1.8.2	Co-ordination Chemistry of Cobalt	30			
		1.8.3	Co-ordination Chemistry of Nickel	31			
		1.8.4	Co-ordination Chemistry of Zinc	32			
		1.8.	Co-ordination Chemistry of Iron	33			

	1.9	Review	of Literature	34
	1.10	Scope a	nd Objectives of Present work	46
	Referen	nces		49
II	EXPEI	RIMENT	AL TECHNIQUES	56 -
	2.1	Chemic	-	56
	2.2		erisation Techniques	56
		2.2.1	Solubility and Melting Points	57
		2.2.2	Elemental Analysis	58
		2.2.3	Chemical Analysis	58
		2.2.4	Molar Conductance Measurement	59
		2.2.5	Magnetic Susceptibility Measurement	60
		2.2.6	<sup>1</sup> H NMR Spectroscopy	60
		2.2.7	Fourier Transform Infrared Spectroscopy	61
		2.2.8	UV-Visible Spectroscopy	61
		2.2.9	EPR Spectroscopy	62
		2.2.10	Mass Spectroscopy	63
		2.2.11	Cyclic Voltammetric Studies	64
		2.2.12	Thermal Decomposition Studies	64
	2.3	Biologi	cal Applications	65
		2.3.1	In Vitro Antibacterial Activity Screening	65
		2.3.2	In Vitro Antifungal Activity Screening	66
		2.3.3	Antioxidant Activity Screening (Free Radical Scavenging Activity)	67
		2.3.4	Antidiabetic Activity Screening	67
			2.3.4.1 α-Amylase Inhibitory Assay	67
			2.3.4.2 α- Glucosidase Inhibitory Assay	68
	2.4	Corrosi	on Inhibition Properties of Schiff base ligands	68
		2.4.1	Weight Loss Method	69
			2.4.1.1 Preparation of the Mild Steel Specimens	69
			2.4.1.2 Chemicals Used	69

		2 4 4 2	D .: CT . C 1 .:	
		2.4.1.3	Preparation of Test Solutions	69
		2.4.1.4	Preparation of the Environment	70
		2.4.1.5	Determination of Surface Area of the Specimens	70
		2.4.1.6	Determination of Inhibition Efficiency and Corrosion Rate	70
		2.4.1.7	Scanning Electron Microscopic Studies (SEM)	71
2.5	Dye ads	sorbent pr	operties of Schiff base ligands	71
	2.5.1	Adsorba	nte	71
	2.5.2	Adsorbe	ent	71
	2.5.3	Experim	nental Methods	71
		2.5.3.1	Batch Adsorption Studies	71
		2.5.3.2	Adsorption Isotherm	72
			2.5.3.2.1 Langmuir Isotherm	72
			2.5.3.2.2 Freundlich Isotherm	73
	2.5.4	Investig	ation of Malachite Green removal ability	73
Referer	nces			75
	ices			13
SYNTI ANTIN ACTIV	HESIS, C MICROB MITIES of	IAL, ANT 2-(methy	TERISATION AND EVALUATION OF FIOXIDANT AND ANTIDIABETIC ylsulfanyl)-N-(1H-pyrrol-2-ID ITS METAL COMPLEXES	76 - 124
SYNTI ANTIN ACTIV	HESIS, C MICROB MITIES of	IAL, ANT f 2-(methy niline AN	FIOXIDANT AND ANTIDIABETIC ylsulfanyl)-N-(1H-pyrrol-2-	
SYNTI ANTIN ACTIV ylmeth	HESIS, C MICROB MITIES of MITIES of ylidene)a Introduc Synthes	IAL, AND  2-(methy niline AN etion  is of Schi	FIOXIDANT AND ANTIDIABETIC ylsulfanyl)-N-(1H-pyrrol-2-	76 - 124
SYNTI ANTIN ACTIV ylmeth 3.1	HESIS, C MICROBI /ITIES of ylidene)a Introduc Synthes ylmethy	IAL, ANT f 2-(methy niline AN etion his of Schil ylidene)an	FIOXIDANT AND ANTIDIABETIC ylsulfanyl)-N-(1H-pyrrol-2-ID ITS METAL COMPLEXES  ff base 2-(methylsulfanyl)-N-(1H-pyrrol-2-	<b>76 - 124</b>
SYNTI ANTIN ACTIV ylmeth 3.1 3.2	HESIS, C MICROBI /ITIES of ylidene)a Introduct Synthes ylmethy Synthes	IAL, ANT f 2-(methy niline AN etion his of Schil ylidene)an	rioxidant and antidiabetic ysulfanyl)-N-(1H-pyrrol-2-ID ITS METAL COMPLEXES  ff base 2-(methylsulfanyl)-N-(1H-pyrrol-2-Iline MPMA al Complexes of MPMA	<b>76 - 124</b> 76  77
SYNTI ANTIN ACTIV ylmeth 3.1 3.2	HESIS, C MICROBI /ITIES of ylidene)a Introduct Synthes ylmethy Synthes	IAL, ANT f 2-(methy niline AN etion is of Schir rlidene)an is of Meta and Discu	rioxidant and antidiabetic ysulfanyl)-N-(1H-pyrrol-2-ID ITS METAL COMPLEXES  ff base 2-(methylsulfanyl)-N-(1H-pyrrol-2-Iline MPMA al Complexes of MPMA	<b>76 - 124</b> 76  77  77
SYNTI ANTIN ACTIV ylmeth 3.1 3.2	HESIS, C MICROBI /ITIES of ylidene)a Introduc Synthes ylmethy Synthes Results	IAL, ANT f 2-(methy niline AN etion his of Schir rlidene)an his of Meta and Discu	FIOXIDANT AND ANTIDIABETIC ylsulfanyl)-N-(1H-pyrrol-2-ID ITS METAL COMPLEXES  If base 2-(methylsulfanyl)-N-(1H-pyrrol-2-Iline MPMA In Complexes of MPMA In Sission	76 - 124 76 77 77 78
SYNTI ANTIN ACTIV ylmeth 3.1 3.2	HESIS, C MICROBI VITIES of ylidene)a Introduct Synthes ylmethy Synthes Results 3.4.1	IAL, ANT f 2-(methy niline AN etion his of Schir rlidene)an his of Meta and Discu Element Molar C	FIOXIDANT AND ANTIDIABETIC ylsulfanyl)-N-(1H-pyrrol-2-ID ITS METAL COMPLEXES  If base 2-(methylsulfanyl)-N-(1H-pyrrol-2-Iline MPMA In Complexes of MPMA In Composition	76 - 124  76 77 77 78 78
SYNTI ANTIN ACTIV ylmeth 3.1 3.2	HESIS, C MICROBI VITIES of ylidene)a Introduct Synthes ylmethy Synthes Results 3.4.1 3.4.2	IAL, ANT f 2-(methy niline AN etion his of Schir rlidene)an his of Meta and Discu Element Molar C	FIOXIDANT AND ANTIDIABETIC ylsulfanyl)-N-(1H-pyrrol-2-ID ITS METAL COMPLEXES  If base 2-(methylsulfanyl)-N-(1H-pyrrol-2-iline MPMA  In Complexes of MPMA  Ital Composition  Conductivity  R Spectra	76 - 124  76 77 77 78 78 80
SYNTI ANTIN ACTIV ylmeth 3.1 3.2	HESIS, C MICROBI /ITIES of ylidene)a Introduct Synthes ylmethy Synthes Results 3.4.1 3.4.2 3.4.3	IAL, ANT f 2-(methy niline AN etion his of Schi vlidene)an his of Meta and Discu Element Molar C  H-NMI FT-IR S	FIOXIDANT AND ANTIDIABETIC ylsulfanyl)-N-(1H-pyrrol-2-ID ITS METAL COMPLEXES  If base 2-(methylsulfanyl)-N-(1H-pyrrol-2-iline MPMA  In Complexes of MPMA  Ital Composition  Conductivity  R Spectra	76 - 124  76 77 77 78 78 80 80

	3.4.6	Electron Paramagnetic Resonance Spectrum of [Cu(MPMA) <sub>2</sub> (H <sub>2</sub> O) <sub>2</sub> ]Cl <sub>2</sub>	93
	3.4.7	LC-MS Spectrum of [Zn(MPMA) <sub>2</sub> ]SO <sub>4</sub>	94
	3.4.8	Cyclic Voltammetry Studies	94
	3.4.9	Thermal Decomposition Studies	99
3.5	Biologic	cal Studies	104
	3.5.1	Evaluation of Antimicrobial Activities of Synthesized Compounds	104
	3.5.2	Evaluation of Antioxidant Activity (DPPH free radical scavenging Method)	114
	3.5.3	Evaluation of Antidiabetic Activity	117
3.6	Conclus	ion	120
Referen	nces		122
ACTIV	ITIES O	AL, ANTIOXIDANT AND ANTIDIABETIC F (E)-2-(methylthio)-N-(pyridin-2- line AND ITS METAL COMPLEXES	
yimetny 4.1	yıene)anıı Introduc		125
4.2			126
4.2	•	is of (E)-2-(methylthio)-N-(pyridin-2- lene)aniline MTPMA	120
4.3	Synthes	is of Metal Complexes of MTPMA	126
4.4	Results	and Discussion	127
	4.4.1	Elemental Composition	127
	4.4.2	Molar Conductivity	129
	4.4.3	<sup>1</sup> H-NMR Spectra	129
	4.4.4	FT-IR Spectra	131
	4.4.5	UV-Visible Spectra and Magnetic Moment	136
	4.4.6	Electron Paramagnetic Resonance Spectrum of [Cu(MTPMA) <sub>2</sub> ]Cl <sub>2</sub>	141
	4.4.7	LC-MS Spectrum of [Cu(MTPMA) <sub>2</sub> ]Cl <sub>2</sub>	143
	4.4.8	Cyclic Voltammetry Studies	143
	4.4.9	Thermal Decomposition Studies	147
	4.4.10	Unit Cell Parameters of Ligand MTPMA	151

4.5	Biological S	Studies	151
	4.5.1	Evaluation of Antimicrobial Activities of Synthesized Compounds	151
	4.5.2	Evaluation of Antioxidant Activity (DPPH free radical scavenging Method)	161
	4.5.3	Evaluation of Antidiabetic Activity	164
4.6	Conclusion		167
Referen	ices		168
ANTIC (Z)-N-(	XIDANT A	RACTERISATION, ANTIMICROBIAL, ND ANTIDIABETIC ACTIVITIES OF v1)methylene-2-(methylthio)aniline AND ITS XES	171 - 218
5.1	Introdu	ction	171
5.2	Synthes (methyl	sis of (E)-N-(1H-indol-3-yl)methylene-2-thio)aniline IMMA	172
5.3	Synthes	sis of Metal Complexes of IMMA	172
5.4	Results	and Discussion	172
	5.4.1	Elemental Composition	172
	5.4.2	Molar Conductivity	174
	5.4.3	<sup>1</sup> H-NMR Spectra	175
	5.4.4	FT-IR Spectra	177
	5.4.5	UV- Visible Spectra and Magnetic Moment	182
	5.4.6	Electron Paramagnetic Resonance Spectrum of $[Cu(IMMA)_2)(H_2O)_2]Cl_2$	187
	5.4.7	LC-MS Spectrum of [Zn(IMMA) <sub>2</sub> ]SO <sub>4</sub>	188
	5.4.8	Cyclic Voltammetry Studies	189
	5.4.9	Thermal Decomposition Studies	193
5.5	Biologi	cal Studies	199
	5.5.1	Evaluation of Antimicrobial Activities of Synthesized Compounds	199
	5.5.2	Evaluation of Antioxidant Activity (DPPH free radical scavenging Method)	209
	5.5.3	Evaluation of Antidiabetic Activity	211

APPLICAT INHIBITO 6.1	RS AND I	Ses as Corr Introduc	osion Inhibetion  nd Discussi	itors	216 219 - 2 219 219 219 221
INHIBITO	RS AND I Schiff Ba 6.1.1	oye ADSO ses as Corr Introduc Result a 6.1.2.1	ORBENTS  Posion Inhibetion  and Discussion	itors	219 219
6.1	6.1.1	Introduce Result a 6.1.2.1	etion nd Discussi		219
		Result a 6.1.2.1	nd Discussi	ion	
	6.1.2	6.1.2.1		ion	221
			Weight L		221
		6.1.2.2		oss Measurement	221
			Molecula Propertie	ar Structure and Inhibitor	223
		6.1.2.3	-	on Isotherm and ynamics Calculation	224
		6.1.2.4	SEM: Sc Microsco	anning Electron ppe	226
	6.1.3	Conclus	ion		227
6.2	Dye Adso	orbent Prop	erties of Sc	chiff Bases	228
	6.2.1	Introduc	etion		228
	6.2.2	Result a	nd Discussi	ion	229
		6.2.2.1	Batch Ads	sorption Experiments	229
			6.2.2.1.a	Effect of Contact Time	229
			6.2.2.1.b	Effect of Initial Dye Concentration	230
		6.2.2.2	Adsorptio	n Isotherm Models	232
			6.2.2.2.a	Langmuir Isotherm	233
			6.2.2.2.b	Freundlich Isotherm	234
	6.2.3	Conclus	ion		237
References					238
SUMMARY	Y AND CO	ONCLUSI	ON		240 - 2
LIST OF PA	APER PU	BLICATI	ONS		246
LIST OF P.	APERS P	RESENTE	D IN CON	IFERENCES	247

# LIST OF TABLES

Table No.	Description	Page No.
2.1	Molar Conductivity Values (Ω <sup>-1</sup> cm <sup>2</sup> mol <sup>-1</sup> ) and Electrolytes Types	59
2.2	Preparation of the Environments for Weight Loss Method	70
3.1	Analytical Data and Physical Properties of the Ligand MPMA and its Metal Complexes	79
3.2	Molar Conductance Values of the MPMA Metal Complexes	80
3.3	<sup>1</sup> H NMR Spectral Data of the Ligand MPMA	81
3.4	<sup>1</sup> H NMR Spectral Data of the [Zn(MPMA) <sub>2</sub> ]SO <sub>4</sub>	82
3.5	Selected FT-IR Absorption Frequencies (cm <sup>-1</sup> ) of the Ligand MPMA and its Metal Complexes	84
3.6	Electronic Spectral Data of the Ligand MPMA and its Metal Complexes	89
3.7	Cyclic Voltammetric Data for MPMA Metal Complexes in DMF solution at 298 K	96
3.8	Stepwise Thermal Degradation Data of MPMA Metal Complexes obtained from TG-DTG Curve	100
3.9	Antibacterial Activities of Ligand MPMA and its Metal Complexes	106
3.10	Antifungal Activities of Ligand MPMA and its Metal Complexes	107
3.11	Antioxidant Activities of Ligand MPMA and its Metal Complexes	116
3.12	IC50 (µM) and R2 values of Standard Drug, Ligand MPMA and its Metal Complexes	117
3.13	Antidiabetic Activities of Ligand MPMA and its Metal Complexes Measured by $\alpha$ - Amylase Method	118
3.14	Antidiabetic Activities of Ligand MPMA and its Metal Complexes Measured by $\alpha\text{-}$ Glucosidase Method	119
4.1	Analytical Data and Physical Properties of the Ligand MTPMA and its Metal Complexes	128
4.2	Molar Conductance Values of the MTPMA Metal Complexes	129
4.3	<sup>1</sup> H NMR Spectral Data of the Ligand MTPMA	130
4.4	<sup>1</sup> H NMR Spectral Data of the [Zn(MTPMA)SO <sub>4</sub> ]	131

4.5	Selected FT-IR Absorption Frequencies (cm <sup>-1</sup> ) of the Ligand MTPMA and its Metal Complexes	133
4.6	Electronic Spectral Data of the Ligand MTPMA and its Metal Complexes	138
4.7	EPR Spectral data of [Cu(MTPMA) <sub>2</sub> ]Cl <sub>2</sub>	142
4.8	Cyclic Voltammetric Data for MTPMA Metal Complexes in DMF solution at 298 K	145
4.9	Thermal Degradation Data of Metal Complexes obtained from TG-DTG Curve	148
4.10	Antibacterial Activities of Ligand MTPMA and its Metal Complexes	153
4.11	Antifungal Activities of Ligand MTPMA and its Metal Complexes	158
4.12	Antioxidant Activities of Ligand MTPMA and its Metal Complexes	162
4.13	$IC_{50}$ ( $\mu M$ ) and $R^2$ values of Standard Drug, MTPMA and its Metal Complexes.	163
4.14	Antidiabetic Activities of Ligand MTPMA and its Metal Complexes Measured by $\alpha\text{-}$ Amylase Method	165
4.15	Antidiabetic Activities of Ligand MTPMA and its Metal Complexes Measured by $\alpha\text{-}$ Glucosidase Method	166
5.1	Analytical Data and Physical Properties of the Ligand IMMA and its Metal Complexes	173
5.2	Molar Conductance Values of the IMMA Metal Complexes	175
5.3	<sup>1</sup> H NMR Spectral Data of the Ligand IMMA	176
5.4	<sup>1</sup> H NMR Spectral Data of the [Zn(IMMA) <sub>2</sub> ]SO <sub>4</sub>	176
5.5	Selected FT-IR absorption Frequencies (cm <sup>-1</sup> ) of the Ligand IMMA and Metal Complexes	178
5.6	Electronic Spectral Data of the Ligand IMMA and Metal Complexes	183
5.7	Cyclic Voltammetric Data for IMMA Metal Complexes in DMF solution at 298 K.	190
5.8	Stepwise Thermal Degradation Data of Metal Complexes obtained from TG-DSC Curve	195
5.9	Antibacterial Activities of Ligand IMMA and Metal Complexes	201
5.10	Antifungal Activities of Ligand IMMA and Metal Complexes	202

5.11	Antioxidant Activities of Ligand IMMA and Metal Complexes	210
5.12	$IC_{50}\ (\mu M)$ and $R^2$ values of Standard Drug, IMMA and Metal Complexes	211
5.13	Antidiabetic Activities of Ligand IMMA and Metal Complexes Measured by $\alpha\text{-}$ Amylase Method	212
5.14	Antidiabetic Activities of Ligand IMMA and Metal Complexes Measured by α- Glucosidase Method	213
6.1	Corrosion Parameters from Weight Loss Measurement in 10% HCl Solution containing 500ppm Schiff base Ligand	222
6.2	Corrosion Parameters from Weight Loss Measurement in 10%HCl solution containing 1000ppm Schiff base Ligand	222
6.3	Corrosion Parameters from Weight Loss Measurement in 10%HCl solution containing 1500ppm Schiff base Ligand	222
6.4	Corrosion Parameters from Weight Loss Measurement in 10%HCl solution containing 2000ppm Schiff base Ligand	223
6.5	Relation between C/θ and C	224
6.6	Relation between $\Delta G^0_{ad}$ and $K_{ad}$ Values of Schiff Bases 1-3	226
6.7	Effect of initial concentration on the adsorption of the malachite green by Schiff base -1	231
6.8	Effect of initial concentration on the adsorption of the malachite green by Schiff base -2	232
6.9	Effect of initial concentration on the adsorption of the malachite green by Schiff base -3	232
6.10	Langmuir sorption parameters for malachite green adsorption using SB 1-3 adsorbents	232
6.11	Freundlich sorption parameters for malachite green adsorption using SB 1-3 adsorbents	235

# LIST OF FIGURES

Figure No.	Description	Page No.
1.1	Palladium (II) complex of Monodentate Schiff base	7
1.2	Structure of Bidentate Schiff base and Complex	8
1.3	Metal complexes with Schiff base coordinated through 'N' and 'O' donor atoms	9
1.4	Structures of Tridentate (NOO, NNO and NSO donor atom) Schiff bases	10
1.5	Structure of Tetradentate (NNOO and NNNO donor atom) Schiff base	10
1.6	Structure of Vanadium complex with Pentadentate Schiff base ligand	11
1.7	Structure of Hexadentate Schiff base	12
1.8	Morphology structure of Gram-positive and Gram-negative bacteria	20
1.9	Morphology Structure of Fungus	22
2.1	Structure of Malachite Green	74
3.1	Synthesis of Schiff base Ligand MPMA and its Metal Complexes	78
3.2	<sup>1</sup> H NMR Spectrum of the Ligand MPMA	81
3.3	<sup>1</sup> H NMR Spectrum of the [Zn(MPMA) <sub>2</sub> ]SO <sub>4</sub>	82
3.4	FT-IR Spectrum of Schiff Base MPMA	84
3.5	FT-IR Spectrum of [Fe(MPMA) <sub>2</sub> (H <sub>2</sub> O) <sub>2</sub> ]Cl <sub>3</sub>	85
3.6	FT-IR Spectrum of [Co(MPMA) <sub>2</sub> (H <sub>2</sub> O) <sub>2</sub> ](NO <sub>3</sub> ) <sub>2</sub>	85
3.7	FT-IR Spectrum of [Ni(MPMA) <sub>2</sub> ]SO <sub>4</sub>	86
3.8	FT-IR Spectrum of [Cu(MPMA) <sub>2</sub> (H <sub>2</sub> O) <sub>2</sub> ]Cl <sub>2</sub>	86
3.9	FT-IR Spectrum of [Zn(MPMA) <sub>2</sub> ]SO <sub>4</sub>	87
3.10	UV- Vis Spectrum of Schiff Base MPMA	90
3.11	UV- Vis Spectrum of Schiff Base [Fe(MPMA) <sub>2</sub> (H <sub>2</sub> O) <sub>2</sub> ]Cl <sub>3</sub>	90
3.12	UV- Vis Spectrum of Schiff Base [Co(MPMA) <sub>2</sub> (H <sub>2</sub> O) <sub>2</sub> ](NO <sub>3</sub> ) <sub>2</sub>	91
3.13	UV- Vis Spectrum of Schiff Base [Ni(MPMA) <sub>2</sub> ]SO <sub>4</sub>	91
3.14	UV- Vis Spectrum of [Cu(MPMA) <sub>2</sub> (H <sub>2</sub> O) <sub>2</sub> ]Cl <sub>2</sub>	92
3.15	UV- Vis Spectrum of [Zn(MPMA) <sub>2</sub> ]SO <sub>4</sub>	92

3.16	EPR Spectrum of [Cu(MPMA) <sub>2</sub> (H <sub>2</sub> O) <sub>2</sub> ]Cl <sub>2</sub>	93
3.17	LC-MS Spectrum of [Zn(MPMA) <sub>2</sub> ]SO <sub>4</sub>	94
3.18	Cyclic Voltammogram of [Fe(MPMA) <sub>2</sub> (H <sub>2</sub> O) <sub>2</sub> ]Cl <sub>3</sub>	96
3.19	Cyclic Voltammogram of [Co(MPMA) <sub>2</sub> (H <sub>2</sub> O) <sub>2</sub> ](NO <sub>3</sub> ) <sub>2</sub>	97
3.20	Cyclic Voltammogram of [Ni(MPMA) <sub>2</sub> ]SO <sub>4</sub>	97
3.21	Cyclic Voltammogram of [Cu(MPMA) <sub>2</sub> (H <sub>2</sub> O) <sub>2</sub> ]Cl <sub>2</sub>	98
3.22	Cyclic Voltammogram of [Zn(MPMA) <sub>2</sub> ]SO <sub>4</sub>	98
3.23	TG-DTA curve of [Fe(MPMA) <sub>2</sub> (H <sub>2</sub> O) <sub>2</sub> ]Cl <sub>3</sub>	102
3.24	TG-DTA curve of [Co(MPMA) <sub>2</sub> (H <sub>2</sub> O) <sub>2</sub> ](NO <sub>3</sub> ) <sub>2</sub>	102
3.25	TG-DTA curve of [Ni(MPMA) <sub>2</sub> ]SO <sub>4</sub>	103
3.26	TG-DTA curve of [Cu(MPMA) <sub>2</sub> (H <sub>2</sub> O) <sub>2</sub> ]Cl <sub>2</sub>	103
3.27	TG-DTA curve of [Zn(MPMA) <sub>2</sub> ]SO <sub>4</sub>	104
3.28	Antibacterial Activities of Ligand MPMA and its Metal complexes	109
3.29	Diameter of Inhibition Zone of Complexes against Bacteria	110
3.30	Antifungal Activities of Ligand MPMA and its Metal complexes	112
3.31	Diameter of Inhibition Zone of Complexes against Fungi	113
3.32	Free Radical Scavening of Ligand MPMA and its Metal Complexes	116
3.33	Antidiabetic Activities of Ligand MPMA and its Metal Complexes Measured by α-amylase Method	119
3.34	Antidiabetic Activities of Ligand MPMA and its Metal Complexes Measured by α-Glucosidase Method	120
4.1	Synthesis of Schiff base Ligand MTPMA and its Metal Complexes	127
4.2	<sup>1</sup> H NMR Spectrum of the Ligand MTPMA	130
4.3	<sup>1</sup> H NMR Spectrum of the [Zn(MTPMA)SO <sub>4</sub> ]	131
4.4	FT-IR Spectrum of Schiff Base MTPMA	133
4.5	FT-IR Spectrum of [Fe(MTPMA) <sub>2</sub> ]Cl <sub>3</sub>	134
4.6	FT-IR Spectrum of [Co(MTPMA) <sub>2</sub> ](NO <sub>3</sub> ) <sub>2</sub>	134
4.7	FT-IR Spectrum of [Ni(MTPMA) <sub>2</sub> ]SO <sub>4</sub>	135
4.8	FT-IR Spectrum of [Cu(MTPMA) <sub>2</sub> ]Cl <sub>2</sub>	135
4.9	FT-IR Spectrum of [Zn(MTPMA)SO <sub>4</sub> ]	135

4.10	UV- Vis Spectrum of Schiff Base MTPMA	138
4.11	UV- Vis Spectrum of [Fe(MTPMA) <sub>2</sub> ]Cl <sub>3</sub>	
4.12	UV- Vis Spectrum of [Co(MTPMA) <sub>2</sub> ](NO <sub>3</sub> ) <sub>2</sub>	
4.13	UV- Vis Spectrum of [Ni(MTPMA) <sub>2</sub> ]SO <sub>4</sub>	
4.14	UV- Vis Spectrum of [Cu(MTPMA) <sub>2</sub> ]Cl <sub>2</sub>	
4.15	UV- Vis Spectrum of [Zn(MTPMA)SO <sub>4</sub> ]	
4.16	EPR Spectrum of [Cu(MTPMA) <sub>2</sub> ]Cl <sub>2</sub>	
4.17	LC-MS Spectrum of [Cu(MTPMA) <sub>2</sub> ]Cl <sub>2</sub>	
4.18	Cyclic Voltammogram of [Co(MTPMA) <sub>2</sub> ](NO <sub>3</sub> ) <sub>2</sub>	145
4.19	Cyclic Voltammogram of [Cu(MTPMA) <sub>2</sub> ]Cl <sub>2</sub>	
4.20	Cyclic Voltammogram of [Zn(MTPMA)SO <sub>4</sub> ]	146
4.21	TG-DTG Curves of [Fe(MTPMA) <sub>2</sub> ]Cl <sub>3</sub>	149
4.22	TG-DTG Curves of [Co(MTPMA) <sub>2</sub> ](NO <sub>3</sub> ) <sub>2</sub>	149
4.23	TG-DTG Curves of [Ni(MTPMA) <sub>2</sub> ]SO <sub>4</sub>	150
4.24	TG-DTG Curves of [Cu(MTPMA) <sub>2</sub> ]Cl <sub>2</sub>	150
4.25	Antibacterial Activities of Ligand MTPMA and its Metal Complexes	152
4.26	Diameter of Inhibition Zones of Complexes against Bacteria	157
4.27	Antifungal Activities of Ligand MTPMA and its Metal Complexes	
4.28	Diameter of Inhibition Zones of Complexes against Fungi	160
4.29	Free Radical Scavening of Ligand MTPMA and its Metal Complexes	163
4.30	Antidiabetic Activities of Ligand MTPMA and its Metal Complexes Measured by α-Amylase Method	165
4.31	Antidiabetic Activities of Ligand MTPMA and its Metal Complexes Measured by α- Glucosidase Method	166
5.1	Synthesis of Schiff base Ligand IMMA and Metal Complexes	174
5.2	<sup>1</sup> H NMR Spectrum of Schiff Base Ligand IMMA	176
5.3	<sup>1</sup> H NMR Spectrum of [Zn(IMMA) <sub>2</sub> ]SO <sub>4</sub>	177
5.4	FT-IR Spectrum of Schiff Base IMMA	179
5.5	FT-IR Spectrum of [Fe(IMMA) <sub>2</sub> (H <sub>2</sub> O) <sub>2</sub> ]Cl <sub>3</sub>	179
5.6	FT-IR Spectrum of [Co(IMMA) <sub>2</sub> (H <sub>2</sub> O) <sub>2</sub> ](NO <sub>3</sub> ) <sub>2</sub>	180
5.7	FT-IR Spectrum of [Ni(IMMA) <sub>2</sub> ]SO <sub>4</sub>	180

5.8	FT-IR Spectrum of [Cu(IMMA) <sub>2</sub> )(H <sub>2</sub> O) <sub>2</sub> ]Cl <sub>2</sub>	181
5.9	FT-IR Spectrum of [Zn(IMMA) <sub>2</sub> ]SO <sub>4</sub>	181
5.10	UV-Vis Spectrum of Schiff Base IMMA	184
5.11	UV-Vis Spectrum of [Fe(IMMA) <sub>2</sub> (H <sub>2</sub> O) <sub>2</sub> ]Cl <sub>3</sub>	184
5.12	UV-Vis Spectrum of [Co(IMMA) <sub>2</sub> (H <sub>2</sub> O) <sub>2</sub> ](NO <sub>3</sub> ) <sub>2</sub>	185
5.13	UV-Vis Spectrum of [Ni(IMMA) <sub>2</sub> ]SO <sub>4</sub>	185
5.14	UV-Vis Spectrum of [Cu(IMMA) <sub>2)</sub> (H <sub>2</sub> O) <sub>2</sub> ]Cl <sub>2</sub>	186
5.15	UV-Vis Spectrum of [Zn(IMMA) <sub>2</sub> ]SO <sub>4</sub>	186
5.16	EPR Spectrum of [Cu(IMMA) <sub>2)</sub> (H <sub>2</sub> O) <sub>2</sub> ]Cl <sub>2</sub>	188
5.17	LC-MS Spectrum of [Zn(IMMA) <sub>2</sub> ]SO <sub>4</sub>	188
5.18	Cyclic Voltammogram of [Fe(IMMA) <sub>2</sub> (H <sub>2</sub> O) <sub>2</sub> ]Cl <sub>3</sub>	191
5.19	Cyclic Voltammogram of [Co(IMMA) <sub>2</sub> (H <sub>2</sub> O) <sub>2</sub> ](NO <sub>3</sub> ) <sub>2</sub>	191
5.20	Cyclic Voltammogram of [Ni(IMMA) <sub>2</sub> ]SO <sub>4</sub>	192
5.21	Cyclic Voltammogram of [Cu(IMMA) <sub>2</sub> (H <sub>2</sub> O) <sub>2</sub> ]Cl <sub>2</sub>	192
5.22	Cyclic Voltammogram of [Zn(IMMA) <sub>2</sub> ]SO <sub>4</sub>	193
5.23	TG-DSC Curve of [Fe(IMMA) <sub>2</sub> (H <sub>2</sub> O) <sub>2</sub> ]Cl <sub>3</sub>	197
5.24	TG-DSC Curve of [Co(IMMA) <sub>2</sub> (H <sub>2</sub> O) <sub>2</sub> ](NO <sub>3</sub> ) <sub>2</sub>	197
5.25	TG-DSC Curve of [Ni(IMMA) <sub>2</sub> ]SO <sub>4</sub>	198
5.26	TG-DSC Curve of [Cu(IMMA) <sub>2</sub> (H <sub>2</sub> O) <sub>2</sub> ]Cl <sub>2</sub>	198
5.27	TG-DSC Curve of [Zn(IMMA) <sub>2</sub> ]SO <sub>4</sub>	199
5.28	Antibacterial Activity of Ligand IMMA and Metal complexes	200
5.29	Diameter of Inhibition Zone of Complexes against Bacteria	206
5.30	Antifungal Activity of Ligand IMMA and Metal complexes	206
5.31	Diameter of Inhibition Zone of complexes against Fungi	208
5.32	Free Radical Scavening of Ligand IMMA and Metal Complexes	210
5.33	Antidiabetic Activities of Ligand IMMA and Metal Complexes Measured by $\alpha\text{-Amylase Method}$	213
5.34	Antidiabetic Activities of Ligand IMMA and Metal Complexes Measured by $\alpha\text{-Glucosidase Method}$	214

# LIST OF SYMBOLS AND ABBREVIATIONS

Symbols	Abbreviations
DMF	Dimethyl formamide
DMSO	Dimethyl sulphoxide
CHCl <sub>3</sub>	Chloroform
cm <sup>-1</sup>	Wavenumber
ppm	Parts per million
g	Gram
h	Hour
MHz	Megahertz
GHz	Gigahertz
kHz	Kilohertz
mL	Millilitre
°C	Degree Celsius
%	Percentage
TMS	Tetramethylsilane
nm	Nanometer
mg	Milligram
mm	Millimetre
μm	Micrometre
kg	Kilogram
μΑ	Microampere
sec	Seconds
min	Minutes
mmol	Millimole
M	Molarity
Λm	Molar Conductance
BM	Bohr magneton
μ <sub>eff</sub>	Effective magnetic moment

χ <sub>M</sub> corr	Corrected Magnetic susceptibility
mV	Millivolt
Δ	Delta
G	Gauss in EPR Spectroscopic Studies
λ	Lambda
ν	Frequency
δ	Chemical shift
μg/mL	Microgram per millilitre
IC <sub>50</sub>	The half maximal inhibitory concentration
CHNS analysis	Carbon, Hydrogen, Nitrogen and Sulphur analysis
<sup>1</sup> H NMR	Proton nuclear magnetic resonance spectroscopy
FT-IR	Fourier Transform Infrared spectroscopy
UV-Vis	Ultraviolet visible spectral studies
CV	Cyclic voltammetry
EPR	Electron paramagnetic resonance spectra
TG	Thermo Gravimetry
DTA	Differential Thermal Analysis
DSC	Differential Scanning Calorimetry
B.subtilis	Bacillus subtilis
S.aureus	Staphylococcus aureus
E.coli	Escherichia coli
P.aeruginosa	Pseudomonas aeruginosa
A.niger	Aspergillus niger
C.albicans	Candida albicans
DPPH	1, 1-diphenyl-2-picryl-hydrazyl
MPMA	2-(methylsulfanyl)–N–(1H-pyrrol-2-ylmethylidene)aniline
MTMPA	(E)-2-(methylthio)-N-(pyridin-2-ylmethylene)aniline
IMMA	(Z)-N-(1H-indol-3-yl)methylene-2-(methylthio) aniline

# SYNTHESIS, CHARACTERISATION AND BIOLOGICAL STUDIES ON SCHIFF BASE METAL COMPLEXES: CORROSION INHIBITION AND DYE ADSORBENT PROPERTIES OF SCHIFF BASES

# Abstract

Transition metal complexes were prepared using Schiff base ligands derived from the condensation of 2-(methylthio)aniline with pyrrole-2-carboxaldehyde, pyridine-2-carboxaldehyde and indole-3-carboxaldehyde respectively. The geometry of the metal complexes was concluded from elemental analysis, molar conductivity,  $^{1}$ H NMR, FT-IR, UV-Vis, EPR, Mass, CV, magnetic and thermal studies. The synthesized Schiff base metal complexes were inspected for *in vitro* antimicrobial activities against human pathogenic microorganisms. The antioxidant activities of the Schiff base metal complexes were measured by DPPH method. The *in vitro* antidiabetic activities of the Schiff base metal complexes were studied against carbohydrate hydrolysing enzymes such as  $\alpha$ - amylase and  $\alpha$ - glucosidase. Corrosion inhibition property of Schiff bases was studied using mild steel in 10% HCl solution. Dye adsorbent property of Schiff bases was studied using malachite green.

# Introduction

In recent years, coordination compounds have sparked a lot of interest due to their practical suitability, operational flexibility and interesting structural features. This branch of chemistry has now amalgamated into various areas of science such as metallurgy, analytical chemistry, materials science, industrial chemistry and medicinal chemistry. The trend towards the design, synthesis, characterisation, and application of coordination compounds is undeniably expanding for educational, economic, environmental, and societal reasons. Especially, development of biologically active compounds such as pharmaceuticals, agrochemicals, flavours and fragrances, as well as advanced materials, has received a great attention. Coordination compounds containing bonds between a central metal atom and surrounding ligands, play acute role in regulating the structure and function of many enzymes and their metabolism. Coordination compounds of the organic ligands accounting for more than fifty percent of carbon, are included under inorganic chemistry, may be due to the fact that the central metal ion is responsible for their reactivity. Earlier works reported that some drugs showed an increase in activity when administered as metal chelates rather than as organic compounds and hence metal complexes are used as diagnostic and therapeutic agents.[1]

Coordination compounds plays important role in our day-to-day life, ranging from biology to industrial applications. In biology, classical organic drugs are now replaced by the coordination complexes, because of their excellent selectivity and target specificity in treating a variety of life-threatening disorders. Hence, gaining a knowledge about the nature and bonding of coordination complexes grabs attention. Metals, which are an integral part

of enzymes and proteins, play a critical role in the normal functioning of enzymes in living systems.[2]

There are several synthetic metal complexes that replicate the behaviour of complex biomolecules, and the investigation of such compounds is currently attracting a lot of attention. Several studies have linked particular transition metal ion concentrations to a variety of disorders. Wilson's disease is diagnosed by a low serum copper level in blood. In a large number of chronic and acute illnesses such as Hodgkin's disease, Leukaemia and many other malignancies serum copper levels are found to be high.[3] For many metalloenzymes, zinc is an chief nutritive factor as well as a cofactor. Zinc is required for cell growth and division, particularly in the early stages of life when growth rates are high. Syndromes that cause short structure and dwarfism are associated with zinc deficiency. Human bodies require trace metals such as iron and cobalt. Some disorders can be caused by a lack of these important components, and if they are consumed in excess, they can be toxic and detrimental.

The fourth richest element in the earth's crust is iron and it occurs as both Fe<sup>2+</sup> and Fe<sup>3+</sup> ions in all types of rock and soil minerals. In the biosphere, iron plays a chief role because it is the active centre of proteins that transfer oxygen and electrons, as well as metalloenzymes including oxidases, reductases, and dehydrases. Schiff bases as ligands have played a significant role in the growth of coordination chemistry as a whole.

The field of research on transition metal complexes of Schiff bases has grown enormously in recent years, encompassing a wide range of topics, including vast areas of organometallic compounds and various aspects of bioinorganic chemistry. [4]

Schiff base complexes find their place in the fields of condensed matter physics, material chemistry, and inorganic chemistry due to their unique magnetic properties. [5].

When the coordination environment of the metal ion is unsaturated, some additional binders can bridge the metal ions to form polynuclear complexes. Schiff base compounds containing azomethine group (-RC=N-) appear to be a point of interest for many inorganic chemists as these are widely used as liquid crystals, in heterogeneous catalysis, [6] for designing molecular ferromagnets, in biological modelling applications and also in self-assembling cluster complexes [7].

Schiff bases offer chances for inducing chirality in the substrate molecule, tuning the electronic factor of central metal ion and increasing the solubility and stability of either homogeneous or heterogeneous catalyst. Schiff base transition metal complexes having oxygen and nitrogen donors possess unusual configuration and are sensitive to molecular environment. The key factor required for metallo-proteins to carry out specific physiological activities is the environment around the metal centre, such as coordination geometry, the number of coordinated ligands, and their donor groups. Furthermore, the biological activity of donor atoms is triggered by their presence in the coordination sphere. The studies of Schiff base metal complexes cover a wide range of topics, from general academic interest to a wide spectrum of biological activity and practical applications in a variety of fields, including medicine, agriculture, trace metal determination, pharmaceutical products and ion selective electrodes.

Schiff bases find application in dye manufacturing, liquid crystal manufacturing, and medicine. They act as synthetic oxygen carriers and they have been produced from enzymatic reaction intermediate products and also used as antitumor agents.[8] Therefore it is very essential to synthesise Schiff bases and their transition metal complexes. For a long time, researchers have shown interest in studying, transition metal Schiff base complexes derived from heterocyclic aldehydes. [9, 10]

# 1.1 Schiff base ligands

Schiff base, is one of the potent organic moieties which can form metal complexes. They are synthesized from the direct condensation of aldehydes or ketones and primary amines. This condensation was first completed by Hugo Schiff in 1864 (hence the name of the compounds) [11]. Condensation of primary amine with an aldehyde or ketone occurs according to **Scheme: 1** 

$$\begin{array}{c}
R \\
C = O + H_2N - R \longrightarrow R \xrightarrow{\text{Azomethine linkage}} R^1 \\
R^1 & R^1 & Schiff base
\end{array}$$

Scheme -1 Synthesis of Schiff base

where R can be either an alkyl or an aryl group. Schiff bases with aryl substituents are significantly more stable and easier to prepare, but those with alkyl substituents are relatively unstable and they easily polymerize. The –N=CH- (imine) group in Schiff bases, is important for understanding the mechanism of transamination and racemisation in biological systems. The azomethine group has a lot of chemical importance because of the lone pair of electrons in the sp<sup>2</sup>- hybridised orbital of the nitrogen atom, and it has a lot of chelating potential, especially when combined with one or more donor atoms close to the azomethine group. This chelating capacity of the Schiff bases, combined with their ease of production and versatility in modifying the chemical environment around the C=N group, make them an interesting ligand in coordination chemistry, and they are commonly referred to as privileged ligands. [12]

The formation of a Schiff base, from an aldehyde or ketone is a reversible reaction and commonly takes place under acid or base catalysis, or upon heating (**Scheme 2**).

Scheme-2 Mechanism for formation of Schiff base

The formation of Schiff base is usually driven to completion by separation of the product or removal of water, or both. Many Schiff bases can be hydrolysed by aqueous acid or base to give back their aldehydes or ketones and amines. The mechanism for the formation of Schiff base can be seen on the theme of nucleophilic addition to the carbonyl group. In this case, the nucleophile is the amine. In the first part of the mechanism, unstable addition compound called carbinolamine is formed, when amine reacts with the aldehyde or ketone. The carbinolamine undergoes dehydration by either acid or base-catalysed pathways. Since the carbinolamine is an alcohol, it undergoes acid-catalysed dehydration.

The rate determining step of Schiff base formation is typically the dehydration of the carbinolamine. However, amines are basic molecules and hence the concentration of acid used for dehydration cannot be too high. When an amine is protonated and becomes non-nucleophilic, equilibrium is shifted to the left, preventing carbinolamine production. As a result, many Schiff base syntheses are best performed at mildly acidic pH. Carbinolamine dehydration is also catalysed by base. This reaction is slightly equivalent to the E<sub>2</sub> elimination of alkyl halides except that it is not a concerted reaction. It takes place in two steps through an anionic intermediate.

# 1.1.1 Types of Schiff bases based on chelating property with metal ion

A Schiff base shows strong coordination ability due to the presence of azomethine linkage. The nitrogen atom of the azomethine moiety (C=N-) has a tendency to donate the lone pair of electrons.[13] The presence of an acidic group, such as phenolic OH, or another donor group adjacent to the azomethine group, strengthens the coordinating effect of the lone pair of electrons thereby increasing the stability of the metal complex. The basicity of the amino group and steric factors play a vital role in the stability of the Schiff base complex. The accessibility of the lone pair of electrons is reduced by the presence of an electron withdrawing ring structure in the ligand. Schiff base ligands are known to coordinate as mono-, bi-, tri-, tetra-, penta- and hexa -dentate ligands.

#### **Monodentate Schiff bases**

The C=N group of the Schiff base is insufficiently basic to produce stable complexes when the azomethine nitrogen atom is coordinated to a metal ion. For this reason, the presence of at least one additional group is required to maintain the metal-nitrogen bond. Several research groups have suggested that the Schiff bases seem to be monodentate in nature. Kose et al. came out with two monodentate Schiff base ligands, based on N, N'-bis(2-methoxy phenylidene)-1, 5-diaminonaphthalene and N, N-bis(3,4,5-trimethoxyphenylidene)-1, 5-diamino naphthalene.[14] The palladium (II) complex shown in the **Fig.1.1** is an example of monodentate Schiff base complex where Schiff base acts as a ligand which is stabilised by the recommended interaction of Pd-H [15]

Fig. 1.1 Palladium (II) complex of Monodentate Schiff base [15]

# **Bidendate Schiff bases**

The following subsections provide a quick overview of potential bidentate ligands in terms of their donor atom set.

# a) N, N donor atom set

Schiff bases with two nitrogen donors are formed via condensation of dialdehydes or diketones between two amine molecules or by interaction of diamines with aldehydes or ketones. The typical example may be N-(pyridyl)-3-methoxy-4-hydroxy-5-nitrobenzaldimine [16]. The synthesis, structure and coordination activities of these ligands have been widely studied. 2-Pyrrole carboxaldehyde and ammonia combines to give N, N donor ligand which forms a stable complex [17] with copper (II) ion (shown in **Fig.1.2**).

$$\begin{array}{c|c} & & & & \\ & & & \\ & & & \\ & & & \\ & & & \\ & & & \\ & & & \\ & & & \\ & &$$

Fig.1.2 Structure of Bidentate Schiff base and Complex [16, 17]

#### b) N, O donor atom set

Schiff bases with N, O donor atoms operate as ligands for numerous metal ions, because oxygen is present there in phenolic group and these ligands generally act as chelating monoanions. The Schiff bases, which have the composition  $ML_2(2H_2O)$  operate as a bidentate monobasic donor where M = Mn(II), Co(II), Ni(II), Cu(II) and  $ML_2(H_2O)$  Cl where M = Fe(III) as shown in the **Fig.1.3.** Physicochemical data confirm the octahedral geometry of Mn(II), Co(II), Ni(II), Cu(II), and Fe(III) complexes. Here, Schiff bases are derived from 3-(4-chlorophenoxymethyl)-4-amino-5-mercapto-1, 2, 4-triazole and substituted aldehydes. All of the dark coloured amorphous metal complexes listed above are soluble in DMF and DMSO. The molar conductance values for these complexes are in the range of 20-30 ohm<sup>-1</sup> cm<sup>2</sup> mol<sup>-1</sup>. As a result, these complexes are classified as non-electrolytes [18]. The ligand 2-[(E)-{3-[(4-chlorophenoxy) methyl]-5-mercapto-4H1, 2, 4-triazol-4-yl}imino]-phenol (CITHS) acts as a monobasic bidentate one coordinating through 'N' and 'O' of OH group.

M=Fe(III)

M=Co(II), Cu(II), Ni(II) and Mn(II)

Fig. 1.3 Metal complexes with Schiff base coordinated through 'N' and 'O' donor atoms [18].

#### **Tridentate Schiff bases**

In the literature, a considerable number of tridentate Schiff bases with NNO, NNS, NOO, NNN, and NSO donor sets have been reported [19-23]. The majority of them are made by reacting salicyaldehyde with amines that include an OH or SH group. Some typical tridentate ligands are given in, **Fig.1.4**. Antibacterial and antiviral medicines have been developed using different types of tridentate ligands and their metal complexes with new structural, magnetic, and spectroscopic properties. [22, 23] The presence of a soft sulphur atom lowers the hardness of oxygen atoms, allowing the formation of a wide range of metal complexes with remarkable structural variation.

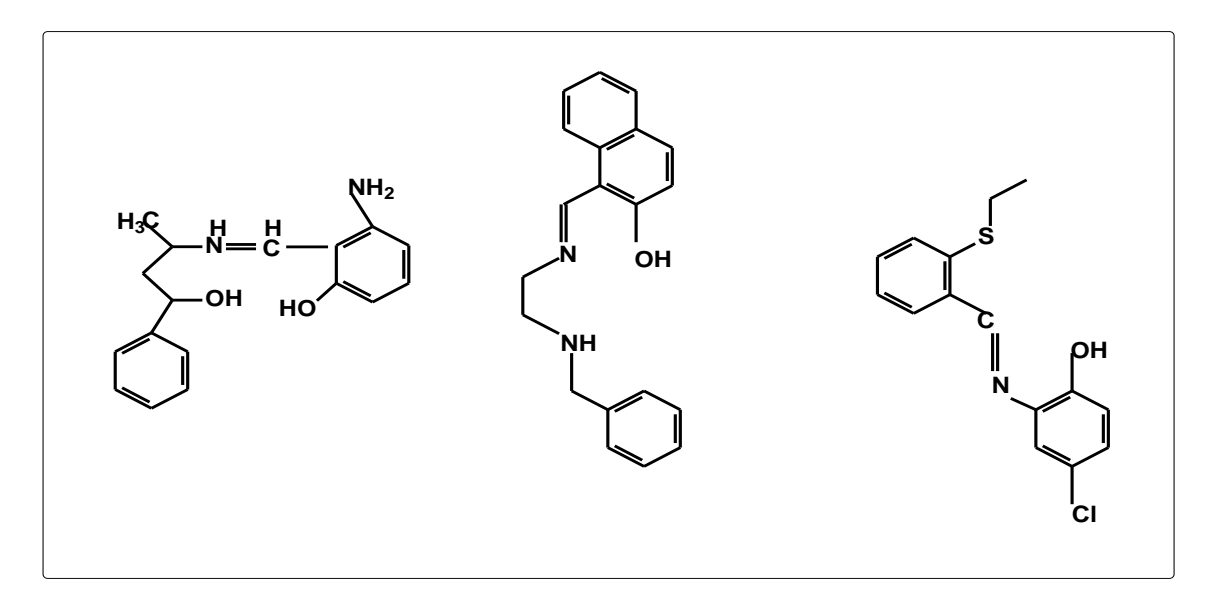


Fig.1.4 Structures of Tridentate (NOO, NNO and NSO donor atom) Schiff bases [19-23]

# **Tetradentate Schiff bases**

Tetradentate Schiff bases viz N<sub>2</sub>O<sub>2</sub> or N<sub>3</sub>O have been studied for their ability to coordinate metal ions. [24, 25] The properties of complexes formed by these ligands are governed by their electrical nature and conformational behaviour. Tetradentate Schiff bases are used to make acen, salen, salophen, and melen type compounds, as shown in **Fig.1.5.** 

Fig.1.5 Structure of Tetradentate (NNOO and NNNO donor atom) Schiff base [24, 25]

#### **Pentadentate Schiff bases**

Metal complexes containing pentadentate Schiff base ligands have also been extensively studied in recent decades. Boca et al. produced mononuclear and binuclear Fe (III) complexes with pentadentate Schiff-base ligands and their magnetic properties were also explored. [26] Mukherjee et al. discovered an insulin-stimulating oxidovanadium (IV) Schiff base complex generated from vitamin B6.It is shown in **Fig.1.6** .It is found to be a five coordinated complex. [27]

Fig.1.6 Structure of Vanadium complex with Pentadentate Schiff base ligand [27].

# **Hexadentate ligands**

In the domain of coordination chemistry, polydentate ligands and their metal complexes are presently of great interest. These compounds have a wide range of uses in analytical, synthetic, and biological chemistry. Sarkar et al. have condensed 3-formylsalicylic acid and 1, 2-di(o-amino phenylthio) ethane to form a novel interesting hexadentate dibasic  $N_2S_2O_2$  donor Schiff base ligand, 1, 2-di{(3-carboxyl)o-salicylal dimino phenylthio}ethane (abbreviated as H4dcsalpte) (**Fig.1.7**) Under various reaction conditions, the ligand reacted with various metal salts such as manganese(III), iron(III),

cobalt(II), cobalt(III), nickel(II), copper(II), and palladium(II) ions to produce a range of metal complexes.[28]

Fig.1.7 Structure of Hexadentate Schiff base [28]

# 1.1.2 Biological Importance of Schiff Bases

Schiff bases, which are formed by condensation of a carbonyl compounds and amino acids, are an astonishing class of ligands that coordinates to metal ions by imine nitrogen. Presence of azomethine (C=N) linkage in Schiff base ligand system is crucial for biological activities. The lone pair on sp² hybridized nitrogen atom of the azomethine linkage plays a key role to show biological activities. These types of metal complexes have also received an excessive attention because of their active part in metalloenzymes and as biomimetic model compounds. It is found that nitrogen atom has a vital role in the coordination of metals as an active site of numerous metallobiomolecules. The ligands in transition metal complexes containing some hetero atoms, like nitrogen, oxygen and sulphur donors show carcinostatic, antitumor, antiviral, antidiabetic, antifungal, antibacterial activities [29] and their capability to bind oxygen reversibly, their catalytic activity in the hydrogenation of olefins, their photochromic properties and their complexing ability towards some toxic metals.

In particular, Schiff bases derived from amino acids are active against a wide range of organisms as they play an essential role in carboxylation, transamination and C-C bond cleavage in living organisms [30]. Furthermore, Schiff bases are found to have mild antitumour activities; a huge number of these compounds have been synthesized in order to find compounds with greater antitumour activities. Antitumour activity has also been discovered in certain polymeric Schiff bases. At pH 5, Schiff bases have the highest degree of hydrolysis and solubility in water. The antitumour efficacy of Schiff bases towards malignant tumours increases significantly with the slight increase in water solubility.

With the aid of molecular models, stereochemical investigations were carried out on Schiff bases formed between methylglyoxal and the amino group of the lysine. Side chains of proteins can bend back in such a way towards the nitrogen atom of peptide group, so that a charge transfer can occur between these groups and the oxygen atoms of the Schiff bases

Schiff bases are significant in enzyme catalysis because they form a covalent bond with the substrate, thereby preventing the diffusion of substrate in the middle of the reaction and they act as electron source. Many Schiff bases are recognised to have medicinal value and are employed in the development of pharmaceuticals. Schiff bases appear to be main intermediates in a number of enzymatic reactions involving the interaction of an enzyme's amino group with a substrate's carbonyl group.

Schiff bases are shown to have a pharmacological impact that is much enhanced when metal ions are present. These facts have sparked a lot of curiosity in the chemistry of these complexes. As a result, the research field involving these metal complexes is highly broad, encompassing a variety of interdisciplinary fields such as bioinorganic chemistry, catalysis, photo chemistry, and magneto chemistry. Again, with the progresses in inorganic chemistry, researchers are having novel concepts regarding versatile uses of metal complexes as therapeutic agents and as medications for the treatment of numerous human

diseases. Synthesis of Schiff base metal complexes, particularly those of transition metal ions, with various molecular topologies and sets of donor atoms, is becoming an emerging area of research due to their potential applications in pharmaceuticals, antibacterial [31-36], antifungal [37], anticancer, anticonvulsant [38], and anti-inflammatory actions. Finally, the heterocyclic Schiff base ligands and their metal complexes have been the subject of extensive investigation because of their wide use in biological field [39].

## 1.2 Metallo-Elements in Biological Systems

The study of metal ions in the fields of medicine, pharmacology and toxicology have long history but recently the extent and variety of metal ion involvement is much appreciated. The metalloelements either in trace or ultra - trace quantities play major roles in living system at molecular level. For example, the elements V, Cr, Mn, Fe, Co, Ni, Cu, Zn and Mo are found to be an essential to life and the elements Au, Ag, Pt, Pd, Ir, Os, Ti and others have either been used in therapy or claimed to be of therapeutic values. The proper functioning of different enzymes are controlled by the transition metal ions. Metal ions play indispensable roles in about one third of enzymes. These ions can control an enzyme-catalysed reaction effectively by modifying the electron flow in a substrate or enzyme. In the active site, metal ions serve to bind and orient substrate with respect to functional groups, and if the metal ion has several valence states, it provides a site for redox activity. In the absence of appropriate metal ion, a biochemical reaction catalysed by a particular metalloenzyme would proceed very slowly. It is found that the transition metals are biological active and it is mainly due to coordination with different bioligands.

Thermodynamic and kinetic properties of the complexes govern the mode of biological action. Sometimes, *in vivo*, formation of chelates increases the lipophilicity which in turn increases the drug action that results in much more effective penetration of drug into the site of action. Further, in various *in vivo* compartments the correct metal ion balance is

important for the functioning of specific metal containing sites in many enzymes and proteins. For example, if the concentrations of some metal ions are significantly higher than normal, blockage of transport sites might occur and symptoms more commonly attributed to depletion of metal ions can result. They are inactive in the absence of all metals. The toxicity of heavy metal ions is partially due to their binding nature with the nucleic acids. Furthermore, the knowledge of binding of metal ions is useful in developing effective anticancer drugs.[40, 41] Changes in the *in vivo* concentration of naturally occurring low molecular weight ligands or protein complexing sites might affect metal ion distribution. Chromium metabolism plays an important role in diabetes. Metabolism of inorganic constituents are responsible for number of diseases and their remedies.

When considering *in vivo* activities, the most likely complex species can be anticipated in terms of concentration and relative abundance. A wide range of microenvironments are present *in vivo* and each would be expected to impact the metal's chemistry in the same way that a change in the solvent or the absorption of metal ions on a surface would. While discussing the *in vivo* chemistry, the metal ions are divided into class I and class II acids based on their *in vitro* reactivity.

Class I metal ions (eg., Na<sup>+</sup>, K<sup>+</sup>, Mg<sup>2+</sup>) are small and are neither oxidised nor reduced easily and relatively have high positive charge while class II metals (e.g., Cu<sup>+</sup>, Au<sup>+</sup>, Hg<sup>+</sup>, Cd<sup>2+</sup>, Pt<sup>2+</sup>) are large with low positive charge. First row transition metal ions lie in between those two extremes. Class I metal ions coordinate with oxygen and nitrogen donor ligands whereas class II metal ions coordinate with sulphur and phosphorus donor ligands. This concept is absolutely difficult to apply, but it is useful in a relative sense. Transition metal ions are good Lewis acids, generating a wide spectrum of complexes with donor ligands such as nitrogen, oxygen, and sulphur.

In recent years, considerable interest has been developed in copper complexes. Copper is an essential metal and it is an active site of several metallo proteins and enzymes such as haemocyanin, tyrosinase, cytochrome C oxidase, and ascorbate oxidase [42]. Copper can exist in four oxidation states (0, 1, 2 and 3) under normal condition. Biological electron-transfer reaction, oxygen atom insertion into substrates, dioxygen reduction to hydrogen peroxide or water and hydrolytic reactions are some of the biological processes in which copper proteins are involved. Unusual spectral and structural properties of blue copper proteins have received considerable interest. Copper (II) Schiff base complexes are well-known among transition metal complexes for their preparational accessibility, displaying the flexibility of the coordination geometry around the metal centre. It also acts as key intermediates in some pyridoxal dependent enzyme processes and in collagen cross linkage by lysyl oxidase. [43] The oxidation of amine to aldehyde using molecular oxygen as oxidant and pyridoxal phosphate as cofactor is catalysed by amino oxidase a copper protein. A type II copper protein which is found in mammalian liver acts as a catalyst for the oxidation of uric acid to allentrin haemocyanin. This type of protein is also responsible for oxygen transport in lower invertebrates such as mollusks, arthropods and annelids. Ceruloplasmin, an intensely blue coloured copper protein is found in the blood plasma of the vertebrates. [44]

Cobalt plays an important role in vitamin  $B_{12}$  for a wide range of life forms from microorganisms to human being.[45] Cobalt both in the di- and trivalent states, forms stable complexes with nitrogen donor ligands, and both are associated with the catalytic action of the vitamin. The cobalt (III) corrin complex which bounds to blood plasma protein fractions and passed to the tissue, bounds to various protein receptors which are required for haemoglobin synthesis. [46, 47] Vitamin  $B_{12}$  enzymes are also associated with hydrogen and methyl transfers. Conversion of amino alcohols into aldehydes is catalysed by Vitamin  $B_{12}$  enzyme.

Four types of enzymes namely urease, carbon monoxide dehydrogenase (CODH) and hydrogenase and methyl-S-coenzyme M reductases contain nickel as an essential component. Square planar nickel-salen complex in presence of oxidizing agents is used for cleavage of plasmid DNA. [48] This was reported by Morrow and Kolasa. Urease an enzyme which comprise dimeric Ni centre where nickel atom is octahedrally coordinated and probably act as Lewis acid for substrate binding. It also catalyses the hydrolysis of urea to ammonium and carbamate ions. In some bacteria, hydrogen uptake or liberation is catalysed by an enzyme called Nickel Iron hydrogenase. Synthesis of acetyl-coenzyme A is catalysed by enzymes of certain methanogenic organism containing nickel. Methyl-coenzyme M reductase is an enzyme which contains redox active NiN4 macro cycle (factor F430) as prosthetic group. [49]

### 1.3 Anti-Bacterial Activity

One of the great success stories of medicinal chemistry is the fight against bacterial infection. The discovery of antibacterial agents is so important that it is more selective in combating bacterial cells rather than animal cells due to structural differences and biosynthetic mechanisms that develop within them.

Antibiotics are microorganism-produced chemical substances that inhibit the growth of other microbes. Many antibiotics are currently in use, either fully synthetic or produced through chemical modification of natural products, and are thus referred to as antimicrobial agents (AMA)

### Mechanisms of anti-bacterial action

Based on their mechanism of action, Antibiotics can be divided into two classes

Bacteriostatic – the agent inhibits bacterial growth or reproduction and limits bacterial growth by interfering with bacterial protein production, DNA replication, or other aspects of bacterial cellular metabolism.

Bactericidal - a substance that kills or destroys bacteria. It kills bacteria by blocking cell wall formation and bacterial enzymes, as well as protein translation.

These antibacterial agents primarily work through five different methods.

#### **Inhibition of cell metabolism**

Antimetabolites are antibacterial drugs that block cell metabolism. The metabolism of a microbe is inhibited by these compounds, but not the metabolism of the host. They accomplish this by blocking an enzyme-catalyzed process found in bacterial cells but not in animal cells.

# Inhibition of bacterial cell wall synthesis

Inhibition of cell wall synthesis causes bacterial cell lysis (bursting) and death.

Because animal cells lack a cell wall, such antibiotics (penicillins and cephalosporins) have no effect on them.

### Interactions with the plasma membrane

Some antibacterial drugs affect membrane permeability by interacting with the plasma membrane of bacterial cells. The cell will die as a result of this.

## Disruption of protein synthesis

Protein synthesis, bacterial chromosome binding, and other aspects of protein synthesis are all inhibited. Rifamycins, aminoglycosides, tetracyclines, and chloramphenicol are examples of agents that affect protein synthesis.

### Inhibition of nucleic acid transcription and replication.

Cell division and/or the production of essential enzymes are prevented when nucleic acid function is inhibited. Nalidixic acid and proflavin are two agents that work in this fashion. The antibacterial properties of produced Schiff base metal complexes were investigated using two different types of bacteria.

#### 1.3.1 Bacteria

Bacteria are prokaryotic microorganisms that are single-celled and lack nuclei and other organised cell structures. The differential staining technique known as Gram staining was invented by Danish physician Christian Grams. Bacteria are classified as Gram-positive or Gram-negative based on the results of the gram staining method, which uses an agent to bind the bacteria's cell wall. Gram-positive bacteria absorb the crystal violet dye and remain blue or violet in colour. Gram-negative bacteria, on the other hand, do not absorb the crystal violet dye and look red or pink.

#### **Bacillus subtilis (Gram-positive)**

Bacillus subtilis is a Gram-positive, rod-shaped bacteria, also known as the hay bacillus or grass bacillus. It is found in soil and the gastrointestinal tract of ruminants, humans and marine sponges. Christian Gottfried Ehrenberg termed it Vibrio subtilis, but Ferdinand Cohn renamed it *Bacillus subtilis* in 1872. *B. subtilis* cells are typically rod-shaped, and are about 4–10 micrometres (μm) long and 0.25–1.0 μm in diameter, with a cell volume of about 4.6 fL at stationary phase. To survive under high heat and desiccation, it can create an endospore. The bacterium *Bacillus subtilis* is an excellent model for investigating chromosomal duplication and cell division in bacteria. It is one of the pioneers in the manufacture of secreted enzymes and has been employed in biotechnology on a large scale. *B. subtilis* is only known to infect highly immuno compromised persons and to cause food poisoning in a small number of cases.

### E.coli (Gram negative)

Escherichia coli also known as *E. coli* is a Gram-negative, facultative anaerobic, rod-shaped, coliform bacterium of the genus. Cells are typically rod-shaped, and are about 2.0 μm long and 0.25–1.0 μm in diameter, with a cell volume of 0.6–0.7 μm, *Escherichia coli* that is commonly found in the lower intestine of warm-blooded organisms. Most *E. coli* strains are harmless, but some serotypes can cause serious food poisoning in their hosts, and are occasionally responsible for food contamination . Antibiotics can effectively treat E. coli infections outside the digestive tract and most intestinal infections but are not used to treat intestinal infections by one strain of these bacteria. E. coli has several practical uses besides its use as a vector for genetic experiments and processes. For example, E. coli can be used to generate synthetic propane.

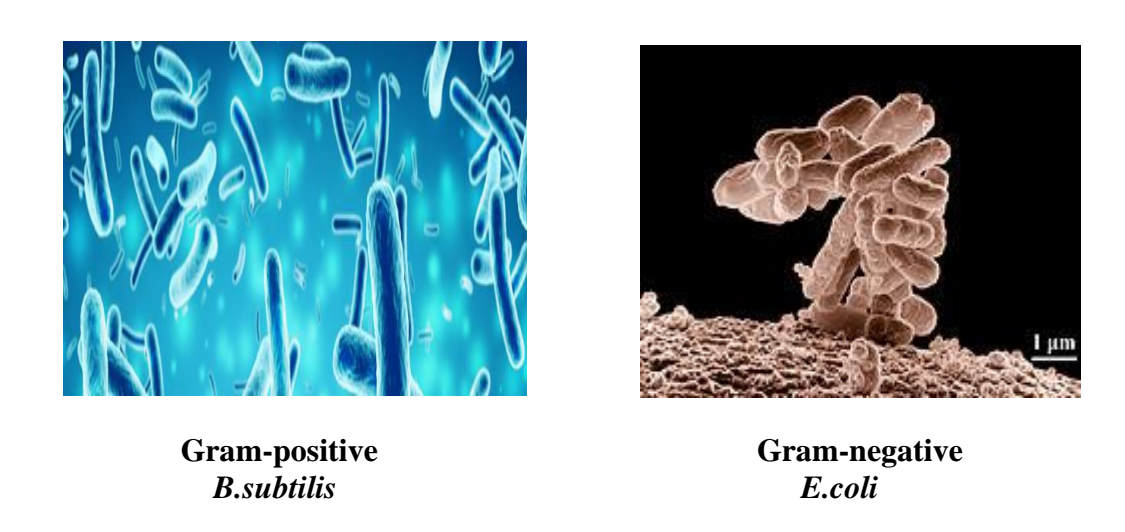


Fig.1.8 Morphology structure of Gram-positive and Gram-negative bacteria

#### 1.4 Anti-Fungal Activity

Anti-fungals are drugs that destroy or stop fungus from growing. They're used to treat diseases like athlete's foot, ringworm, and thrush in medicine, and they function by exploiting distinctions between mammalian and fungal cells. They eliminate the fungus organism without causing harm to the host. The disc method is used to investigate the antifungal activity of ligands and their metal complexes.

### **1.4.1** Fungi

A fungi is an eukaryotic organisms that includes microorganisms such as yeasts and molds. Fungi, like animals, are heterotrophs; they acquire their food by absorbing dissolved molecules, typically by secreting digestive enzymes into their environment. Fungi do not photosynthesize. Fungi are the principal decomposers in ecological systems. Fungi perform an essential role in the decomposition of organic matter and have fundamental roles in nutrient cycling and exchange in the environment. They have long been used as a direct source of human food, in the form of mushrooms and truffles; as a leavening agent for bread; and in the fermentation of various food products.

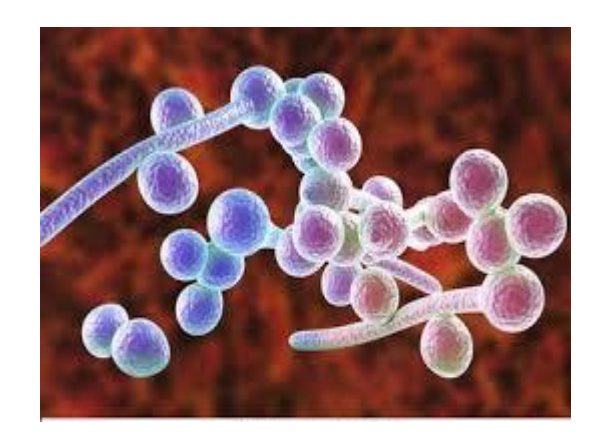
## Aspergillus Niger

Aspergillus niger is one of the most common Aspergillus species. The black mould, Aspergillus niger, frequently contaminates bacteriological and mycological cultures. It is present naturally in soil and causes food to rot. The fungus Aspergillus niger is used to make citric acid and other organic acids. A. niger culture produces enzymes that are employed in industrial fermentation. They produce diseases such as aspergilloses of the lungs and external ear.

#### Candida albicans

*C. albicans* is frequently used as a model organism for fungi. Candida is a yeast genus that can be found in the human intestinal flora. It can cause vaginal yeast infection, as well as infections in other moist parts of your body like your mouth (thrush), skin folds, and fingernail beds. Candida is prevalent all around the world, but it is more common in immuno - compromised individuals who are diagnosed with serious illnesses like HIV or cancer.





Aspergillus Niger

Candida albicans

Fig.1.9 Morphology Structure of Fungus

#### 1.5 Antioxidant Activity

Free radicals, which are formed during normal or pathological cell metabolism, contain one or more unpaired electrons. These free radicals are easily reacted with reactive oxygen species (ROS), which then become radicals. ROS are activated oxygen species that include free radicals like superoxide anion radicals (O<sub>2</sub>) and hydroxyl radicals (OH'), as well as non-free radical species like hydrogen peroxide (H<sub>2</sub>O<sub>2</sub>) and molecular oxygen (O<sub>2</sub>). Peroxisomes, activated polymorphonuclear leukocytes and macrophages, and regular aerobic respiration are some examples by which they are created in living creatures.[50] They are metabolic by-products that occur naturally in human bodies. Our tissues are completely damaged by free radicals and reactive oxygen species (ROS), and this type of damage can be avoided by using antioxidants.

The amount of ROS that is eliminated is detoxified by mitochondria, whereas ROS is created at the mitochondrial site at the same time. The capacity of mitochondria to remove ROS could be vastly different from that of produced ROS. The discrepancy between ROS elimination and creation causes ROS to be emitted outside of the mitochondria. The steady state ROS concentration is determined by the rate of ROS emission and generation by extra mitochondrial resources.[51]

Certain complexes improve antioxidant defence in cells. They chelate transition metals, preventing their free radicals from acting as catalysts. Transferrin and ferritin are iron-chelating proteins. Selenium and zinc are important antioxidants as well. Cell reinforcements can be either hydrophilic or lipophilic. Hydrophilic antioxidants respond to oxidants in cell cytosol and blood plasma. Lipophilic antioxidants protect cell membranes. Gluthione and ubiquinone are antioxidants found in the cells of various organisms' bodily fluid and tissues, while uric acid is eliminated.[52, 53]

## 1.6 Anti-Diabetic Activity

Inorganic salts of vanadium and zinc have been used to control glucose levels in blood plasma. It has been demonstrated that elements in their inorganic forms are poorly absorbed and require significant doses. With enhanced solubility and lipophilicity, vanadium complexes have proven to be less hazardous. There have been several vanadium compounds produced, all of which show insulin-mimetic characteristics. The activation of numerous major components of insulin signalling pathways has been revealed to be involved in the molecular mechanism responsible for vanadium compounds' insulin-like actions. In addition, higher zinc intake has been linked to a lower risk of type 2 diabetes in women.[54]

### 1.7 Review of the Ligands

#### 1.7.1 Heterocyclic Compounds

In the field of Schiff base metal complexes, the incorporation of the heterocyclic moiety serves as a noteworthy feature in drug discovery, elevating the pharmacological capabilities of heterocyclic nucleus to a new level. [55] Because of their inherent versatility and unique natural characteristics, heterocyclic Schiff base metal complexes have emerged as true pillars of medicinal chemistry. Heterocycles with nitrogen in their structure are abundant in nature and essential to life since their structural subunits are found in a wide

range of natural products, including vitamins, hormones, antibiotics, alkaloids, essential amino acids, and haemoglobin.[56, 57] The heterocyclic fragments have remarkable capacity to operate as biomimetics and active pharmacophores which contribute to their particular significance as the traditional components of numerous drugs.[58] Efforts are being made all around the world to find effective metal-based biologically active chemicals that could be used as antimicrobials. Among the various therapeutic approaches for eradicating these microbial hazards, the use of transition metal complexes such as metallodrugs has shown great promise for enzyme inhibition, interaction with intracellular biomolecules, improved lipophilicity, alteration of cell membrane functions, cell cycle arrest, and other applications.[59-61] Schiff base complexes containing to heterocyclic moieties such as pyrrole, pyridine, indole, benzimidazole and pyrazole have attracted a lot of attention as antibacterial, antifungal, and anticonvulsant drugs. The unique structures that the heterocyclic systems provide to such ligands and their metal complexes are related with the tremendous enthusiasm for the synthesis of heterocyclic Schiff base compounds.

### **1.7.1.1 Pyrrole**

Pyrrole is a five-membered heterocyclic aromatic organic molecule with the formula C<sub>4</sub>H<sub>4</sub>NH. It's a clear, colourless liquid that darkens quickly when exposed to air.. Porphobilinogen is a trisubstituted pyrrole that serves as a biosynthetic precursor to a variety of natural compounds, including heme. Pyrroles are found in a variety of macrocycles, such as heme porphyrins, bacteriochlorins, chlorophyll, and porphyrinogens.[62] Proline and hydroxyproline are the amino acids which contain pyrrole ring, a heterocyclic moiety in hydrogenated forms. Alkaloids, a wide class of alkaline organic nitrogen compounds generated by plants, contain these amino acids. Pyrrole is generally recognised as a pharmacologically active scaffold with a wide range of functions. More active compounds have resulted from the combination of different pharmacophores in a pyrrole ring structure. Pyrrole-containing analogues are thought to be a potential source of physiologically active

molecules with a wide range of beneficial qualities that can be found in a variety of natural products. The pyrrole ring signifies a valuable framework for developing novel therapeutic agents. [63]

Pyrrole subunit has diverse applications in therapeutically active compounds including fungicides, antibiotics, anti-inflammatory drugs, cholesterol reducing drugs, antitumor, anti-viral, anti-malarial, antitubercular, enzyme inhibiting and anticancer agents and many more. They are known to hinder reverse transcriptase [human immunodeficiency virus type 1 (HIV-1)] and cellular DNA polymerases protein kinases. Furthermore, they are also a constituent of polymers, indigoid dyes and of larger aromatic rings. Pyrroles are widely used as a catalyst in catalytic reactions for polymerization, corrosion inhibitor, preservative, resin solvent, terpenes, transition metal complex catalyst chemistry for uniform polymerization, luminescence chemistry, and spectrochemical analysis.. Furthermore, some of these compounds are useful intermediates in the synthesis of biologically important naturally occurring alkaloids and synthetic heterocyclic derivatives.[64]

#### Pyrrole-2-carboxaldehyde

Pyrrole-2-carboxaldehyde, also known as alpha-pyrrolaldehyde or 2-carboxaldehyde-pyrrole, belongs to the class of organic compounds known as arylaldehydes. Aryl-aldehydes are compounds containing an aldehyde group directly attached to an aromatic ring. Pyrrole-2-carboxaldehyde is an ethereal tasting compound. Pyrrole-2-carboxaldehyde is found, on average, in the highest concentration within beer. Pyrrole-2-carboxaldehyde has also been detected, but not quantified in, several different foods, such as evergreen blackberries (Rubus laciniatus), teas (Camellia sinensis), green tea, red tea, and robusta coffees (Coffea canephora). This could make 1H-pyrrole-2-carboxaldehyde a potential biomarker for the consumption of these foods.

### **1.7.1.2 Pyridine**

Pyridine is a basic six membered heterocyclic organic compound with the chemical formula C<sub>5</sub>H<sub>5</sub>N. Pyridine is an azaarene with a benzene core and a nitrogen atom in place of one of the -CH groups. It's a highly flammable, slightly alkaline, water-miscible liquid with an obnoxious fish-like odour. Pyridine is colourless, however it can appear yellow on older or in impure samples. Many useful compounds, such as agrochemicals, medicines, and vitamins, include the pyridine ring. Despite their industrial application, pyridine moieties can be found in a variety of natural compounds such as vitamins, coenzymes, and alkaloids, as well as in a variety of medications and pesticides. Pyridine moieties are frequently utilised in pharmaceuticals due to their basicity, water solubility, stability, and capacity to form hydrogen bonds, as well as their small molecular size. Because pyridine rings can operate as bioisosteres for amines, amides, heterocyclic rings with nitrogen atoms, and benzene rings, replacing them with pyridine moieties is essential in drug development.

Series of BACE1 inhibitors were recently synthesised using silico conformational structure-based drug design, and the pyridine moiety was discovered to play an essential role as a scaffold. The importance of pyridines in medicinal chemistry, as well as development of  $\beta$ -secretase inhibitors with pyridine scaffolds for Alzheimer's disease treatment was studied recently. When exposed to pyridine, it is generally inhaled and absorbed into the lungs and gastrointestinal tract, where it is either unaltered or metabolised. N-Methylpyridiniumhydroxide, which is produced by N-methyltransferases (e.g., pyridine N-methyltransferase), pyridine N-oxide, and 2-, 3-, and 4-hydroxypyridines, which are produced by monooxygenase, are the main products of pyridine metabolism. Pyridine is solely converted into N-methylpyridiniumhydroxide in humans.

Bacteria quickly breakdown pyridine to ammonia and carbon dioxide. Picoline, lutidine, chloropyridine, and aminopyridines breakdown more slowly than unsubstituted

pyridine rings, and a number of pyridine degraders have been reported to overproduce riboflavin in the presence of pyridine. Pyridine and other ionisable N-heterocyclic compounds interact with environmental surfaces (such as soils and sediments) through a multiple pH-dependent mechanisms, including partitioning to soil organic matter, cation exchange, and surface complexation. The bioavailability of pyridines for microbial degraders and other species is reduced as a result of such adsorption to surfaces, thus slowing degradation rates and reducing ecotoxicity.

### Pyridine-2-carbaldehyde

It is a heterocyclic aromatic aldehyde with chemical formula NC<sub>5</sub>H<sub>4</sub>CHO. It is also as called 2-formylpyridine. It is one of the three isomeric pyridinaldehydes. The other isomers are pyridine-3-carboxaldehyde and pyridine-4-carboxaldehyde.

Pyridine-2-carbaldehyde is an oily, colourless liquid with a strong odour. Impurities in older samples cause them to turn brown. In coordination chemistry and pharmacology, it acts as a precursor to other compounds of interest. Typically, pyridine aldehydes are made by oxidising hydroxymethyl- or methyl pyridines.

### 1.7.1.3 Indole

Indole is an aromatic heterocyclic organic compound with formula C<sub>8</sub>H<sub>7</sub>N. It has a bicyclic structure, consisting of a six-membered benzene ring fused to a five-membered pyrrole ring. Indole is widely distributed in the natural environment and can be produced by a variety of bacteria. Indole regulates many aspects of bacterial physiology including spore formation, plasmid stability, drug resistance, biofilm formation, and virulence as an intercellular signal molecule. A number of indole derivatives have significant cellular functions, including neurotransmitters such as serotonin.

### Indole-3-carboxaldehyde

Indole-3-carboxaldehyde also known as indole-3-aldehyde and 3-formylindole, is a metabolite of dietary L-tryptophan synthesised by human gastrointestinal bacteria, specifically Lactobacillus species. It is a biologically active metabolite that acts as a receptor agonist at the aryl hydrocarbon receptor in intestinal immune cells, stimulating the production of interleukin-22 and improving mucosal reactivity.

The reactivity of indole-3-carboxaldehyde is typical of aromatic aldehydes. It is oxidised easily to indole-3-carboxylic acid. In a Henry reaction, it condenses with nitro methane to form 3-nitrovinyl indole.

Indole-3-carboxaldehyde has antifungal properties, and it partially accounts for the protection from chytridiomycosis seen in amphibian species which carry Janthinobacterium lividum on their skin.

#### 1.7.2 2-(Methylthio)aniline

2-(Methylthio)aniline is a clear pale yellow liquid with molecular formula C<sub>7</sub>H<sub>9</sub>NS. It is also called as 2-Aminothioanisole. It used as important raw material and intermediate used in organic synthesis, pharmaceuticals and agrochemicals.

#### 1.8 Metallo-Elements under Investigation

#### **1.8.1** Co-ordination Chemistry of Copper

Copper is an element of IB group along with gold and silver. The most common oxidation state of copper is +2. The outer electronic configuration of copper in +2 state is  $3d^9$ .

Copper complexes are distorted often resulting in unequal bond length, angles and a large number of possible geometries. Jahn-Teller distortion is possible, when Cu<sup>+2</sup> ion is located in an octahedral or tetrahedral environment. The extent of Jahn –Teller distortion

affects the geometry of the complexes. All the octahedral copper complexes are distorted tetragonally.

Cu<sup>+2</sup> complexes have also been found to have distorted tetrahedral and trigonal bipyramidal structures. In a few situations, the symmetry is  $D_{3h}$ , while in most cases the structure is distorted. [65, 66] Waters et al investigated the absorption spectra of a number of copper (II) complexes.[67, 68] Almost all complexes were observed to be green or blue in colour. The interference of the charge transfer band in the visible region caused the complex to be brown or red in some situations. A normal octahedral complex is unlikely to form when the Cu(II) ion is subjected to Jahn Teller distortion. This is reflected strongly in the spectral and magnetic properties. Three transitions namely  $^2B_{1g} \rightarrow ^2A_{1g}$ ,  $^2B_{1g} \rightarrow ^2B_{2g}$  and  $^2B_{1g} \rightarrow ^2E_g$ . are predicted by the energy level diagram for ligand fields with  $D_{4h}$  symmetry. However, due to the overlap of these bands in some circumstances, only one band is seen. Regardless of stereochemistry, the magnetic moments of simple Cu(II) complexes are typically in the range of 1.8 - 2.20 BM.[69-71]

Copper (II) is found in a variety of polynuclear compounds that have magnetic anomalies. The magnetic moments of these compounds suggest a significant interaction between two copper atoms [72]. The magnetic moment will be reduced as a result, and the value will be temperature dependent. [73, 74] To interpret these magnetic anomalies, detailed research with copper (II) carboxylates were carried out [75]. Copper (II) can also be found in dimeric forms. Copper acetate, a dimer with bridging carboxylate groups, is a classic example of this kind. In the Cu (II) complexes of pthalocyanines, true square planar coordination is found, but in some square planar complexes, the molecules are stacked, resulting in a weak affinity between the Cu (II) and the central carbon atom of the neighbouring molecule.

### 1.8.2 Co-ordination Chemistry of Cobalt

Smaltite (CoAs<sub>2</sub>) and cobaltite (CoAs<sub>S</sub>) are the two most important cobalt minerals. This bluish-white metal is extremely inert. Cobalt has a variety of oxidation states, but the cobalt (II) and cobalt (III) complexes are the most stable. Because of the minor difference in ligand field stabilisation energy between octahedral and tetrahedral configurations, tetrahedral complexes of Co(II) are more prevalent than other transition metal ions. The ground state of the free Co(II) ion corresponds to <sup>4</sup>F. For the free ion, a further quartet state, <sup>4</sup>P of higher energy, is also feasible. Tetrahedral complexes are blue, but octahedral complexes are pale red or purple. For octahedral complexes, the permitted transitions are  ${}^4T_{1g(F)} \rightarrow {}^4T_{1g(P)}$ ,  ${}^4T_{1g(F)} \rightarrow {}^4A_{2g}$  and  ${}^4T_{1g(F)} \rightarrow {}^4T_{2g}$ . For tetrahedral complexes the permitted transitions are  ${}^4A_2 \rightarrow {}^4T_1$  (P),  ${}^4A_2 \rightarrow {}^4T_1$  (F) and  ${}^4A_2 \rightarrow {}^4T_2$ . Magnetic characteristics of octahedral and tetrahedral complexes are also different. The ground state of  ${}^4T_{1g}$  offers an unquenched orbital contribution to the magnetic moment for Co(II) high spin complexes. Co(II) octahedral complexes with low spin are uncommon. The electronic configuration in this situation is  $t_{2g}^{6}eg^{1}$  indicating the possibility of Jahn-Teller distortion. As a result, entirely octahedral low spin Co(II) complexes are uncommon, and these systems tend to lose ligands, resulting in low spin five or four coordinate complexes. Magnetic moments of Co(II) square planar complexes range from 2.2 to 2.7 BM. Five coordinate complexes will have either square pyramidal or trigonal bipyramidal stereochemistry. For both geometries high spin complexes with three unpaired electrons and low spin complexes with one unpaired electron are known. Co(III) forms a variety of complexes, the majority of which are octahedral.[76] The free cobalt (III) ion with the d<sup>6</sup> configuration has the lowest energy state <sup>5</sup>T<sub>2g</sub> in the presence of an octahedral field. However, the <sup>1</sup>A<sub>1g</sub> state, which originates from one of the free ion's high-energy singlet states, drops very rapidly. As a result, the majority of Co(III) octahedral complexes are diamagnetic and low spin. It is also been reported that some binuclear cobalt (IV) pthalocyanines can be synthesised.[77]

### 1.8.3 Co-ordination Chemistry of Nickel

The most common coordination numbers for Ni are 4, 5 and 6. These complexes have octahedral, trigonal bipyramidal, square pyramidal, square planar, and tetrahedral geometries.[78]

Nickel has the highest coordination number of six. The electronic absorption spectra of Ni(II) octahedral complexes are characterised by three transitions:  ${}^3A_{2g} \rightarrow {}^3T_{2g}$ ,  ${}^3A_{2g} \rightarrow {}^3T_{1g(F)}$ , and  ${}^3A_{2g} \rightarrow {}^3T_{1g(P)}$ , all of which are allowed transitions. Ni(II) octahedral complexes have two unpaired electrons and magnetic moments ranging from 2.9 to 3.4 BM, depending on the magnitude of orbital contribution. Ni(II) square pyramidal and trigonal bipyramidal five coordinate complexes with high spin and low spin magnetic moments have been observed.[79-81] The symmetry of a pure trigonal bipyramidal structure must be  $D_{3h}$ , however in many Ni(II) complexes, the symmetry drops to  $C_{3v}$ , as evidenced by the electronic spectra. The other five-coordinated complexes, which do not contain "tripod" ligands, have a trigonal bipyramidal stereochemistry. A few square pyramidal complexes are also possible.

Ni(II) tetrahedral complexes with stoichiometries [NiX<sub>4</sub>]  $^{2-}$ , [Ni X<sub>3</sub>L]<sup>-</sup>, [NiL<sub>2</sub>X<sub>2</sub>] and [Ni(L-L)<sub>2</sub>] (X = halogen, L-L bidendate ligand) are possible. Only the complexes [NiX<sub>4</sub>]  $^{2-}$  are expected to have perfect tetrahedral symmetry. In many cases, the dihedral angle is less than 90°, resulting in a geometry that is somewhere between tetrahedral and square planar. The degree of distortion will be reflected in the magnetic characteristics as tetrahedral complexes are paramagnetic and square planar complexes are diamagnetic. The ground state of tetrahedral Ni(II) complexes is  $^{3}T_{1(F)}$ , and the electronic absorption spectrum is determined by the transition  $^{3}T_{1(F)} \rightarrow ^{3}T_{1(P)}$ , which falls in the visible region . The magnetic moment of a perfect tetrahedral Ni (II) complex should be around 4.2 BM. The deviations from tetrahedral symmetry are widespread, resulting in a loss in magnetic moment. For

irregular tetrahedral complexes, magnetic moments in the range of 3.5 to 4 BM have been found. If the distortion is extreme, the magnetic moment can possibly drop to 3.0 BM. In the vast majority of four coordinate complexes, Ni (II) prefers square planar geometry. This is due to the fact that antibonding d orbital being unoccupied. However, in a tetrahedral form, antibonding orbital occupancy is unavoidable. Ni (II) square planar complexes are diamagnetic. Because of the potential involvement of these oxidation states in nickel-containing metalloenzymes, researchers are increasingly studying both Ni(I) and Ni(II) species.

## 1.8.4 Co-ordination Chemistry of Zinc

Zinc is an element that belongs to group 12 of the periodic table.  $Zn^{2+}$  ions have the electronic configuration [Ar]  $3d^{1o}$  in their compounds. As a result, its complexes, ZnO and zinc sulphide, ZnS (zinc blende), are symmetrical, with the oxide and sulphide ions tetrahedrally bonded to four zinc ions. Tetrahedral compounds, such as  $ZnCl_4^{2-}$ , are common. Metallo-enzymes like carbonic anhydrase include tetrahedrally coordinated zinc. The ion  $[Zn(H_2O)_6]^{2+}$ , which is formed when zinc salts are dissolved in water, is an example of a six-coordinate octahedral complex. Special organic ligands can impose five- and seven-coordination numbers. The Zn-ligand bonds in Zn(II) complexes are kinetically labile, meaning they swap with other ligands quickly. As a result, zinc ions are found in many catalytic centres of enzymes.

 $Zn^{2+}$  is classified as a class A acceptor by Ahrland, Chatt, and Davies, which means it forms stronger complexes with first-row donor atoms like oxygen or nitrogen than with second-row donor atoms like sulphur or phosphorus.  $Zn^{2+}$  is a hard acid according to HSAB theory.

### 1.8.5 Co-ordination Chemistry of Iron

Iron is a chemical element with symbol Fe and atomic number 26. It is a metal that belongs to the first transition series and group 8 of the periodic table. It's outer most electronic configuration is [Ar] 3d<sup>6</sup> 4s<sup>2</sup>. The most common oxidation states of iron are +2 and +3. Iron shares many properties of other transition metals, including the other group 8 elements, ruthenium and osmium. Iron forms compounds in a wide range of oxidation states, +2 to +7. Iron also forms many coordination compounds; some of them, such as ferrocene, ferrioxalate, and Prussian blue, have substantial industrial, medical, or research applications. Electron acceptor ligands, such as carbon monoxide, isocyanide, and phosphorus donors, stabilise low-oxidation state iron complexes. The most frequent coordination geometry found in iron compounds is octahedral, while other options include tetrahedral, trigonal bipyramidal, and square pyramidal.

Although there are cases of four-, five-, and even eight-coordination, most iron(II) complexes have an octahedral shape. In an octahedral crystal field,  ${}^5D_2$  ground state of the iron(II) complex splits into  ${}^5T_{2g}$  and  ${}^5E_g$  states. Magnetic moments of high-spin octahedral iron(II) complexes are around 5.2 BM. The broad  ${}^5T_{2g} \rightarrow {}^5E_g$  absorption in the visible/near infrared is the only spin-allowed d-d transition. Low-spin iron(II) complexes are formed when high-field ligands, such as aromatic nitrogen donors, are used, and their spectra are generally dominated by a strong metal to ligand charge-transfer band. Due to a temperature-independent paramagnetic contribution, their magnetic moments are typically around 1 BM.

Due to orbital contributions, tetrahedral iron(II) complexes have magnetic moments that are larger than predicted for four unpaired electrons. Magnetic moments are usually in the range of 5.0–5.2 BM when the  $^5E \rightarrow ^5T_2$  transition occurs at about 4000 cm<sup>-1</sup>. Phosphocyanines and porphyrins are examples of tetradentate macrocycles that form square-planar iron(II) complexes with an intermediate spin (S = 1) ground state. Additional

axial ligands are easily added to these complexes, resulting in six-coordinate complexes with low spin. The majority of iron(III) complexes are octahedral in shape. The d<sup>5</sup> centre is frequently high-spin in simple complexes, such as red [Fe(acac)<sub>3</sub>], with magnetic moments close to the predicted 5.9 BM. Iron(III) has a low affinity for amine ligands, but not for oxygen donors, which results in the formation of bridged species with antiferromagnetic coupling between the iron atoms.[82]

#### 1.9 Review of Literature

This chapter presents the findings of numerous researchers in the same field of application and synthesis of metal complexes using various methods, as well as their distinct features.

Fatemeh Dashi Rahmatabadi et al., [83] have synthesized tripodal heptadentate Schiff base ligand from pyrrole-2-carboxaldehyde and tris(2-aminoethyl)amine (tren) and its complexes with Cd (II), Co (II), Mn (II) and Ni(II) metal ions. The synthesised compounds were identified by IR, UV-Vis, <sup>1</sup>H-NMR, <sup>13</sup>C- NMR, TGA and elemental analysis. These complexes showed greater anti-bacterial property than the ligand. Co (II) complex showed best activity against *Bascillus cercies* and Mn (II) complex showed weak activity against *E.coli*.

Subarani et al., [84] have studied the anti-bacterial, anti-fungal and super oxidase dismutase activities of newly synthesized Schiff base metal complexes in which the Schiff base was derived from pyrrole-2-carboxaldehyde and L-glycine. The ligand and metal complexes were characterised by XRD, SEM and EDAX. From the results they concluded that the copper complex exhibited higher anti-microbial activity than the ligand and other metal complexes.

Bibhesh K.Singh et al., [85] have prepared a new symmetrical Schiff base N, N' bis(pyrrole-2-carboxaldehye) ethylene diammine and its Mn(II), Co(II), Ni(II) and Cu(II) complexes. These complexes were characterised by IR, UV-Vis, <sup>1</sup>H-NMR, EPR, Mass, Magnetic and electrochemical studies. These metal complexes were found to possess octahedral geometry. The cell parameters of the metal complexes were measured by powder X-ray diffraction method. The bio efficacy of the complexes were found to be greater than that of the ligand.

Sulekh Chandra et al., [86] have prepared Ni (II) and Cu (II) complexes of Schiff base thiosemicarbazones and semicarbazones derived from pyrrole-2-carboxaldehyde. These complexes were characterized by elemental analysis, molar conductance measurement, IR, electronic and EPR spectral studies . EPR spectra of the Cu complexes measure the exchange interaction which is less than 4. The geometry of Ni (II) complexes were found to be octahedral and Cu (II) complexes were found to be tetragonal.

Mangamamba et al., [87] reported the synthesis of new Schiff bases and their metal complexes. They were studied by IR, UV-Vis, TGA and magnetic susceptibility measurements. These metal complexes were screened for their toxicity against the chosen fungal and bacterial organisms. Here, Vo (II) complexes were found to be more active when compared to the activity of the commercial standard.

Emad Yousif et al., [88] synthesised a total of five new metal complexes of 2N-salicylidene-5-(p-nitro phenyl)-1, 3, 4-thiadiazole (HL) with metal ions Vo (II), Co(II), Rh(II), Pd (II) and Au(III). The obtained complexes were characterized quantitatively and qualitatively by using microelemental analysis, FT-IR spectroscopy, UV-Vis spectroscopy, mass spectroscopy, NMR spectroscopy, magnetic susceptibility and conductivity measurements. From these studies the metal complexes were found to have a monomeric structure and it was 4 co-ordinated with square planar geometry except Vo (II) and Co (II)

complexes which possessed square pyramidal and tetrahedral geometry respectively. *In vitro* anti-bacterial screening activity revealed that the complexes showed moderate activity against bacterial strain.

Jisha et al., [89] have came out with Schiff base ligand from furan -3-carboxaldehyde and 3-amino pyridine and its metal complexes. The synthesized ligand and its complexes were characterized by elemental analysis, molar conductance, magnetic moment, <sup>1</sup>H-NMR, IR, UV-Vis and SEM. The analytical data revealed that the metal to ligand ratio was 1:2. The molar conductance data revealed that all the complexes were non-electrolytes. The metal complexes were found to have greater anti-microbial activity than the ligand.

Bibhesh K.Singh et al., [90] have synthesised a new Schiff base from 2-aminophenol and pyrrole-2-carboxaldehyde and its Zn (II), Cd (II), Sn (II) and Pb (II) complexes. They were characterised by physiochemical studies and spectral studies which indicated deprotonation and co-ordination of phenolic oxygen, azomethine nitrogen, pyrrole nitrogen and anions with metal ions. The presence of water molecules in the lattice were confirmed by TG/DTA studies. Kinetics and thermodynamics parameters were computed from the thermal data using Coats and Red fern method which revealed first order kinetics. The antibacterial potentials of the ligand and its metal complexes were examined *in vitro* against the *E-coli* and *S-auerus*. The structure of the complexes was found to be tetrahedral and was confirmed by MM2 calculation.

Subarani et al., [91] have prepared Schiff base ligand by condensation of pyrrole-2-carboxaldehyde with alanine and its metal complexes. The synthesised ligand and complexes were described by spectroscopic studies, powder XRD, SEM and EDAX. The bio efficacies of the ligand and metal complexes were studied. Antioxidant activities of the complexes were found to be higher than that of the ligand. The DNA cleavage activities of

the ligand and the metal complexes were studied and found that Zn (II) complex showed effective cleavage toward pUC 18 DNA.

Charles et al., [92] have come out with a new N-((1 H-pyrrol-2-yl)methylene)-4-methyl aniline (PMM) Schiff base ligand by condensing pyrrole-2-carboxaldehyde with p-toluidine. Using the above synthesized ligand they prepared nine metal complexes and characterized them on the basis of spectral analysis. The anti-bacterial and anti-fungal activities of the ligand and metal complexes have been screened for various pathogenic bacteria and fungi. From the data, it was confirmed that iron, nickel, copper and zinc complexes showed anti-bacterial activity whereas other metal complexes did not show.

Minu G. Bhowon et al., [93] have prepared Schiff base ruthenium (II) complexes using pyrrole-2-carboxaldehyde and various imines and 2-amino phenol. The structures of these complexes were confirmed using spectral and analytical studies. These Ru (II) metal complexes were found to be more effective catalysts for the oxidation of primary alcohol in the presence of N-methyl morpholine-N-oxide as oxidant.

Chaudhary [94] prepared copper, cobalt and zinc metal complexes using Schiff base as a ligand which were derived from pyrrole-2-carboxaldehyde and amoxicillin trihydrate in aqueous methanol solution in weak acidic medium. The prepared metal complexes and ligand were characterized by IR, UV-Vis, NMR, TOR mass and elemental analysis. It was confirmed that metal ions were coordinated to Schiff base ligand through nitrogen and sulphur donor atoms. The anti-bacterial evaluation against various pathogenic bacteria was done by measuring zone of inhibition. The metal complexes and ligand were found to possess higher bacterial activities than the control drug. Zinc complex had strong activity against *E. coli* and *B. subtilis* and copper complex was more active against *S. aureus*.

Charles et al., [95] have synthesized Schiff base ligands namely N-((IH-pyrrol-2-yl)methyleneaniline(1), N-((1H-pyrrol-2-yl)methyleneethylaniline(2), N-((1H-pyrrol-2-yl)methylene)-4methoxyaniline(3) and N-((1H-pyrrol-2-yl)methylene)-3, 5dimethylaniline (4). These four Schiff base ligands were characterized using <sup>1</sup>H NMR and IR studies. The corrosion inhibiting capacity of the prepared products were evaluated using weight loss method in a 0.1 M HCl solution for mild steel. They identified that tridentate Schiff base was found to have more corrosion inhibiting capacity.

Ahamed et al., [96] have prepared three Schiff base ligands by refluxing ethanolic solution of benzoyl acetone with ethylene diamine, o-phenylenediamine and 1, 6 -hexane diamine and fourth Schiff base ligand by condensing o-phenylenediamine with benzoin. These four ligands formed coordination complexes with different metal ions in1:1metal ligand ratio. The newly prepared products were characterized using techniques like elemental analysis, molar conductivity, IR spectra, electronic spectra, thermal analysis and magnetic susceptibility measurements. The analysis confirmed the formation of mono and bi-nuclear metal complexes.

Asha et al., [97] have synthesized N, O type Schiff base ligand by condensing 6-acetyl-7-hydroxy-4, 8-dimethyl-2H-chromen-2-one with o-phenylenediamine in alcoholic medium. Using this ligand, they prepared five new metal complexes of Co (II), Cu (II), Zn (II), Cd (II) and Ni (II) ions. The newly prepared products were characterized quantitatively and qualitatively by using micro elemental analysis, FT-IR, <sup>1</sup>H NMR, Mass, UV-Vis, TG/DTG, ESR, Magnetic susceptibility and molar conductance data. These studies confirmed that the metal complexes were found to possess octahedral geometry. The antimicrobial activity of these complexes were screened using *in vitro* diffusion method.

The results revealed that due to the presence of metal ions, most of the synthesized complexes exhibited good biological activities.

Sadu Suryakant et al., [98] have synthesized a new Schiff base by refluxing salicylaldehyde and 3-amino-5-bromobenzene-2-carboxamide. This Schiff base formed coordination complexes to six different metal ions namely Co(II), Ni(II), Cu(II), Hg(II), Cd(II) and Zn(II). These complexes were characterised by various studies *viz*. IR, UV-Vis, <sup>1</sup>H NMR, ESR and mass spectra. The molar conductivity measurements indicated all the complexes were non-electrolytes in nature. The tentative structure of the synthesised Cu (II), Ni (II) and Co (II) complexes was octahedral and that of Cd (II), Zn (II) and Hg (II) was tetrahedral. These complexes were found to possess better anti-microbial activity than the ligand.

Gangadhar et al., [99] have synthesised series of metal complexes using cobalt (II), nickel (II) and copper (II) ions with a newly derived biologically active ligand. This ligand was obtained by condensing 2-amino-4-phenyl-1, 3-thiazole with 8-formyl-7-hydroxy-4-methyl coumarin. The probable structure of the synthesized complexes was confirmed on the basis of analytical and spectroscopic data. Electrochemical study on the copper complex revealed the degree of reversibility of the one electron transfer reaction and its quasi-reversible character. The geometry of these complexes were found to be octahedral. From DNA cleavage study it was concluded that those compounds inhibited the growth of the pathogenic organism by cleaving the genome.

Kiran Singh et al., [100] have prepared two new heterocyclic Schiff bases namely 4-amino-5-mercapto-3-H/propyl-1, 2, 4-triazole and 5-nitrofurfuraldehyde. Using these ligands, they prepared transition metal complexes and characterized them by elemental

analysis, spectral (UV-Vis, IR, <sup>1</sup>H NMR, fluorescence, and ESR )studies, thermal techniques and magnetic moment measurements. The heterocyclic Schiff bases acted as bidentate ligands and coordinated to metal ions through nitrogen atom of azomethine linkage and sulphur atom of the thiol group. The structure of the metal complexes was found to be octahedral for Co (II), Ni (II) and Zn (II) ions, and it was square planar for Cu (II) ion. No signal at half field was observed in ESR spectrum of copper (II) complex which showed the absence of dimeric form. The anti-microbial studies suggested that the Schiff bases were found to be biologically active and their metal complexes showed enhanced anti-microbial activity against microbial strains in comparison to the free ligand.

Anant Prakash et al., [101] have come out with new complexes of Co (II), Ni (II) and Cu (II) with Schiff bases obtained by condensing pyridine-2-carboxaldehye with L-histidine and L-valine. These new products were confirmed by various physico-chemical techniques. These complexes were found to be 1:2 (M: L) ratio. The spectral studies suggested octahedral geometry for the metal complexes. TG studies showed the absence of water molecules in all the complexes.

Mini et al., [102]synthesised five new complexes of Mn (II), Co (II), Cu (II), Zn (II) and Ni (II) with the Schiff base{2-{furan-2-yl methylene amino}pyridine -3-ol}and characterized them by elemental analyses, FT-IR, <sup>1</sup>H NMR, electronic, ESR, mass spectra, magnetic susceptibility and electrolytic conductance. It was reported that the Schiff base acted as uni-anionic bidentate ligand with all the metal ions. The M:L ratio of the formed complexes was 1:1 except in the case of Ni where it was 1:2. The anti-microbial activity of the Schiff base and its complexes were studied. The metal complexes were found to possess better anti-microbial activity than the ligand .The Mn(II) complex showed noticeable antioxidant activity when compared to the standard.

Chen.et al., [103] have synthesised an ambidentate Schiff base ligand by condensing pyridine-2-carboxaldehyde with 4-[(E)-2-phenyldiazenyl]aniline. Hydrothermal reaction of the ligand with silver nitrate and Cd(ClO<sub>4</sub>)<sub>2</sub>.6H<sub>2</sub>O afforded AgLNO<sub>3</sub>.and [CdL<sub>2</sub>(H<sub>2</sub>O)ClO<sub>4</sub>]ClO<sub>4</sub> complexes respectively. These complexes were characterised by elemental analysis and IR spectroscopy. Both the complexes were found to be mononuclear which was confirmed by single crystal XRD analysis. The silver complex was found to have distorted trigonal geometry whereas Cd complex was in a distorted octahedral geometry with an equatorial plane composed of four nitrogen atoms from two bidentate Schiff base ligands and the apical position occupied by one oxygen atom from aqua ligand and one oxygen atom from perchlorate.

Selma Bal et al., [104] have investigated on two novel Schiff base ligands (E)-N, N'-bis (pyridin-2-ylmethylene)cyclohexane-1, 4-diamine and (E)-N, N'-bis(pyridine-2-ylmethylene)benzene-1, 4-diamine by condensing 2-pyridine carboxaldehyde with 1, 4-diaminobenzene and trans1, 4-diaminocyclohexane. Characterisation of the synthesised products was carried out by analytical, spectroscopic and thermal methods. The catalytic activity of the complexes was found to be high towards oxidation of styrene and low towards oxidation of cyclohexane. Thermal studies revealed that except copper complex, all other complexes were more resistant to temperature. This indicated their chance to be used as catalyst towards chemical reactions carried out at high temperatures.

Mohammed Habibi et al., [105] worked on the synthesis of a tridentate Schiff base ligand from 2-pyridine carboxaldehyde and 4-nitro-o-phenylenediamine. This ligand was coordinated to Ni(II) metal ions and the coordination complexes were characterised by IR and NMR spectroscopies together with elemental analysis. In addition, optimized geometries, the nature of bond orbital analysis, assignment of the IR bands and NMR

chemical shifts of the synthesised compounds were computed by using DFT studies. In the optimized geometry of the ligand, aromatic rings were not found in the same plane. But the nickel complex was in square planar geometry. The deprotonated Schiff base acted as a N<sub>3</sub> tridentate ligand. The chloro ligand occupied another coordination position of the complex. The DFT- calculated vibrational wave numbers and NMR chemical shifts were in agreement with the experimental values, confirming correctness of the optimized geometries for the ligand and Ni(II) complex.

Omyma Ali et al., [106] have synthesised 2-[(pyridine-2-ylmethylidene)amino]-6-aminopyridine by condensing 2-pyridine carboxaldehyde and 2, 6-diaminopyridine in 1:1 ratio. The ligand and its complexes were characterized by different physico-chemical studies with analytical and spectroscopic tools. These studies confirmed the geometry of the complexes. Vibrational spectra indicated the coordination of ligand to metal ions through its pyridyl and azomethine nitrogen atoms. The TG/DTA studies proved the presence of water molecules in all complexes. The prepared ligand and its complexes exhibited intraligand  $(\pi$ - $\pi$ \*) fluorescence and could potentially serve as photoactive materials. Decomposition of H<sub>2</sub>O<sub>2</sub> was catalysed by this complex measured anti-bacterial activities of the ligand and the complexes confirmed that the complexes possessed better activity than the ligand.

Narendra Kumar Chaudhary et al., [107] made a novel Schiff base of type HL by mixing amoxicillin trihydrate and nicotinaldehyde. This ligand was used to prepare metal complexes of Co (II), Ni (II), Cu (II) and Zn (II) ions. These newly prepared products were characterised and investigated by physical and spectral techniques. Thermal techniques were used to gain better insight into the thermal stability and kinetic properties of the complexes. The low molar conductivity values implied that all the prepared complexes were non-electrolytes. The powder XRD pattern revealed triclinic crystal system for copper

complex and amorphous nature for all other complexes. The EPR study recommended tetrahedral geometry for the copper complex. The geometry of all the complexes were confirmed by MM force field calculation through Argus lab 4.01 software program. The *in vitro* anti-bacterial activities of the compounds were screened against four bacterial pathogens namely *E.coli*, *P.vulgaris*, *K.pneumoniae* and *S.aureus* and the compounds were found to possess better activity than parent drug and control drug.

Eliene Leundro de Aranjo et al., [108] have synthesised Schiff bases from the biopolymer chitosan and various substituted salicylaldehyde. These Schiff bases were used as ligands for formation of transition metal complexes in 1:1.5 mol ratio. The ligands were characterised by NMR, FT-IR which confirmed the substitution of various substituents from 43.7% to 78.7%. Complexes were characterised by FT-IR, electronic spectra and XPRD. Electronic spectral values confirmed square planar geometry for the complexes. Thermal techniques showed the loss of water molecules and decomposition with characteristic events for ligand and complexes. Compared to chitosan, Schiff base ligands showed low thermal stability and crystallinity. Surface morphologies were analysed with SEM-EDAX. Cell viability studies revealed that the Zn (II) complexes were most cytotoxic.

Kiran Singh et al., [109] have condensed 4-amino-3-mercapto-6-methyl-5-oxo-1, 2, 4-triazine with 2-acetyl pyridine. This product was coordinated to cobalt (II), nickel (II), copper (II) and zinc (II) metal ions and the resulting complexes were characterised by elemental analysis, conductivity measurements, IR, UV-Vis, NMR spectral data, magnetic and thermo gravimetric analyses. All the complexes were found to exist in polymeric state which was confirmed by insolubility in water and other organic solvents and infusibility at higher temperature. Except copper complex, all other complexes were found to be octahedral whereas copper complex was square planar. These prepared compounds were

screened against 3 Gram positive bacteria and 2 Gram negative bacteria. All the complexes were found to possess more pronounced effect on the microbes than the ligand.

T.B.S.A. Ravoof et al., [110] prepared metal complexes by mixing the individual metal acetates with the Schiff bases. Compounds were described by different physicochemical techniques and spectral approaches. The configuration of six-coordinate complexes with tridentate NNS ligand was shown by magnetic and spectroscopic studies. The molar conductivity ranged from 6.49 to 12.18 Ohm<sup>-1</sup> cm<sup>2</sup> mol<sup>-1</sup>. The azomethine frequency in the IR spectra ranged between 1584 and 1632 cm<sup>-1</sup>. Electronic spectra revealed peaks at 275-360 nm (n-  $\pi$ \*) and 400-440 nm (LMCT). Copper complexes had magnetic moments in the range of 1.65-1.98 BM, while nickel complexes had magnetic moments in the range of 2.82-3.02 BM. The octahedral structure of all three compounds was distorted. Antimicrobial agents frequently form complexes with transition metal ions.

Sivasankaran Nair et al., [111] have investigated Co(II), Ni(II), Cu(II), and Zn(II) 1:2 complexes with the Schiff base ligand Indal-4- AAP which is produced from indole-3-carboxaldehyde and 4-aminoantipyrine. Elemental analyses, mass, IR, electronic spectra, magnetic moment, molar conductance, and cyclic voltammetry were used to characterise Indal-4- AAP. [ML<sub>2</sub>Cl<sub>2</sub>] was discovered to be the generic formula for the complexes (M = Co(II), Ni(II), Cu(II), and Zn(II)). The co-ordination sites of the Schiff base ligand were the azomethine nitrogen and carbonyl oxygen atoms, according to the IR measurements. The electronic spectral and magnetic measurement data indicate that the complexes exhibit octahedral geometry around the metal centre. The *in vitro* biological screening of the synthesized compounds against several microbial species suggested that the metal complexes were more biologically active than the ligand. The DNA cleavage activity of the ligand and its complexes was assayed on pUC18 DNA using gel

electrophoresis. The result shows that Ni (II), Cu (II), and Zn (II) complexes had completely cleaved the DNA.

Quraishi and Sardar [112] have prepared three organic compounds namely 5-mercapto-3-butyl-4-salicylidine-l, 2, 4-triazole(MBST), 5-mercapto-3-butyl4-enzilidineiminio-l, 2, 4-triazole (MBBT) and 5-mercapto-3-butyl-4-cinnamylidineimino-l, 2, 4-triazole(MBCT) and explored their corrosion inhibition capacity by weight loss and potentiodynamic polarization techniques on MS in IN HCl and IN H<sub>2</sub>SO<sub>4</sub> Temperature, concentration, and immersion time all had an effect on inhibition efficiency. Temkin's adsorption isotherm was found to govern the adsorption of these compounds on the steel surface for both acids. The results of potentiodynamic polarisation revealed that the substances investigated are mixed type inhibitors.

Desai et al. [113] investigated seven Schiff bases as corrosion inhibitors for MS in HCl solutions by weight loss and electrochemical methods. According to polarization data, all these compounds act as cathodic inhibitors.

E.M. El-Sayed et al [114] have studied the adsorption of methyl orange dye onto cross-linked Chitosan derivate Schiff bases obtained from the coupling of Chitosan with 1-vinyl 2- pyrrolidone [Schiff base (I)] and 4-amino acetanilide (Schiff base (II)) in aqueous solutions.. FT-IR and thermal gravimetric analyses were used to describe the structure of the newly synthesised Schiff bases. A batch experiment was carried out to investigate the adsorption of Methyl orange dye from aqueous solutions utilising novel Chitosan Schiff bases (I) and (II) in comparison to cross-linked Chitosan. On dye adsorption, the effects of contact time, initial dye concentration, temperature, system pH, agitation speed, and adsorbent dosage were studied. The maximum percent dye removal was achieved at pH 7 (pH 8 in the case of Schiff base (I)), temperature 80°C, 250 rpm, and contact duration 70 minutes, according to the data. Langmuir and Freundlich isotherm models were used to

examine the adsorption equilibrium data. The Langmuir model fully describes the equilibrium information. According to the experimental kinetics data, the kinetics of the removal of methyl orange dye using the prepared sorbents followed a pseudo-first-order model.

Gutha Yuvaraja et al., [115] developed a novel, eco-friendly aminated chitosan Schiff's base (ACSSB@ZnO) and utilized to remove MO from aqueous environment. Batch process was used to investigate the effects of many significant parameters such as pH (3-11), adsorbent dose (0.1-0.6 g), contact time (0-120 min), and temperature (303-323 K). The pseudo-second-order model was used to depict the kinetic data, and the isotherms fit well with the Langmuir isotherm model. At 323 K, the maximum sorption capacity of ACSSB@ZnO was found to be 111.11 mg/g. The MO adsorption method was endothermic, as evidenced by positive enthalpy and entropy values. Negative Gibbs free energy values indicated that the adsorption mechanism was spontaneous. Furthermore, reusability tests revealed that it may be regenerated using NaOH as an effluent.

#### 1.10 Scope and Objectives of the Present Work

Schiff base ligands have been extensively studied in recent years, due to their biological importance. The chelating ability, ready accessibility and pharmacological properties such as analgesic, antipyretic, anticancerous, bacteriocidal, fungicidal, antidiabetic, antioxidant activities have raised the importance of Schiff base ligands. According to current medical research, drug resistance has become a major issue in the treatment of many infectious diseases caused by bacteria, viruses, and other pathogens in recent years. Despite of availability of various chemotherapeutic agents on the market, pathogenic bacteria develop resistance to these drugs, posing a global threat to medical science. Hence, still there is a necessity to synthesize new novel chemotherapeutic agents which will be more effective and safer than existing agents. A review of literature on Schiff

base ligands and its metal complexes reveals that only a few studies have been made on Schiff base ligands derived from heterocyclic aldehydes and (2-methylthio)aniline and their metal complexes. In view of these factors, we have synthesized the transition metal complexes of some new Schiff base ligands and studied their physic-chemical and biological properties.

The present research work embodied in this thesis mainly was attempted with a view to synthesize novel Schiff base ligands and their metal complexes containing heterocyclic moieties. Due to its strong chelating capacity and various biological functions, the heterocyclic nucleus has acquired prominence in medicinal chemistry. In highlighting this point, the objectives of the current work are as follows:

- ❖ To synthesize three new Schiff base ligands having N, S donor atoms.
  - > 2-(methylsulfanyl)–N–(1H-pyrrol-2-ylmethylidene)aniline MPMA from pyrrole-2-carboxaldehyde and (2-methylthio)aniline.
  - ➤ (*E*)-2-(methylthio)-N-(pyridin-2-ylmethylene)aniline MTPMA from pridine-2-carboxaldehyde and (2-methylthio)aniline.
  - > (Z)-N-(1H-indol-3-yl)methylene-2-(methylthio) aniline IMMA from indole 3-carboxaldehyde and (2-methylthio)aniline.
- ❖ To synthesize coordination complexes with transition metal ions like iron (III), cobalt (II), nickel (II), copper (II) and zinc (II) using synthesized ligands.
- ❖ To characterise the ligands and their complexes by using physic-chemical techniques like molar conductance, chemical analysis. elemental analysis, magnetic susceptibility, ¹H NMR, FT- IR, UV-Visible, EPR, mass, thermal decomposition studies and X-ray diffraction measurements.

- ❖ To study the redox behaviour of certain metal complexes by using cyclic voltammetry
- ❖ To study antimicrobial activities of the ligands and their metal complexes against human pathogenic bacteria and fungi by agar disc diffusion method.
- ❖ To evaluate antioxidant activities of the ligands and their metal complexes.
- ❖ To evaluate the antidiabetic activities of the ligands and their metal complexes by inhibiting carbohydrate hydrolysing enzymes.
- ❖ To study the anticorrosion properties of the Schiff base ligands by weight loss method.
- ❖ To study the dye adsorbent properties of the Schiff base ligands towards malachite green.

### REFERENCES

- 1. U.I.Singh, R.K.B.Singh, W.R.Devi and Ch.B.Singh, *J. Chem. Pharm.*, 2012, **4(2)**, 1130-1135.
- 2. Z.H. Abd El-Wahab and M.R. El-Sarrag, *Spectrochim. Acta A Mol. Biomol. Spectrosc.*, 2004, **60(1-2)** 271-277.
- 3. F.A Cotton and G. Wilkinson, "Advanced Inorganic Chemistry", 1972, **3<sup>rd</sup>** Edn. Wiley Eastern.
- 4. J. Chakraborty and R.N.Patel, *J. Chem. Soc.*, 1996, **73** (April-May), 191-193.
- 5. J.Ribas, M. Monfort, C. Diaz, C. Bastos, C. Mer and X. Solans, *Inorg. Chem.*, 1995, **34(20)** 4986–4990.
- 6. D.B.C.O. Rodriguez, N.A.Bailey, D.E Fenton and Q.Y.He, *J. Chem. Soc., Dalton Trans.*, 1997, (2) 161-166.
- 7. A.Mukherjee, R. Raghunathan, M.K. Saha, M. Nethaji, S. Ramasesha and A.R. Chakroborty, *Chem. Eur. J.*, 2005, **11(10)**, 3087-3096.
- 8. R. Klement, F. Stock, H. Elias, H. Paulus, P. Pelikan, M. Valko and M. Muzur, *Polyhedron*, 1999, **18**, 3617-3628.
- 9. D.X. West, S.B. Padhye and P.B. Sonawane, *Struct-Bond.*, 1991, **76**, 1-50.
- 10. A. Cukurovali, I. Yilmaz, H.Ozmen and M.Ahmedzade, *Trans. Met. Chem.*, 2002, **27**, 171-177.
- 11. K.I.Ansari, J.D.Grant, S.Kasiri, G.Woldemeriam, B.Shrestha, and S.S.Mandal, *J.I norg. Bio Chem.*, 2009, **103(5)**, 818-826.
- 12. P.G. Cozzi, Chem. Soc. Rev., 2004, **33(7)**, 410-422.
- (a) S.K.Tadavi, A.A.Yadav and R.S.Bendre, *J. Mol. Struc.*, 2018, 1152, 223-231.
   (b) N.M. Abdul Khader, J.A. Xavier and A. Ramu, *Mater. Today: Proc.*, 2018, 5(10) 22200-22214.
- 14. M. Köse, G. Ceyhan, M. Tümer, I. Demirtas, I. Gönül, and V. McKee, *Spectrochim. Acta A*, 2015, **137**, 477-485.
- 15. S. Dayagi and Y. Degani, in 'The Chemistry of the Carbon-Nitrogen Double Bond', ed S. Patai, Wiley-Interscience, New York, 1970, **71.**

- 16. M. Calligaris and L.Randccio in *'Comprehensive coordination Chemistry'*, eds. G.Wilkinson, R.D. Gillard and J.A.Mccleverty Pergaman, Oxford, 1987, **2**(20), 1.
- 17. Ekk Sinn, *Inorg. Chem.*, 1976, **15(2)**, 369-375.
- 18. V. Reddy, N. Patil, T. Reddy and S. D. AngadiI, *E-Journal of Chemistry*, 2008, **5(3)**, 529-538.
- 19. W.J. Geary, Coord. Chem. Rev., 1972, 1, 81-122.
- 20. D. Biswal, N. R. Pramanik, S. Chakrabarti, M. G. B. Drew, B. Sarkar, M. R. Maurya, S. K. Mukherjee and P. Chowdhury, *New J. Chem.*, 2017, **41**, 4116-4137.
- 21. P. Roy, A. Sau Mondal, A. K. Pramanik and T. K. Mondal, *J. Organomet. Chem.*, 2017, **828**, 1-9.
- 22. A.P. Hatfield and C.W. Inmen, *J. Inorg. Nucl. Chem.*, 1969, **31**, 1376-1380.
- 23. K.H. Thompson, J. Chiles, V.G. Yuen, J. Tse, J.H. McNeill and C. Orvig, *J. Inorg. Biochem.*, 2004, **98**, 683-686.
- 24. J. P. Costes, F. Dahan and A. Dupuis, *Inorg. Chem.*, 2000, **39**, 165-168.
- 25. K. Das, G. W. Woyessa, A. Datta, B. B. Beyene, S. Goswami, E. Garribba, A. Frontera and C.Sinha, *J. Mol. Struct.*, 2018, **1173**, 462-468.
- 26. R.Boca, Y. Fukuda, M. Gembicky, R. Herchel, R. Jarosciak, W. Linert, F. Renz, and J. Yuzurihara, *Chem. Phys. Lett.*, 2000, **325**, 411-419.
- 27. T. Mukherjee, J. C. Pessoa, A. Kumar and A. R. Sarkar, *Inorg. Chem.*, 2011, **50** (**10**), 4349-4361.
- 28. S. Sarkar, and K. Dey, *Spectrochim. Acta A Mol. Biomol. Spectrosc.*, 2005, **62(1-3)**, 383-393.
- 29. N.Raman, A.Kulandaisamy, A.Shunmugasundaram, and K.Jeya Subramanian, *Transition Met. Chem*, 2001, **26(1)**, 131-135.
- 30. M. Nath and R Yadov, *Bull Chem.Soc. Jpn.*, 1998, **71(6)**, 1355-1362.
- 31. N. Sari, S. Arslan, E. Logoglu and I. Sakiyan, *Gazi Univ. J. Sci.*, 2003, **16(2)**, 283-288.
- 32. F.D. Karia and P. H. Parsania, *Asian J. Chem.*, 1999, **11**(3), 991-995.

- 33. P.G. More, R.B. Bhalvankar and S.C. Pattar, *J. Indian Chem. Soc.*, 2001, **78(9)**, 474-475.
- 34. M. Amir, S.M. Hasan and A. Wadood, *Orient. J. Chem.*, 2002, **18(2)**, 351-353.
- 35. S.K.Sridhar, M.Saravanan and A.Ramesh, Eur. J.Med.Chem., 2001, **36** (**7-8**), 615-625.
- 36. A. Halve and A. Goyal, *Orient. J. Chem.*, 1996, **12**(1), 87-92.
- 37. P. Mazza, M. Orcesi, C. Pelizzi, G. Pelizzi, G. Predieri and F.Zani, *J. Inorg. Biochem.*, 1992, **48(4)**, 251-270.
- 38. S.K. Sridhar, S.N. Pandeya, J.P. Stables and A. Ramesh, *Eur.J. Pharm. Sci.*, 2002, **16(3)**, 129-132.
- 39. D.C. Brown, "Progress in Inorganic Chemistry", 1973, Vol.18, Wiley, New York.
- 40. A.L. Lehninger, "Biochemistry", 1974, 2<sup>nd</sup> Ed, Worth publishers, New York
- 41. R.Singh, N.Gupta and N.Fahmi, *Indian J, Chem.*, 1999, **38A**, 1150-1158.
- 42. B. Abolmaali, H.V-Taylor and U. Weser, *Bioinorg. Chem. Springer*, Berlin, Heidelberg, 1998, 91-190.
- 43. E.D. Harris, R.A. Disilvestro and J.A. Balthrop, *'Inflammatory Disease and Copper'*, 1982 ed. J.R.J. Sorenson, Humana Press, New Jersey, 183.
- 44. J.R.J.Sorenson, 'Inflammatory Diseases and Copper', 1982, Humana Press, New Jersey.
- 45. J.M. Wood and D.G. Brown, Struct. Bond, 1972, 11, 47-105.
- 46. Ponka, H.M. Schulman and R.D. Woodworth (Eds.), "*Iron Transport and Storage*", 1990, Boca Raton, Flourida.
- 47. J.W. Buchler, *Angew. Chem.*, 1978, **17**(6), 407-423.
- 48. R. Morrow and K.A. Kolasa, *Inorg. Chim-Acta*, 1992, **195**, 245-248.
- 49. L.G. MacDonald, D.H.Brown and W.E. Smith, *Inorg. Chim. Acta*, 1982, 67, 7-12.
- 50. J. Qiu, M. Lu, Y. Yao, Y. Zhang, Y. Wang and Q. Shen, *Dalton Trans.*, 2013, **42**, 10179-10184.
- 51. Li, C.W. Yan and X.C. Zeng, *Pol.*, 2000, **74**, 631-637.

- 52. K. Sampath, and C.Jayabalakrishnan, *Inorg. Nano-Met.*, 2015, 45(8), 1145-53.
- 53. A.C. Ekennia, A.A. Osowole, L.O. Olasunkanmi, D.C. Onwudiwe and E.E. Ebenso, *Res. Chem. Intermed.*, 2017, **43(7)**, 3787-37811.
- 54. Q.Sun, R.M.Van Dam and W.L.Willet, *F.B.Hu.*, 2009, **32(4)**, 629-634.
- 55. D.Mohanambal, G.Sridevi, S.Arulantony and R.Angayarkani, *Asian J. Pharm. Clin. Res.*, 2018, **11(4)**, 66-74.
- 56. R.Vasanthi, P.ShyamSundar, H.Ramana, K.N.V.Rao, S.Nayyar and K.Rajeswardutt, *Indo Am. j. pharm. sci.*, 2017, **4(10)**, 3859-3863.
- 57. M.T.P.Ferreira and H.Maia, *Tetrahedron Lett.*, 2002, **43**, 4491-4493.
- 58. C.Y.D. Leon and B.Ganem, *Tetrahedron*, 1997, **53**, 7731-7752.
- 59. P.Krishnamoorthy, P.Sathyadevi, A.H.Cowley, R.R.Butorac and N.Dharmaraj, *Eur. J. Med. Chem.*, 2011, **46(8)**, 3376–3387.
- 60. F.Arjmand, A.Jamsheera and D.K.Mohapatra, *J. Photochem. Photobiol. B: Biol.*, 2013, **121**, 75–85.
- 61. K.S.Bharti and K. S.Singh, *Der Pharm. Lett.*, 2009, **1**, 39–51.
- 62. C.P.Meher, S.P.Sethy and M.Madhavi, *Pharmatutor*, 2012, **2**, 1528-1537.
- 63. G. Carullo, S.Mazzotta, F. Giordano and F.Aiello, *Hindawi J.Chem.*, 2021, 1-8.
- 64. V. Bhardwaj, D. Gumber, V.Abbot, S. Dhimana and P. Sharmaa, *Rsc Adv.*, 2015, **5(20)**, 15233–15266.
- 65. K.N. Raymond, D.W Meek, and J.A.Ibers, *Inorg. Chem.*, 1968, **7**, 1111-1121.
- 66. B.J. Hathway, and D.E.Billing., *Coord. Chem. Rev.*, 1970, **5(2)**, 143-149.
- 67. T.N.Waters, and D.J. Hall, *Chem. Soc.*, 1959, 1200-1203.
- 68. J.M.Waters, and T.N. Waters, *J. Chem. Soc.*, 1964, 2489-2491
- 69. A.B.P.Lever, *Coord. Chem. Rev.*, 1968, **3(2)**, 119-140.
- 70. J. Lewis and R.A. Walton, *J. Chem, Soc. A*, 1966, 1557.
- 71. B.N. Figgis, *Nature*, 1958, **182**, 1568-1570.

- 72. M. Kato, H.B. Jonassen and J.C. Fanning., *Chem. Rev.*, 1964, **64**, 99-128.
- 73. J.C.Scott and A.F. Garito, *Phys. Rev. B*, 1975, **12**, 5927-5931.
- 74. S.L. Lembert, *Inorg. Chem. Acta.*, 1978, **29**, 223-234.
- 75. L.P. Battaglia, J. Chem. Soc. Dalton Tans., 1986, 1653-1671.
- 76. W. Levason, and C.A. McAuliffe, *Coord. Chem. Rev.*, 1974, **12**, 151-159.
- 77. H. P.Boniecka, and W. Wojciecho, *Wski, Mater. Sci.*, 1975, **1**, 27-35.
- 78. L. Sacconi, *Transition Metal Chem.*, 1968, **4**, 199-206.
- 79. M. Ciampolini, *Struct Bond*, 1969, **6**, 52-61.
- 80. J.K. Stalick, and J.A. Ibers, *Inorg. Chem.*, 1970, **9**, 453-460.
- 81. P.L. Orioli and C.A. Ghilardi, *J. Chem. Soc. A*, 1970, 1511-1516.
- 82. J. Burgess and M.V. Twigg, Encyclopaedia of Inorganic Chemistry, 2006, 1-45.
- 83 F .D. Rahmatabadi, R.R. Khojasteh, H. K. Fard and F.Tadayon, *Eurasian Chem. Commun.* 2020, **2**, 587-594.
- 84. R. Subarani and P.Metilda, *Int. J. Sci. Eng.*, 2017, **8**(**9**), 336-340
- 85. B. K.Singh, P. Mishra, A. Prakash, and N. Bhojak, *Arab. J. Chem.*, 2017, **10(1)**, S472-S483.
- 86. S.Chandra and P.Ballah, *Int. J. Pharm. Sci.*, 2013, **4(6)**, 2393-2399.
- 87. T.Mangamba, M.C.Ganorkar and G.Swarnabala, *Int. J. Inorg. Chem.*, 2014, 1-22.
- 88. E. Yousif and A.Majeed, Khulood Al-Sammarrae Nadia Salih, Jumat Salimon Bashar Abdullah, *Arab. J. Chem.*, 2017, **10**, S1639-S1944.
- 89. M.J.Nisha and C.Isac Sobanaraj, *Int. J. Sci. Res. Publ.*, 2017, **7(10)**, 10-19.
- 90. B. K. Singh, A. Prakash, H. K. Rajour, N. Bhojak and D. Adhikari, *Spectrochim. Acta A Mol. Biomol.*, 2010, **76**(3-4), 376–383.
- 91. R.Subarani and P.Metilda, *J. Emerg.*, 2019, **6(5)**, 53-9-62.
- 92. A. Charles and K. Sivaraj, *Res. J. Life Sci.*, 2019, 5(2), 982-992.

- 93. M. G. Bhowon, H. Li Kam Wah, A. Dosieah, M. Ridana, O. Ramalingum and D. Lacour, *Synthesis and Reactivity in Inorganic and Metal Organic Chemistry*, 2004, **34(1)**, 1–16.
- 94. N.K.Chaudhary, World J Pharm Pharm Sci, 2013, **2(6)**, 6016-6025.
- 95. A. Charles, K. Sivaraj and S. Thanikaikarasan, *Mater. Today: Proc.*, 2020, 1-4.
- 96. A. A. Ahmed, S. A. Benguzzi and A.A.EL.Hadi, J. Sci., 2007, 1(1), 79-90
- 97. M. S. Asha, O. Pinto, J. N Sebastian, S. Naik and S. A. Khanum. *Int. J. Adv. Res.*, 2017, **5(8)**, 2189-2204.
- 98. M.B. Halli, S. Sadu SuryaKant, N Shaishta and M Kinni, *Indian J. Appl. Res.*, 2014, **4**(2), 4-6.
- 99. G. B Bagihalli, P.S. Badami, S.A. Patil, *J. Enzyme Inhib. Med. Chem.*, 2009, **24(2)**, 381-394.
- 100. K. Singh, Y. Kumar, P. Puri and G. Singh, Bioinorg. Chem. Appl., 2012, 1-9.
- 101. A. Prakash, S. Kabir, M. Agrawal, R. Sharma and A. K. Gupta, *Int. J. Chemtech. Res.*, 2014, **6(2)**, 1276-1280.
- 102. S Mini and V Sadasivan, Int. J. Adv. Res., 2016, 4(8), 1555-1562.
- 103. Z.-F. Chen, Y.-Z. Tang, H. Liang, H.-K. Fun and K.-B. Yu, *J. Coord. Chem.*, 2006, **59**(2), 207–214.
- 104. S. Bal and S. S Bal, *Monatsh. Chem.*, 2015, **146(6)**, 903-912.
- 105. M. Habibi, S. A. Beyramabadi, S. Allameh, M. Khashi, A.Morsali, M. Pordel and M. Khorsandi-Chenarboo, *J. Mol. Struct.*, 2017, **1143**, 424-430.
- 106. O.A. Ali, S.M. El-Medani, D. A. Ahmed and D. A. Nassar, *Spectrochim. Acta A: Mol. Biomol. Spectrosc.*, 2015, **144**, 99–106.
- 107. N. K. Chaudhary and P. Mishra, *Bioinorg Chem Appl.*, 2013, 1-13.
- 108. E.L. de Araujo, H. F. G. Barbosa, E. R. Dockal and E. T.G. Cavalheiro, *Int. J. Biol. Macromol.*, 2017, **95**, 168-176.
- 109. K Singh, M.S. Barwa and P. Tyagi, Eur. J. Med. Chem., 2007, 42 (3), 394-402.
- 110. T.B.Ravoof, K.A Crouse, E.R Tiekink, M.I Tahir, E.M. Yusof, R. Rosli, *Polyhedron.* 2017, **5(133)**, 383-392.

- 111. M. S. Nair, D. Arish and J. Johnson, J. Saudi Chem. Soc., 2016, 20, S591-S598.
- 112. M.A. Quraishi and R. Sardar; *Indian J. Chem. Techn.*, 2004, **11**, 103-107.
- 113. M.N. Desai, M. B. Desai, C. B. Shah and S. M. Desai; *Corros. Sci.*, 1986, **26(10)**, 827-837.
- 114. E.M. El-Sayeda, T.M. Tamerb, A.M. Omerb and M.S. Mohy Eldinb, *Desalination Water Treat.*, 2016, 1-14.
- 115. G.Yuvaraja, D.Y. Chen, J.L.Pathak, J.Long, M.V.Subbaiah, JC. Wen and CL.Pan, *Int. J. Biol. Macromol.*, 2020, **1(146)** 1100-1110.

# **Experimental Techniques**

This chapter provides a brief account on used chemicals and various analytical, physico-chemical and biological techniques employed for characterisation, structural elucidation and applications for Schiff base ligands and its metal complexes isolated in solid state.

### 2.1 Chemicals

All the reagents and chemicals used for the current work were purchased from commercial sources (Sigma Aldrich, Merck and Loba chemicals, India) and used without further purification. The solvents were purified and dried according to standard methods available methods in literature. [1]

The compounds such as pyrrole-2-carboxaldehyde, pyridine-2-carboxaldehyde, indole-3- carboxaldehyde and 2-(methylthio)aniline were obtained from Sigma-Aldrich and Alfa aesar. Metals salts such as FeCl<sub>3</sub>.6H<sub>2</sub>O, Co(NO<sub>3</sub>)<sub>2</sub>.6H<sub>2</sub>O, NiSO<sub>4</sub>.7H<sub>2</sub>O, CuCl<sub>2</sub>.2H<sub>2</sub>O and ZnSO<sub>4</sub>.6H<sub>2</sub>O were Merck products. The solvents used for current research work such as methanol, ethanol, chloroform, DMSO and DMF were obtained from Merck.

# 2.2 Characterisation Techniques

Various physico-chemical techniques have been used to characterize synthesized Schiff base ligands and their metal complexes. Each technique is distinct and provides crucial information on level of complexity, type of coordination and the stability of the complexes. Following physico-chemical techniques were used to characterize the synthesized products.

- Solubility
- Melting point
- Elemental analysis
- Chemical analysis
- Molar conductance
- Magnetic susceptibility
- <sup>1</sup>H NMR spectra
- FT-IR spectra
- UV-Visible spectra
- EPR spectra
- Mass spectra
- Cyclic Voltammetric studies
- Thermal Decomposition Studies
- X-Ray Diffraction Measurements

# 2.2.1 Solubility and Melting Point

### **Solubility**

Solubilities of the prepared Schiff base ligands and their metal complexes were tested in hot and cold water, CHCl<sub>3</sub>, dimethylformamide (DMF), dimethylsulfoxide (DMSO) by shaking a small amount each compound with the respective solvent in a test tube. The synthesized ligands and their metal complexes were established to be water insoluble, slightly soluble in ethanol, methanol and completely soluble in DMF and DMSO.

# **Melting Point**

Minimum amount of the ligand or metal complexes was taken in a clean dry mortar with pestle. It was powdered well and taken in a small capillary tube with one end fused and tied to a thermometer. Then, this arrangement was inserted into a glycerol bath and heated slowly. The temperature at which the compound began to melt was recorded.

# 2.2.2 Elemental Analysis

Quantitative microanalyses of elements such as carbon, hydrogen, nitrogen and sulphur of synthesized compounds provide vital data in finding out the empirical formula. It was carried out on a Perkin-Elmer 2400 CHNS/O elemental analyzer at SAIF, Indian Institute of Technology, Madras. In the microanalysis, sample weighing about 10 mg concealed in a tin capsule was injected into the instrument and the computerized elemental percentages for the synthesized compound were obtained. Based on the elemental composition possible structures were drawn using the Chemsketch / Chemdraw software. The results of microanalysis for synthesized Schiff bases and their metal complexes are briefly discussed in each chapter (III-V).

# 2.2.3 Chemical Analysis

# **Estimation of Anions**

A known weight of a chloro complex was carefully mixed with fusion mixture of Na<sub>2</sub>CO<sub>3</sub> and KNO<sub>3</sub> in 1:3 weight ratio in a nickel crucible. The contents of the crucible were strongly heated to decompose the complex and cooled and then water extracted. The extract was acidified with dilute nitric acid to decompose the carbonate, and the chloride content was estimated volumetrically by Volhard's method. The sulphato complexes were decomposed by digesting with concentrated nitric acid and the sulphate was estimated gravimetrically as BaSO<sub>4</sub>. Nitrate was not separately estimated.

### **Estimation of Metal ions**

The metal complex was digested with concentrated nitric acid or concentrated nitric acid and concentrated hydrochloric acid mixture (1:3 v/v). The excess acid was fumed off and the resulting solution was evaporated to dryness. The residue was then extracted with distilled water and used for the estimation of the metal ions. Copper was estimated volumetrically by iodometric method. Zinc was estimated volumetrically by titrating against

EDTA using Eriochrome Black-T as indicator. Cobalt and Nickel were estimated gravimetrically as Hg[Co(SCN)<sub>4</sub>] and [Ni(DMG)<sub>2</sub>] respectively. Iron was estimated colorimetrically by adding potassium thiocyanide. [2]

### 2.2.4 Molar Conductance Measurement

The molar conductance value of an electrolyte in a particular solvent depends upon various properties of the solvent such as dielectric constant, viscosity, specific conductance, purity and donor capacity towards metal ions. The electrical conductance measurements were carried out to know whether the anions of the metal salts were coordinated to the metal centre or remained as uncoordinated ions outside the sphere.

The conductances of the different types of electrolytes in various non-aqueous solutions have been studied by Geary [3]. Table 2.1 furnishes the range of values of molar conductivities of different electrolytes in common organic solvents at room temperature.

Table 2.1 Molar Conductivity Values (Ω<sup>-1</sup> cm<sup>2</sup> mol<sup>-1</sup>) and Electrolytes Types

Solvent	1:1	1:2	1:3	1:4
Acetone	100-140	160-200	270	360
Acetonitrile	120-140	220-300	340-420	500
DMF	65-90	130-170	200-140	300
Ethanol	35-45	70-90	120	160
Methanol	80-115	160-220	290-350	450
Nitrobenzene	20-30	50-60	70-80	90-150
Nitromethane	75-95	150-180	220-260	290-300

The conductance data of the metal ion complexes in the present study were obtained in  $\sim 10^{-3}$  M DMF solutions at room temperature using Equiptronics conductivity metre Model No. EQ 665 with a dip type cell having platinum electrodes. The cell constant of the conductivity cell used was  $1.06 \text{ cm}^{-1}$ .

### 2.2.5 Magnetic Susceptibility Measurement

Magnetic susceptibility measurements can be used in conjunction with the electronic spectra to establish the geometries of the complexes. Tetrahedral, square planar or octahedral stereochemistries and spin-free or spin –paired nature of the complexes could be distinguished from the magnetic criteria in the cases of d<sup>5</sup>, d<sup>6</sup>, d<sup>7</sup>, d<sup>8</sup> and d<sup>9</sup> metal complexes.

The magnetic measurements of the new complexes of Fe <sup>III</sup>, Co <sup>II</sup>, Ni <sup>II</sup> and Cu <sup>III</sup> were carried out to find out the effective magnetic moments for metal atoms in the complexes at room temperature by using a Gouy magnetic balance. The Gouy tube was calibrated using mercury(II) tetrathiocyanatocobaltate (II).[4] The diamagnetic corrections for various atoms and structural units were computed from Pascal's constants.[5] The effective magnetic moments were calculated from the corrected molar magnetic susceptibilities ( $\chi_M^{corr}$ ) of the complexes using Curie's relation  $\mu_{eff} = 2.84 \ [\chi_M^{corr} T_{abs}]^{1/2} \ B.M.$  where  $T_{abs}$  is the absolute temperature at which the measurements were done. The number of unpaired electrons 'n' possessed by the metal ion can be determined from the effective magnetic moment,  $\mu_{eff}$  of the metal ion. The contribution to the magnetic moment from the electron spin effect ( $\mu_{s}$ ) only is given by the equation  $\mu_{s}=\mu_{eff}=[n(n+2)]^{1/2}$ .

### 2.2.6 <sup>1</sup>H NMR Spectroscopy

<sup>1</sup>H NMR spectra for the Schiff base ligands and metal complexes were recorded in DMSO on a Bruker Avance III, 400MHz NMR spectrometer at room temperature using TMS as internal standard. Nuclear Magnetic Resonance (NMR) spectroscopy is an analytical technique that exploits the magnetic properties of nuclei and useful in determining the molecular structures of organic compounds. Proton Nuclear magnetic resonance spectroscopy is one of the most powerful tools for elucidating the number of hydrogen atoms or protons in the compound. An NMR spectrum is a plot of the intensity of a peak against its chemical shift, measured in parts per million (ppm). [6]

# 2.2.7 Fourier Transform Infrared Spectroscopy

The FT-IR spectroscopy is extensively used as a characterisation technique for metal complexes. FT- IR spectra of the synthesized compounds were recorded on the Shimadzu FTIR 470 IR spectrophotometer by dispersing the solid substance in KBr discs (pellet technique) in the region 4000-250 cm<sup>-1</sup>. FT-IR analysis may simply involve the characterisation of compound with respect to presence or absence of specific group frequency associated with one or more fundamental modes of vibration or by complex pattern recognition when an unknown spectrum is compared with existing reference data base. Upon complexation the stretching modes of ligands change due to weakening /strengthening of the bonds involved in the bond formation leading to a number of subsequent changes in the position of bands. Changes in the structural features of the ligands and metal complexes are observed mainly in the fingerprint region i.e., at 1600 - 750 cm<sup>-1</sup> and in the far IR region i.e., 50 - 500 cm<sup>-1</sup>. [7]

# 2.2.8 UV-Visible Spectroscopy

UV-Visible spectroscopy is a significant and valuable tool for many chemists to draw important details about the geometric features of the metal complexes. UV-Vis spectra were recorded on a Shimadzu UV-Vis.160A UV-Visible spectrophotometer between 200-800 nm using DMSO as the solvent. The electronic spectra of ligands and metal complexes depend upon the transition of unpaired electron from ground state to excited state. In the ground state, the spins of the electrons in each molecular orbital are essentially paired. The highly probable transition due to absorption of quantized energy involves the promotion of one electron from the highest occupied molecular orbital to the lowest available unfilled molecular orbital. In most of the cases, several transitions occur resulting in the formation of several bands. [8] The transition metal complexes mostly appear as coloured substances due to d-d transitions in visible region. Generally, four types of electronic transitions are observed with transition metal complexes. They are as follows:

The d-d or ligand field spectra usually appear in 400-800 nm region due to the transition that arise between divided d levels of central metal atom. Ligand—metal charge transfer transition occurred due to transition from molecular orbital located primarily on ligands to non-bonding or anti-bonding molecular orbital located primarily on metal atoms. Electrons when excited from non-bonding or anti-bonding orbital located primarily on metal atom to antibonding orbital of ligand produce metal-ligand charge transfer. This usually occurs in UV region, but rarely is found tailing off into the visible region. Intra-ligand transitions occur due to the electrons excited from one ligand orbital to another orbital and usually occur in UV region. These bands are not adversely affected by chelation and can be easily distinguished from near charge transfer bands. Octahedral, square-planar and tetrahedral fields cause splitting of d orbitals in different ways and thus the stereochemistry of the metal ion will have a significant impact on the d-d transitions in a metal complex. Therefore, the spectral data provide useful information about the structure of a complex.

# 2.2.9 EPR Spectroscopy

EPR is a spectroscopic technique that is useful for the study of systems having unpaired electrons. An unpaired electron that is not subject to the interactions with other electrons or magnetic nuclei will show a sharp single absorption for its transition, which corresponds to the position of the magnetic field at which it comes into resonance. The resonance position of the spectral line is referred to as 'g' value and is directly determined by the separation of the energy levels of the system under investigation. [9] The different 'g' values are interpreted in terms of the first and the second order perturbations by the spin orbit interactions. The line width is produced by the relaxation of the spin energy state. Hyperfine splitting pattern arises from the interaction of the unpaired metal electron with magnetic nuclei on the ligand, it can be used to determine the distribution of the unpaired electron in a molecule. It decides the extent to which the electron is delocalized over the

ligands. EPR spectroscopy along with the magnetic susceptibility measurement is used to study magnetic interactions mainly in polynuclear Cu <sup>II</sup> complexes.

Electron paramagnetic resonance (EPR) spectra (X-band, 0.4 T, 9.452 GHz) were obtained with a JEOL Model JES FA200 spectrometer, equipped with a variable-temperature facility in the following conditions: 0.99800 mW power, 100.0 kHz modulation frequency, 10.0 GS amplitude and 120 seconds sweep time. The EPR spectra of the Cu  $^{II}$  complexes in the powdered form were recorded at room temperature. Polycrystalline DPPH with a g value of 2.0036 was used as g factor marker. The spin Hamiltonian parameters ( $g_{II}$ ,  $g_{\perp}$ ,  $g_{av}$ , G) were computed.

# 2.2.10 Mass Spectroscopy

Mass spectrum is used to determine the molecular mass of a compound with high accuracy, which leads to the exact deduction of the molecular formula. In the structure analysis, fragmentation pattern of the molecular ion is much useful. The fragmentation may be due to simple cleavages, rearrangements and ion –molecule reaction. This leads to the identification of the presence of recognizable groups within the molecule. In the electron impact (EI) mode, a high-energy electron beam bombards the molecule in the vapour phase to produce molecular ions. The unstable parent ions split into fragments. The result of electron impact is recorded as a spectrum of positive ions separated, based on mass/charge (m/z) ratios.

The mass spectral study of the ligands and a few metal complexes were carried out using Agilent 6530 LC/Q-TOF mass spectrometer. The accurate molecular weights of the compounds studied were confirmed from their electron impact mass spectra.

### 2.2.11 Cyclic Voltammetric Studies

CHI instrument model 760 was used for recording the cyclic voltammogram of the metal complexes. Cyclic voltammetric studies were carried out using DMF as solvent with 0.1M TBAP as supporting electrolyte. A three-electrode configuration was used *viz.*, glassy carbon electrode as working, a Pt-wire as auxiliary and Ag/AgCl as reference electrode. Cyclic voltammetry is the most widely used technique for acquiring qualitative information about electrochemical reactions. This technique is based on varying the applied potential at the working electrode (compared to the reference electrode) in both forward and reverse directions while monitoring the current between the auxiliary electrode and reference electrode. Peaks will be observed at potentials that initiate a chemical reaction in the solution (reduction or oxidation) because they involve a flow of electrons. The power of cyclic voltammetry results from its ability to provide considerable information on the thermodynamics of redox processes and the kinetics of heterogeneous electron transfer reactions and on coupled chemical reactions of adsorption processes. In particular, it offers a rapid location of redox potentials of the electro active species. [10]

### 2.2.12 Thermal Decomposition Studies

In thermal analysis some physical properties of a material are measured as a function of temperature. The techniques used are

- 1) TG (Thermogravimetry) –measuring the change of weight on programmed heating,
- DTA (Differential Thermal Analysis) temperature difference ( $\Delta T$ ) between the sample and the reference is measured. The DTA curve is a plot of  $\Delta T$  on an ordinate with endothermic reaction downward and exothermic reaction upward and time (t) or temperature (T) on the abscissa,
- 3) DSC (Differential Scanning Calorimetry)-Absorption of heat is measured and recorded against sample temperature.

TG is useful to find the decomposition temperature, thermal stability and composition. Evolved gas and decomposition kinetics can also be studied using TG.

In the present study, thermal analysis of the ligands and their metal complexes was carried out to understand the modes of decomposition of the compounds, thermal stabilities and the decomposition temperatures of the compounds and to detect the presence of crystalline or lattice or coordinated water molecules and the nature of the phase changes taking place during the programmed heating.

Simultaneous TG/DTG patterns were recorded on SDT Q600 V20.9 Build 20 TG/DTG analyser. The analyses were carried out on horizontal differential type balance, in a nitrogen atmosphere with the flow time of 100 mL min<sup>-1</sup> at heating rate of 20°C min<sup>-1</sup> from ambient to 850° C using heated alumina as the standard reference material. A sample of less than 10mg was subjected to programmed heating to record thermograms.

# 2.3 Biological Applications

### 2.3.1 *In Vitro* Antibacterial Activity Screening

Muller Hinton agar medium was used to screen the newly synthesised ligands and their metal complexes for antibacterial activity using the agar well diffusion method. [11] The *in vitro* antibacterial activities of the test compounds were tested against two Gram positive bacteria and two Gram negative bacteria. Base plates were prepared by pouring 20 mL of autoclaved Muller Hinton agar into each sterilized petri dish and allowing them to settle. Broth cultures of *B.subtilis*, *S.aureus*, *P.aeruginosa* and *E.coli* bacteria were incubated with molten autoclaved Muller Hinton agar that had been maintained at 38° C for 15 minutes for adsorption. Wells were drilled into the seeded agar plates with a sterile cork borer of 8mm diameter, and these wells were injected with test chemical solutions. The stock solution of each test compounds was prepared by dissolving 10 mg of the test compound in 10 mL of freshly distilled DMSO. Further, various concentrations of the

compounds (100, 75, 50, 25  $\mu$ g/mL) were prepared by diluting the stock solution with the required volume of distilled DMSO. All the plates were incubated at 38°C for 24 hours and the zones of inhibition were measured around the wells. As the organism grows, it develops a turbid layer except in the region where the concentration of antibacterial agent is above Minimum Inhibition Concentration (MIC) and a zone of inhibition is observed. The diameter of the inhibition zone depends upon the culture medium, rate of diffusion, concentration of antimicrobial agent and incubation condition. Gentamicin was used as a reference. For each organism and for each test compound, the procedure was repeated three times on three replicate plates.

# 2.3.2 *In Vitro* Antifungal Activity Screening

Potato dextrose medium was used to screen the newly synthesised ligands and their metal complexes for antifungal activities by agar well diffusion method. [12] Antifungal activity screening was carried out against Candida albicans and Aspergillus Niger. Base plates were prepared by pouring 20 mL of autoclaved potato dextrose into each sterilized petridish and allowing them to settle. They were maintained at 38°C and incubated with the broth cultures of Candida albicans and Aspergillus niger and kept for 15 minutes for adsorption. Wells were bored into the seeded dextrose plates using sterile cork borer of 8 mm diameter, and these wells were loaded with the test compound solutions. Stock solution of each test compound was prepared by dissolving 10 mg of each test compound in 10 mL of freshly distilled DMSO. Further various concentrations of the test compounds (100, 75, 50, 25 μg/mL) were prepared by diluting the stock solution with the required volumes of distilled DMSO. Plates were incubated at 38°C for 24 hours and the zone of inhibition was measured around each well. As the organism grows, it forms a turbid layer except in the region where the concentration of the antifungal agent is above MIC and a zone of inhibition is seen. Ketoconazole was used as reference. For each organism and for each test compound, the procedure was repeated three times on three replicate plates.

### 2.3.3 Antioxidant Activity Screening (Free Radical Scavenging Activity)

2, 2 -Diphenyl -1-picryl hydrazyl (DPPH) assay was used for determining the free radical scavenging activity of the Schiff base ligands and their metal complexes. 0.9 mL of 1.5x10<sup>-4</sup> M DPPH radical solution in methanol was prepared and mixed with different concentrations of test samples (5, 10, 15, 20 μg/mL) and to the standard L-ascorbic acid that were taken in different test tubes and the volume of solution in each test tube was adjusted to 100 μL by adding DMSO and kept in dark for 30 minutes. The absorbance of DPPH remaining in the mixed solution was measured at 520nm. The reduction in the absorbance of the DPPH solution indicated the free radical scavenging activity of the particular test sample. Methanol without the sample was used as the control. The DPPH radical scavenging activity was calculated according to the following formula.

Scavenging activity 
$$\% = [\underline{Abs_{control} - Abs_{sample}}] \times 100.$$
 [Abs\_control]

### 2.3.4 Antidiabetic Activity Screening

### 2.3.4.1 α-Amylase Inhibitory Assay

Using the synthesized silver nanoparticles, the  $\alpha$  - amylase inhibitory assay was performed. In a test tube, 250µL of sample solution (20-100 g/mL) was added, followed by 250µL of 0.02 M sodium phosphate buffer (pH 6.9) containing  $\alpha$ - amylase solution (0.5 mg/mL). The solution was pre-incubated for 10 minutes at 25°C, after which 250 µL of 1% starch solution in 0.02M sodium phosphate buffer (pH 6.9) was added at regular intervals and incubated for another 10 minutes at 25°C. The reaction was terminated by the addition of 500 µL of dinitrosalicylic acid (DNS) reagent. The tubes were then incubated in boiling water for 5 minutes and cooled to room temperature. The reaction mixture was diluted by adding 5 mL distilled water and the absorbance was measured at 540nm using a spectrophotometer. A control was prepared using the same procedure by replacement of the

sample solution with distilled water. The  $\alpha$ - amylase inhibitory activity was calculated in terms of percentage.

### 2.3.4.2 α- Glucosidase Inhibitory Assay

The activity of a sample solution on  $\alpha$ -glucosidase was determined by using  $\alpha$ -glucosidase from saccharomyces cerevisiae. p-Nitrophenol glucopyranoside (p-NPG) was prepared in 20mM phosphate buffer as a substrate solution at pH 6.9 . 100 $\mu$ L of  $\alpha$ -glucosidase (1.0 U/ mL) was pre-incubated with 50  $\mu$ L of the sample solutions containing different (20-100  $\mu$ g/ml) concentrations of sample for 10 minutes. Then 50  $\mu$ L of 3.0 mM (p-NPG) substrate was a dissolved in 20 mM phosphate buffer (pH 6.9) and added to initiate the reaction. The reaction mixture was incubated at 37°C for 20 minutes and then the reaction is stopped by adding 2 mL of 0.1M sodium carbonate. The  $\alpha$ -glucosidase activity was determined by measuring the yellow colour of p- nitro phenol released from p-NPG at 405nm. The results were expressed in percentages of the blank control. The  $\alpha$ - glucosidase inhibitory activity was calculated by percentage inhibition.

% inhibition ratio = [
$$\underline{Abs_{control} - Abs_{sample}}$$
] x 100 [ $\underline{Abs_{control}}$ ]

# 2.4 Corrosion Inhibition Properties of Schiff base ligands

This experimental work was planned to study the corrosion inhibiting properties of three newly synthesised Schiff base ligands. The chemicals and solvent used in this work were of analar grade and used without further purification. All the glass apparatus were washed with distilled water and dried in an oven.

# 2.4.1 Weight Loss Method

### **2.4.1.1 Preparation of the Mild Steel Specimens**

Mild steel specimens (0.14 % C, 0.35 % Mn, 0.17 % Si, 0.03 % P and Rest Fe) of the dimensions  $2.0 \times 4.0 \times 0.34$  cm were subjected to pre-treatment such as cleaning by sandpaper, washing with Clerk's solution (5 g of SnCl<sub>2</sub> and 2 g of Sb<sub>2</sub>O<sub>3</sub> in 100mL HCl) and polishing by emery paper, finally degreasing using acetone. [13] The specimens were stored in a desiccator.

### 2.4.1.2 Chemicals Used

- Analar grade hydrochloric acid
- Schiff base (SB) 1 (derived from condensing pyrrole-2-carboxaldehyde and 2-(methylthio)aniline),
- Schiff base (SB) 2 (derived from condensing pyridine-2-carboxaldehyde and 2-(methylthio)aniline)
- Schiff base(SB) 3 (derived from condensing indole-3-carboxaldehyde and 2-(methylthio)aniline)
- DMF
- Double distilled Water

### **2.4.1.3 Preparation of Test Solutions**

Exactly 10% hydrochloric acid solution was prepared using double distilled water in a 1000 mL standard measuring flask and its strength was determined by titrating with standard sodium carbonate. Inhibitor solutions of various concentrations such as 500, 1000, 1500 and 2000 ppm of Schiff base 1 (SB 1), Schiff base 2 (SB 2) and Schiff base 3 (SB 3) were prepared. For example, 2 g of Schiff base is dissolved in minimum amount of DMF and diluted to 1000 mL using double distilled water. This is 2000 ppm solution. From this, remaining lower concentrations can be prepared.

### 2.4.1.4 Preparation of the Environment

The details regarding the preparation of various environments used for weight loss method in the present study are given in Table 2.2 for one set of solutions

Table 2.2 Preparation of the Environments for Weight Loss Method

S.No	Schiff Base 1		Volume of 10% HCl	Total volume		
	ppm	mL	(mL)	( 100 mL)		
1.	500	10	90	100		
2.	1000	10	90	100		
3.	1500	10	90	100		
4.	2000	10	90	100		

In the same way four sets of solutions were prepared for remaining two inhibitor compounds.

# 2.4.1.5 Determination of Surface Area of the Specimens

The length, breadth and the thickness of a mild steel specimen were determined with the help of Vernier Caliper of high precision and the surface area of each specimen was calculated.

### 2.4.1.6 Determination of Inhibition Efficiency and Corrosion Rate

The initial weight of the specimen was noted using single pan balance and then immersed into the corrosive medium and boiled for 30 minutes. After 30 minutes the weight of the specimen was noted. The change in weights was calculated from initial weight. The percentage of weight loss was calculated by usual method. From this, inhibition efficiency and the corrosion rate for each specimen was obtained by using the following formula. [14, 15].

### Inhibition Efficiency = $(W_0-W_1/W_0) \times 100$

Where,  $W_0$  is the weight loss without inhibitor and  $W_1$  is weight loss with inhibitor.

87600 x Weight loss in grams

Corrosion Rate =

(Area in cm<sup>2</sup>) x (Time in Hours) x (Density of coupon in g/cc)

# 2.4.1.7 Scanning Electron Microscopic Studies (SEM)

The mild steel specimen was first immersed in blank and then in the inhibitor solution and heated for a period of 30 minutes. The specimen was removed, rinsed with double distilled water, dried and observed in a Scanning Electron Microscope to examine the surface morphology. The surface morphology of the mild steel was examined using CAREL ZEISS Model: EVO 18 computer controlled scanning electron microscope.

# 2.5 Dye Adsorbent Properties of Schiff base Ligands

### 2.5.1 Adsorbate

Malachite green, a cationic dye.

### 2.5.2 Adsorbent

Schiff base ligands SB1, SB2 and SB3

# 2.5.3 Experimental Methods

# 2.5.3.1 Batch Adsorption Studies

A stock solution of malachite green (1000ppm, 1g/L) was prepared by dissolving appropriate amount of the dye in distilled water. From this stock solution, various concentrations were obtained by dilution. Batch adsorption experiments were conducted in 100 mL Erlenmeyer flasks by adding 0.1 g of each Schiff bases (1-3) to 20 mL of malachite green solution at pH = 8 at room temperature. They were placed on an orbital shaker for a given time. The initial and final concentrations of the adsorbate in aqueous solution were measured using a photoelectric colorimeter. From the difference between initial and final

concentrations and the equilibrium concentration, the amount of the adsorbed dye was calculated. [16]

The percentage of dye adsorbed was calculated using the following equation.

Dye adsorption (%) = 
$$(\text{Co - Ce}) / \text{Co X } 100$$

where Co is the initial dye concentration and Ce is the final dye concentration in the supernatant.

### 2.5.3.2 Adsorption Isotherm

It is the fundamental idea in the design of adsorption system. It is a relation between the mass of the dye adsorbed on the surface of the adsorbent at equilibrium at constant temperature and adsorbate in the liquid phase.

The design of an isotherm provides not only the information about the affinity of dye molecules for adsorption but also give the possible mode of adsorption. Adsorption isotherm is useful in determining the initial and final concentrations of the dye. Several attempts have been made to determine the adsorbed amount. Several isotherms have been developed and employed for such analysis and the two important isotherms, the Langmuir and Freundlich isotherm are applied in this study.

### 2.5.3.2.1 Langmuir Isotherm

Langmuir isotherm is given by the linear equation

$$C_e/q_e = (1/q_m.K) + (1/q_m)$$

where,  $q_e$  is the concentration of the solid phase in equilibrium with the concentration of the liquid phase  $C_e$ .  $q_m$  is the final sorption capacity (in mg/g) and K is an equilibrium constant (L/mg).

This isotherm indicates the maximum adsorption capacity of the adsorbent from complete mono layer coverage on the surface.

### 2.5.3.2.2 Freundlich Isotherm

Adsorbents having heterogeneous surfaces with sites possessing variation in potential obeys Freundlich isotherm equation.

$$q_e = K_f C_e^n$$

where  $q_e$  is the concentration of the solid phase in equilibrium with the concentration of the liquid phase  $C_e$ .  $K_f$  is constant (a function of energy of adsorption and temperature) and n is a constant.

Taking log on both sides, we get

$$\log q_e = \log K_f + n \log C_e$$
,

We, plot A plot of log  $q_e$  versus log  $C_e$  gives a straight line with slope n and intercept log  $K_f$  from which these constants can be obtained.

### 2.5.4 Investigation of Malachite Green removal ability

Malachite green is a cationic dye (Fig 2.1) and is used to control the fungus saprolegnia in the fish breeding industry and various absorbents were used for removal of malachite green from aqueous solution.

On the basis of the previously reported works on the removal of malachite green at various pH values, we have chosen and studied the removal of malachite green at pH of 8. As shown in the **Fig.2.1**, malachite green has three aromatic rings and one N<sup>+</sup> group and one electronegative nitrogen group with a lone pair of electrons. Therefore there exists an electrostatic interaction and hydrogen bond between them and the active groups of Schiff bases 1-3 leading to adsorption of malachite green on the adsorbent. But at lower pH's, there

exists a competition between  $H^+$  ions, active groups of the adsorbent and dye molecules. Being smaller and lighter it is easier for  $H^+$  ions to interact with both adsorbate and adsorbent molecules, thus disabling the active groups to interact with malachite green .The adsorption of malachite green on to the Schiff bases 1-3 were studied at pH = 8 with 0.1g of adsorbent.

$$CI \\ H_3C \\ V \\ H_3 \\ CH_3$$

Fig.2.1 Structure of Malachite Green

### REFERENCES

- 1. A.I.Vogel, *Text Book of Practical organic chemistry*, 1989, **5**<sup>th</sup> ed. Longman, London.
- 2. J.Bassett, R.C.Denney, G.H. Jeffery and J.Hendham, "Vogel's Text Book of Qualitative Analysis," 1986, 4th ed., ELBS, Longman, London.
- 3. W.J.Geary, *Coord.Chem.REV*, 1971, **7**, 81.
- 4. J.Lewis and R.J.Wilkins., Eds, "Modern Coordination Chemistry", 1963, Interscience, Newyork.
- 5. A.Earnshaw, "Introduction to Magneto-Chemistry", 1968, Academic Press, New York.
- 6. G.R. Chatwal, "Instrumental Methods of Chemical Analysis", 2018, 5th ed.
- 7. K.Nakamoto, "Infrared and Raman spectra of inorganic and coordination compounds", 1978, 3<sup>rd</sup> ed, John Wiley and Sons, New York.
- 8. Y.R Sharma, "Elementary Organic Spectroscopy", 2007, 4th ed.
- 9. R.L.Dutta and Syamal, "Electron Spin Resonance Responses, In elements of Magnetochemistry,"1992, **2**<sup>nd.</sup> **ed**, East-West Press, New Delhi.
- 10. S.S.Beshahwored, "International Research Journal of Natural Sciences", 2020, **8**, 52-59.
- 11. A.W.Bauer, W.M.Kirby, J.C.Sherries and M.Turck, *Am. J. Clin. Pathol.*, 1966, **45**, 493–496.
- 12. C.Perez and C.Anesini, *J. Ethnopharmacol.*, 1993, **44**, 41-46.
- 13. R. K. Upadhyay and S. P. Mathur, *E-J. Chem.*, 2007, **4** (3), 408-414.
- 14 H. Uhlig, "Corrosion Hand Book", 1948, Wiley Publications, New York.
- A. Wachter and R.S. Treseder in "Corrosion Engineering" Edts. 1987, 3rd Edn. M.G. Fontana, McGraw-Hill International Editions, New York.
- 16. I.A.Amar, A. Sharif, M.M. Alkhayali, M. A. Jabji, F. Altohami, M.A.A.Qadir, M.M. Ahwidi, *IJEE*, 2018, **4**, 247-254.

# Synthesis, Characterisation and Evaluation of Antimicrobial, Antioxidant And Antidiabetic Activities of 2-(methylsulfanyl)-N-(1H-pyrrol-2-ylmethylidene)aniline and its Metal Complexes

### 3.1 Introduction

For decades, Schiff base ligands are considered as privileged ligands because they play a major role as chelating ligands in coordination chemistry and also they are easily prepared by condensation of carbonyl compounds with primary amines. Their structural flexibility are associated with various applications. [1]

Schiff base ligands have high tendency to coordinate with many metals and stabilize them in various oxidation states. These metal complexes of Schiff bases have been used as drugs and their structure activity relationships have been studied since they possess better antitumor, antimicrobial and antiviral activities. [2, 3] Various metal complexes with biand tridentate Schiff bases containing sulphur and nitrogen donor atoms play vital role in biological systems and act as exciting models for metalloenzymes which efficiently catalyze the reduction of dinitrogen and dioxygen.

Schiff base complexes with phenolic groups in the ligand as chelating moieties are used to model important biological events and replicate the catalytic activity of metalloenzymes. In addition, macrocyclic derivatives of these Schiff bases have numerous important biological roles, including photosynthesis and oxygen transport in mammalian and animal respiratory systems. [4]

In view of these ideas, here the present work deals with the synthesis of Schiff base ligand 2-(methylsulfanyl)-N-(1H-pyrrol-2-ylmethylidene)aniline and its metal complexes.

Various physico-chemical methods such as molar conductance, chemical analysis, elemental analysis, magnetic susceptibility, <sup>1</sup>H-NMR, FT-IR, UV-Vis, EPR, mass spectra, cyclic voltammetry and thermal decomposition studies are utilized to determine the structure of Schiff-base ligand and its metal complexes. The bio-efficacy of the free ligand and its complexes are tested *in vitro* against microbes with various dilutions, in order to evaluate their antimicrobial potential. In addition, antioxidant and antidiabetic activities of the titled compounds are also evaluated.

# 3.2 Synthesis of 2-(methylsulfanyl)-N-(1H-pyrrol-2- ylmethylidene)aniline MPMA

The Schiff base MPMA was prepared by mixing pyrrole-2-carboxaldehyde (0.95 g, 1mmol) in 20 mL of ethanol slowly to 2-(methylthio)aniline (0.139 g, 1 mmol) in 20 mL of ethanol with constant stirring. Then the mixture was refluxed for 4 h till a yellow precipitate was formed. The mixture was kept for slow evaporation and the yellow precipitate (MPMA) was collected. The collected yellow coloured Schiff base was washed with cold ethanol and dried in a desiccator over anhydrous calcium chloride

# 3.3 Synthesis of Metal Complexes of MPMA

The ethanolic solution of corresponding salt [iron (III) chloride hexahydrate/cobalt (II) nitrate hexahydrate/ nickel (II) sulphate heptahydrate /copper(II) chloride dihydrate /zinc (II) sulphate hexahydrate] was slowly mixed to a hot stirring ethanolic solution of 2-(methylsulfanyl)-N-(1H-pyrrol-2-ylmethylidene)aniline (MPMA) in 1:2 (M:L) molar ratio. The reaction mixture was refluxed for 3 h, then allowed to cool and by slow evaporation coloured precipitate was formed. The complex precipitated by each metal salt was filtered, washed with cold ethanol and dried in a desiccator over anhydrous calcium chloride.

### 3.4 Results and Discussion

# 3.4.1 Elemental Composition

The Schiff base MPMA was obtained as a yellow solid and it was soluble in common organic solvents. Metal complexes of Schiff base MPMA are found to be solids, non-hygroscopic, stable at room temperature and are soluble in DMF and DMSO but sparingly soluble in common organic solvents. The analytical data and physical properties of the MPMA and its complexes are furnished in **Table-3.1**.

The complexes gave satisfactory analytical data which indicate that all the metal complexes are in 1:2 metal to ligand ratio. The schematic diagram for the synthesis of Schiff base MPMA and metal complexes are shown in **Fig.3.1**.

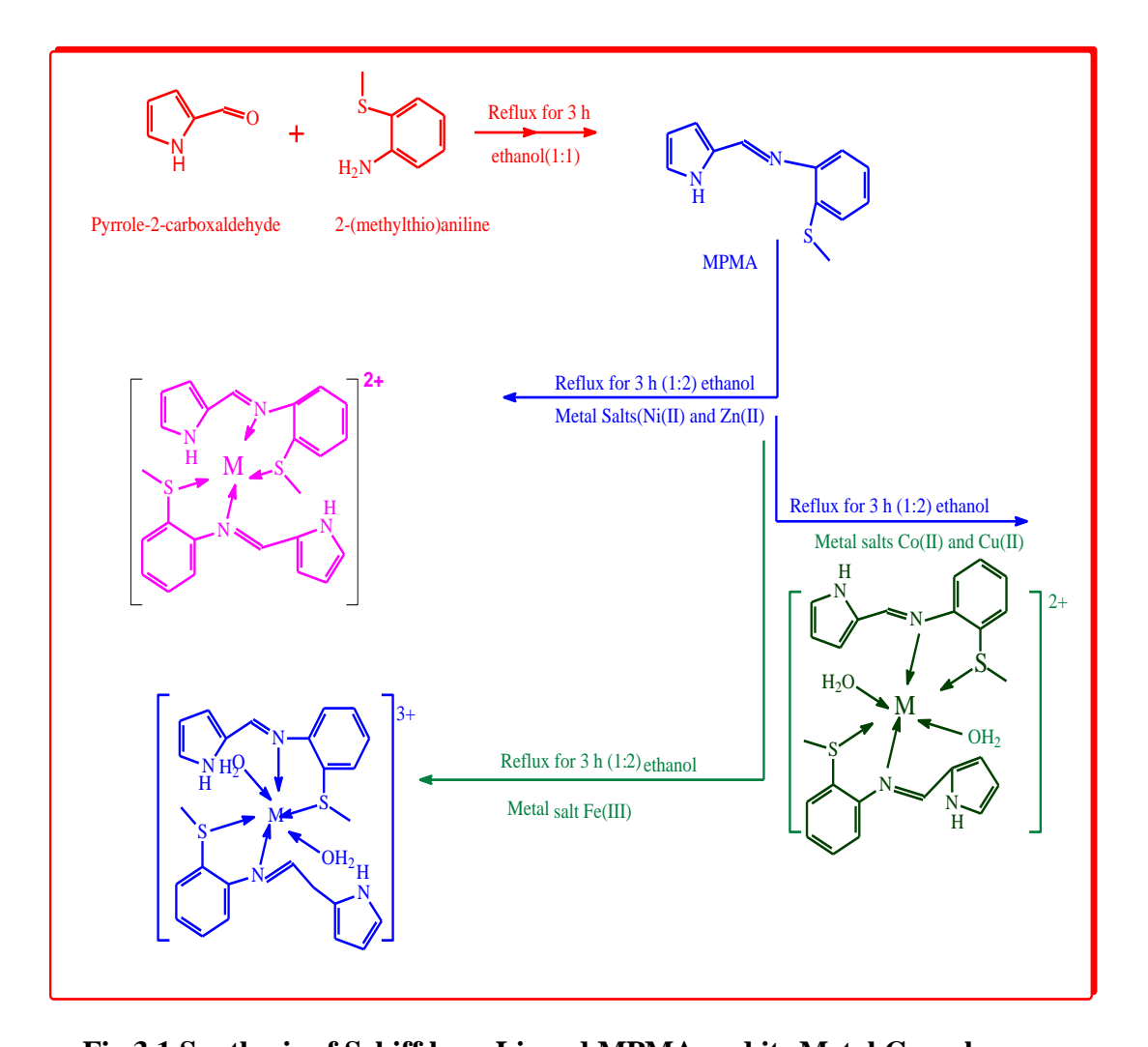


Fig.3.1 Synthesis of Schiff base Ligand MPMA and its Metal Complexes

Table-3.1: Analytical Data and Physical Properties of the Ligand MPMA and its Metal Complexes

Compound	Empirical formula	Colour	Yield	Yield M. Wt. g.mol <sup>-1</sup>	Melting Point °C	Elemental Analysis % Found (Calc)					
_			(%)			C	Н	N	S	Cl	Metal
MPMA	$C_{12}H_{12}N_2S$	Yellow	75	216.30	162	66.63 (66.59)	5.59 (5.62)	12.95 (12.89)	14.84 (14.85)	-	-
[Fe(MPMA) <sub>2</sub> (H <sub>2</sub> O) <sub>2</sub> ]Cl <sub>3</sub>	FeC <sub>24</sub> H <sub>28</sub> N <sub>4</sub> S <sub>2</sub> O <sub>2</sub> Cl <sub>3</sub>	Red Brown	80	630.77	>200	45.69 (45.63)	4.47 (4.45)	8.88 (8.82)	10.16 (10.13)	16.86 (16.81)	8.85 (8.80)
[Co(MPMA) <sub>2</sub> (H <sub>2</sub> O) <sub>2</sub> ](NO <sub>3</sub> ) <sub>2</sub>	CoC <sub>24</sub> H <sub>28</sub> N <sub>6</sub> S <sub>2</sub> O <sub>8</sub>	Light Brown	75	651.54	>200	44.23 (44.20)	4.33 (4.31)	12.89 (12.87)	9.84 (9.85)	-	9.04 (9.01)
[Ni(MPMA) <sub>2</sub> ]SO <sub>4</sub>	NiC <sub>24</sub> H <sub>24</sub> N <sub>4</sub> S <sub>3</sub> O <sub>4</sub>	Dark Blue	65	587.34	>200	49.07 (49.01)	4.11 (4.09)	9.53 (9.51)	16.37 (16.37)	-	9.99 (9.91)
[Cu(MPMA) <sub>2</sub> (H <sub>2</sub> O) <sub>2</sub> ]Cl <sub>2</sub>	CuC <sub>24</sub> H <sub>28</sub> N <sub>4</sub> S <sub>2</sub> O <sub>2</sub> Cl <sub>2</sub>	Dark Green	85	603.16	>200	47.78 (47.71)	4.67 (4.63)	9.28 (9.31)	10.63 (10.59)	11.77 (11.69)	10.53 (10.60)
[Zn(MPMA) <sub>2</sub> ]SO <sub>4</sub>	ZnC <sub>24</sub> H <sub>24</sub> N <sub>4</sub> S <sub>3</sub> O <sub>4</sub>	Dirty White	85	594.03	>200	48.52 (48.49)	4.07 (4.01)	9.43 (9.46)	16.19 (16.17)	-	11.01 (11.09)

# 3.4.2 Molar Conductivity

The molar conductance values obtained for the complexes in DMF at the concentration 10<sup>-3</sup> M are presented in **Table-3.2**.

**Table-3.2: Molar Conductance Values of the MPMA Metal Complexes** 

S.No.	Complexes	Molar Conductance $(\Omega^{-1} \operatorname{cm}^2 \operatorname{mol}^{-1})$
1.	$[Fe(MPMA)_2(H_2O)_2]Cl_3$	189
2.	[Co(MPMA) <sub>2</sub> (H <sub>2</sub> O) <sub>2</sub> ](NO <sub>3</sub> ) <sub>2</sub>	142
3.	[Ni(MPMA) <sub>2</sub> ]SO <sub>4</sub>	75
4.	[Cu(MPMA) <sub>2</sub> (H <sub>2</sub> O) <sub>2</sub> ]Cl <sub>2</sub>	146
5.	[Zn(MPMA) <sub>2</sub> ]SO <sub>4</sub>	82

The data presented in Table-3.2 indicate that all the complexes are electrolytic in nature since their values lies in the range of 75-189 ohm<sup>-1</sup> cm<sup>2</sup> mole<sup>-1</sup>. The data also suggest that anions are present outside the coordination sphere. [5]

### 3.4.3 <sup>1</sup>H-NMR Spectra

The <sup>1</sup>H NMR spectrum of the Schiff base ligand MPMA is shown in **Fig.3.2.**There is a sharp singlet peak at  $\partial$  8.7 ppm assignable to azomethine proton (-HC=N) whereas a multiplet observed at  $\partial$  7.1- 8.7 ppm is due to aromatic protons of pyrrole moiety and 2-(methylthio)aniline. A singlet found at  $\partial$  2.4 ppm corresponds to –CH<sub>3</sub> protons. However, azomethine proton undergoes shielding upon coordination as observed in <sup>1</sup>H NMR spectrum of Zn<sup>II</sup> complex (**Fig.3.3**) and appears at 8.3 ppm confirming the coordination through azomethine nitrogen. The multiplet corresponding to aromatic ring protons appears in the region  $\partial$  6.5–8.9 ppm and are slightly shifted upfield, indicating the involvement of sulphur atom of aromatic ring in coordination. A singlet peak at  $\partial$  2.5 ppm corresponds to aliphatic methyl protons. A sharp singlet peak at  $\partial$  10 ppm is attributed to free -NH protons of pyrrole ring in both the spectra. Thus a comparison of signals due to the ligand and the complex, it

is confirmed that the condensation of pyrrole-2-carboxaldehyde with 2-(methylthio)aniline resulted in the formation of 2-(methylsulfanyl)-N-(1H-pyrrol-2-ylmethylidene) aniline and also coordination of zinc metal to Schiff base. [6-8] The <sup>1</sup>H NMR signals of the ligand MPMA and Zn<sup>II</sup> complex are listed in **Tables-3.3 and 3.4.** 

Table-3.3: <sup>1</sup>H NMR Spectral Data of the Ligand MPMA

S.No.	Signal Position (ppm)	Relative No. Of Protons	Multiplicity	Inference
1.	10	1H	Singlet	Free -NH of pyrrole ring
2.	8.7	1H	Singlet	-HC=N (Azomethine proton)
3.	7.1-8.7	7H	Multiplet	Ar-CH
4.	2.4	3Н	Singlet	-CH <sub>3</sub>

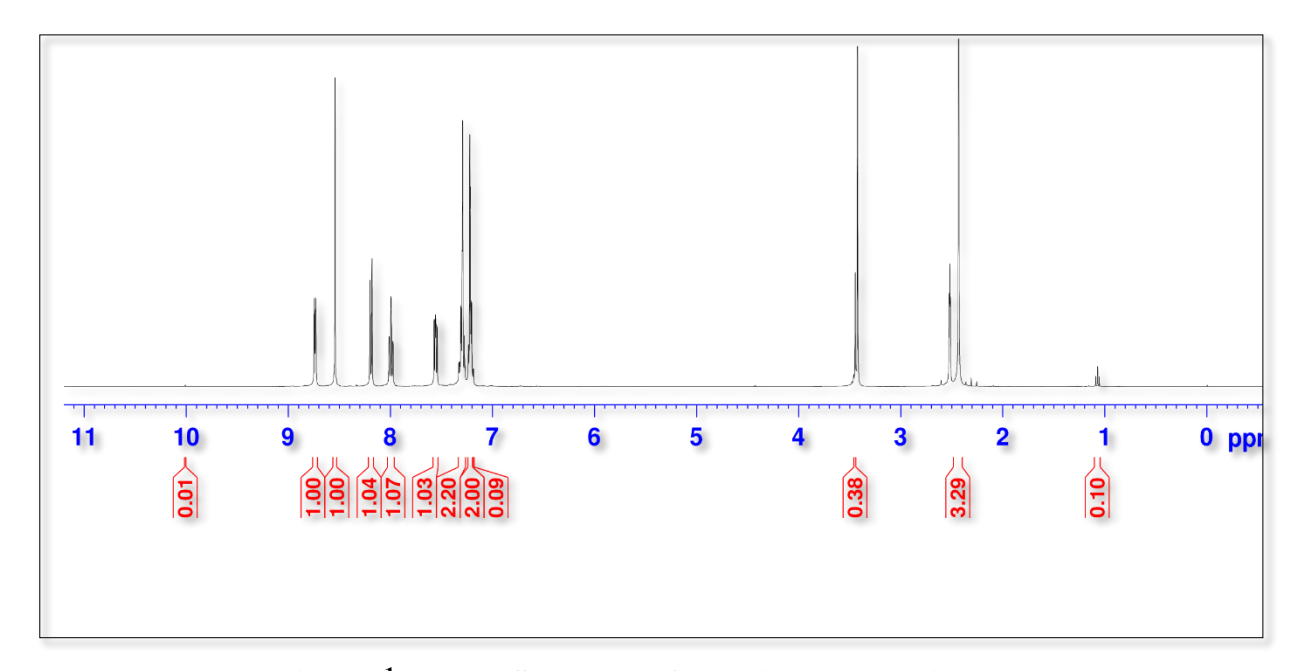


Fig. 3.2 <sup>1</sup>H NMR Spectrum of the Ligand MPMA

Table-3.4: <sup>1</sup>H NMR Spectral Data of the [Zn(MPMA)<sub>2</sub>]SO<sub>4</sub>

S.No.	Signal Position (ppm)	Relative No. Of Protons	Multiplicity	Inference
1.	10	2H	Singlet	Free -NH of pyrrole ring
2.	8.3	2H	Singlet	-HC=N(Azomethine protons)
3.	6.5-8.9	14H	Multiplet	Ar-CH
4.	2.5	6Н	Singlet	-CH <sub>3</sub>

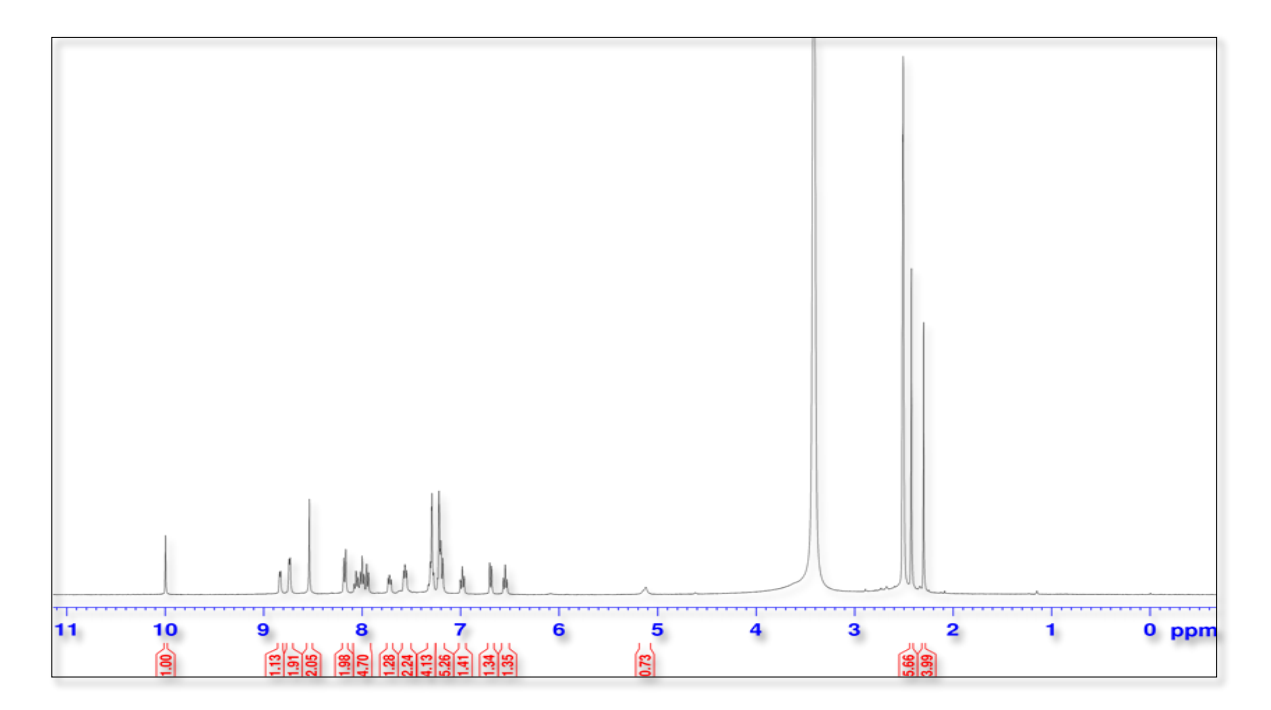


Fig. 3.3 <sup>1</sup>H NMR Spectrum of the [Zn(MPMA)<sub>2</sub>]SO<sub>4</sub>

# 3.4.4 FT-IR Spectra

The structure and bonding in a metal complex can be confirmed by comparing the IR spectrum of the free ligand with that of corresponding metal complex. The nature of the metal-ligand bond, the stability of the complex, and the vibrational modes of the ligand change upon complexation due to weakening/strengthening of the bonds involved. The subsequent changes in the positions of the bands have all been studied using infrared spectra of the metal complexes

**Table-3.5** and **Fig.3.4-3.9** show the FT-IR spectra of the ligand MPMA and its metal complexes. The spectrum of the ligand MPMA shows a strong band at 1670 cm<sup>-1</sup> due to azomethine group (-CH=N) stretching.[9] Coordination of the ligand to the metal ion through the azomethine group, reduces the electron density around nitrogen atom and lowers the  $\dot{\nu}_{\text{(-CH=N)}}$  stretching frequency. The band due to azomethine linkage is now moved to lesser frequencies in the spectra of all complexes (1602 to 1651cm<sup>-1</sup>) signifying the coordination of azomethine nitrogen to metal ions. [10] The coordination of azomethine nitrogen to metal ions is further supported by the presence of bands in the region of 408-452 cm<sup>-1</sup> which are due to M-N linkage.[11]

Band at 787 cm<sup>-1</sup> in the spectra of ligand corresponds to C-S vibration. This band is shifted to lower frequencies (727-758 cm<sup>-1</sup>) in the spectra of all complexes indicating the involvement of sulphur atom in coordination. It is further supported by the presence of bands in the range 630-665cm<sup>-1</sup> which are due to M-S linkage. [12]

From the above observations, it is clear that the Schiff base ligand MPMA is coordinated to the metal ions through sulphur atom and azomethine nitrogen in a bidentate fashion. However, the bands at 3385, 3355 and 3431 cm<sup>-1</sup> in the spectra of iron(III), cobalt(II) and copper(II) complexes respectively are due coordination of water molecules.[13]

Table-3.5: Selected FT-IR Absorption Frequencies (cm<sup>-1</sup>) of the Ligand MPMA and its Metal Complexes

Compound	VCH=N	V C=N	V C-S	VM-N	V M-S	V (O-H) H2O
MPMA	1670	1383	787			-
[Fe(MPMA) <sub>2</sub> (H <sub>2</sub> O) <sub>2</sub> ]Cl <sub>3</sub>	1608	1344	737	452	663	3385
[Co(MPMA) <sub>2</sub> (H <sub>2</sub> O) <sub>2</sub> ](NO <sub>3</sub> ) <sub>2</sub>	1632	1356	758	432	630	3355
[Ni(MPMA) <sub>2</sub> ]SO <sub>4</sub>	1630	1364	756	422	630	-
[Cu(MPMA) <sub>2</sub> (H <sub>2</sub> O) <sub>2</sub> ]Cl <sub>2</sub>	1602	1319	727	416	665	3431
[Zn(MPMA) <sub>2</sub> ] SO <sub>4</sub>	1651	1369	732	408	661	-

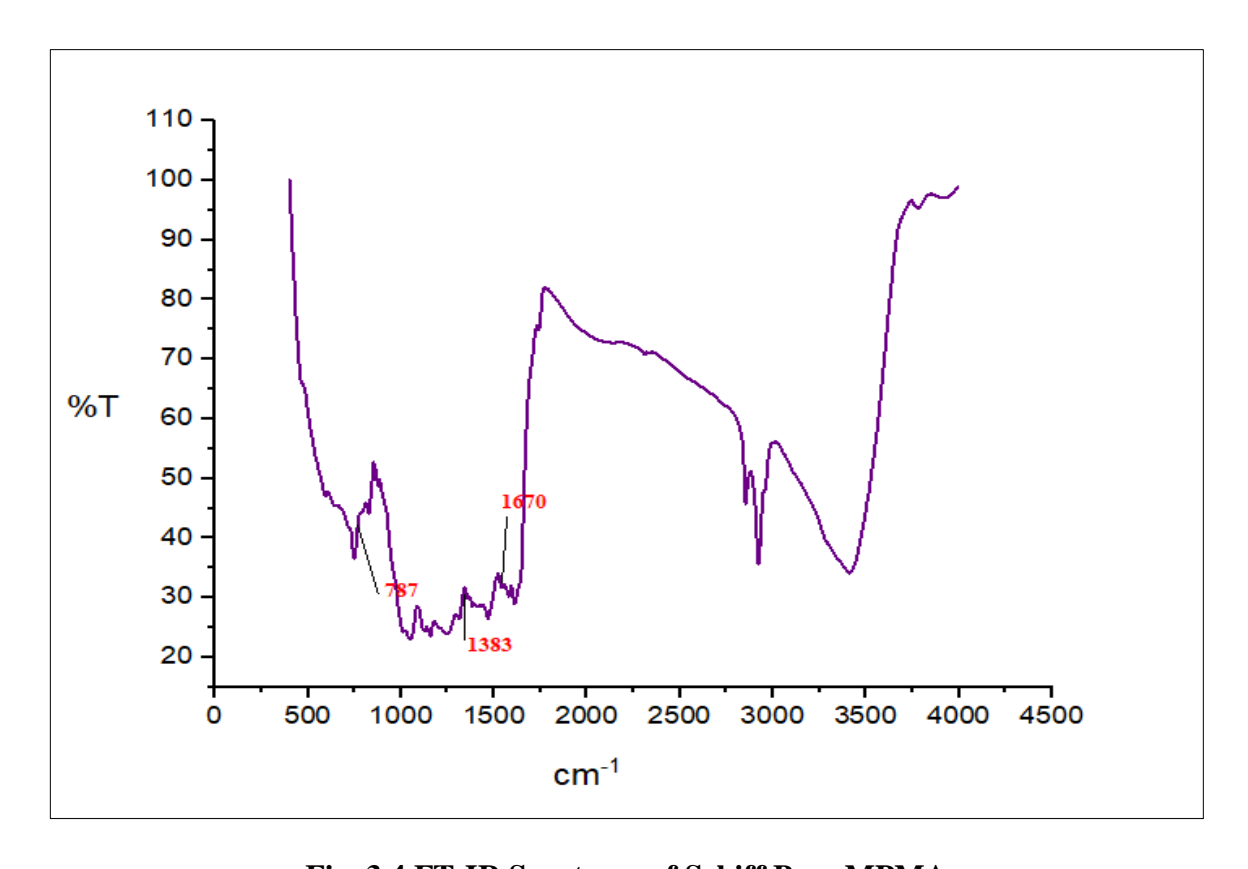


Fig. 3.4 FT-IR Spectrum of Schiff Base MPMA

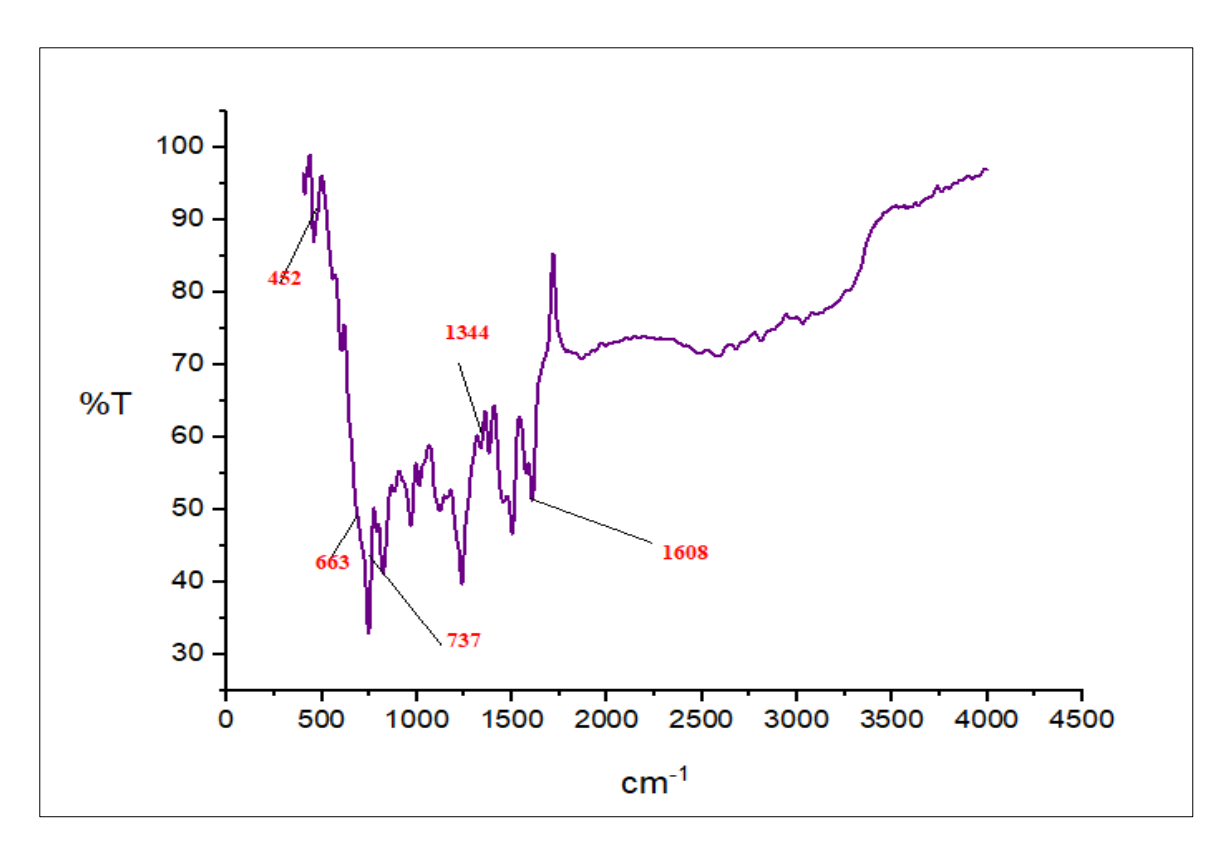


Fig. 3.5 FT-IR Spectrum of [Fe(MPMA)<sub>2</sub>(H<sub>2</sub>O)<sub>2</sub>]Cl<sub>3</sub>

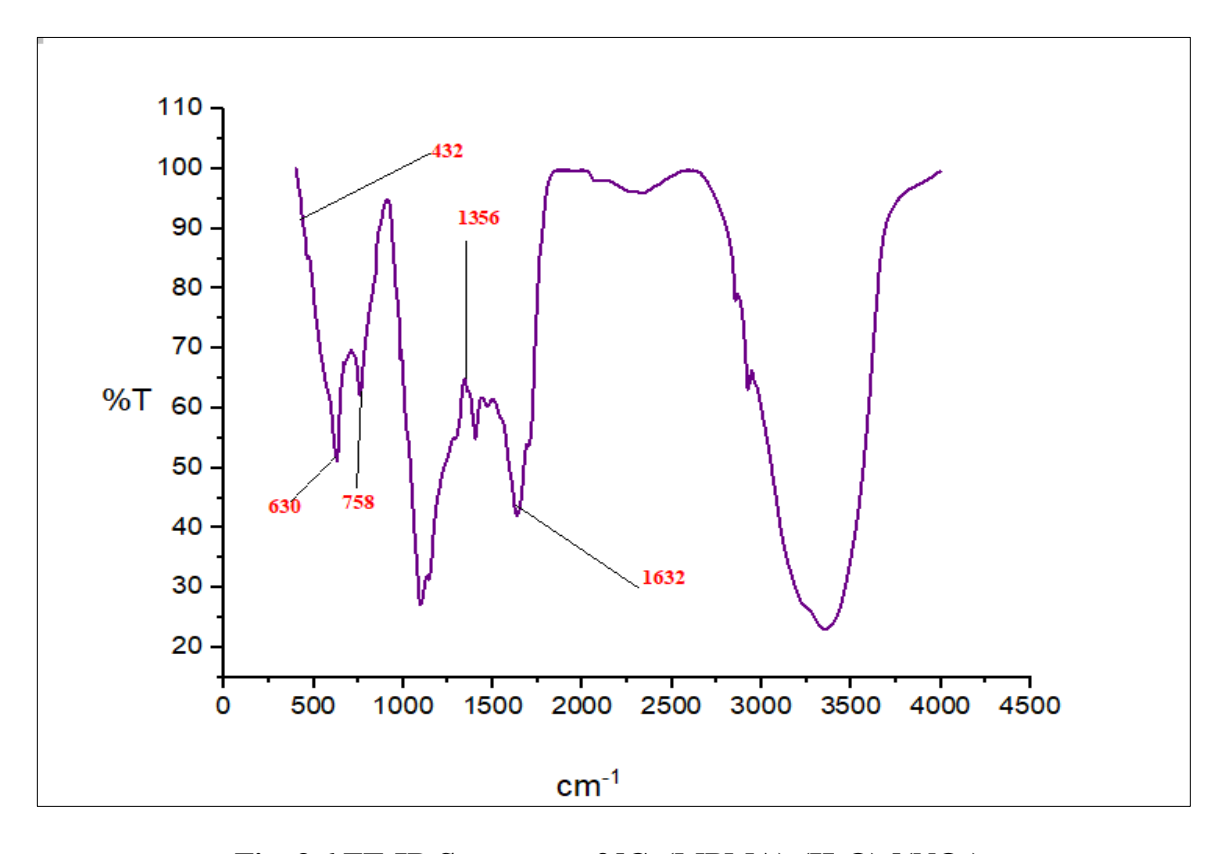


Fig. 3.6 FT-IR Spectrum of  $[Co(MPMA)_2(H_2O)_2](NO_3)_2$ 

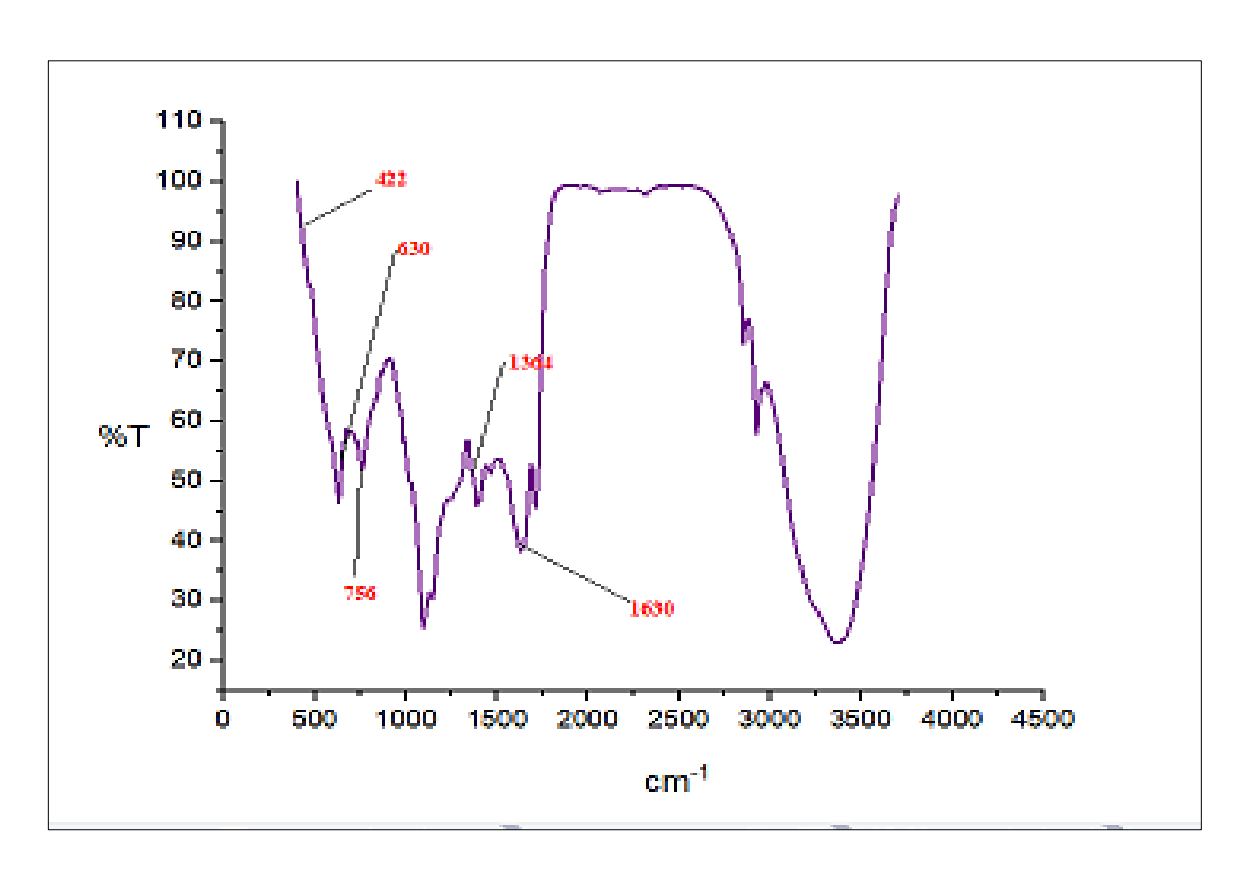


Fig. 3.7 FT-IR Spectrum of [Ni(MPMA)<sub>2</sub>]SO<sub>4</sub>

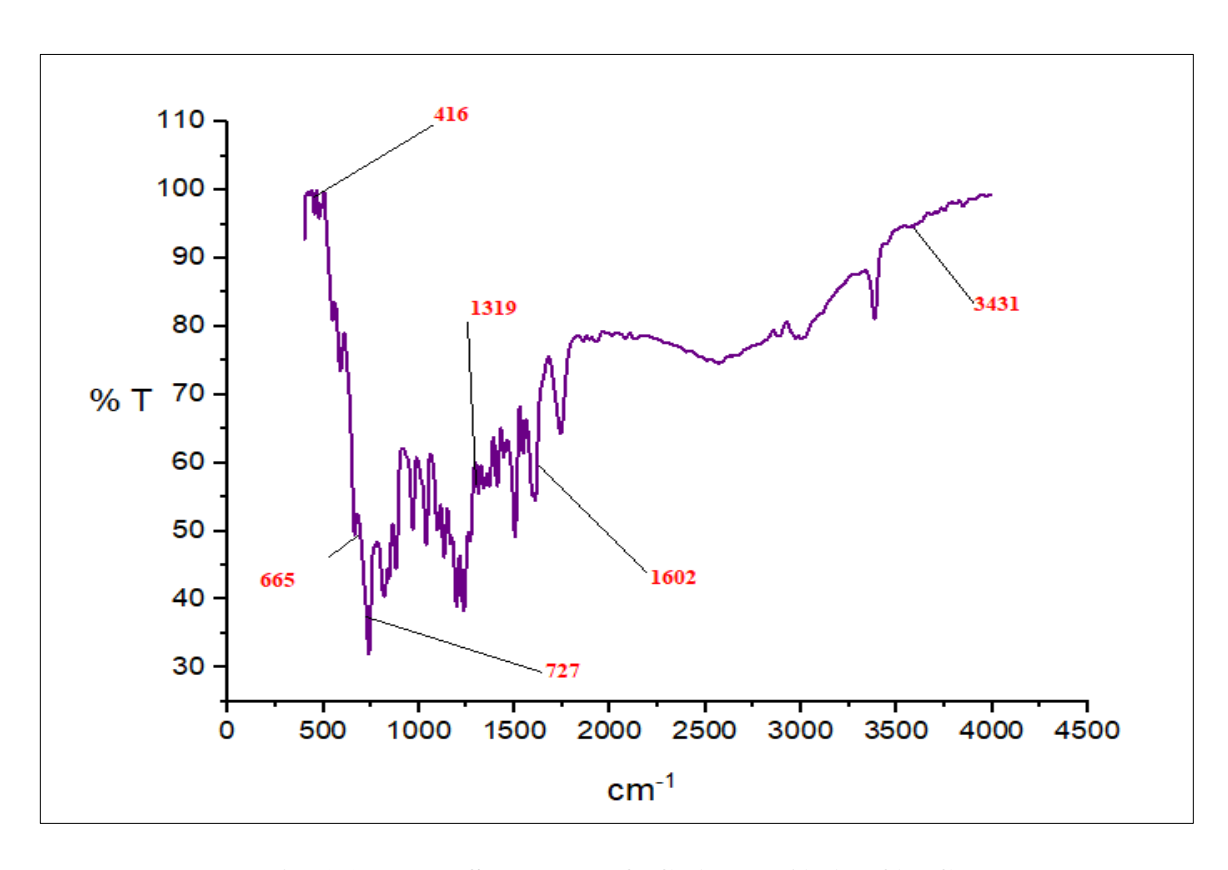


Fig. 3.8 FT-IR Spectrum of  $[Cu(MPMA)_2(H_2O)_2]Cl_2$ 

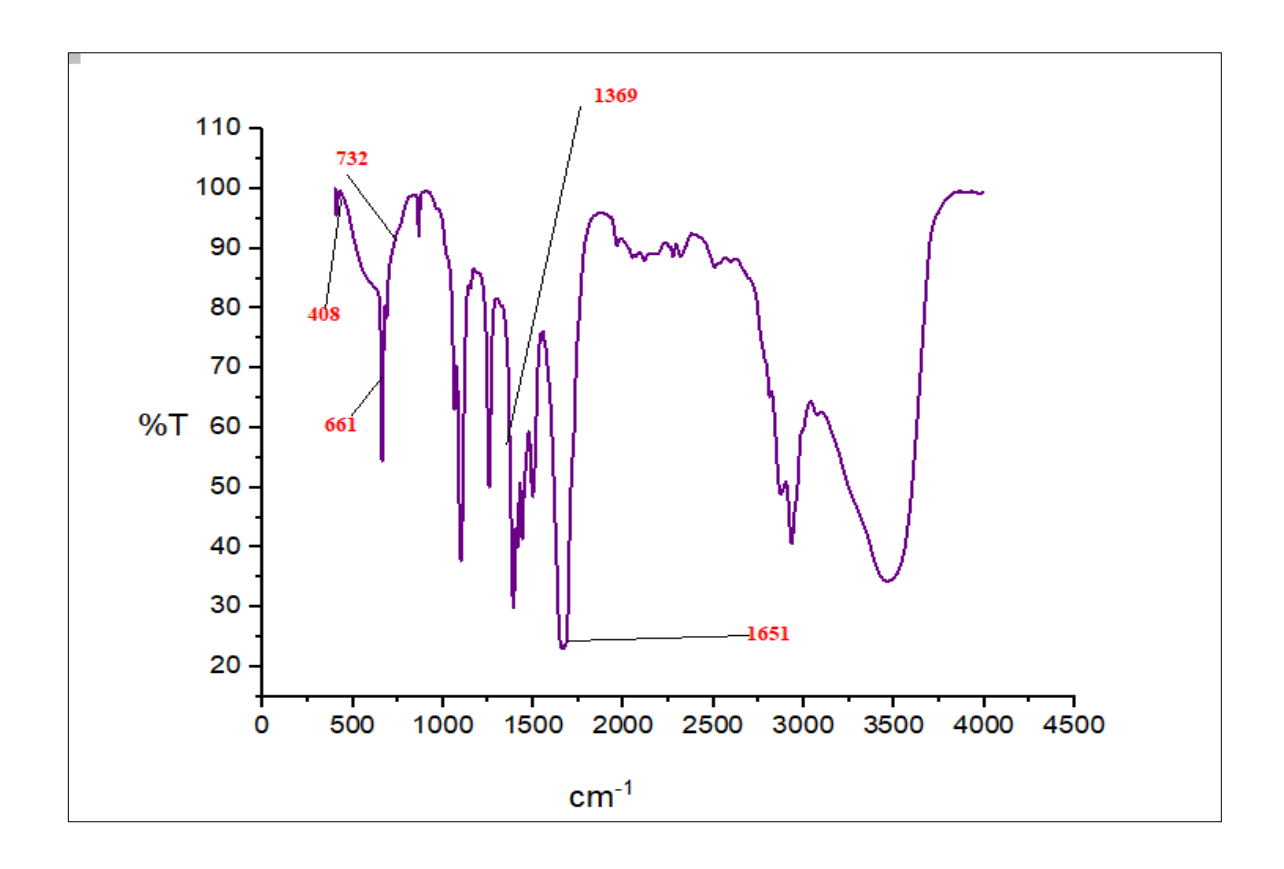


Fig. 3.9 FT-IR Spectrum of [Zn(MPMA)2]SO4

# 3.4.5 UV-Visible Spectra and Magnetic Moment

The electronic spectra of the ligand MPMA and its complexes in DMSO (10<sup>-3</sup>mol<sup>-1</sup>) are furnished in **Fig. 3.10-3.15**. The absorption region, band maxima and their probable assignments are given in **Table-3.6**. The values of magnetic moments of all the metal ions in the complexes are also given in table-3.6.

The electronic spectrum of free Schiff base MPMA shows mainly two bands at  $37,878 \text{ cm}^{-1}$  and  $32,362 \text{ cm}^{-1}$  which are attributed to  $\pi$ - $\pi$ \*and n- $\pi$ \* transition of the azomethine group of ligand and these transitions are shifted to longer wavelengths in the spectra of the complexes. They are in the ranges 37,174 - $36,363 \text{ cm}^{-1}$  and 32,051-  $29,850 \text{ cm}^{-1}$  respectively indicating the coordination of ligand to metal through azomethine moiety. In general, the electronic transitions for Fe<sup>III</sup> systems are spin forbidden and hence weak, and are often masked by charge transfer bands. The broad intense and poorly resolved band

at 32,051 cm<sup>-1</sup> may be assigned to MLCT. The high intensity band at 37,174 cm<sup>-1</sup> is of ligand origin assignable to intraligand  $\pi$  -  $\pi$ \* transition. The other weaker bands are attributed to metal centred d-d transitions. The magnetic moment of iron (III) at room temperature is 1.92 BM and is consistent with octahedral geometry.[14]

The spectrum of cobalt (II) complex is consistent with the formation of an octahedral geometry with the appearance of three absorption bands at 10,266, 24,213 and 24,449 cm<sup>-1</sup> which correspond to  ${}^4T_{1g(F)} \rightarrow {}^4T_{2g(F)}$ ,  ${}^4T_{1g(F)} \rightarrow {}^4A_{2g(F)}$ ,  ${}^4T_{1g(F)} \rightarrow {}^4T_{2g(P)}$  transitions, respectively. The magnetic moment of  $Co^{II}$  complex at room temperature is 4.28 BM which corresponds to three unpaired electrons. This value is consistent with high spin  $d^7$  complexes, which is greater than the spin-only value (3.87) because of the orbital angular momentum contribution in the  $d^7$  -system, and it is close to the values reported for an octahedral geometry. [15] At room temperature,  $Ni^{II}$  complex shows diamagnetic behaviour, indicating the square planar environment around the  $Ni^{II}$  ion [16]. The solution spectrum of the nickel (II) complex exhibits absorption in the region 24,390 cm<sup>-1</sup>. This transition corresponds to  ${}^1A_{1g} \rightarrow {}^1Eg$  ( $d_{xy}$ ,  $d_{yz} \rightarrow d_{x2-y2}$ ) and reveals that the nickel (II) complex possesses square planar geometry.

For octahedral  $Cu^{II}$  complex, the expected transition is  ${}^2E_g \rightarrow {}^2T_{2g}$ . Due to the Jahn–Teller distortions,  $Cu^{II}$  complex gives a broad absorption band at 14,430 cm $^{-1}$ . The  $t_{2g}$  orbitals have a lower energy than the  $e_g$  orbitals in an octahedral crystal field. Because, the  $t_{2g}$  are directed between bond axes whereas the  $e_g$  point along bond axes, this reflects the orientation of the orbitals. The electrons are shielded as a result of this, which explains why the Jahn-Teller effect is only important for odd number occupancy of the  $e_g$  level. These data suggest a distorted octahedral geometry for  $Cu^{II}$  complex. The observed magnetic moment of the  $Cu^{II}$  complex is 1.94 BM which confirms octahedral geometry.[17]

The electronic spectrum of  $Zn^{II}$  complex does not show any d–d transition due to  $d^{10}$  electronic configuration, but only charge transfer absorption is observed at 24, 570 cm<sup>-1</sup>. The Zn (II) complex is diamagnetic in nature. [18]

**Table- 3.6: Electronic Spectral Data of the Ligand MPMA and its Metal Complexes** 

Compound	Wavelength λ <sub>max</sub> (nm)	Wave number $\bar{v}$ (cm <sup>-1</sup> )	Assignment	Geometry and Magnetic Moment
	264	37, 878	π-π*	-
MPMA	309	32, 362	n-π*	
[Fe(MPMA) <sub>2</sub> (H <sub>2</sub> O) <sub>2</sub> ]Cl <sub>3</sub>	269	37, 174	Intraligand π-π*	Octahedral 1.92 BM
	312	32, 051	MLCT	1.72 BW
	974	10, 266	$^{4}T_{1g(F)}>^{4}T_{2g(F)}$	0 1 1 1
$[Co(MPMA)_2(H_2O)_2](NO_3)_2$	413	24, 213	${}^{4}T_{1g(F)}> {}^{4}A_{2g(F)}$	Octahedral 4.28 BM
	409	24, 449	$^{4}T_{1g(F)}> ^{4}T_{2g(p)}$	1.20 511
[Ni(MPMA) <sub>2</sub> ]SO <sub>4</sub>	410	24, 390	$^{1}A_{1g}\rightarrow ^{1}Eg$	Square Planar Diamagnetic
[Cu(MPMA) <sub>2</sub> (H <sub>2</sub> O) <sub>2</sub> ]Cl <sub>2</sub>	693	14, 430	$^{2}\text{E}_{g} \rightarrow ^{2}\text{T}_{2g}$	Distorted Octahedral 1.94 BM
[Zn(MPMA) <sub>2</sub> ]SO <sub>4</sub>	407	24, 570	LMCT	Tetrahedral Diamagnetic

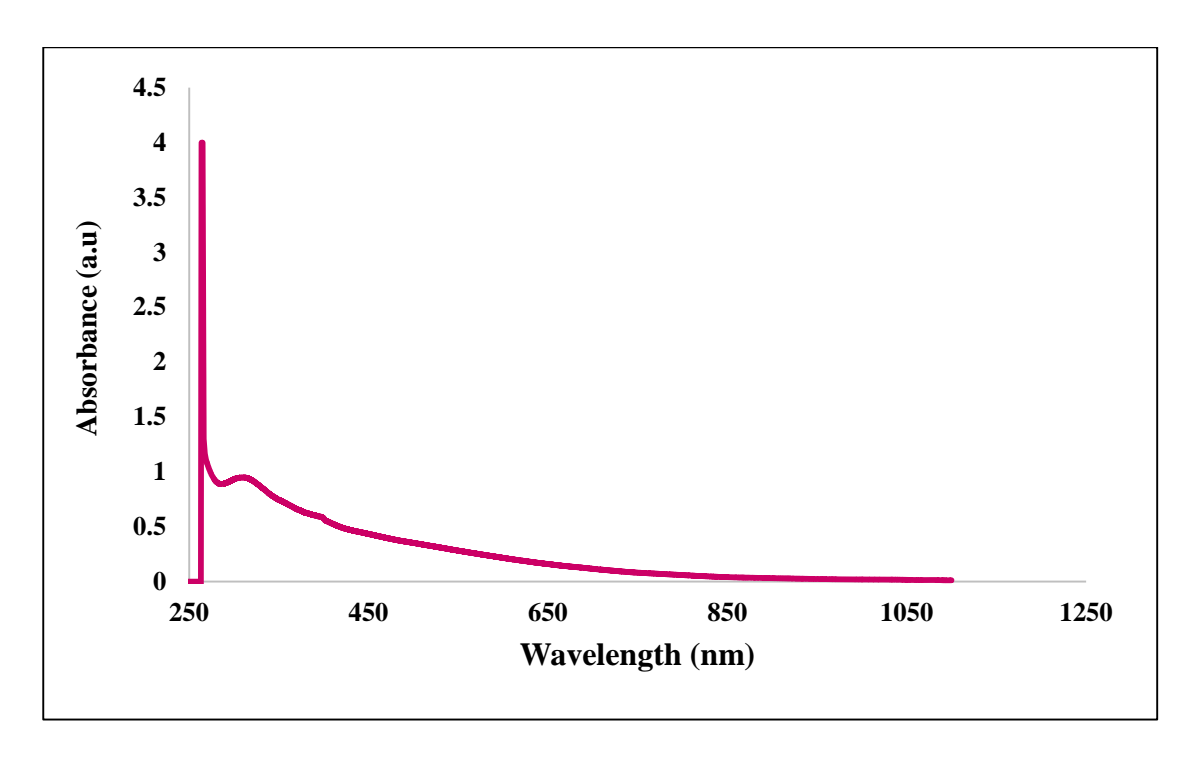


Fig. 3.10 UV- Vis Spectrum of Schiff Base MPMA

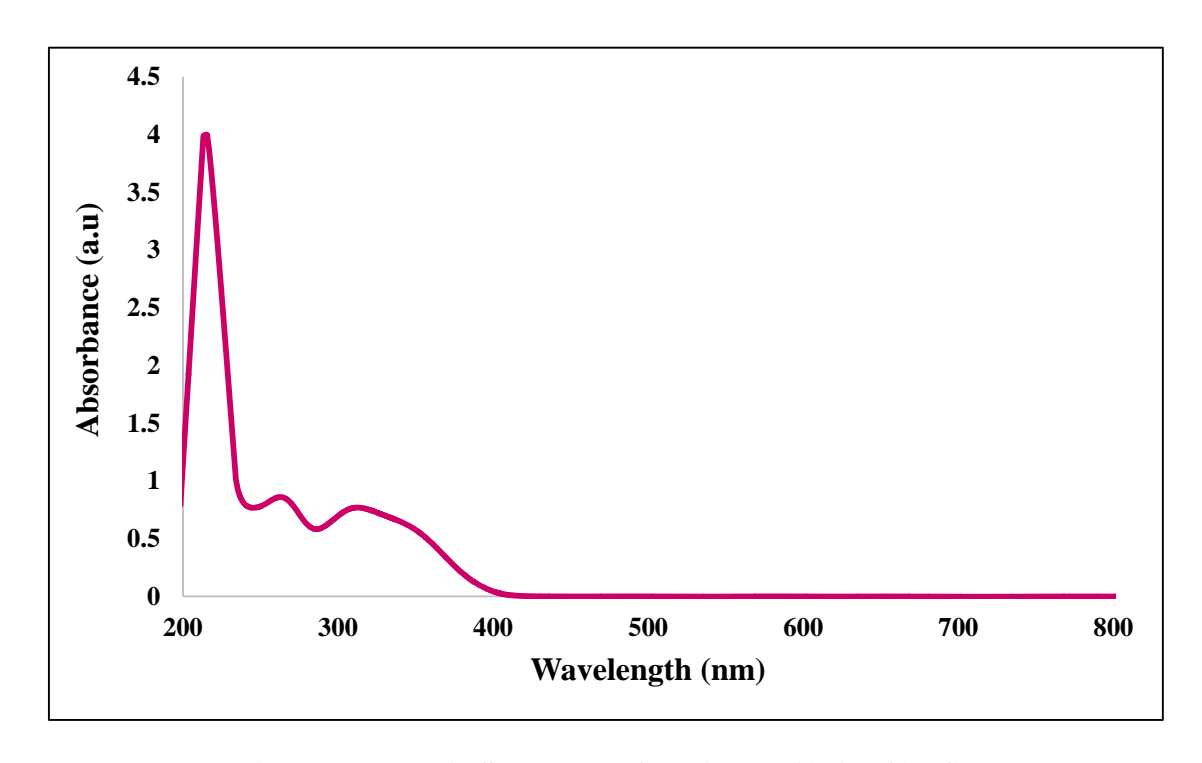


Fig. 3.11 UV- Vis Spectrum of [Fe(MPMA)<sub>2</sub>(H<sub>2</sub>O)<sub>2</sub>]Cl<sub>3</sub>

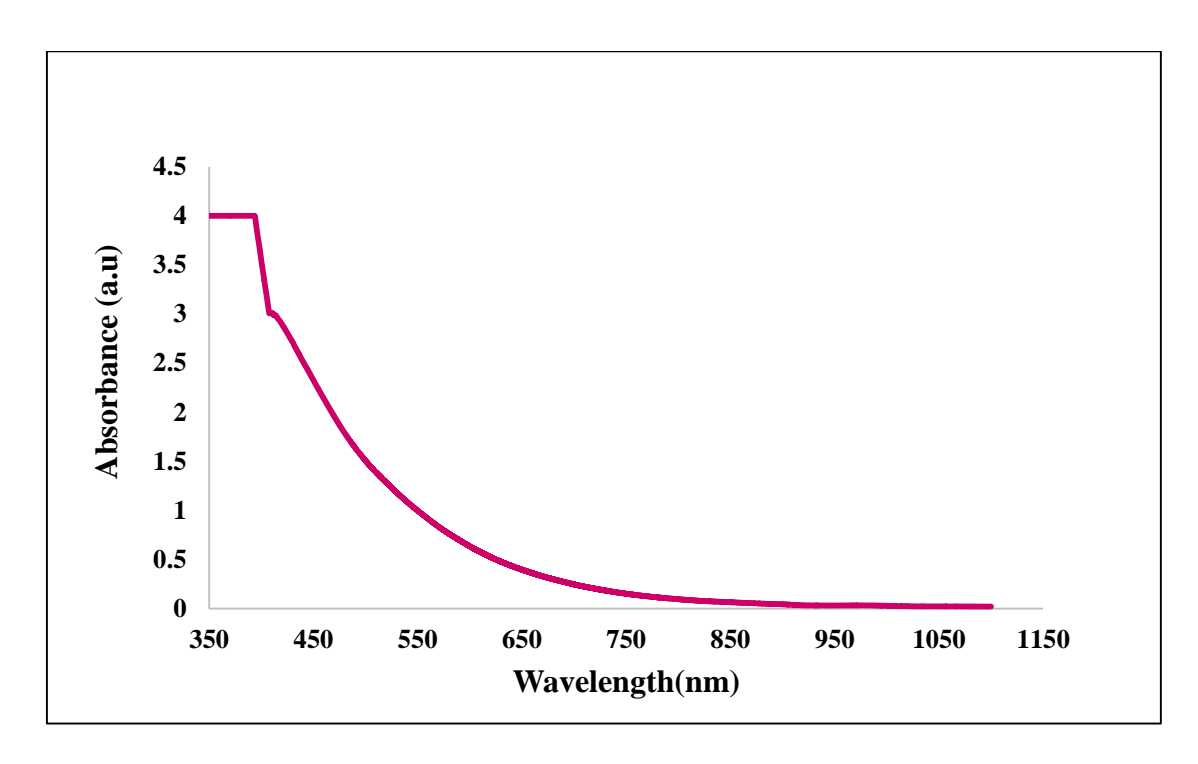


Fig. 3.12 UV- Vis Spectrum of [Co(MPMA)<sub>2</sub>(H<sub>2</sub>O)<sub>2</sub>](NO<sub>3</sub>)<sub>2</sub>

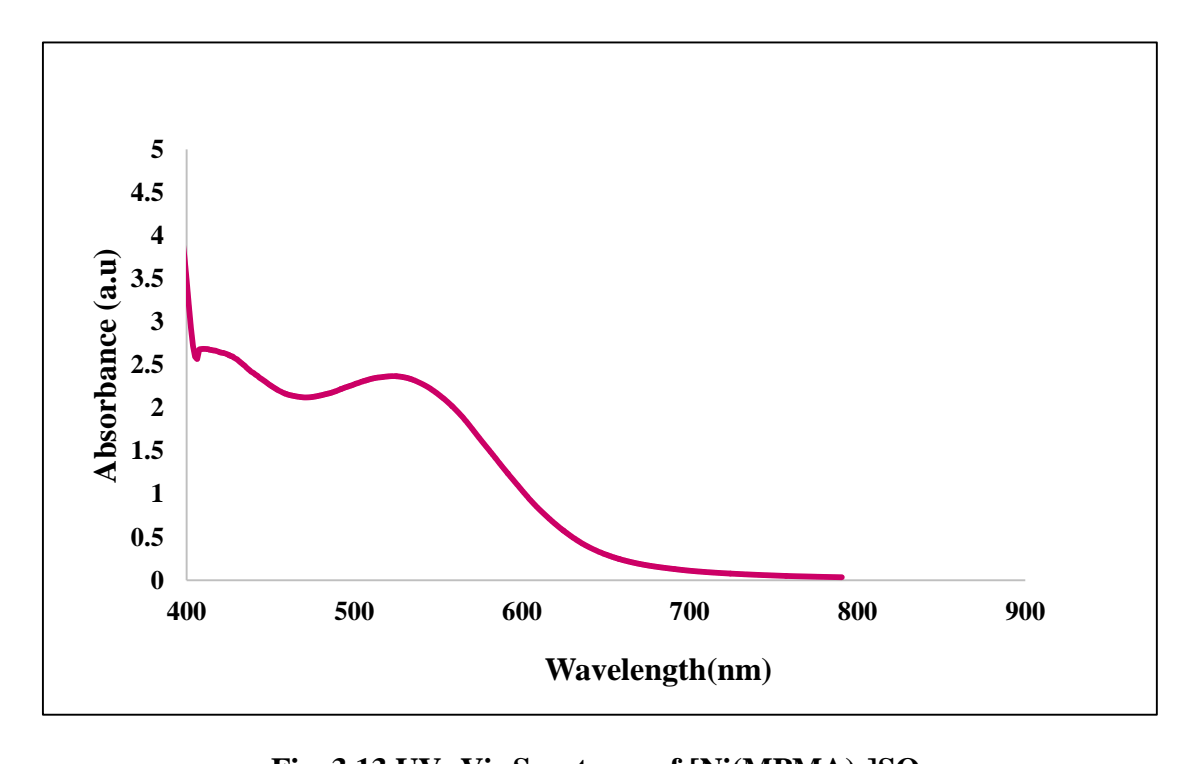


Fig. 3.13 UV- Vis Spectrum of [Ni(MPMA)2]SO4

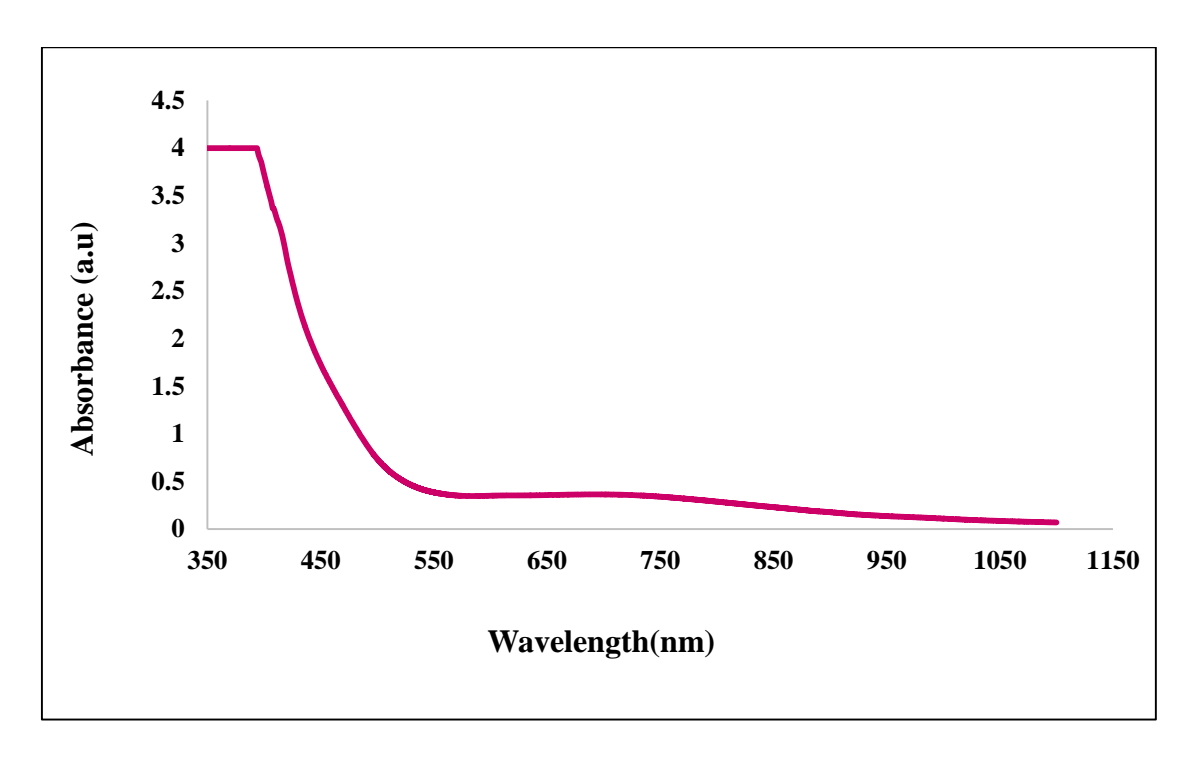


Fig. 3.14 UV- Vis Spectrum of  $[Cu(MPMA)_2(H_2O)_2]Cl_2$ 

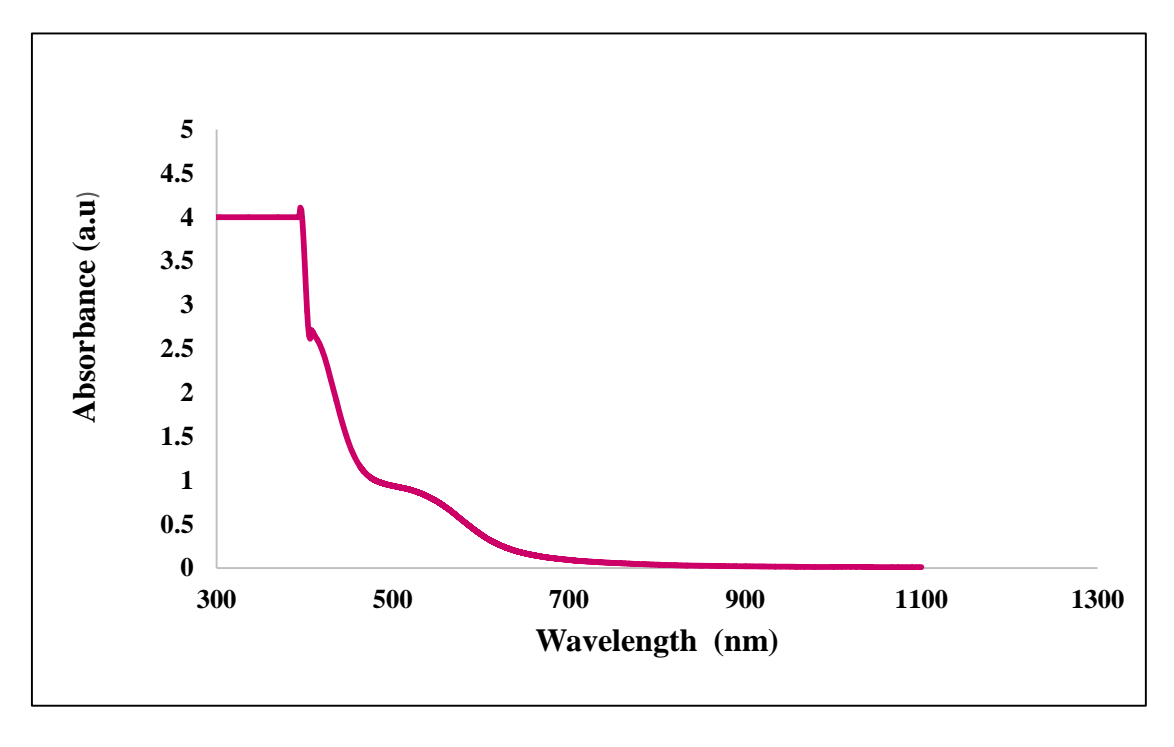


Fig. 3.15 UV- Vis Spectrum of [Zn(MPMA)2]SO4

## 3.4.6 Electron Paramagnetic Resonance Spectrum of [Cu(MPMA)2(H2O)2]Cl2

The EPR spectra of the metal complexes provide information that are important in understanding the environment of metal ion in complexes such as the geometry, nature of the ligating sites and the degree of covalency of the metal-ligand bonds.

The room temperature X band EPR spectrum of the Cu<sup>II</sup> complex is shown in **Fig.3.16**. The Cu<sup>II</sup> complex shows one intense absorption band in the high field region and is found to be isotropic due to the tumbling motion of the molecules.

The  $g_{iso}$  value of the copper (II) complex is found to be 2.08 which is slightly higher than g value of free electron (2.0023), indicating the covalent nature of the metal-ligand bonds and the presence of one unpaired electron in the  $d_{x^2-y^2}$  orbital of the  $Cu^{II}$  ion.

The magnetic moment of 1.94 BM for the copper complex indicates the presence of one unpaired electron, showing the complex to be mononuclear in nature. Thus, the electronic spectrum, magnetic moment value and the relative isotropic g parameter indicate octahedral geometry around Cu<sup>2+</sup> metal ion.[19]

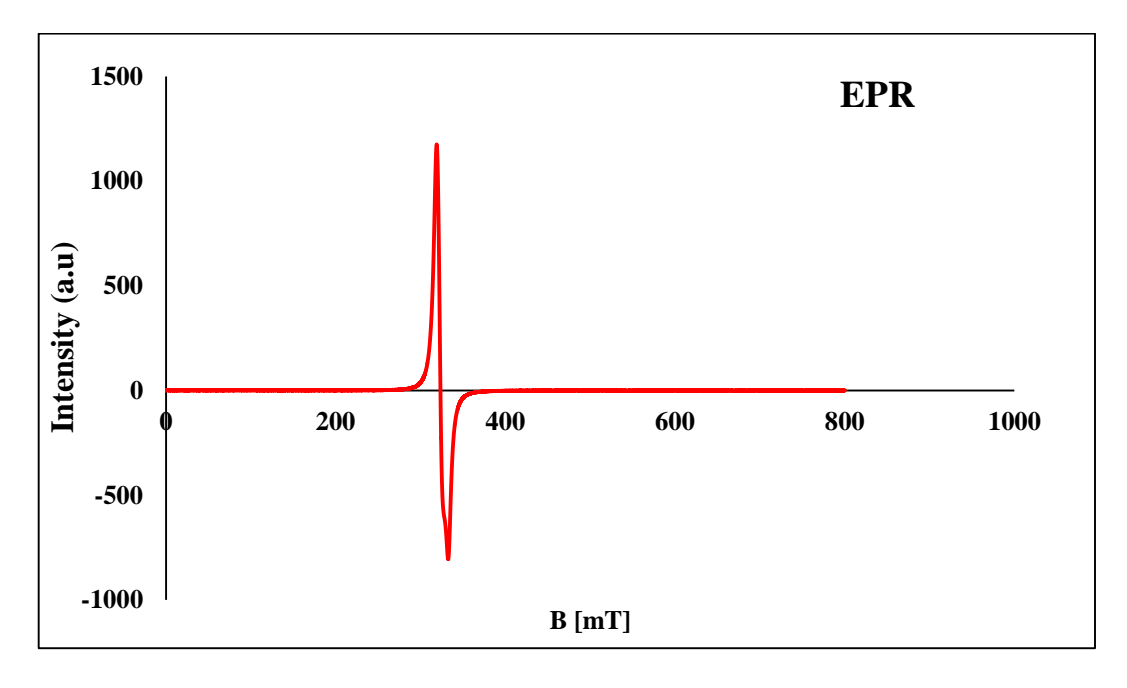


Fig.3.16 EPR Spectrum of [Cu(MPMA)<sub>2</sub>(H<sub>2</sub>O)<sub>2</sub>]Cl<sub>2</sub>

# 3.4.7 LC-MS Spectrum of [Zn(MPMA)2]SO4

The LC-MS spectrum of zinc complex is shown in Fig. 3.17.The zinc complex  $(ZnC_{24}H_{24}N_4S_3O_4)$  with ligand shows the molecular ion peak at  $m/z = 597(M+3)^+$  which corresponds to protonated species. The data confirms the stoichiometry of the metal complex as tetrahedral type.

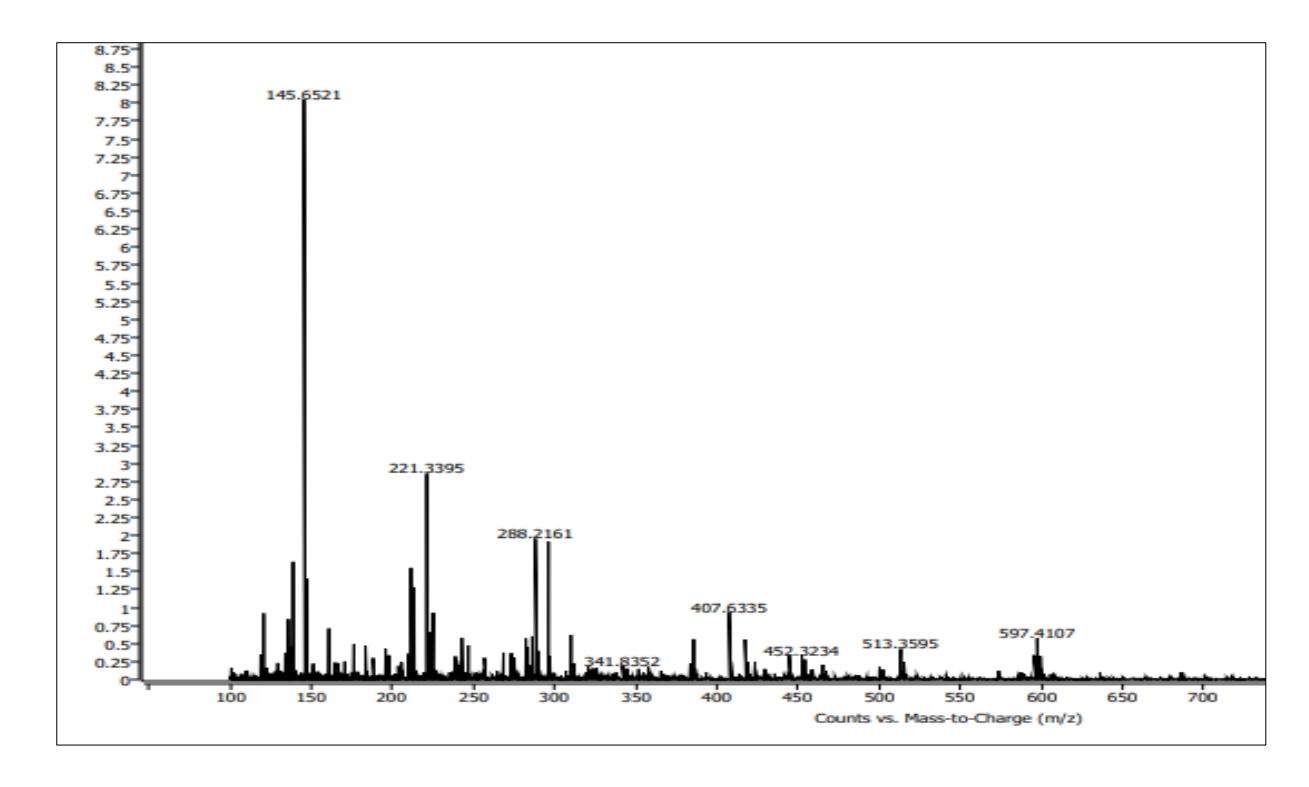


Fig. 3.17 LC-MS Spectrum of [Zn(MPMA)<sub>2</sub>]SO<sub>4</sub>

# 3.4.8 Cyclic Voltammetry Studies

The cyclic voltammograms obtained for metal complexes are shown in **Fig.3.18** - **3.22** and the data are summarized in **Table-3.7**.

The cyclic voltammogram of  $[Fe(MPMA)_2(H_2O)_2]Cl_3$  complex in DMF solution measured at  $0.1Vs^{-1}$  registers a cathodic peak potential  $(E_{pc})$  value at -1051 mV and corresponding anodic peak potential value  $(E_{pa})$  at -682.72 mV. These peak potential values suggest the reduction of  $Fe^{III}$  to  $Fe^{II}$ . The separation between the anodic and cathodic peak potential  $(\Delta E_p)$  is 368.28 mV. This indicates a quasi- reversible redox couple. The ratio of

current peaks  $(I_{pa}/I_{pc})$  at  $0.1 \text{Vs}^{-1}$  is -1.76. This value is less than one suggesting one electron transfer is followed by a chemical reaction. (i.e. EC mechanism is observed).[21]

The cyclic voltammogram of  $[Co(MPMA)_2(H_2O)_2](NO_3)_2$  complex in DMF solution measured at  $0.1Vs^{-1}$  records a cathodic peak potential  $(E_{pc})$  value at -522.01 mV and corresponding anodic peak potential value  $(E_{pa})$  at -43.55 mV. These peak potential values suggest the reduction of  $Co^{II}$  to  $Co^{I}$ . The separation between the anodic and cathodic peak potential  $(\Delta E_p)$  is 478.46 mV. This indicates a quasi-reversible redox couple. The ratio of current peaks at  $0.1Vs^{-1}$  is -2.85. This value is less than one signifying one electron transfer is followed by a chemical reaction. (ie EC mechanism is observed).[22]

The cyclic voltammogram of [Ni(MPMA)<sub>2</sub>]SO<sub>4</sub> complex in DMF solution measured at  $0.1 \text{Vs}^{-1}$  registers a cathodic peak potential ( $E_{pc}$ ) value at -1247 mV and corresponding anodic peak potential value ( $E_{pa}$ ) at -575.82 mV. These peak potential values suggest the reduction of Ni<sup>II</sup> to Ni<sup>I</sup>. The separation between the anodic and cathodic peak potential ( $\Delta E_p$ ) is 671.18 mV. This indicates a quasi-reversible redox couple. The ratio of current peaks at  $0.1 \text{Vs}^{-1}$  is -1.51. This value is less than one suggesting one electron transfer is followed by a chemical reaction. (ie EC mechanism is observed).[23]

The cyclic voltammogram of  $[Cu(MPMA)_2(H_2O)_2]Cl_2$  measured at 0.1 Vs<sup>-1</sup> scan rate features the reduction of  $Cu^{II}$  to  $Cu^{II}$  at cathodic peak potential of -1006 mV. Reoxidation of  $Cu^{II}$  to  $Cu^{II}$  occurs at -819.21 mV at anodic peak potential upon scan reversal. The separation between the anodic and cathodic peak potentials ( $\Delta Ep$ ) is 186.79mV. This indicates a quasi-reversible redox couple. Further, the current peaks ratio at 0.1 Vs<sup>-1</sup> is 0.23. This value is less than one suggesting one electron transfer is followed by a chemical reaction. [24, 25]

The cyclic voltammogram of  $[Zn(MPMA)_2]SO_4$  complex in DMF solution measured at  $0.1Vs^{-1}$  registers a cathodic peak potential  $(E_{pc})$  value at -982.07 mV and corresponding

anodic peak potential value ( $E_{pa}$ ) at -753.27 mV. These peak potentials suggest the reduction of  $Zn^{II}$  to  $Zn^{I}$ . The separation between the anodic and cathodic peak potential ( $\Delta E_{p}$ ) is 228.8 mV. This indicates a quasi- reversible redox couple. The ratio of current peaks at 0.1Vs<sup>-1</sup> is -2.48. This value is less than one suggesting one electron transfer is followed by a chemical reaction (ie EC mechanism is observed).[26]

Table- 3.7: Cyclic Voltammetric Data for MPMA Metal Complexes in DMF solution at 298 K

Compound	E <sub>pc</sub> (mV)	$\begin{array}{c} E_{pa} \\ (mV) \end{array}$	$\begin{array}{c} \Delta E_p \\ (mV) \end{array}$	E <sub>1/2</sub> (mV)	I <sub>pc</sub> (μA)	I <sub>pa</sub> (μA)	$I_{\mathrm{pa}}/I_{\mathrm{pc}}$
[Fe(MPMA) <sub>2</sub> (H <sub>2</sub> O) <sub>2</sub> ]Cl <sub>3</sub>	-1051	-682.72	368.28	-866.86	-14.9	26.3	-1.76
$[\text{Co}(\text{MPMA})_2(\text{H}_2\text{O})_2](\text{NO}_3)_2$	-522.01	-43.55	478.46	-282.78	-12.7	36.2	-2.85
[Ni(MPMA) <sub>2</sub> ]SO <sub>4</sub>	-1247	-575.82	671.18	-911.41	-29.1	44.1	-1.51
$[Cu(MPMA)_2(H_2O)_2]Cl_2$	-1006	-819.21	186.79	-912.60	-78.8	-18.2	0.23
[Zn(MPMA) <sub>2</sub> ] SO <sub>4</sub>	-982.07	-753.27	228.8	-867.67	-11.81	29.3	-2.48

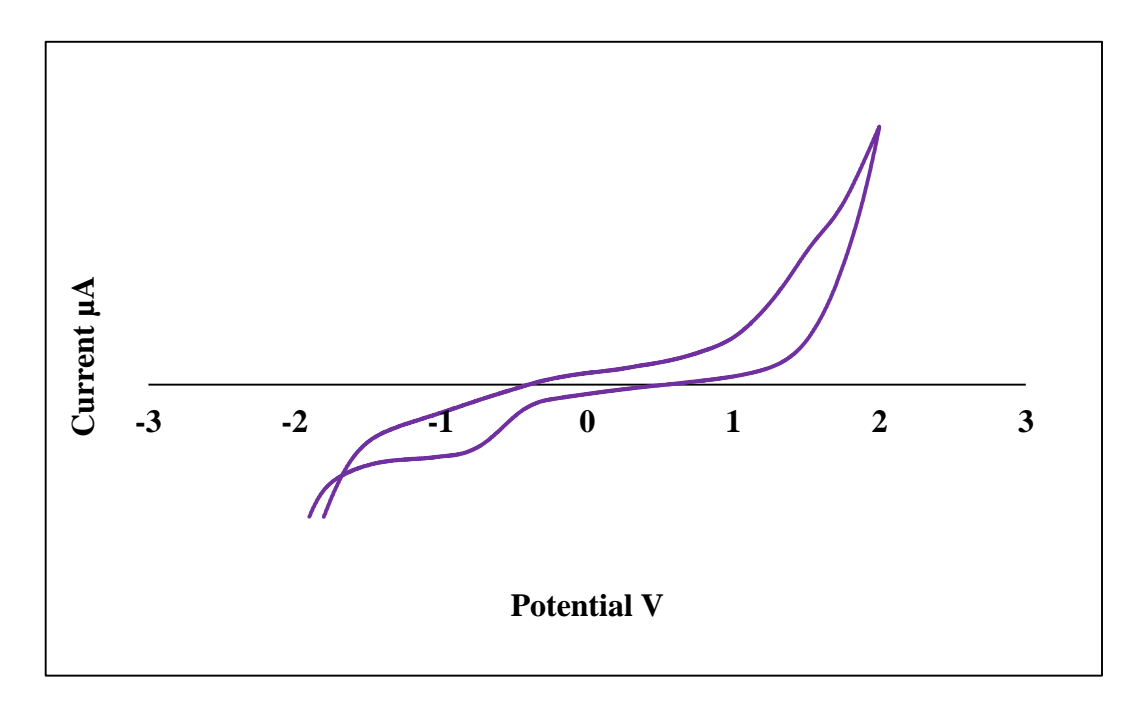
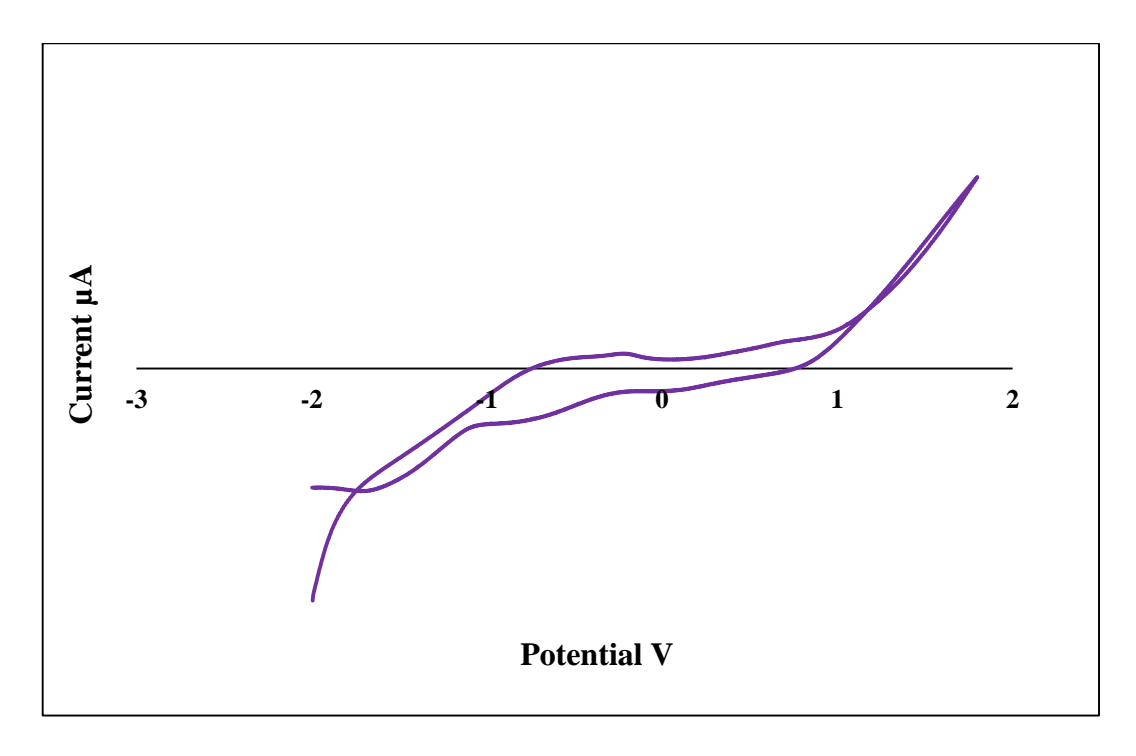
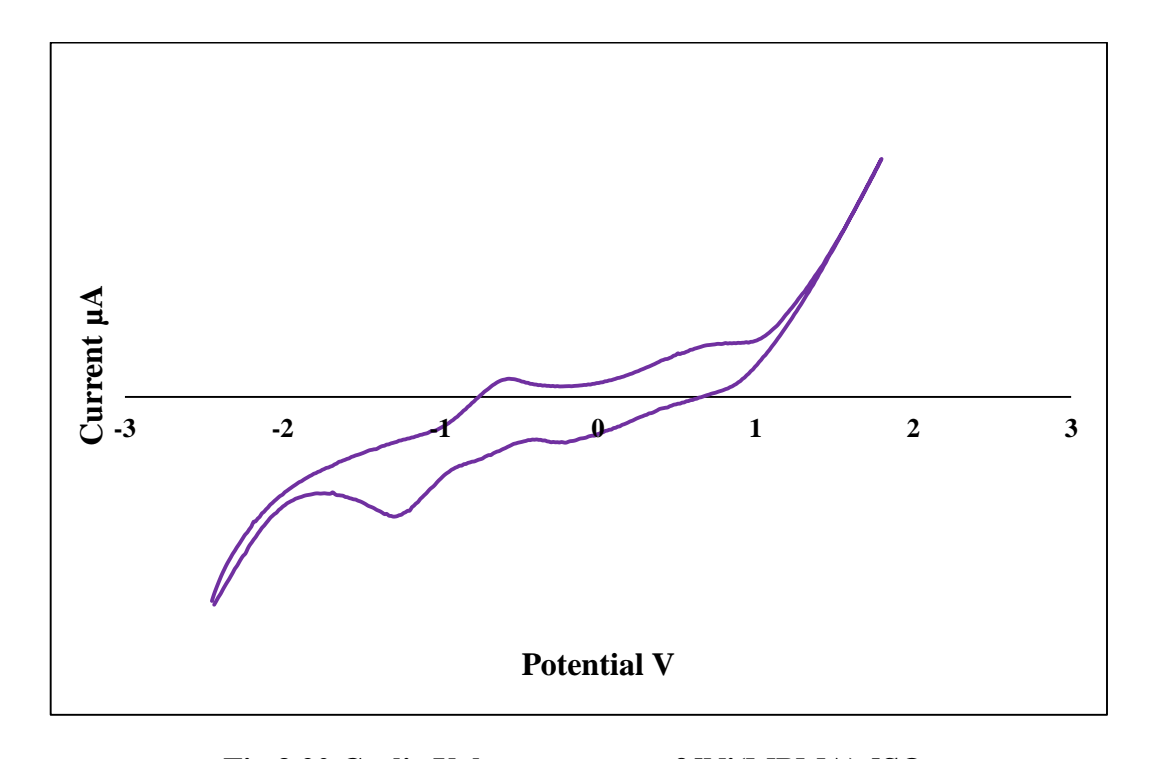


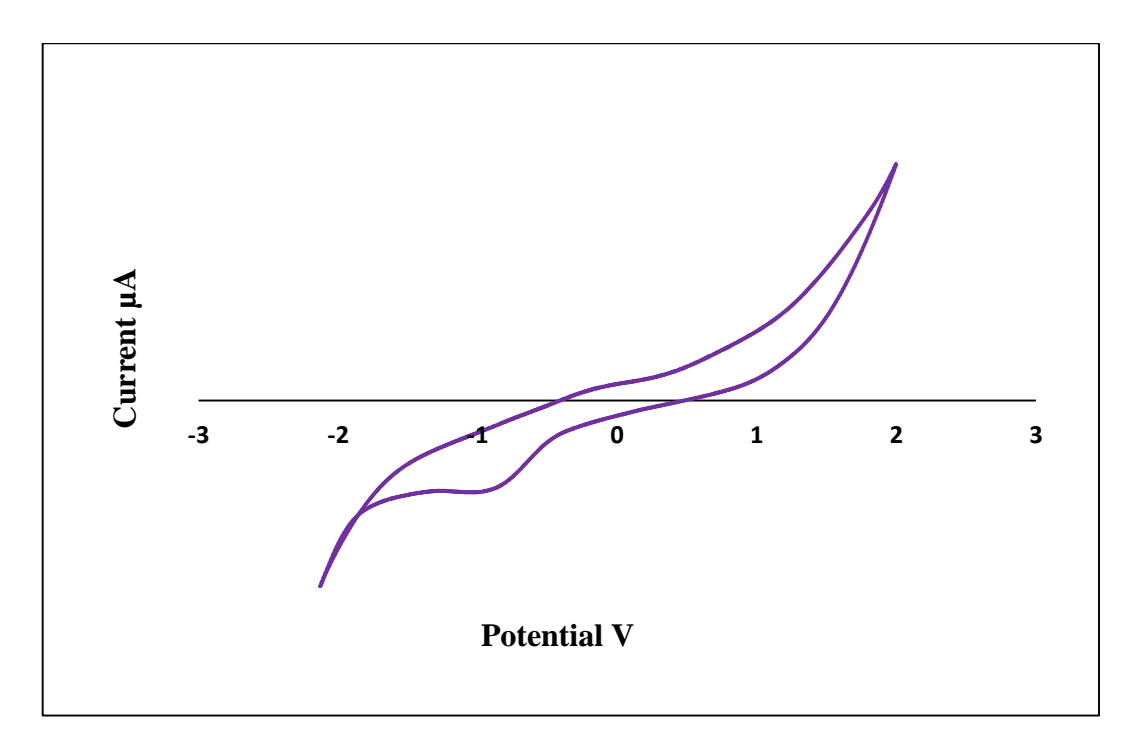
Fig. 3.18 Cyclic Voltammogram of [Fe(MPMA)<sub>2</sub>(H<sub>2</sub>O)<sub>2</sub>]Cl<sub>3</sub>



 $Fig. 3.19 \ Cyclic \ Voltammogram \ of \ [Co(MPMA)_2(H_2O)_2](NO_3)_2$ 



 $Fig. 3.20 \ Cyclic \ Voltammogram \ of \ [Ni(MPMA)_2]SO_4$ 



 $Fig. 3.21\ Cyclic\ Voltammogram\ of\ [Cu(MPMA)_2(H_2O)_2]Cl_2$ 

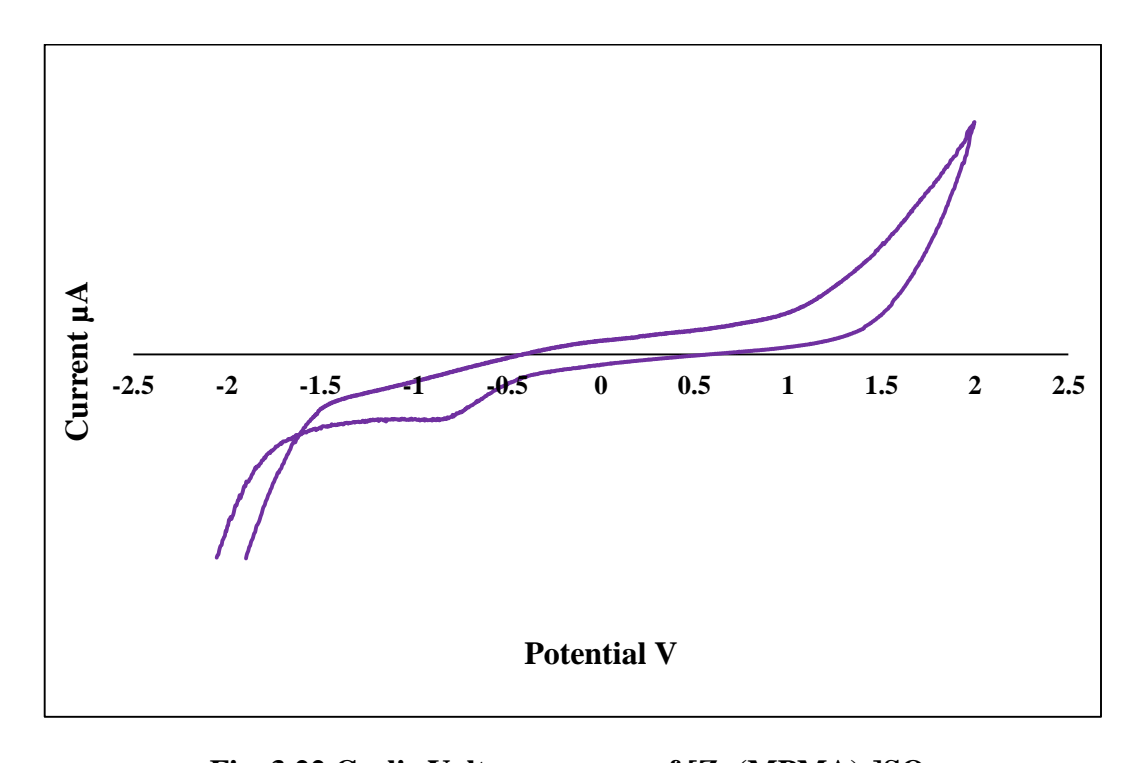


Fig. 3.22 Cyclic Voltammogram of [Zn(MPMA)<sub>2</sub>]SO<sub>4</sub>

### **3.4.9** Thermal Decomposition Studies

The thermograms of Schiff base metal complexes are given in the **Fig.3.23-3.27**. The correlation between different decomposition steps of the compounds and the corresponding weight losses are discussed in terms of the proposed formula of the compounds. The decomposition temperatures of the metal complexes acquired from their thermograms and other thermal data are presented in **Table-3.8** 

The TG/DTG curves of the [Fe(MPMA)<sub>2</sub>(H<sub>2</sub>O)<sub>2</sub>]Cl<sub>3</sub> complex is shown in Fig 3.22 and the thermal data are furnished in Table-3.8. This aqua complex on programmed heating records an endothermic peak at 164 °C corresponding to elimination of coordinated water molecules. The observed mass loss is 5.8% while the calculated mass loss is 5.7%. The existence of the anhydrous complex is seen in the temperature range 164-195 °C. The decomposition of the anhydrous complex occurs between 195 and 345 °C. The decomposition of the anhydrous complex is marked by the DTG peaks at 250 and 320° C. The mass of the final residue calculated as Fe<sub>2</sub>O<sub>3</sub> is 12.66% whereas the observed mass of the final residue is 13.5% of the original mass of the complex. It indicates a total mass loss of 86.5% i.e. the organic ligands and chloro groups are removed completely to produce iron(III) oxide as the final product of the thermal reaction.

The TG/DTG curves of [Co(MPMA)<sub>2</sub>(H<sub>2</sub>O)<sub>2</sub>](NO<sub>3</sub>)<sub>2</sub> complex is shown in Fig 3.23 and the thermal data are furnished in table-3.8. On programmed heating the complex exhibits 5.5% mass loss (calculated mass loss: 5.53%) and a DTG peak at 160 °C corresponding to removal of two water molecules. The anhydrous complex is available in the temperature range of 165-270 °C as shown by the horizontal portion of the TG plot. The anhydrous complex undergoes decomposition as revealed by DTG peak centered at 327 °C to form the final product of Co<sub>3</sub>O<sub>4</sub>. The observed mass of the metal oxide is 37% while the calculated value is 36.9%.

Table- 3.8: Stepwise Thermal Degradation Data of MPMA Metal Complexes obtained from TG-DTG Curve

G 1	a.	Temperature		% We	ight loss	% of I	NI. 4	
Compound Stages Range (° C)		Range (° C)	Assignments	Obs.	Calc.	Obs.	Calc.	Nature
IE-(MDMA) (II O) ICI	I	164	Loss of coordinated water molecules	5.8	5.7	12.5	12.66	E <sub>2</sub> O
$[Fe(MPMA)_2(H_2O)_2]Cl_3$	II	195-345	Loss of organic ligands and chloro groups	80.7	86.5	13.5	12.66	Fe <sub>2</sub> O <sub>3</sub>
[Co(MPMA) <sub>2</sub> (H <sub>2</sub> O) <sub>2</sub> ](NO <sub>3</sub> ) <sub>2</sub>	I	160	Loss of coordinated water molecules	5.5	5.53	37	36.9	Co <sub>3</sub> O <sub>4</sub>
	II	327	Loss of ligands	55.5	57.57			
[Ni(MPMA)2]SO4	I	250	Loss of ligands	70.5	73.65	20.6	12.7	NiO
[Cu(MPMA) <sub>2</sub> (H <sub>2</sub> O) <sub>2</sub> ]Cl <sub>2</sub>	I	175	Loss of coordinated water molecules	6.7	6.0	17.09	13.17	CuO
	II	285	Loss of ligands	73.3	71.72			
[Zn(MPMA) <sub>2</sub> ]SO <sub>4</sub>	I	200	Loss of ligands	70.43	72.82	20.57	13.69	ZnO

The TG/DTG curves obtained for [Ni(MPMA)<sub>2</sub>]SO<sub>4</sub> are shown in Fig. 3.24 and the thermal data are furnished in Table- 3.8.The DTG peak centered at 250°C indicates the decomposition of sulphato complex to form NiSO<sub>4</sub> as an intermediate. The existence of NiSO<sub>4</sub> as intermediate is revealed by the horizontal portion of TG curve in the temperature range 280-475 °C .The DTG peak centered at 535°C further shows the decomposition of NiSO<sub>4</sub>.

The TG/ DTG patterns obtained for [Cu(MPMA)<sub>2</sub>(H<sub>2</sub>O)<sub>2</sub>]Cl<sub>2</sub> complex are shown in the Fig. 3.25. The experimental data are listed in Table-3.8. The initial mass loss of 6.7% is due to the coordinated water (expected 6.0%). The DTG peak centered at 175°C indicates the elimination of water molecules. Another DTG peak centered at 285°C signifies the decomposition of the anhydrous complex to form copper chloride as an intermediate. Copper chloride is found to exist in the temperature range of 300 - 475°C after which it gradually decomposes to form copper oxide as the final residue. The DTG peak centered at 550°C is indicating the decomposition of copper chloride intermediate.

The TG/DTG patterns of [Zn(MPMA)<sub>2</sub>]SO<sub>4</sub>complex are reproduced in the Fig. 3.26 and the decomposition data are provided in Table 3.8. The stable complex begins to decompose at about 200 °C and decomposition continues upto 325 °C. This decomposition is indicated by the DTG peak centered at 275 °C to formation of zinc sulphate as an intermediate. The horizontal portion of the TG curve in the temperature range 350 -450 °C indicates the availability of zinc sulphate as an intermediate. The intermediate zinc sulphate further decomposes into zinc oxide as noted from the DTG peaks centered at 475 and 600 °C.

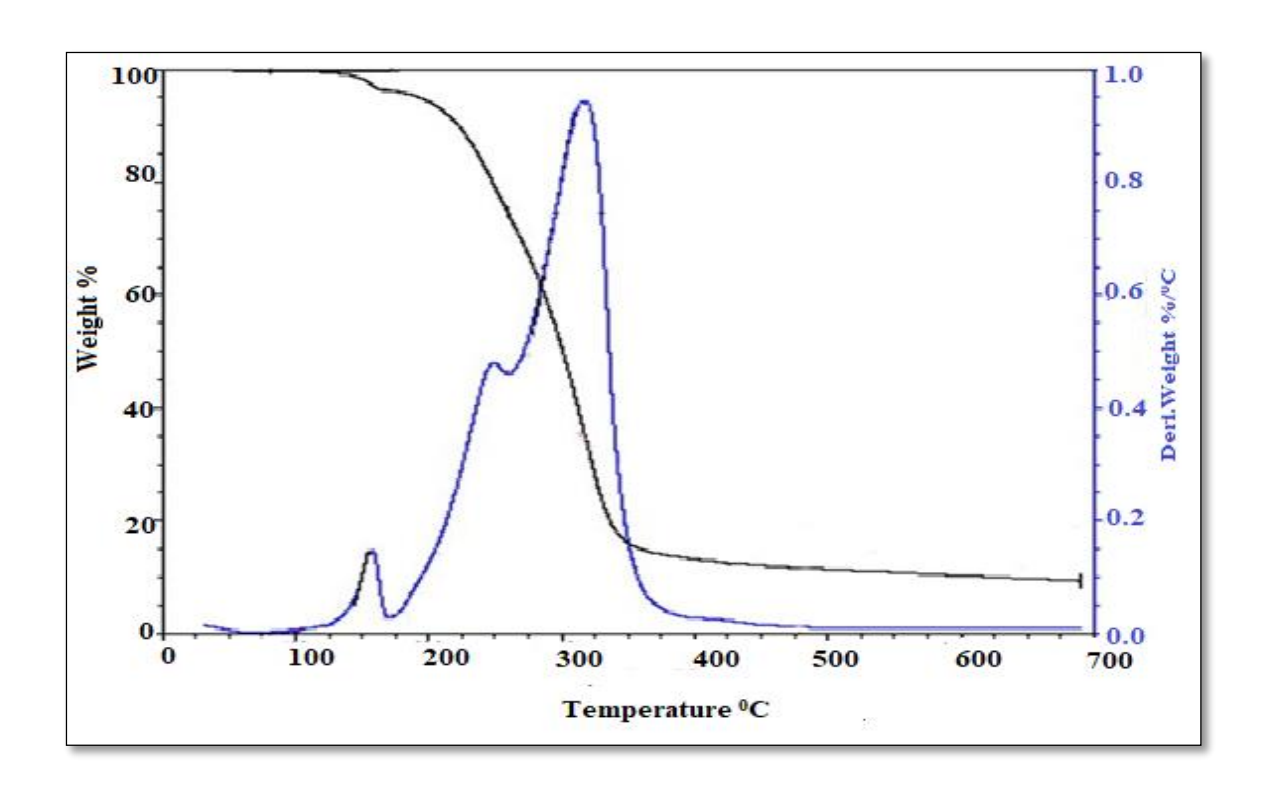


Fig.3.23 TG-DTG Curves of [Fe(MPMA)<sub>2</sub>(H<sub>2</sub>O)<sub>2</sub>]Cl<sub>3</sub>

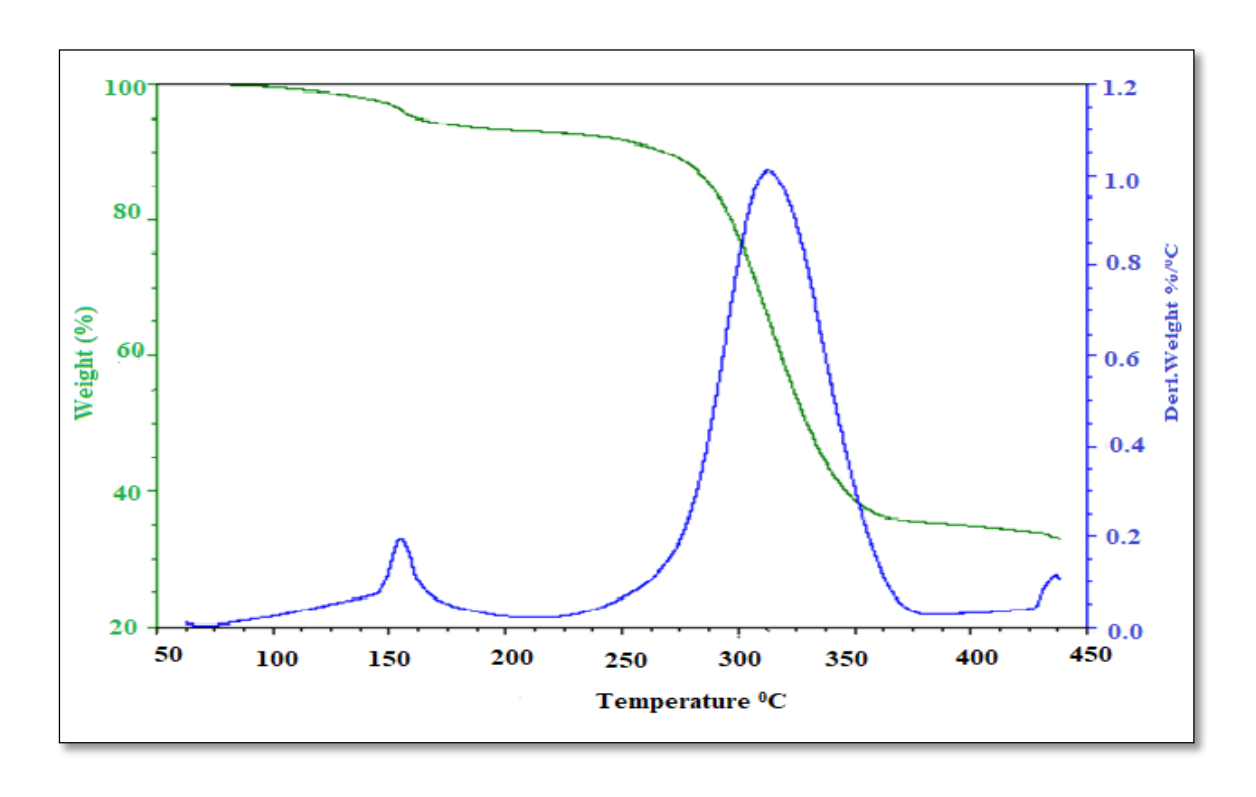


Fig.3.24 TG-DTG Curves of [Co(MPMA)2(H2O)2](NO3)2

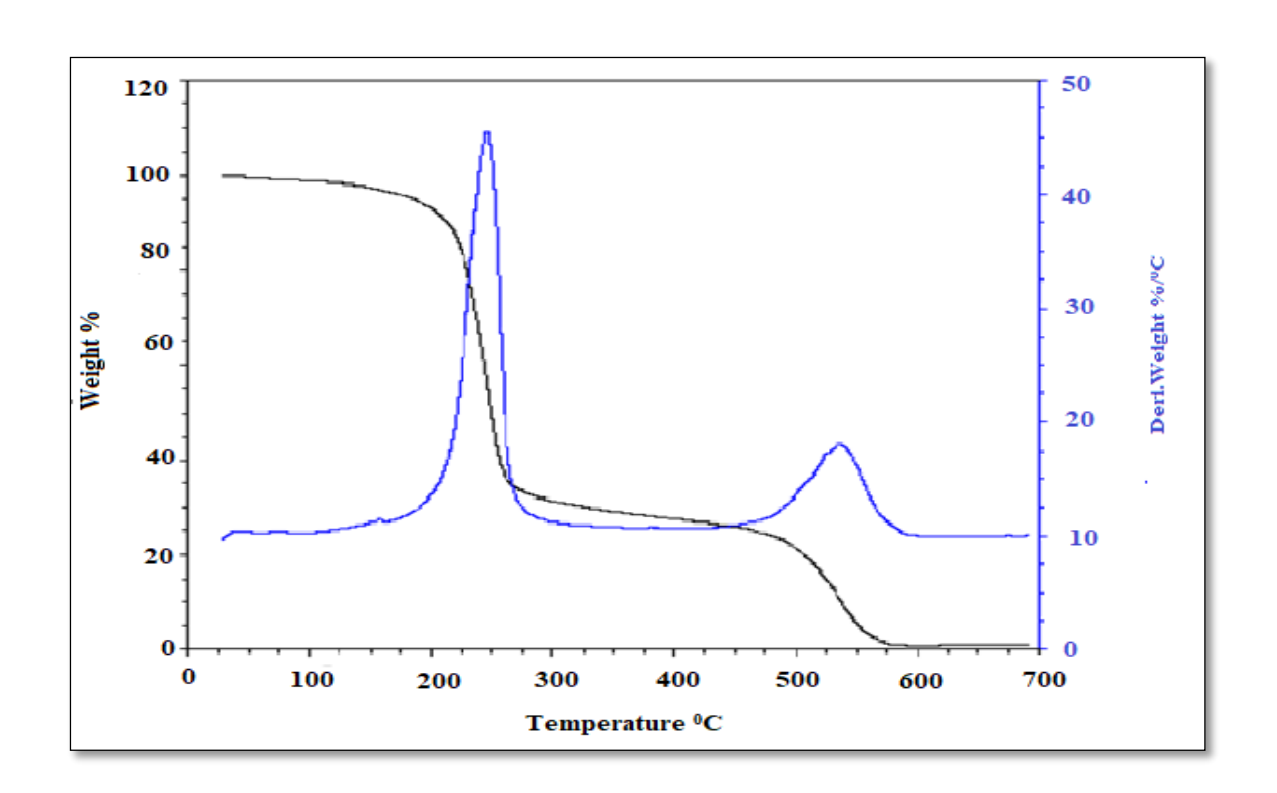
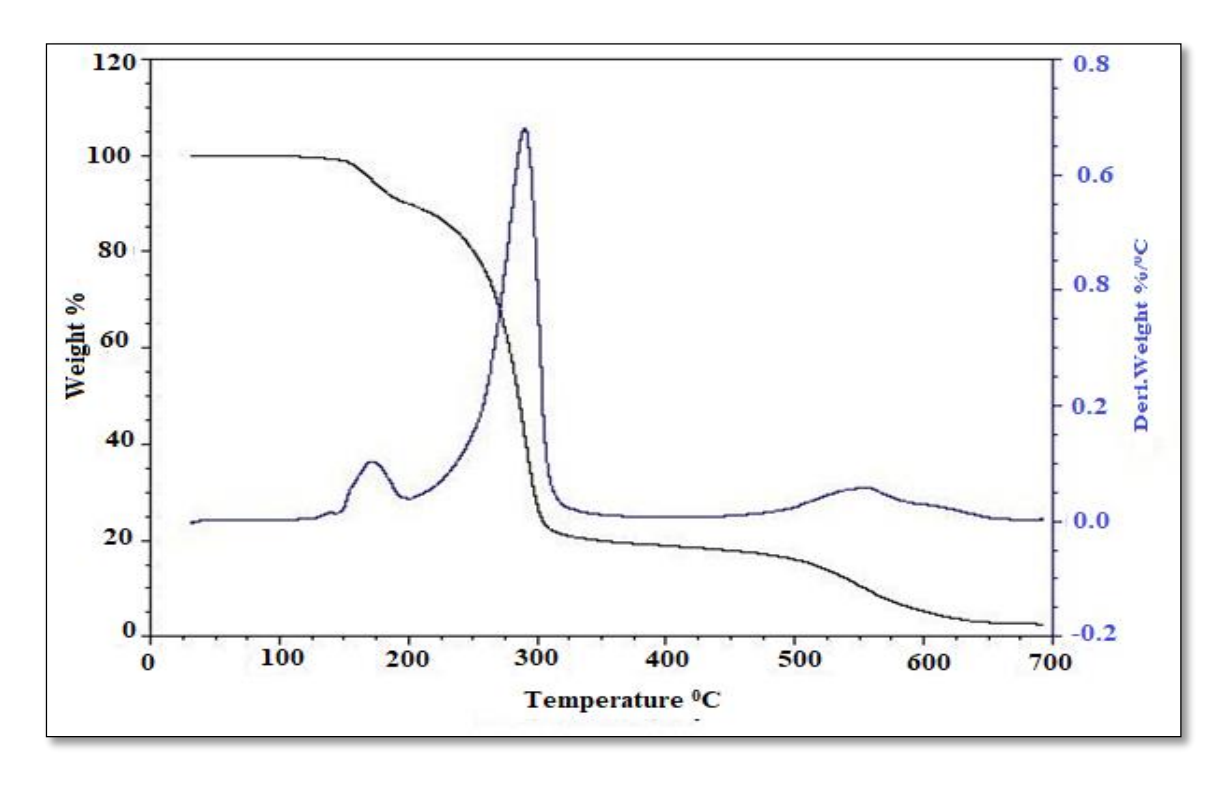


Fig.3.25 TG-DTG Curves of [Ni(MPMA)<sub>2</sub>]SO<sub>4</sub>



 $Fig. 3.26\ TG-DTG\ Curves\ of\ [Cu(MPMA)_2(H_2O)_2]Cl_2$ 

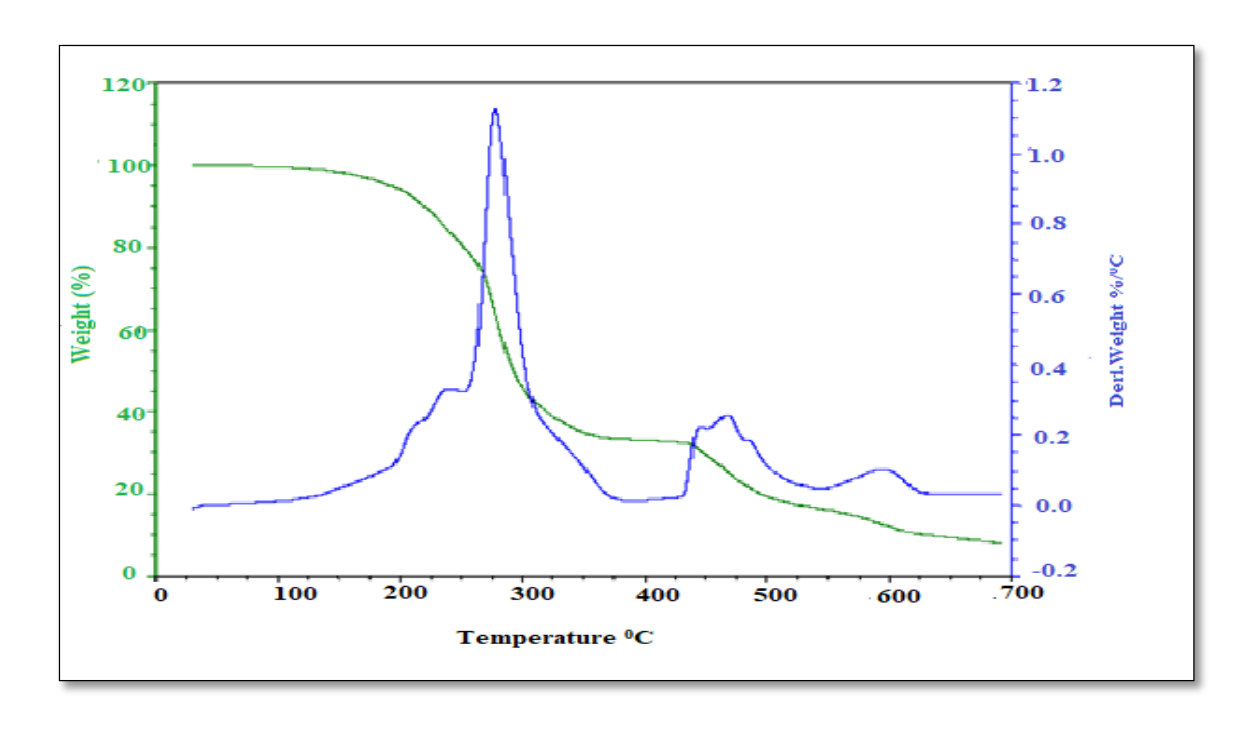


Fig.3.27 TG-DTG Curves of [Zn(MPMA)2]SO4

# 3.5 Biological Studies

### 3.5.1 Evaluation of Antimicrobial Activities of Synthesized Compounds

The *in vitro* antimicrobial activity of the compounds is tested against the bacteria, namely *B.subtilis*, *S.aureus*, *E.coli*, *P.aeruginosa*, and fungi such as *C.albicans and A.niger* by agar well diffusion method. By comparing the diameters of zones of inhibition obtained for the ligand and its complexes, it is found that the complexes exhibit higher antimicrobial activity than the free ligand.

Compounds having >C = N group have enriched antimicrobial activity than those with >C= C< group. Certain micro-organisms can grow even in anaerobic condition. As a result, compounds containing >C = C< group though capable of absorbing  $O_2$  are not related with the growth of microorganisms. Such enriched activity can be described on the basis of Overtone's concept and Tweedy's chelation theory. On the basis of Overtones's concept of cell permeability, the lipid membrane that covers the cell favours the passage of only the lipid-soluble materials where liposolubility is a crucial factor, which reins the antifungal activity.

The polarity of the metal ion is lowered to a higher extent during chelation due to ligand orbital overlap and partial sharing of the metal ion's positive charge with donor groups. Further, the delocalization of  $\pi$ -electrons across the entire chelate ring increases and enhances the lipophilicity of the complexes. This increased lipophilicity progresses the penetration of complexes with lipid membranes, thereby hindering metal binding sites of microorganism enzymes. These complexes also disrupt the cell's respiration process, preventing the synthesis of proteins that limit the organism's potential to expand further. The effectiveness of different compounds against different species is determined by either the impermeability of microorganisms' cells or changes in ribosome of microbial cells. In general, the antibacterial actions are determined by the electron withdrawing and electron releasing nature of the substituents, as well as their position in the complex.[29]

The lesser activity of complexes could also be explained on the basis of low lipid solubility. As a result, the metal ion is unable to reach the appropriate site of action of the cell wall which hinders the normal cell activity. The nature of metal ion also plays a significant role in determining antifungal properties. It is understood that the uncoordinated hetero atoms and carboxylic moieties are responsible for greater inhibition towards microbial growth. The ligands in the complexes contain some uncoordinated donor atoms that increase the activity of the complexes by binding with trace elements found in microorganisms, which may interact with the uncoordinated site and restrict fungal growth. The mode of action of the compounds may involve the formation of a hydrogen bond through the azomethine group (>C = N-) with the active centres of cell constituents, resulting in interruptions with the process of normal cell. [30, 31]

The *in vitro* antimicrobial effects of the synthesized compounds are tested against some bacterial and fungal species. The outcomes of screening of antibacterial and antifungal activities are given in **Table-3.9 &3.10**.

Table- 3.9: Antibacterial Activities of Ligand MPMA and its Metal Complexes

Compound	Diameter of inhibition Zone (mm)															
	B.subtilis				S.aureus			E.coli			P.aeruginosa					
	25 (µg/mL)	50 (μg/mL)	75 (µg/mL)	100 (µg/mL)	25 (µg/mL)	50 (µg/mL)	75 (µg/mL)	100 (μg/mL)	25 (µg/mL)	50 (µg/mL)	75 (µg/mL)	100 (μg/mL)	25 (μg/mL)	50 (μg/mL)	75 (µg/mL)	100 (µg/mL)
MPMA	8	10	12	13	7	9	12	14	9	11	13	14	7	8	8	10
[Fe(MPMA) <sub>2</sub> (H <sub>2</sub> O) <sub>2</sub> ]Cl <sub>3</sub>	11	13	15	17	12	13	15	17	12	13	14	16	12	14	16	18
[Co(MPMA) <sub>2</sub> (H <sub>2</sub> O) <sub>2</sub> ](NO <sub>3</sub> ) <sub>2</sub>	12	15	18	22	12	14	16	20	12	14	16	18	14	16	18	22
[Ni(MPMA) <sub>2</sub> ]SO <sub>4</sub>	12	14	16	18	15	18	20	24	12	14	16	18	10	12	14	14
[Cu(MPMA) <sub>2</sub> (H <sub>2</sub> O) <sub>2</sub> ]Cl <sub>2</sub>	12	15	17	19	13	15	18	19	13	14	16	18	14	15	17	19
[Zn(MPMA) <sub>2</sub> ]SO <sub>4</sub>	15	17	19	21	14	16	18	20	14	17	20	22	16	18	20	24
Gentamicin	20	20	20	20	20	20	20	20	20	20	20	20	20	20	20	20

Table- 3.10: Antifungal Activities of Ligand MPMA and its Metal Complexes

Compound	Diameter of inhibition Zone (mm)								
	C.albicans			A.niger					
	25 (μg/mL)	50 (μg/mL)	75 (μg/mL)	100 (μg/mL)	25 (μg/mL)	50 (μg/mL)	75 (μg/mL)	100 (μg/mL)	
MPMA	10	12	13	15	8	11	13	15	
[Fe(MPMA) <sub>2</sub> (H <sub>2</sub> O) <sub>2</sub> ]Cl <sub>3</sub>	14	16	17	19	11	14	15	17	
[Co(MPMA) <sub>2</sub> (H <sub>2</sub> O) <sub>2</sub> ](NO <sub>3</sub> ) <sub>2</sub>	12	14	16	18	14	16	19	22	
[Ni(MPMA) <sub>2</sub> ]SO <sub>4</sub>	14	17	20	23	12	14	16	18	
[Cu(MPMA) <sub>2</sub> (H <sub>2</sub> O) <sub>2</sub> ]Cl <sub>2</sub>	13	15	16	18	15	16	18	20	
[Zn(MPMA) <sub>2</sub> ]SO <sub>4</sub>	18	20	22	25	15	18	20	23	
Ketoconazole	20	20	20	20	20	20	20	20	

The ligand MPMA and its metal complexes are screened against two Gram positive bacteria such as *B.subtilis* and *S.aureus* and two Gram negative bacteria such as *P.aeruginos* and *E.coli* to study their antibacterial properties by agar well diffusion method using Muller Hinton Agar as nutrient and gentamicin as standard drug. The inhibition based on zone size around the well is measured. As the concentrations of the metal complexes increase then the antimicrobial activity values also increase. With reference to the standard drug (gentamicin), the ligand shows lesser activity against tested pathogenic microorganisms.

The results provided in **Fig.3.28 and 3.29** indicate that zinc (II) complex possesses highest activity against three bacterial species namely B. subtilis, E. coli and P. aeruginosa followed cobalt (II) and nickel (II) complexes whereas copper (II) and iron (III) complexes show moderate activity when compared to the ligand. The zinc (II) complex exhibited 21, 22 and 24 mm zones of inhibition against B. subtilis, E. coli and P. aeruginosa respectively where these values are greater than those of the ligand MPMA as well as gentamicin. This is due to greater lipophilic nature of the complexes. This can be explained in terms of Tweedy's chelation theory because of partial sharing of its positive charge with donor atoms within the chelate ring system, the coordination of ligand to metal ion reduces the polarity of metal ions, causing an increase in the lipophilicity of the complexes, which favours permeation into the lipid layers of the bacterial cell membrane and hindering the metal binding sites on enzymes of microbes.[32] Metal complexes with antibacterial activity are believed to prevent bacteria from replication by inhibiting their active sites. The different compounds have slight differences in microbial activity against different bacterial species, and this difference in activity could be due to the impermeability of the microbe's cell, which is single layered in Gram +ve and multilayered in Gram –ve bacteria. The results are presented in the **Table-3.9**.

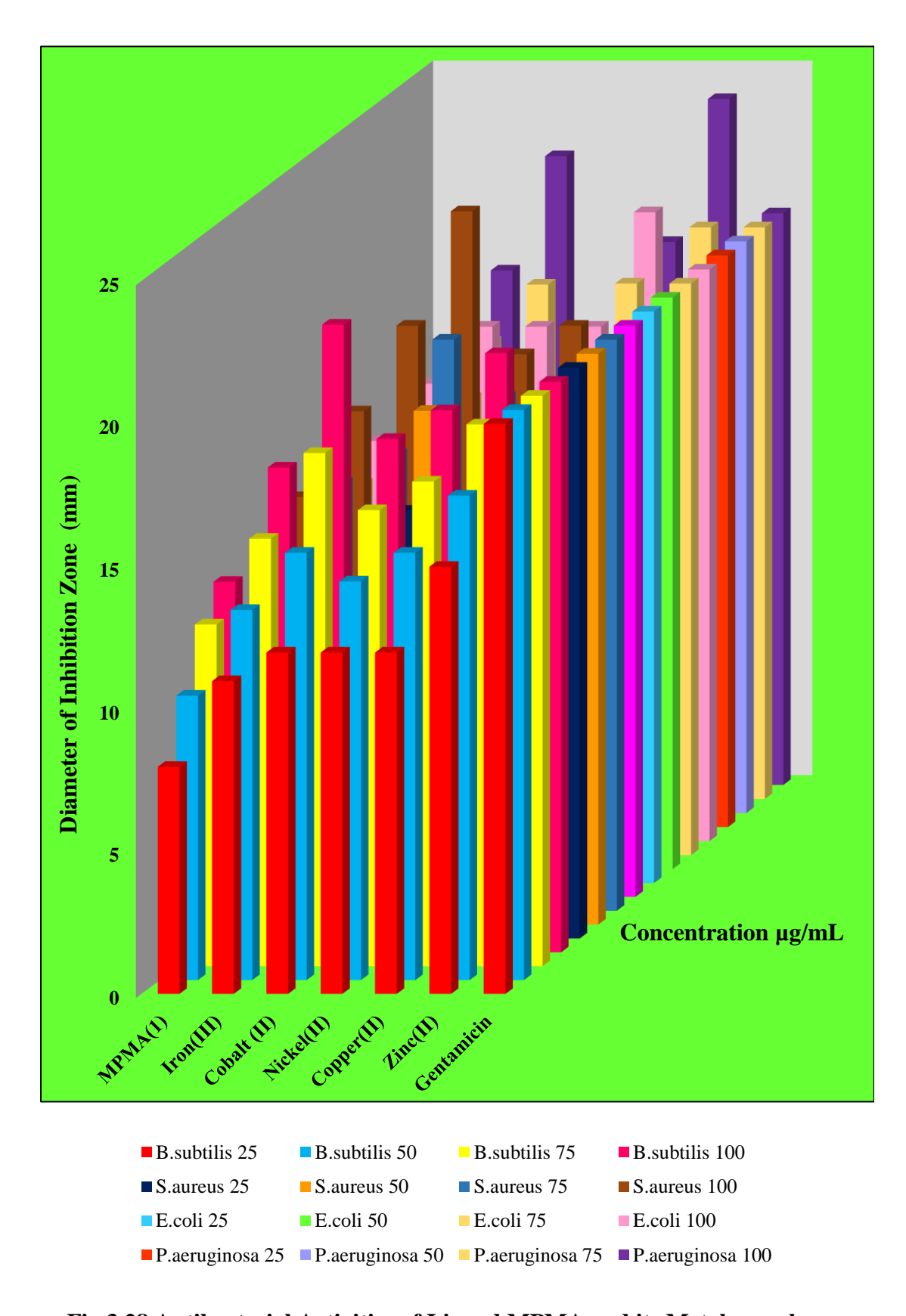


Fig.3.28 Antibacterial Activities of Ligand MPMA and its Metal complexes

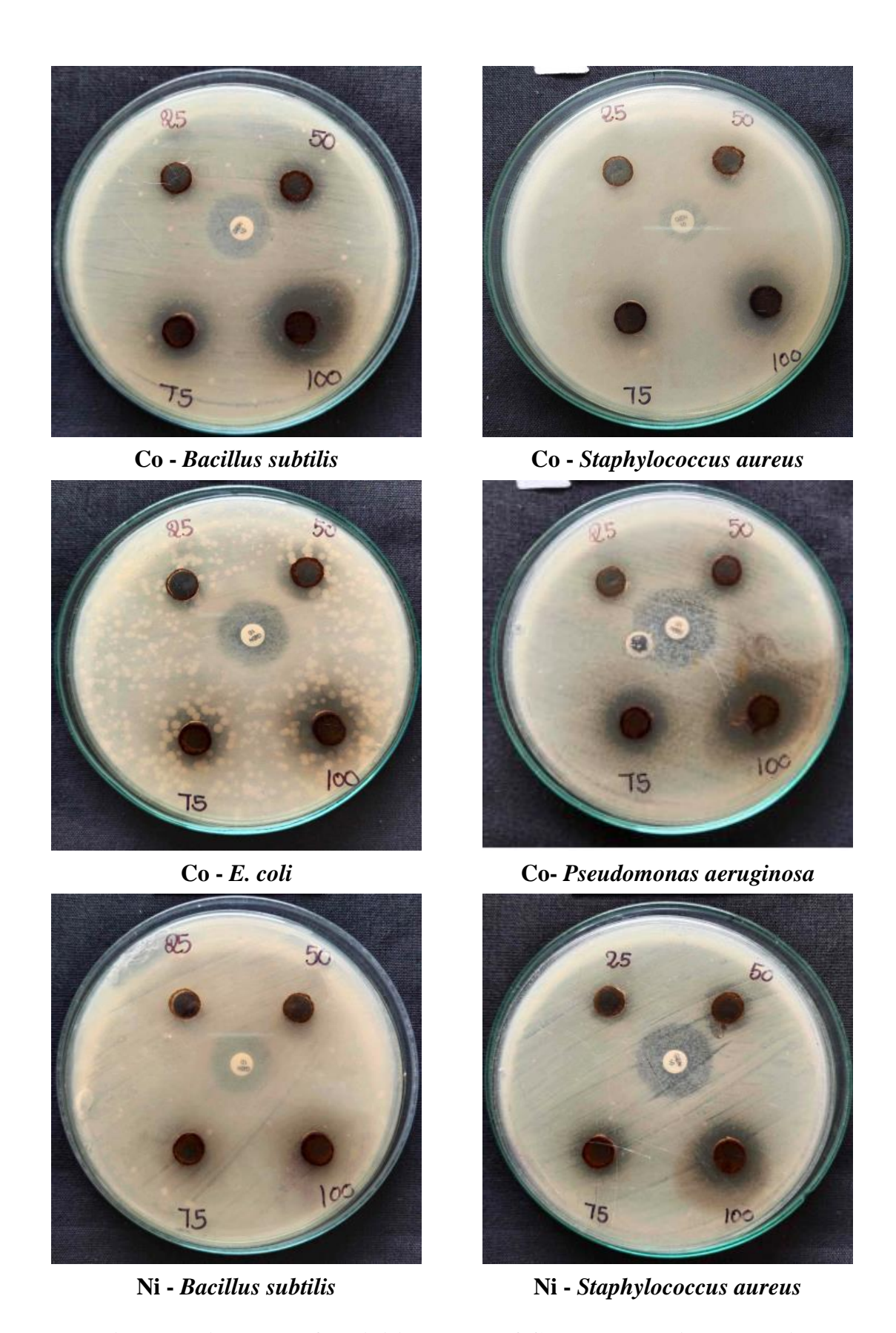


Fig. 3.29 Diameters of Inhibition Zones of Complexes against Bacteria

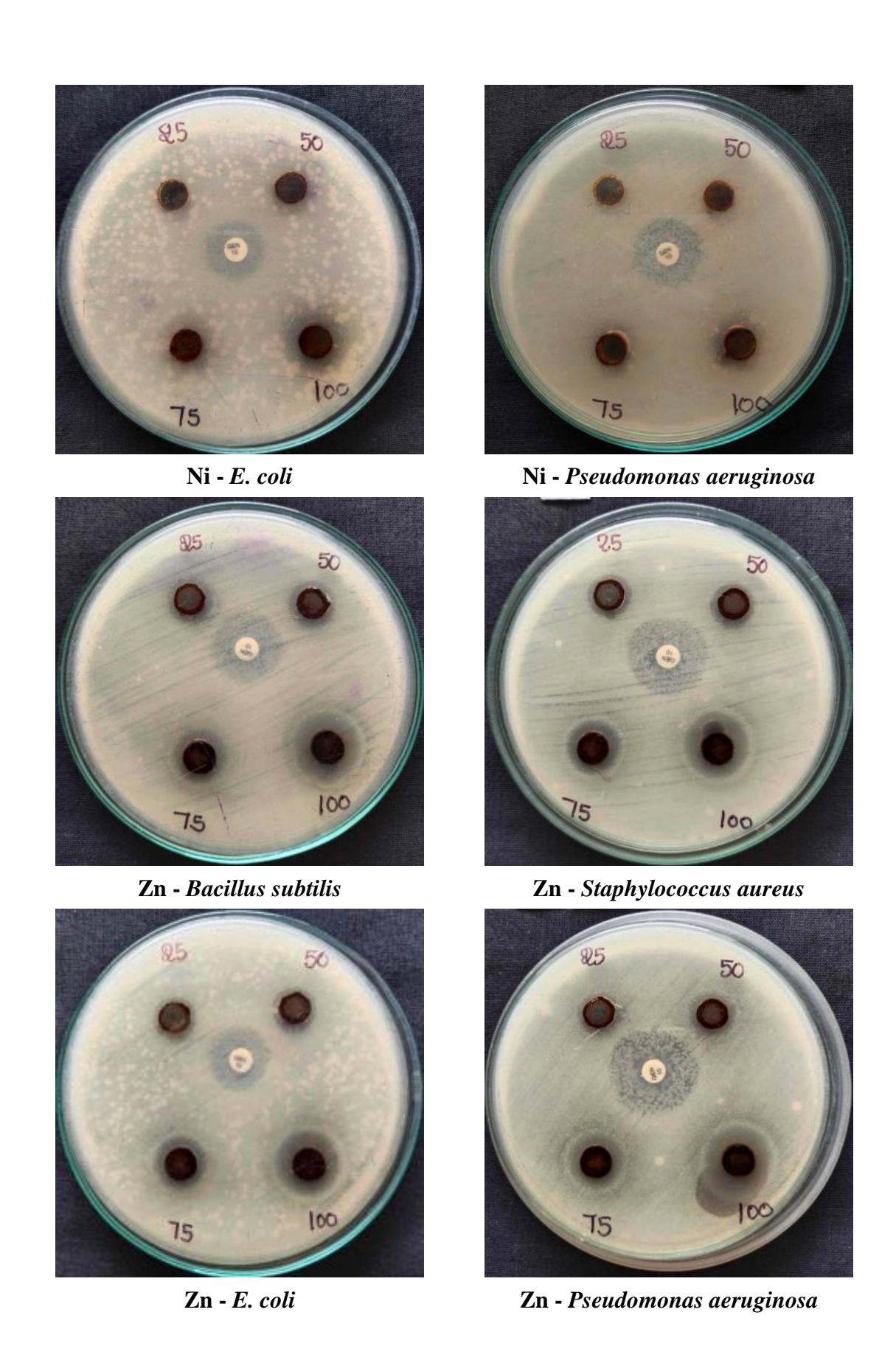


Fig. 3.29 Continued......

The *in vitro* antifungal activities of synthesized ligand MPMA and the complexes shown in the **Fig.3.30** are studied against *C.albicans* and *A.niger* and compared with that of ketoconazole a standard drug. From the results it is clear that ligand has lesser activity against two species with reference to ketoconazole. However, the growth of fungal strains: *C.albicans* and *A.niger* are inhibited much better by zinc (II) complex showing expansion of inhibition zones of 25mm (100 µg/mL) and 20mm (100 µg/mL) respectively, (**Fig.3.31**) followed by cobalt (II) complex which exhibits high activity towards *A.niger* and nickel (II) complex possess high activity against *C.albicans*.[33-35] The impermeability of the cell determines the variation in activity against different microorganisms. The passage of any lipid soluble substances is favoured by lipid membrane which surrounds the cell and leads to liposolubility, which is an essential factor influencing antifungal activity. The results are shown in the **Table-3.10**.

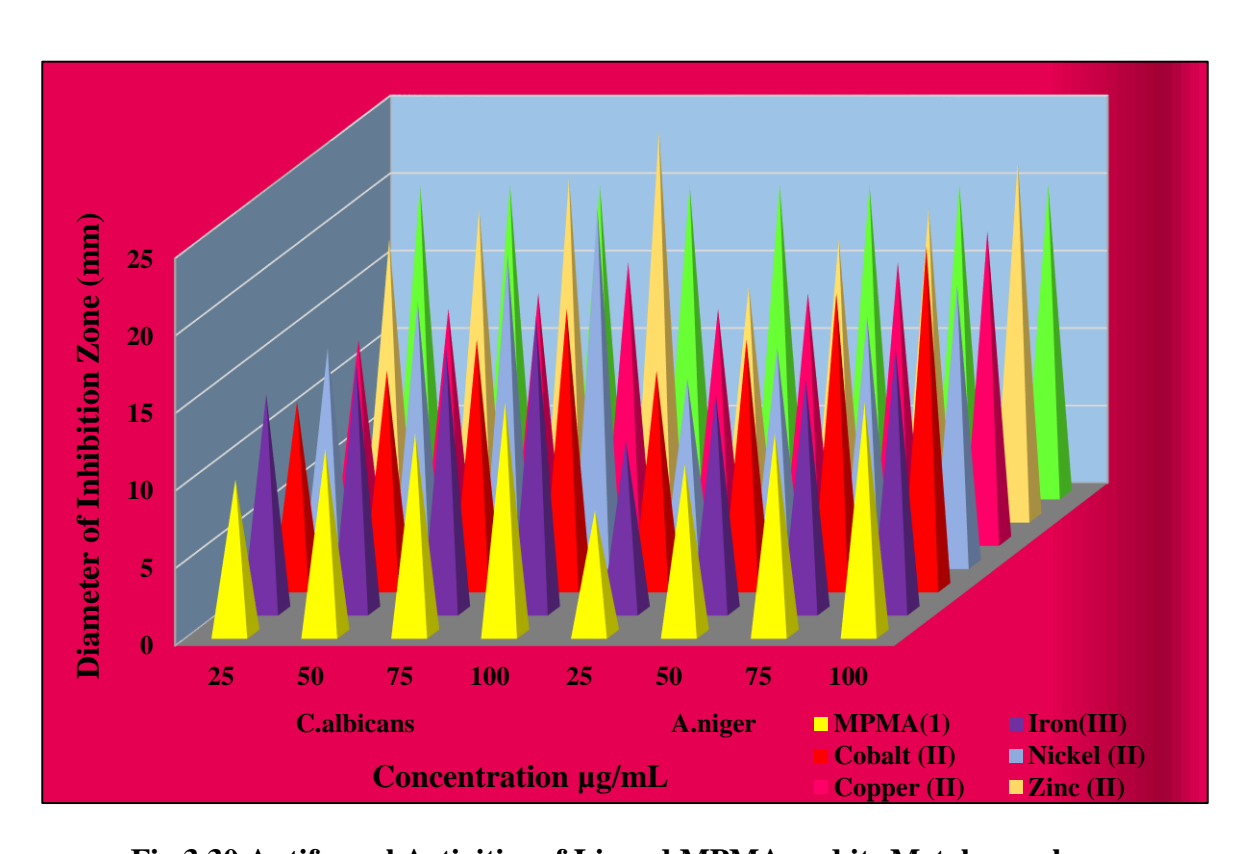


Fig.3.30 Antifungal Activities of Ligand MPMA and its Metal complexes

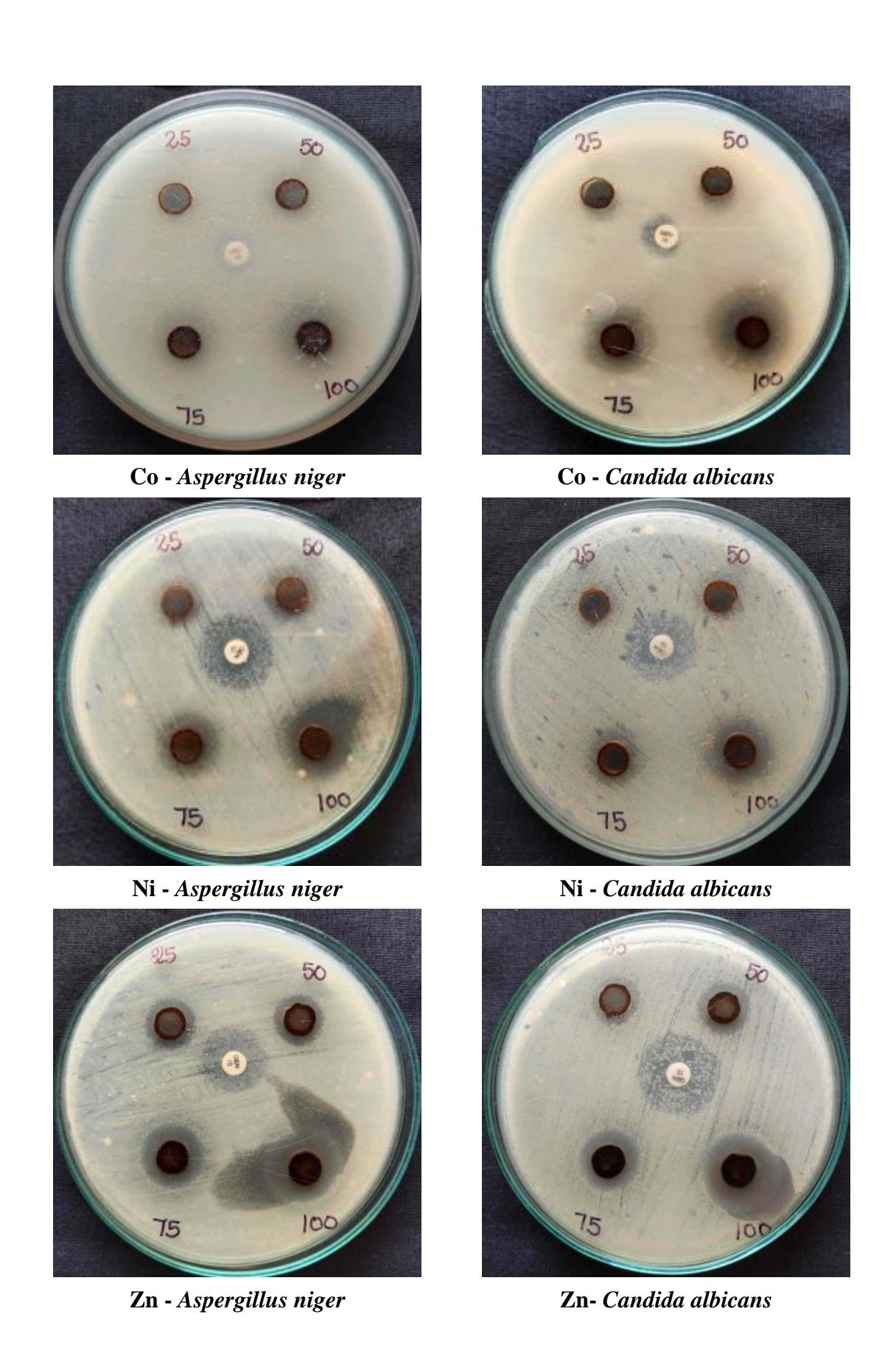


Fig. 3.31 Diameters of Inhibition Zones of Complexes against Fungi

# 3.5.2 Evaluation of Antioxidant Activity (DPPH free radical scavenging Method )

Antioxidants are chemicals that occur naturally and safeguard the living body from damage produced by dangerous species known as free radicals. In response to liberated radicals, bodily cells create these. Free radicals are involved in the etiology of a variety of diseases, including cancer, diabetes, liver injury, autoimmune disorders, cardiovascular diseases, atherosclerosis, and ageing. Antioxidants have an ability to scavenge free radicals and play an important role in the treatment and prevention of various diseases. Antioxidants are commonly utilised as catalysts in antibiotics such as anti-inflammatory, antifungal, antibacterial, and antiviral, as well as in industries as anticorrosion agents. Hence, to prevent the free radical damage in the body, it is important to administer drugs that may be rich in antioxidants. Synthetic antioxidants are now widely used in place of natural antioxidants since they are cheaper and effective. For example, (Z)-2-(pyrrolidin-2- ylidene) hydrazine carbothioamide (L) and its Co(II), Ni(II), and Cu(II) metal complexes have greater free radical scavenging capacity. 2, 2-Diphenyl-1-picryl-hydrazyl (DPPH) is a stable free radical which was used to determine the free radical scavenging ability of these complexes.

The screening of free radical scavenging activities of ligand MPMA and its metal complexes was carried out by DPPH method. Antioxidant activities of the prepared test compounds was observed by measuring radical scavenging effect of DPPH radicals. DPPH is a stable free radical that can accept an electron or hydrogen radical and get converted to a stable, diamagnetic molecule. DPPH has an odd electron and so has a strong absorption band at 517 nm. When this electron becomes paired off, the absorption decreases stoichiometrically with respect to the number of electrons or hydrogen atoms taken up .Such decrease in absorbance, shows the increase in the scavenging activity of the compound. It is observed that the free radical scavenging activity of the compounds are concentration dependent. The results of the free radical scavenging activities of the compounds at different

concentrations are given in the **Table-3.11** and **Fig.3.32.** IC<sub>50</sub> values of the test compounds along with correlation coefficient ( $\mathbb{R}^2$ ) values are displayed in **Table-3.12.** 

Among the examined compounds, metal complexes possess high antioxidant activity than ligand but lower when compared to ascorbic acid. The marked antioxidant activity of the metal complexes may be due to the coordination of metal with imine nitrogen and thio group of amine attached in the second position. In metal complexes, the imine hydrogen -CH=N is more acidic than pyrrole hydrogen -NH. Hence, this imine hydrogen could be easily donated to DPPH free radical and change itself into stable molecule. Furthermore, when imine nitrogen is complexed with metal ions, the acidity of the hydrogen atom linked to it increases. Hence that hydrogen become more vulnerable.

The amount of antioxidant necessary to reduce DPPH concentration by 50% is a commonly used parameter to measure antioxidant activity and is referred to as IC<sub>50</sub>. The lower the IC<sub>50</sub> value, the higher is the antioxidant activity. The copper (II) complex possess high antioxidant activity since there IC<sub>50</sub> values are low and show promise for further investigation to target oxidative damage disease[36].

The order of activities can be given as L-Ascorbic acid  $> Cu^{II} > Co^{II} > Ni^{II} > Zn^{II} >$  Fe<sup>III</sup> >MPMA with IC<sub>50</sub> values as 3.162 > 5.248 > 7.498 > 10.653 > 30.162 > 31.624 > 60.82  $\mu$ M. The oxidizing potentials of the samples are associated with the existence of compounds to exert actions by breaking the free radical chain via hydrogen atom donation. As a result, the findings of this study suggest that the produced compounds could be used to treat oxidative stress-related disorders.[37]

Table-3.11: Antioxidant Activities of Ligand MPMA and its Metal Complexes

Compound	% of Free Radical Scavenging							
	5.0μg/mL	10μg/mL	15μg/mL	20μg/mL				
L-Ascorbic acid	66	70	73	75				
MPMA	15	20	26	31				
[Fe(MPMA) <sub>2</sub> (H <sub>2</sub> O) <sub>2</sub> ]Cl <sub>3</sub>	49	52	59	64				
$[\text{Co}(\text{MPMA})_2(\text{H}_2\text{O})_2](\text{NO}_3)_2$	63	68	72	75				
[Ni(MPMA) <sub>2</sub> ]SO <sub>4</sub>	56	60	64	70				
[Cu(MPMA) <sub>2</sub> (H <sub>2</sub> O) <sub>2</sub> ]Cl <sub>2</sub>	64	69	71	74				
[Zn(MPMA) <sub>2</sub> ]SO <sub>4</sub>	50	55	61	66				

80 % Free Radical Scavenging **70 60 50** 40 **30** 20 **10** 0 5 10 15 20 Concentration µg/mL MPMA(1) L.Ascorbic acid Iron III Complex Cobalt II Complex Nickel II Complex **Copper II Complex** Zinc II Complex

Fig.3.32 Free Radical Scavening Activities of Ligand MPMA and its Metal Complexes

Table-3.12: IC50 ( $\mu$ M) and R<sup>2</sup> values of Standard Drug, Ligand MPMA and its Metal Complexes

Compound	IC50, (µM)	R <sup>2</sup>
L-Ascorbic acid	3.162	0.9783
MPMA	60.82	0.9986
[Fe(MPMA) <sub>2</sub> (H <sub>2</sub> O) <sub>2</sub> ]Cl <sub>3</sub>	31.624	0.9797
[Co(MPMA) <sub>2</sub> (H <sub>2</sub> O) <sub>2</sub> ](NO <sub>3</sub> ) <sub>2</sub>	7.498	0.9877
[Ni(MPMA) <sub>2</sub> ]SO <sub>4</sub>	10.653	0.9888
[Cu(MPMA) <sub>2</sub> (H <sub>2</sub> O) <sub>2</sub> ]Cl <sub>2</sub>	5.248	0.9667
[Zn(MPMA) <sub>2</sub> ]SO <sub>4</sub>	30.162	0.9986

## 3.5.3 Evaluation of Antidiabetic Activity

Diabetes mellitus is a dangerous multifactorial condition marked by hyperglycemia (very high blood glucose levels) and glucose intolerance, which can be caused by a lack of insulin or a reduction in the efficacy of insulin's activity to improve glucose uptake. It can lead to serious problems if left untreated. Hyperlipidaemia (an abnormally high level of lipid in the blood), oxidative stress, and protein enzymatic glycation are examples of these complications.

In this work, the inhibitory effect of Schiff base ligand MPMA and its metal complexes on carbohydrate hydrolysing enzyme alpha amylase and alpha glucosidase are studied. The results of antidiabetic activity are shown in the **Table-3.13** and **Table-3.14**. These enzyme inhibitors work by inhibiting the action of these enzymes and delaying carbohydrate digestion, preventing a rapid rise in blood glucose levels, particularly after meals. Therefore inhibition of these two enzymes is a promising strategy for diabetes management. Metal complexes are found to exhibit more inhibition efficiency than the ligand MPMA and comparable or slightly less efficienct than the standard drug acarbose (**Fig.3.33** and **3.34**)

Cobalt (II) complex showed excellent inhibition efficiency against  $\alpha$ - amylase enzyme and copper (II) complex exhibit high inhibition efficiency towards  $\alpha$ - glucosidase enzyme.[38, 39]

The enhanced activity of cobalt (II) complex was due to the tendency of cobalt to lower the glycemic level and act as an effective agent for diabetes. The enhanced activity of copper (II) complex against diabetes was due to the tendency of copper to increase the tolerance of pancreatic  $\beta$ -cells against oxidative stress.

The enhanced activity of zinc (II) complex was due to the fact that zinc has an insulin mimetic effect and protects against oxidative damage associated with the disease for the treatment of diabetes mellitus. [40, 41]

Table- 3.13: Antidiabetic Activities of Ligand MPMA and its Metal Complexes Measured by α- Amylase Method

Compound	% of Inhibition							
	20μg/mL	40μg/mL	60μg/mL	80μg/mL	100μg/mL			
MPMA	26.75	31.91	37.53	41.30	45.53			
[Fe(MPMA) <sub>2</sub> (H <sub>2</sub> O) <sub>2</sub> ]Cl <sub>3</sub>	41.19	45.76	49.54	53.27	57.82			
$\boxed{ [\text{Co}(\text{MPMA})_2(\text{H}_2\text{O})_2](\text{NO}_3)_2 }$	51.35	57.51	60.27	64.95	68.47			
[Ni(MPMA) <sub>2</sub> ]SO <sub>4</sub>	39.15	43.79	48.39	51.27	55.67			
[Cu(MPMA) <sub>2</sub> (H <sub>2</sub> O) <sub>2</sub> ]Cl <sub>2</sub>	43.73	47.61	51.29	55.64	61.43			
[Zn(MPMA) <sub>2</sub> ]SO <sub>4</sub>	49.39	54.61	58.91	62.71	66.90			
Acarbose	66.90	72.53	77.46	81.69	85.21			

Table-3.14: Antidiabetic Activities of Ligand MPMA and its Metal ComplexesMeasured by  $\alpha$ - Glucosidase Method

Compound	% of Inhibition							
	$20 \mu g/mL$	40μg/mL	60μg/mL	80μg/mL	100μg/mL			
MPMA	21.91	25.81	29.46	33.08	37.67			
[Fe(MPMA) <sub>2</sub> (H <sub>2</sub> O) <sub>2</sub> ]Cl <sub>3</sub>	36.69	41.32	46.87	51.71	55.23			
[Co(MPMA) <sub>2</sub> (H <sub>2</sub> O) <sub>2</sub> ](NO <sub>3</sub> ) <sub>2</sub>	41.34	48.97	52.61	55.72	59.12			
[Ni(MPMA) <sub>2</sub> ]SO <sub>4</sub>	45.73	49.43	53.31	58.67	61.91			
[Cu(MPMA) <sub>2</sub> (H <sub>2</sub> O) <sub>2</sub> ]Cl <sub>2</sub>	51.52	55.01	58.79	62.31	65.61			
[Zn(MPMA)2]SO4	46.13	52.59	56.17	60.48	63.72			
Acarbose	73.63	77.27	80	82.72	85.45			

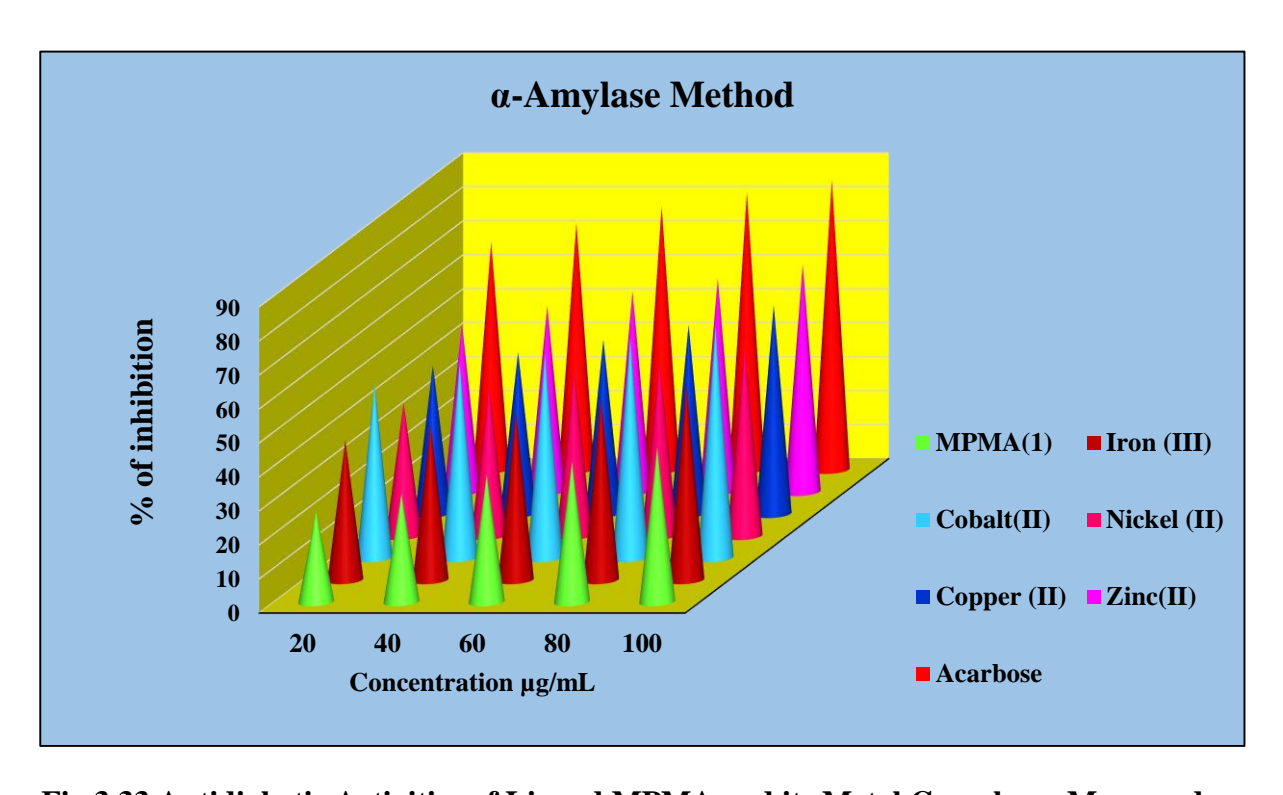


Fig.3.33 Antidiabetic Activities of Ligand MPMA and its Metal Complexes Measured by  $\alpha\textsc{-}\textsc{Amylase}$  Method

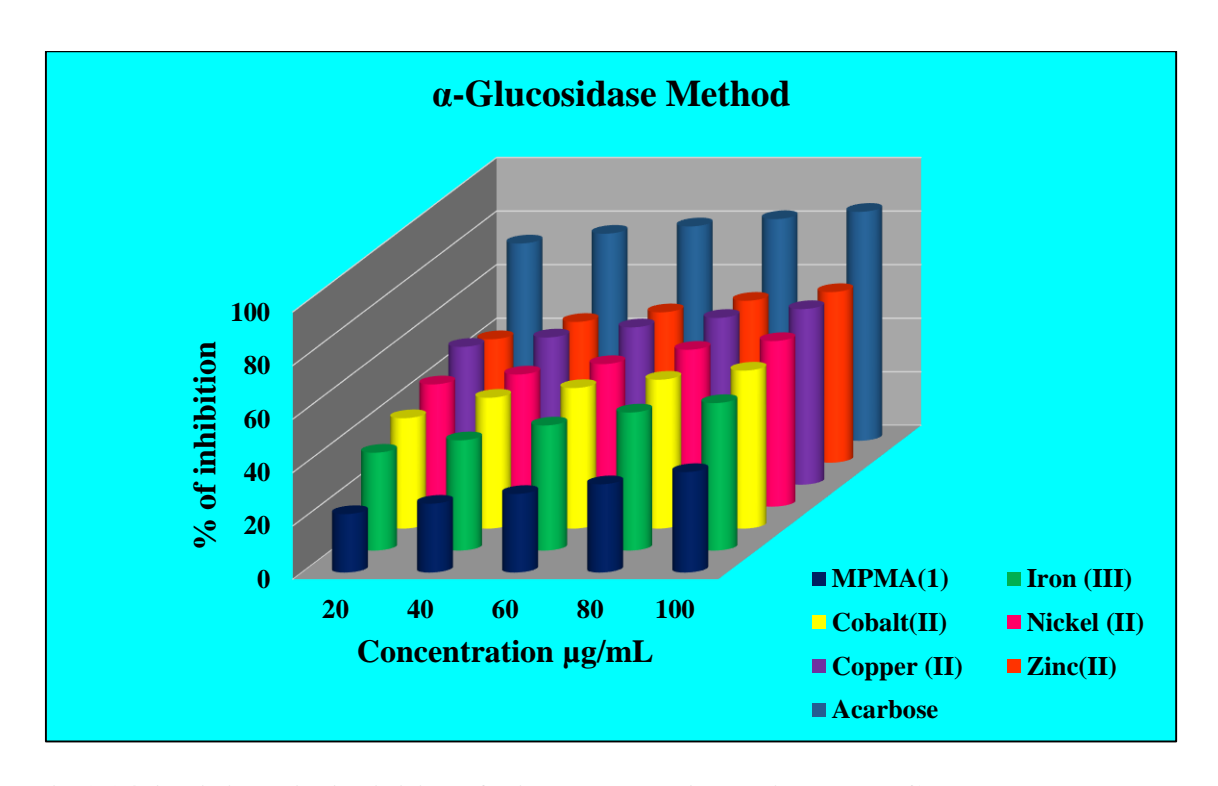


Fig.3.34 Antidiabetic Activities of Ligand MPMA and its Metal Complexes Measured by  $\alpha$ -Glucosidase Method

#### 3.6 CONCLUSION

The condensation reaction pyrrole-2-carboxaldehyde between and 2-(methylthio)aniline in the molar ratio1:1 gave the Schiff base ligand MPMA. The reaction of ligand MPMA with metal ions such as iron (III), cobalt (II), nickel (II) copper(II) and zinc(II) in 2:1 ratio form complexes. Based on spectroscopic studies, the coordinating ability of ligand have been proved as it act as NS donor bidendate ligand. Metal ion is coordinated to ligand through imine nitrogen atom and sulphur atom of thio ether moiety, forming a stable chelate ring. In the light of above discussion, an octahedral geometry is proposed with iron (III), cobalt (II) and copper (II) whereas square planar with nickel (II) and tetrahedral with zinc (II) complexes. Cyclic voltammetric studies reveals that all the complexes, in the applied potential range, undergo one electron quasi-reversible redox reaction. The molar conductance measurements reveal that all the complexes are electrolytic in nature. Antimicrobial, antioxidant and antidiabetic activities reveal that the metal complexes were

more active than the Schiff base ligand which is in agreement with the fact that chelation of metals to the ligand enhances the biological activity of the complexes. Copper (II) complex was found to possess high antioxidant activity and enhanced inhibition activity against  $\alpha$ -amylase enzyme whereas cobalt (II) complex possess high inhibition activity against  $\alpha$ -glucosidase enzyme.

### REFERENCES

- 1. P.Tyagi, S. Chandra, B.S. Saraswat, and D. Sharma, *Spectrochim. Acta A Mol. Biomol. Spectrosc.*, 2015, **143**, 1-11.
- P. Kavitha .M. Saritha and K. Laxma Reddy, *Spectrochim. Acta A Mol. Biomol. Spectrosc.*, 2013, **132**, 159-168.
- 3. A.A.A.Raj, J.Vinnarasi and R.Venkataraman, *Research J. Pharm. and Tech.*, 2013, **6(10)**, 1121-1123.
- 4. G.Rajyalakshmi, R.Narsimhareddy and M.Sarangapani, *Saudi Pharm. J.*, 2011, **19(3)**, 153–158.
- 5. A. K. Sharma and S.Chandra, *Spectrochim. Acta A Mol. Biomol. Spectrosc.*, 2011, 78(1), 337-342.
- 6. L.H. Abdel-Rahman, A.M. Abu-Dief, M.O. Aboelez and A.A.H. Abdel-Mawgoud, *J. Photochem. Photobiol. B: Biol.*, 2017, **170**, 271-285.
- 7. G. T. Tigineh, Y.S.Wen and L.K. Liu, *Tetrahedron*, 2015, **71**(1), 170-175.
- 8. S.A. Nami, I. Ullah, M. Alam, D.U. Lee and N. Sarikavakl, *J. Photochem. Photobiol. B: Biol.*, 2016, **160**, 392-399
- 9. F.D. Rahmatabadi, R.R. Khojasteh, H. K. Fard and F. Tadayon, *Eurasian chemical communication*, 2020, **2(5)**, 587-594.
- 10. K. Singh and P. Dharam, J. Serb. Chem. Soc., 2010, **75**(7), 912-927.
- 11. Z. H. Chohan, S. H. Sumrra, M. H. Youssouf and T. B. Hadda, *Eur. J. Med. Chem.*, 2012, **45**(**7**), 2739-2747.
- 12. S.Malik, M.Kumari, S.Chauhan and D. K. Sharma, *Phosphorus, Sulfur, and Silicon*, 2010, **185(8)**, 1759-1771.
- 13. S. A. Khan, S.A. Nami, S. A. Bhat, A Kareem and N. Nishat, *Microb. Pathog.*, 2017, **110**, 414-425.
- 14. F. Shabani, L. A. Saghatforoush and S. Ghammamy, *Bull. Chem. Soc. Ethiop.*, 2010, **24(2)**, 193-199.
- 15. Z. H. Chohan, H.Pervez, A.Rauf, A. Scozzafava and C. T. Supuran, *J. Enzyme Inhib. Med. Chem.*, 2002, **17(2)**, 117-122.

- 16. R.V. Sakthivel, P. Sankudevan, P. Vennila, G. Venkatesh, S. Kaya and G. Serdaroğlu, *J. Mol. Struct.*, 2021, **1233**, 130097-1300110.
- 17. O.A. El-Gammal, F.S. Mohamed, G.N. Rezk and A.A. El-Bindary, *J. Mol. Liq.*, 2021, **326**, 115223-115240.
- 18. A. M. Abu-Dief, R. M. El-khatib, F. S. Aljohani, S. O. Alzahrani; A. Mahran, M. E. Khalifa and N. M. El-Metwaly, *J. Mol. Liq.*, 2021, **1242**, 130693-1306106.
- 19. Y.P.Singh, and S. K.Patel, *J. Mol. Liq.*, 2021, **1228**, 129457-129475.
- 20. Q.T.Nguyen, P.N.Pham Thi and V.T.Nguyen, *Bioinorg Chem Appl.*, 2021, 1-10.
- 21. S.Bal and S.S. Bal, Adv. Chem., 2014, 1-12.
- A. Jayamani, S. Nagasubramanian, V. Thamilarasan, S.O. Ojwach, G. Gopu and N.Sengottuvelan, *Inorganica Chim. Acta.*, 2018, **482**, 791–799.
- 23. A.Abayneh, T.Gebretsadik, S.Tadesse and M. Thomas, *Adv. Chem. Eng.*, 2018, **8(4)**, 241-254.
- 24. K.Singh, R.Thakur and V. Kumar, *Beni-Suef University Journal of Basic and Applied Sciences*, 2016, **5(1)**, 21-30.
- 25. A.N.Gusev, M.A.Kiskin, E.V. Braga, M. Chapran, G. Wiosna-Salyga, G.V. Baryshnikov and W. Linert, *J. Phys. Chem. C.*, 2019, **123(18)**, 11850-11859.
- 26. R.A. Ahmadi and S.Amani, *Molecules*, 2012, **17(6)**, 6434-6448.
- 27. N. Ahmad, M. Alam, R. Wahab, M. Ahmed and A. Ahmad, *Open Chem. J.*, 2020, **18(1)** 1304–1315.
- 28. B. Bouzerafa, A. Ourari, D. Aggoun, R. Ruiz-Rosas, Y. Ouennoughi and E. Morallon, *Res. Chem. Intermed.*, 2016, **42**(5), 4839–4858.
- 29. S.I.AlResayes, M. Shakir, N. Shahid, M.Azam and A.U. Khan, *Arab. J. Chem.*, 2016, **9**, 335-341.
- 30. B. Soltani, M.Ghorbanpour, C.J. Ziegler, M. Ebadi-Nahari and R.Mohammad-Rezaei, *Polyhedron*, 2020, **180**, 114423-114445
- 31. S.C. Singh, N. Gupta and R.V. Singh, *Ind. J. Chem.*, 1995, **34A(9)**, 733-736.
- 32. J. Mann, M.J.C. Crabbe, *Bacteria and Antibacterial Agents*, Spectrum Academic Publishers, Oxford, UK, 1990, 76.

- 33. K.R. Surati, Spectrochim. Acta A, 2011, **79(1)**, 272 -277.
- 34. R.V. Singh and A. Chaudhary, J. Inorg. Biochem., 2004, 98, 1712 -1721.
- 35. H.Zafar, A. Ahmad, A.U. Khan and T.A. Khan, *J. Mol. Struct.*, 2015, **1097**, 129–135.
- 36. Q.M. Hasi, Y. Fan, X.Q. Yao, D.C. Hu and J.C. Liu, *Polyhedron*, 2016, **109**, 75-80.
- 37. A.A.A. Aziz and H.A. Elbadawy, *Spectrochim. Acta A Mol. Biomol. Spectrosc.*, 2014, **124**, 404–415.
- 38. N. Patel, A.K. Prajapati, R.N. Jadeja, R.N. Patel, S.K. Patel, I.P. Tripathi, N. Dwivedi, V.K. Gupta and R.J. Butcher, *Polyhedron*, 2020, **180**, 114434-114459.
- 39. S.N.Shukla, P.Gaur, S. Jhariya, B. Chaurasia, P. Vaidya, D. Dehariya and M. Azam, *Chem. Sci.*, 2018, **7(3)**, 424-444.
- 40. K. Balan, P. Ratha, G. Prakash, P. Viswanathamurthi, S. Adisakwattana and T. Palvannan, *Arab. J. Chem.*, 2017, **10**(5), 732-738.
- 41. B.J.Okoli and J.S.Modise, *Antioxidants*, 2018, **7**, 113-131.

# Synthesis, Characterisation and Evaluation of Antimicrobial, Antioxidant And Antidiabetic Activities of (E)-2-(methylthio)-N-(pyridin-2-ylmethylene)aniline and its Metal Complexes

### 4.1 INTRODUCTION

Schiff bases and their metal complexes play a vital role due to their catalytic activity and biological activity such as antitumor, antimicrobial, anti-inflammatory, antidiabetic, anticancer, analgesic, pesticidal and antioxidant.[1] The ligands having nitrogen and sulphur donor atoms in their structures can act as better chelating agents for transition metal ions. In recent years, heterocyclic moiety -based medications have become increasingly significant in the medical field. Diabetes, cancer, inflammation, and cardiovascular disease were also treated. For past ten years, transition metal complexes of Schiff bases derived from pyridine -2- carboxaldehyde have gained a lot of attention due to their synthetic and catalytic activities. Pyridine-2-carboxaldehyde Schiff base complexes have been quantified for their catalytic activities towards alkene epoxidation, hydrogenation, and hydroformylation .[2] Pyridine-2- carboxaldehyde Schiff base complexes and derivatives, have also been recognised for high superoxide dismutase activities and found to be effective herbicides for the protection of plants.[3]

Based on these information, here in the present work we deal with the synthesis of Schiff base ligand (E)-2-(methylthio)-N-(pyridin-2-ylmethylene)aniline MTPMA derived from pyridine-2-carboxaldehyde and 2-(methylthio)aniline and its metal complexes. Various physico-chemical methods such as molar conductance, chemical analysis, elemental analysis, magnetic susceptibility, <sup>1</sup>H-NMR, FT-IR, UV-Vis, EPR, mass spectra, cyclic voltammetry, thermal decomposition studies and X-ray diffraction measurements are

utilized to determine the structures of Schiff-base ligand and its metal complexes. The bioefficacies of the free ligand and its complexes are tested *in vitro* against microbes with various dilutions, in order to evaluate their antimicrobial potential. In addition, antioxidant and antidiabetic activities of the title compounds are also evaluated.

## 4.2 Synthesis of (E)-2-(methylthio)-N-(pyridin-2-ylmethylene)aniline MTPMA

Schiff base MTPMA was prepared by adding 2-(methylthio)aniline (0.139 g, 1 mmol) in 20 mL of ethanol slowly to pyridine-2-carboxaldehyde (0.107 g, 1mmol) in 20 mL ethanol with constant stirring. The mixture was then refluxed for 3 h, yellow solution was formed. The solution was kept for slow evaporation and yellow solid was collected. The collected yellow coloured Schiff base was washed with cold ethanol and then dried in a desiccator over anhydrous calcium chloride.

# 4.3 Synthesis of Metal Complexes of MTPMA

(E)- 2-(Methylthio)-N-(pyridin-2-ylmethylene)aniline (2 mmol) in 20 mL of ethanol was added drop wise to a solution containing a metal salts (1 mmol) in 20 mL of ethanol. The mixture was refluxed for 3 hours on a water bath and allowed for slow evaporation. The precipitate of complex obtained was filtered, rinsed with cold ethanol and dried in a desiccator over anhydrous calcium chloride. The metal salts used were iron (III) chloride hexahydrate, cobalt nitrate hexahydrate, nickel sulphate heptahydrate, copper chloride dihydrate and zinc sulphate hexahydrate. The schematic diagram for the synthesis of Schiff base and its complexes is shown in the **Fig. 4.1.** 

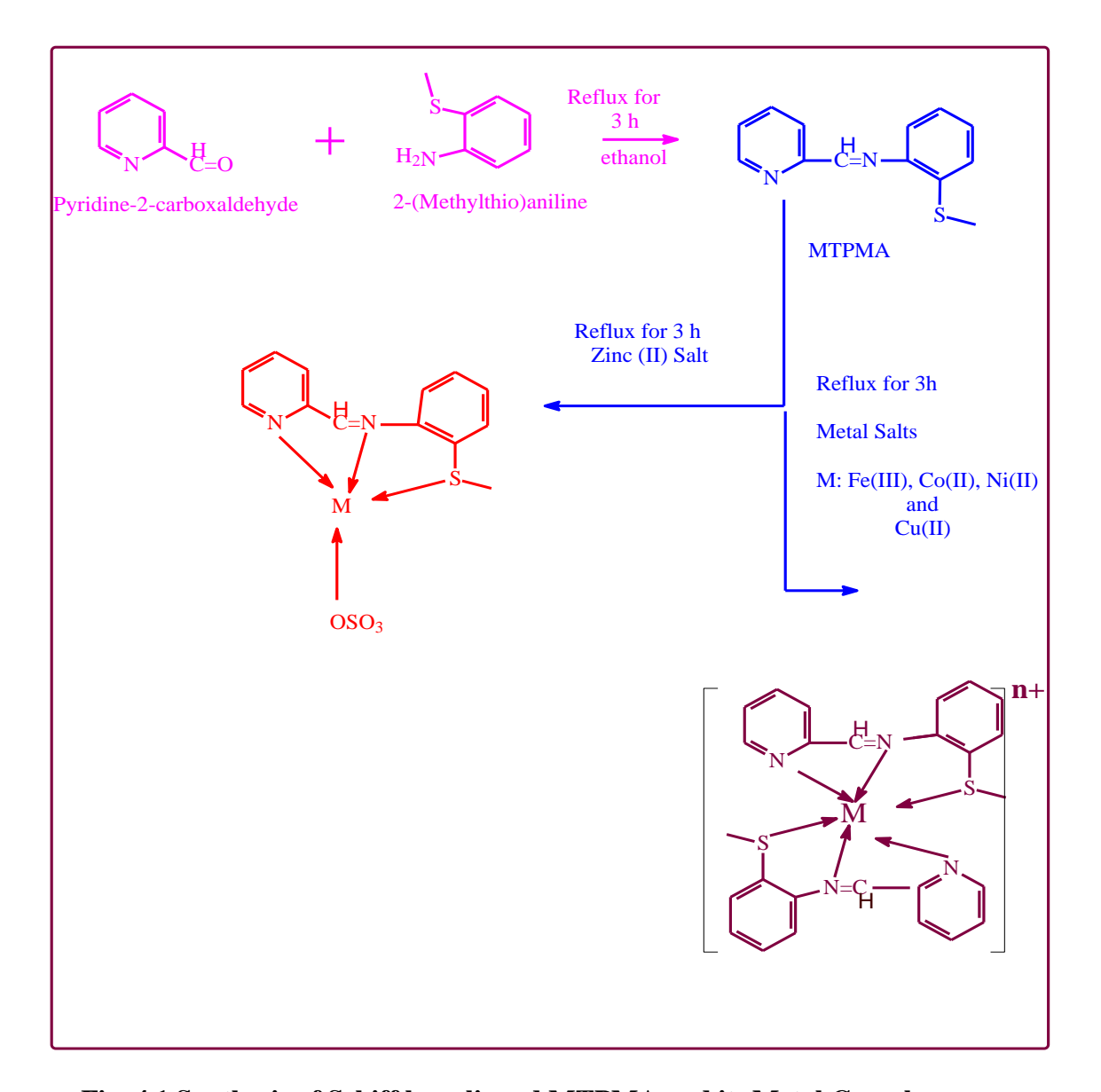


Fig. 4.1 Synthesis of Schiff base ligand MTPMA and its Metal Complexes

## 4.4 Results and Discussion

## 4.4.1 Elemental Composition

The analytical data and some physical properties of the ligand MTPMA and its metal complexes are furnished in **Table-4.1**. The analyses of metal complexes provided satisfactory analytical data indicating that iron (III), cobalt (II), nickel (II) and copper (II) complexes were formed in the ratio 1:2 (M: L) whereas zinc (II) complex was formed in the ratio 1:1 (M: L) stoichiometry. The resulting metal complexes were found to be non-hygroscopic solids and stable at room temperature.

**Table-4.1: Analytical Data and Physical Properties of the Ligand MTPMA and its Metal Complexes** 

Compound	Empirical formula	Colour	Yield M. Wt. g.mol <sup>-1</sup>				Elemental Analysis found (Calc) (%)						
	Tormula			g.moi	<sup>0</sup> С	C	Н	N	S	Cl	Metal		
MTPMA	$C_{13}H_{12}N_2S$	Yellow	85 228.32 1		174	68.39 (68.41)	5.30 (5.25)	12.27 (12.21)	14.05 (14.11)	-	-		
[Fe(MTPMA) <sub>2</sub> ]Cl <sub>3</sub>	FeC <sub>26</sub> H <sub>24</sub> N <sub>4</sub> S <sub>2</sub> Cl <sub>3</sub>	Red Brown	80	618.84	190	50.45 (50.47)	3.90 (3.87)	9.06 (9.02)	10.51 (10.49)	17.18 (17.15)	9.02 (8.99)		
[Co(MTPMA) <sub>2</sub> ](NO <sub>3</sub> ) <sub>2</sub>	CoC <sub>26</sub> H <sub>24</sub> N <sub>6</sub> S <sub>2</sub> O <sub>6</sub>	Brown	75	639.58	223	48.82 (48.79)	3.78 (3.77)	13.13 (13.16)	10.02 (10.04)	-	9.21 (9.16)		
[Ni(MTPMA) <sub>2</sub> ]SO <sub>4</sub>	NiC <sub>26</sub> H <sub>24</sub> N <sub>4</sub> S <sub>3</sub> O <sub>4</sub>	Dark Pink	82	611.33	210	51.07 (51.06)	3.95 (3.90)	9.16 (9.18)	15.73 (15.69)	-	9.60 (9.62)		
[Cu(MTPMA) <sub>2</sub> ]Cl <sub>2</sub>	CuC <sub>26</sub> H <sub>24</sub> N <sub>4</sub> S <sub>2</sub> Cl <sub>2</sub>	Dark Green	85	591.18	235	52.81 (52.79)	4.09 (4.03)	9.47 (9.49)	10.84 (10.83)	12.00 (12.03)	10.74 (10.78)		
[Zn(MTPMA)SO <sub>4</sub> ]	ZnC <sub>13</sub> H <sub>12</sub> N <sub>2</sub> S <sub>2</sub> O <sub>4</sub>	Dirty White	85	389.73	205	40.06 (40.10)	3.10 (3.12)	7.19 (7.14)	16.45 (16.42)	-	16.77 (16.75)		

## 4.4.2 Molar Conductivity

Molar conductance values ( $\Lambda$ m) of all the metal complexes were measured at room temperature in DMF at the concentration of  $10^{-3}$  M and are presented in **Table-4.2**.The values of  $\Lambda_m$  for all the metal complexes except that of zinc(II) fall in the range of 75-180  $\Omega^{-1}$  cm  $^2$  mol $^{-1}$  which indicate that these complexes are electrolytic in nature whereas zinc(II) is non-electrolytic in nature whose value is  $10.5 \Omega^{-1}$  cm  $^2$  mol $^{-1}$ . This is an evidence for both metal to ligand stoichiometry and presence of sulphate group inside the coordination sphere of zinc(II) complex.[4]

**Table-4.2: Molar Conductance Values of the MTPMA Metal Complexes** 

S.No	Complex	Molar Conductance $\Omega^{-1}$ cm $^2$ mol $^{-1}$
1.	[Fe(MTPMA) <sub>2</sub> ]Cl <sub>3</sub>	180
2.	[Co(MTPMA) <sub>2</sub> ](NO <sub>3</sub> ) <sub>2</sub>	150
3.	[Ni(MTPMA) <sub>2</sub> ]SO <sub>4</sub>	75
4.	[Cu(MTPMA) <sub>2</sub> ]Cl <sub>2</sub>	135
5.	[Zn(MTPMA)SO <sub>4</sub> ]	10.5

## 4.4.3. <sup>1</sup>H-NMR Spectra

The <sup>1</sup>H NMR spectrum of the Schiff base ligand MTPMA is shown in **Fig.4.2.**There is a sharp singlet peak at  $\partial$  8.5 ppm assignable to azomethine proton (-HC=N) whereas a multiplet observed at  $\partial$  7.2- 8.7 ppm is due to aromatic protons of pyridine moiety and 2-(methylthio)aniline. A singlet found at  $\partial$  2.5 ppm corresponds to –CH<sub>3</sub> protons. However, azomethine proton undergoes deshielding upon coordination as observed in <sup>1</sup>H NMR spectrum of Zn<sup>II</sup> complex (**Fig.4.3**) and appears at 8.6 ppm confirming the coordination through azomethine nitrogen. The multiplet corresponding to benzene ring protons appears in the region  $\partial$  6.5–8.8 ppm and are slightly shifted upfield, indicating the involvement of

sulphur atom and nitrogen atom of pyridine ring in the coordination. Two singlet peaks at  $\partial$  2.3 ppm and  $\partial$  2.4 ppm corresponds to the aliphatic methyl protons. This is an evidence for E configuration of the complex. Thus a comparison of signals due to the ligand and the complex confirms the condensation of pyridine-2-carboxaldehyde with 2-(methylthio)aniline resulting in the formation of (E)-2-(methylthio)-N-(pyridin-2-ylmethylene)aniline and also coordination of zinc metal to Schiff base.[5, 6] The <sup>1</sup>H NMR signals of the ligand MTPMA and those of Zn complex are listed in the **Tables-4.3 and 4.4.** 

Table-4.3: <sup>1</sup>H NMR Spectral Data of the Ligand MTPMA

S. No.	Signal Position (ppm)	Relative No. Of Protons	Multiplicity	Inference
1.	8.5	1H	Singlet	-HC=N (Azomethine protons)
2.	7.2-8.7	8Н	Multiplet	Ar-CH
3.	2.5	3Н	Singlet	-CH <sub>3</sub>

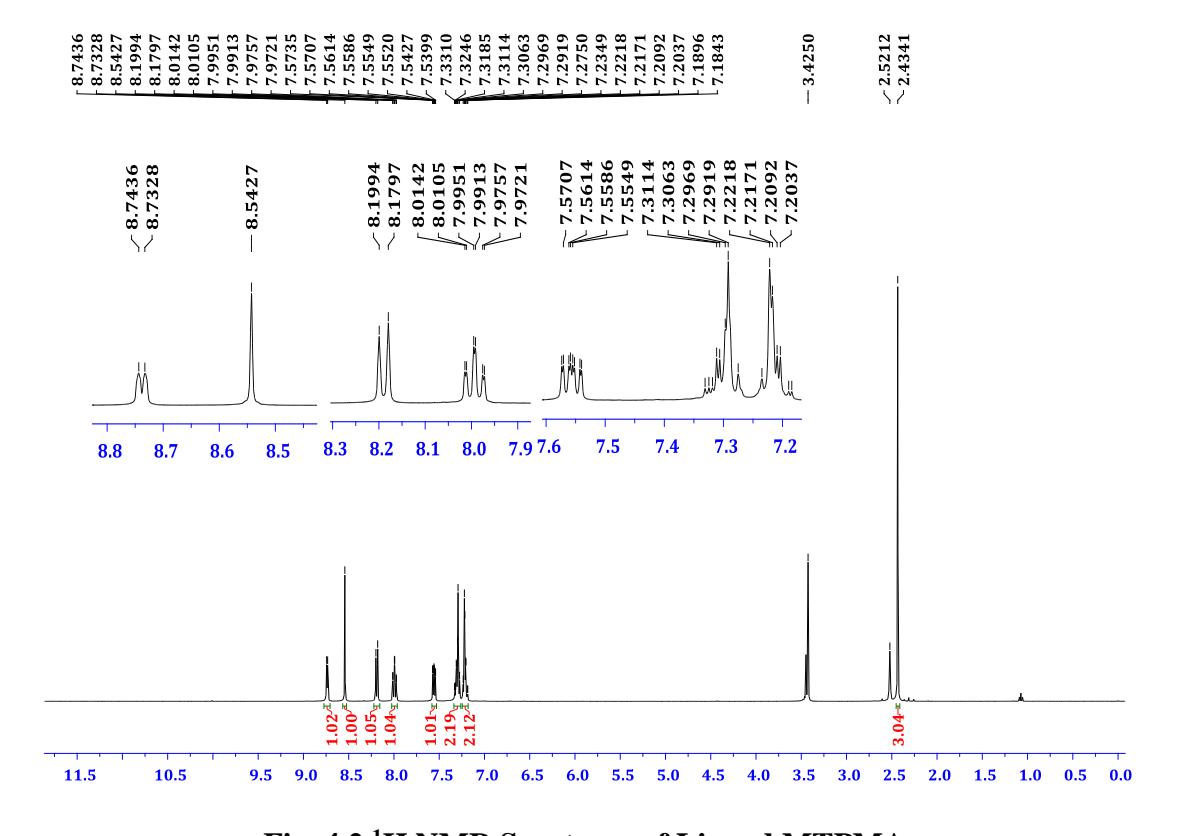


Fig. 4.2 <sup>1</sup>H NMR Spectrum of Ligand MTPMA

Table-4.4: <sup>1</sup>H NMR Spectral Data of the [Zn(MTPMA)SO<sub>4</sub>]

S. No.	Signal Position (ppm)	Relative No. Of Protons	Multiplicity	Inference
1.	8.5	2Н	Singlet	-HC=N(Azomethine proton)
2.	6.5-8.8	16H	Multiplet	Ar-CH
3.	2.3, 2.4	3Н, 3Н	Singlet	-CH <sub>3</sub> , -CH <sub>3</sub> (Two Different environments)

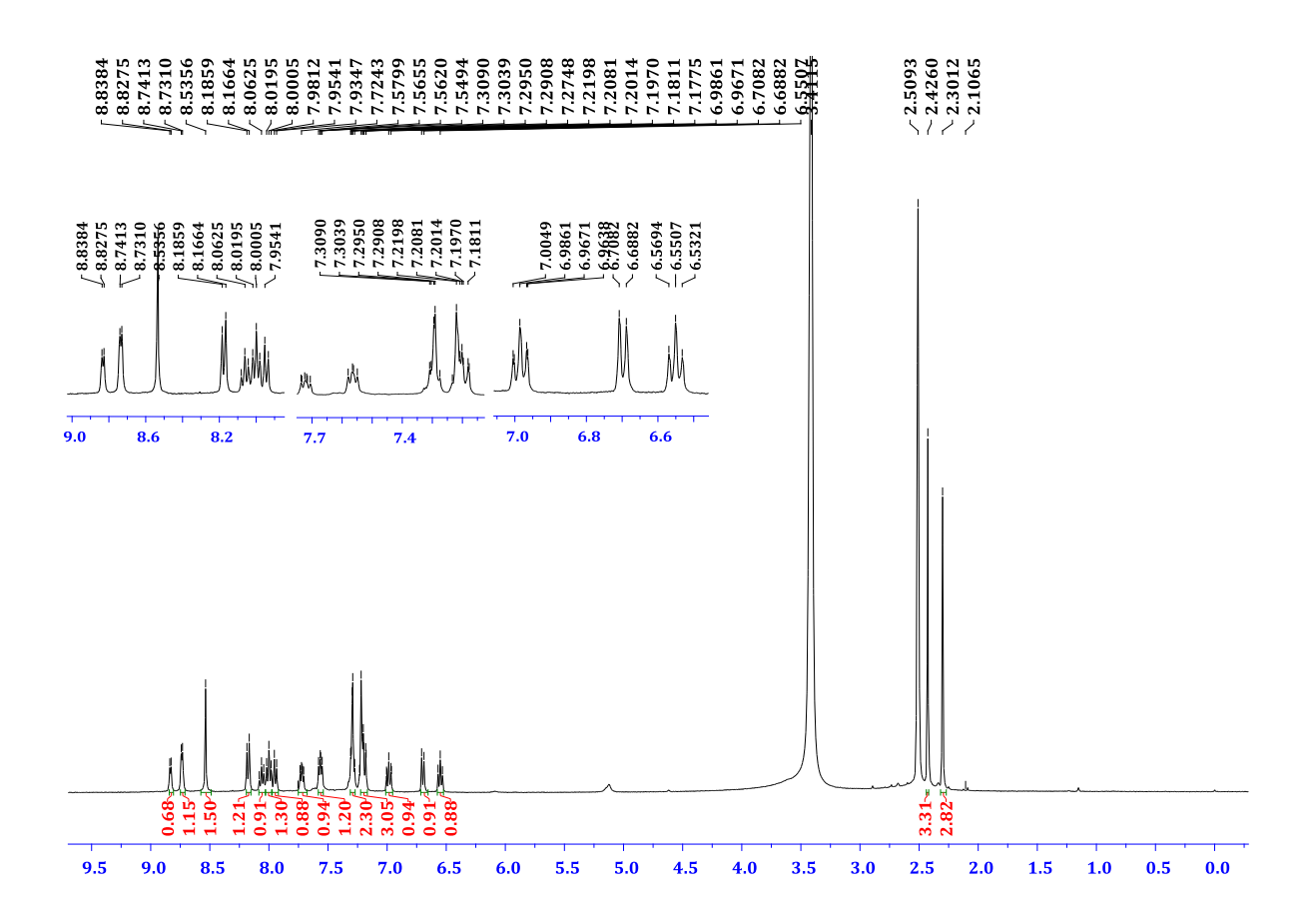


Fig. 4.3 <sup>1</sup>H NMR Spectrum of the [Zn(MTPMA)SO<sub>4</sub>]

# 4.4.4 FT-IR Spectra

IR spectroscopy is an appropriate technique to provide enough information on the mode of bonding of the ligand to the metal ion. The identification of the coordinating atoms has been done on the basis of comparison of the IR spectra of ligand and the complexes. The selected frequencies are shown in the **Table -4.5** and **Fig.4.4-4.9**.

The free Schiff base ligand MTPMA show a strong band at 1673 cm<sup>-1</sup> which is the characteristic band of azomethine linkage (-CH=N). Complexation of the ligand to metal ions through the azomethine linkage, reduces the electron density around nitrogen atom which lowers the ὑ<sub>(-CH=N)</sub> absorption frequency. Thus the bands due to azomethine linkage are now moved to lesser frequencies in the spectra of all the complexes (1621cm<sup>-1</sup> to 1630cm<sup>-1</sup>) signifying the coordination of azomethine nitrogen to metal ions. The coordination of azomethine nitrogen to metal ions is further supported by the presence of bands in the region of 456- 497 cm<sup>-1</sup> which are due to M-N linkage. [7]

In the spectra of the ligand MTPMA, band at  $1585 \text{cm}^{-1}$  is due to  $\dot{\upsilon}_{\text{(-CH=N)}}$  stretching vibration of pyridine ring .This band in the spectra of all complexes are shifted to lower frequencies ( $1435-1531~\text{cm}^{-1}$ ) indicating the coordination of the pyridine ring nitrogen to the metal ions[8].

Band at 783 cm<sup>-1</sup> in the spectrum of the ligand corresponds to C-S stretching vibration. This band is shifted to lower frequencies (745-764 cm<sup>-1</sup>) in the spectra of all complexes indicating the involvement of sulphur atom in coordination. It is further supported by the presence of bands in the range (640-658cm<sup>-1</sup>) which are due to M-S linkage.[9, 10] The presence of very sharp bands in the range (481-511cm<sup>-1</sup>) indicates the formation of M-N bond involving nitrogen atom of pyridine ring.[11]

From the above observation, it is clear that the Schiff base ligand MTPMA are coordinated to the metal ions through sulphur atom, azomethine nitrogen and nitrogen atom of pyridine ring.

All these information suggest that the ligand coordinates to the metal ions in a tridentate fashion.

Table-4.5: Selected FT-IR Absorption Frequencies (cm<sup>-1</sup>) of the Ligand MTPMA and its Metal Complexes

Compound	VCH=N <b>Azomethine</b>	v <sub>C=N</sub> Pyridine	VC-S	VM-N	VM-S	v <sub>M-N</sub> Pyridine
MTPMA	1673	1585	783			
[Fe(MTPMA) <sub>2</sub> ]Cl <sub>3</sub>	1622	1531	764	465	649	484
[Co(MTPMA) <sub>2</sub> ](NO <sub>3</sub> ) <sub>2</sub>	1626	1496	745	497	658	511
[Ni(MTPMA) <sub>2</sub> ]SO <sub>4</sub>	1630	1464	763	456	640	481
[Cu(MTPMA) <sub>2</sub> ]Cl <sub>2</sub>	1621	1435	745	482	645	502
[Zn(MTPMA)SO <sub>4</sub> ]	1622	1487	746	482	656	496

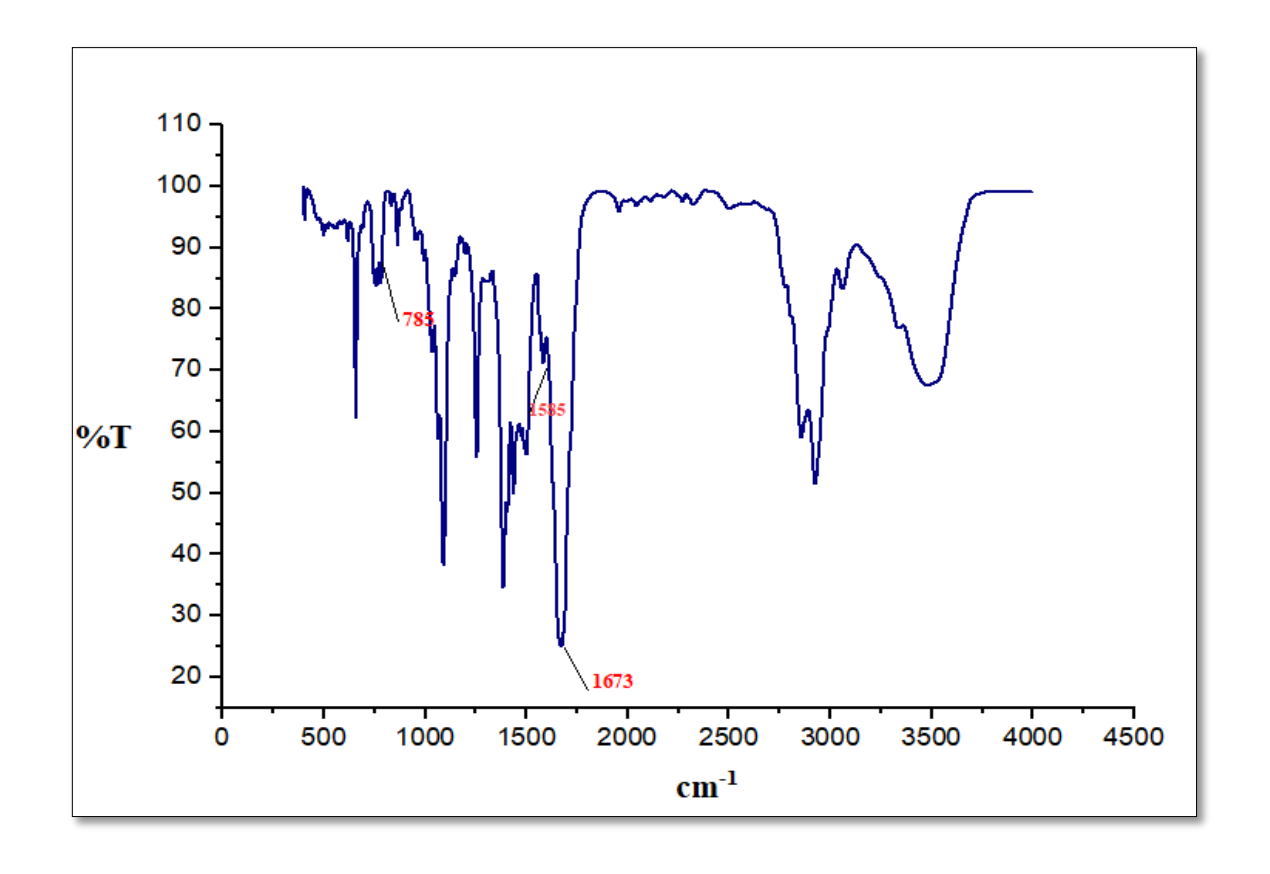


Fig. 4.4 FT-IR Spectrum of Schiff Base MTPMA

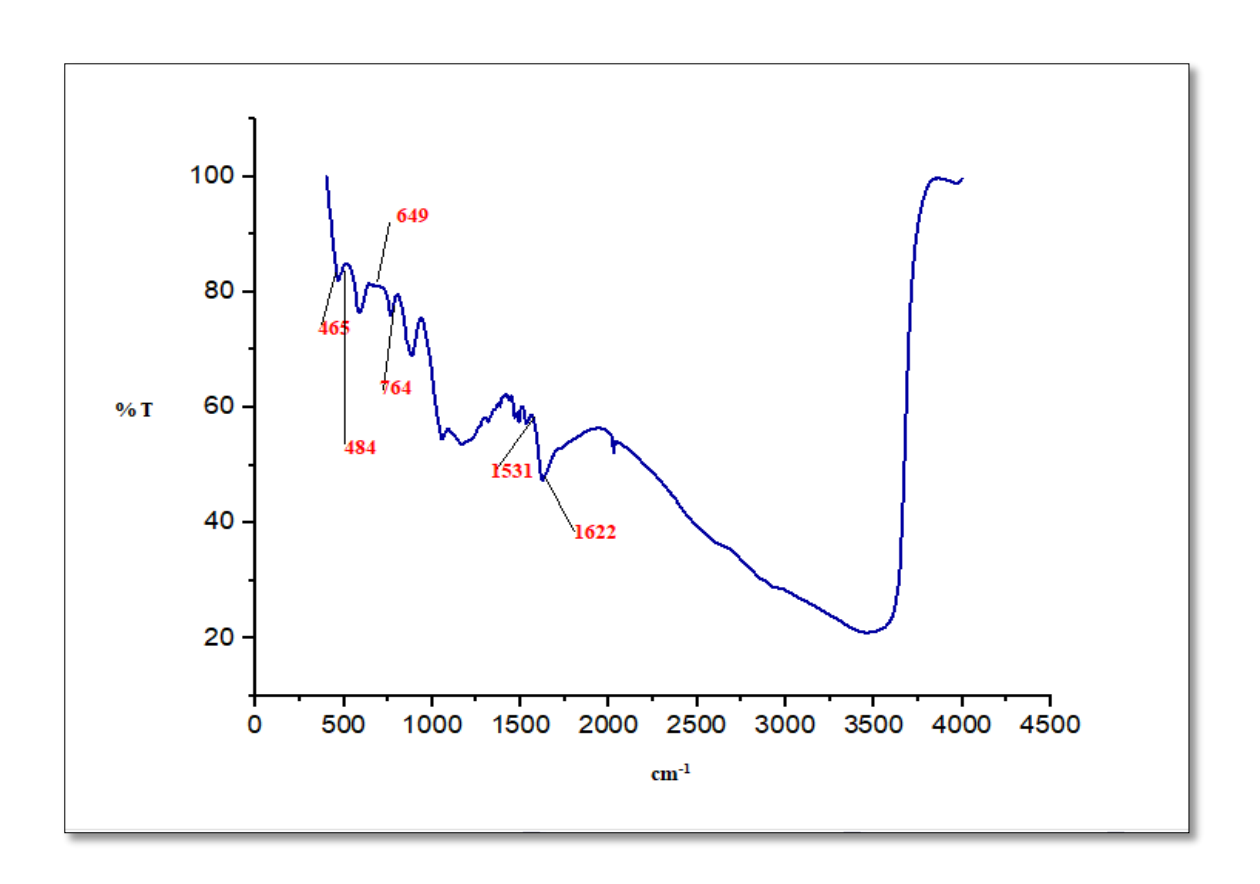


Fig. 4.5 FT-IR Spectrum of [Fe(MTPMA)<sub>2</sub>]Cl<sub>3</sub>

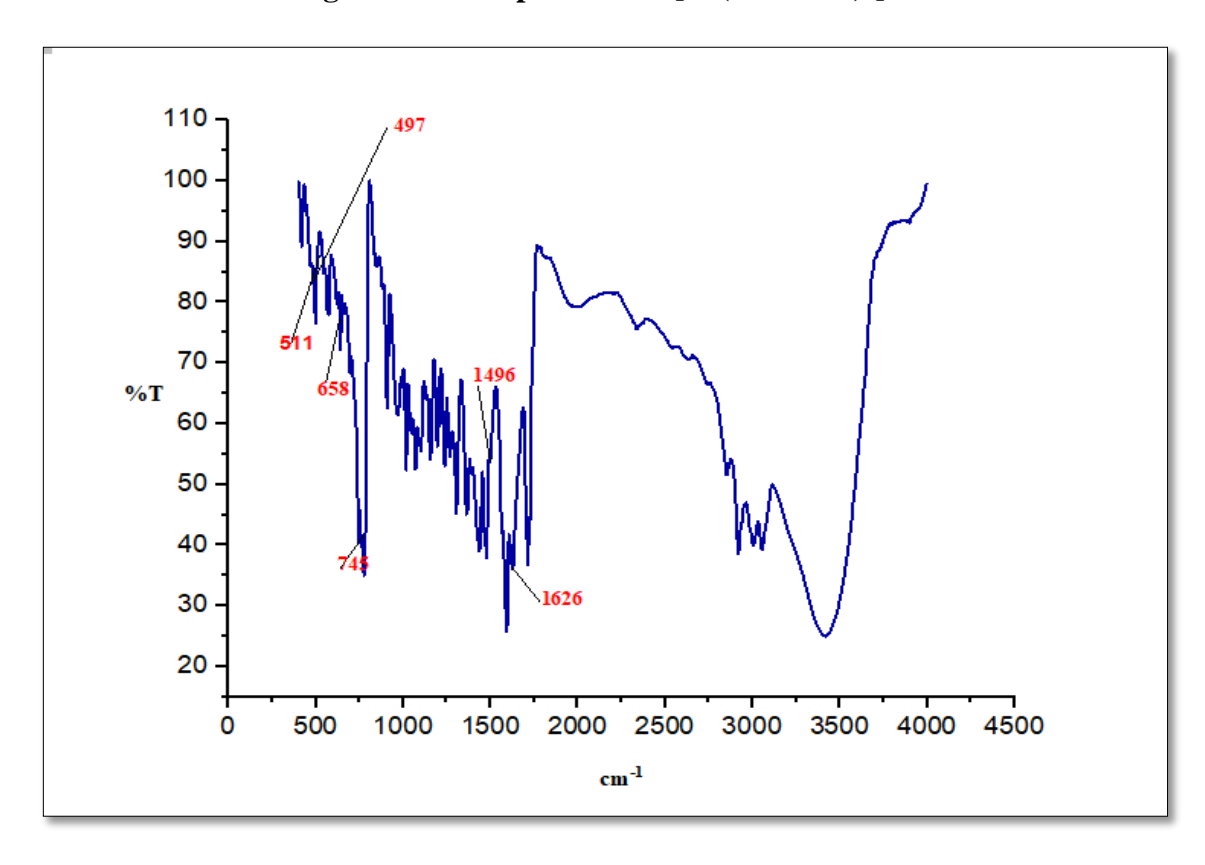


Fig. 4.6 FT-IR Spectrum of [Co(MTPMA)<sub>2</sub>](NO<sub>3</sub>)<sub>2</sub>

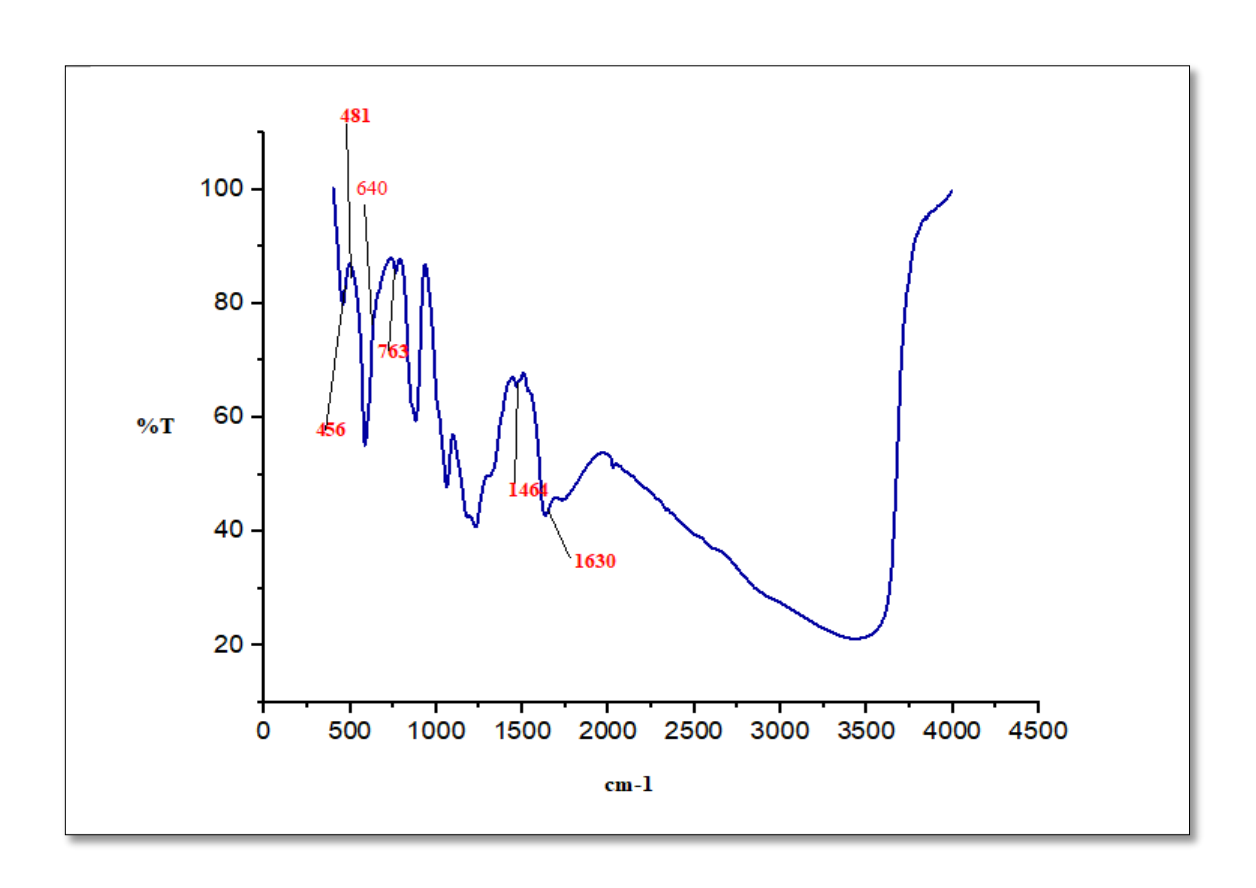


Fig. 4.7 FT-IR Spectrum of  $[Ni(MTPMA)_2]SO_4$ 

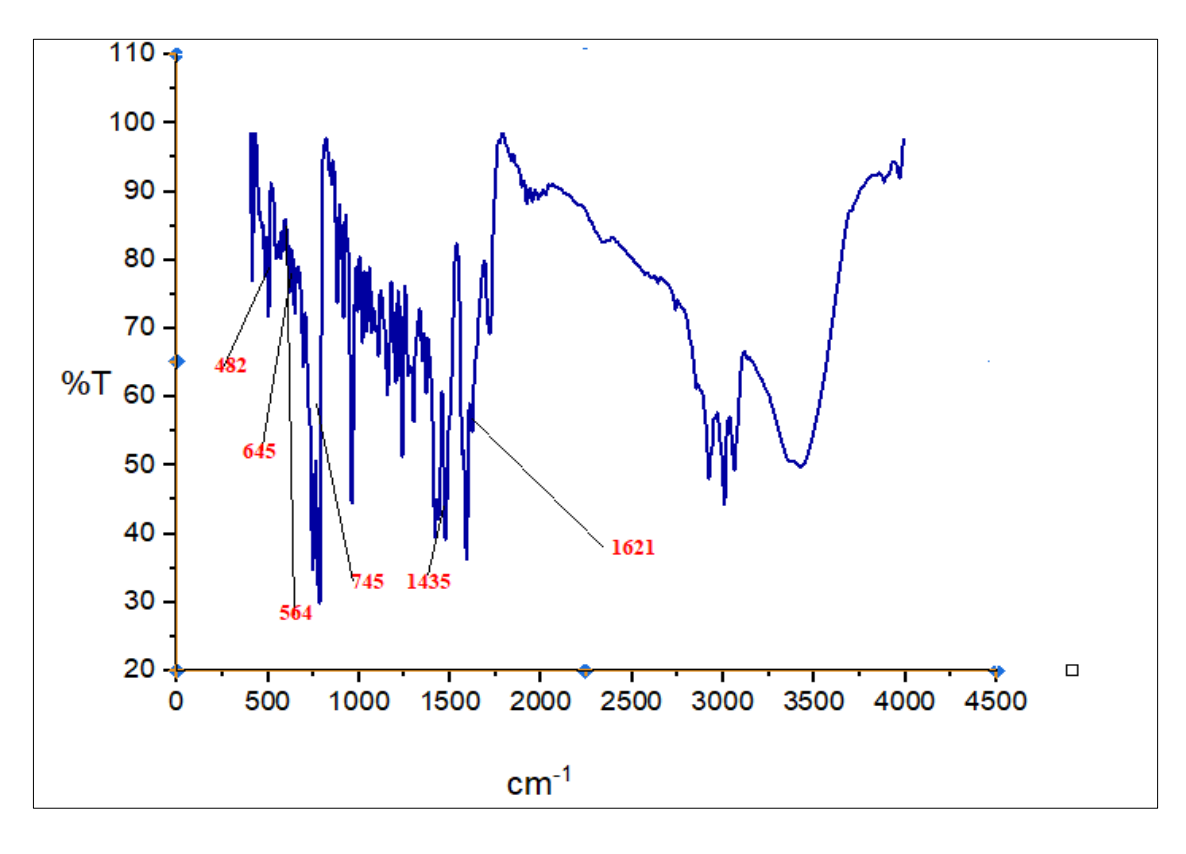


Fig. 4.8 FT-IR Spectrum of  $[Cu(MTPMA)_2]Cl_2$ 

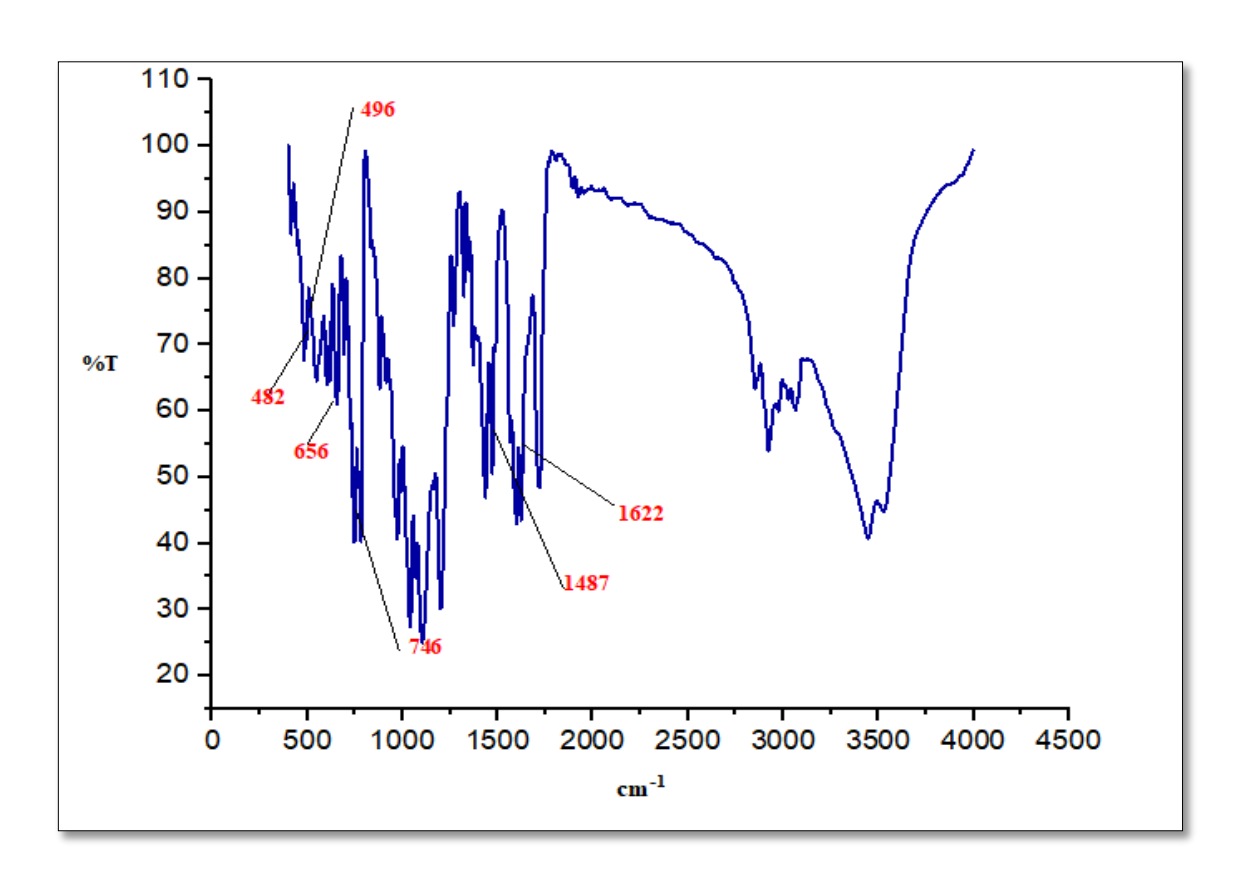


Fig. 4.9 FT-IR Spectrum of [Zn(MTPMA)SO<sub>4</sub>]

# 4.4.5 UV-Visible Spectra and Magnetic Moment

The electronic spectral data and magnetic moments of the metal complexes are used to acquire information about their geometry. The electronic spectra of the synthesized ligand MTPMA and its complexes given in the **Table-4.6** and **Fig.4.10-4.15**. The spectra were recorded at room temperature using DMSO solvent .The spectrum of the Schiff base ligand MTPMA shows two absorption bands at  $35,335\text{cm}^{-1}$  and 29,069 cm<sup>-1</sup> which are due to  $\pi$ - $\pi$ \* and n- $\pi$ \* transitions respectively of the azomethine group and aromatic rings of ligand and these transitions are shifted to longer wavelengths in the spectra of the complexes indicating the coordination of ligand to metal through azomethine and pyridine moieties. The band at 37,453 cm<sup>-1</sup> in the electronic spectra of the iron (III) complex is due to an intraligand  $\pi$ - $\pi$ \* transition. Another band at 30,864 cm<sup>-1</sup> could be due to charge transfer from metal to ligand. The other weaker bands are attributed to metal centre d-d transitions.

The magnetic moment of iron (III) at room temperature is 1.87 BM which is consistent with octahedral geometry. [12]

For high spin octahedral cobalt (II) complex, the ground state is  ${}^4T_{1g}$ , therefore orbital contribution is possible to the magnetic moment. The observed effective magnetic moments at room temperature are much higher than the spin only value and range from 4.70 to 5.20 BM. In the electronic spectrum of cobalt (II) complex, three absorption bands are observed in the range 13,458, 16,650 and 21,834 cm<sup>-1</sup>, which correspond to three spin allowed transitions  ${}^4T_{1g(F)} \rightarrow {}^4T_{2g(F)}$ ,  ${}^4T_{1g(F)} \rightarrow {}^4A_2g_{(F)}$ ,  ${}^4T_{1g(F)} \rightarrow {}^4T_{2g(P)}$  respectively. The magnetic moment of cobalt (II) complex at room temperature is 4.80 BM which confirms an octahedral geometry. [13] The electronic spectrum of the Ni<sup>II</sup> complex displays three bands at 9633 cm<sup>-1</sup> due to  ${}^3$  A<sub>2g</sub> $\rightarrow$   ${}^3$  T<sub>2g</sub>, 10, 905 cm<sup>-1</sup> due to  ${}^3$  A<sub>2g</sub>(F) $\rightarrow$   ${}^3$  T<sub>1g</sub>(F), 17, 158 cm<sup>-1</sup> due to  ${}^{3}A_{2g}(P) \rightarrow {}^{3}T_{1g}(P)$  [14, 15], which clearly indicate the octahedral stereochemistry of the nickel (II) complex. The magnetic moment of Ni (II) complex is 3.2 BM. Electronic spectrum of copper (II) complex show three absorption bands in the regions 28,089, 20,833 and 16,260 cm<sup>-1</sup> which are assigned to  ${}^{2}B_{1g} \rightarrow {}^{2}E_{g}$ ,  ${}^{2}B_{1g} \rightarrow {}^{2}B_{2g}$ , d-d transitions respectively. These values suggest distorted octahedral geometry. The magnetic moment of the copper (II) complex is 1.98 BM which confirms a distorted octahedral geometry for copper. [16, 17].

Zinc (II) complex shows only one band, centred at 27, 473cm<sup>-1</sup> which is attributed to metal –ligand charge transfer. This is well-matched with this complex possessing a tetrahedral geometry.[18, 19]

Table-4.6: Electronic Spectral Data of the Ligand MTPMA and its Metal Complexes

Compound	Wavelength λ <sub>max</sub> (nm)	Wave number $\bar{\upsilon}$ (cm <sup>-1</sup> )	Assignment	Geometry and Magnetic Moment		
A CEDA CA	283	35, 335	π-π*			
MTPMA	344	29, 069	n-π*			
[Fo(MTDMA), lCl.	267	37, 453	Intraligand π-π*	Octahedral 1.87		
[Fe(MTPMA) <sub>2</sub> ]Cl <sub>3</sub>	324	30, 864	MLCT	BM		
	743	13, 458	${}^{4}T_{1g(F)}> {}^{4}T_{2g(F)}$	0 1 1 1 1 00		
$[Co(MTPMA)_2](NO_3)_2$	600	16, 650	${}^{4}T_{1g(F)}> {}^{4}A_{2g(F)}$	Octahedral 4.80 BM		
	458	21, 834	${}^{4}T_{1g(F)}$ > ${}^{4}T_{2g(p)}$	] DIVI		
	1038	9, 633	$^{3}A_{2g} \rightarrow ^{3}T_{2g}$			
[Ni(MTPMA)2]SO4	917	10, 905	$^{3}A_{2g}(F) \rightarrow {}^{3}T_{1g}(F)$	Octahedral 3.2 BM		
	583	17, 158	$^{3}A_{2g}(F) \rightarrow ^{3}T_{1g}(P)$			
	615	16, 260	d-d transition	Distorted		
[Cu(MTPMA) <sub>2</sub> ]Cl <sub>2</sub>	480	20, 833	${}^{2}B_{1g}$ > ${}^{2}B_{2g}$	Octahedral 1.98		
	356	28, 089	${}^{2}B_{1g}> {}^{2}E_{g}$	BM		
[Zn(MTPMA)SO <sub>4</sub> ]	364	27, 473	LMCT	Tetrahedral Diamagnetic		

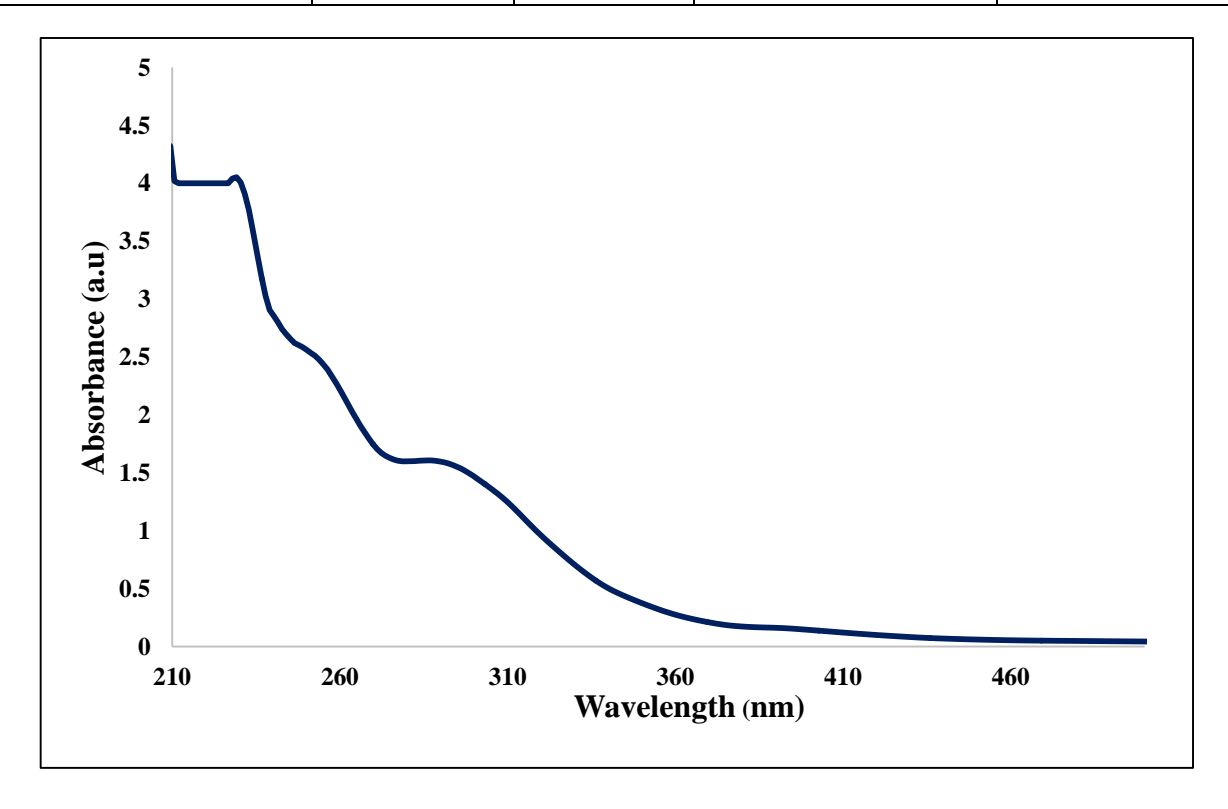


Fig. 4.10 UV- Vis Spectrum of Schiff Base MTPMA

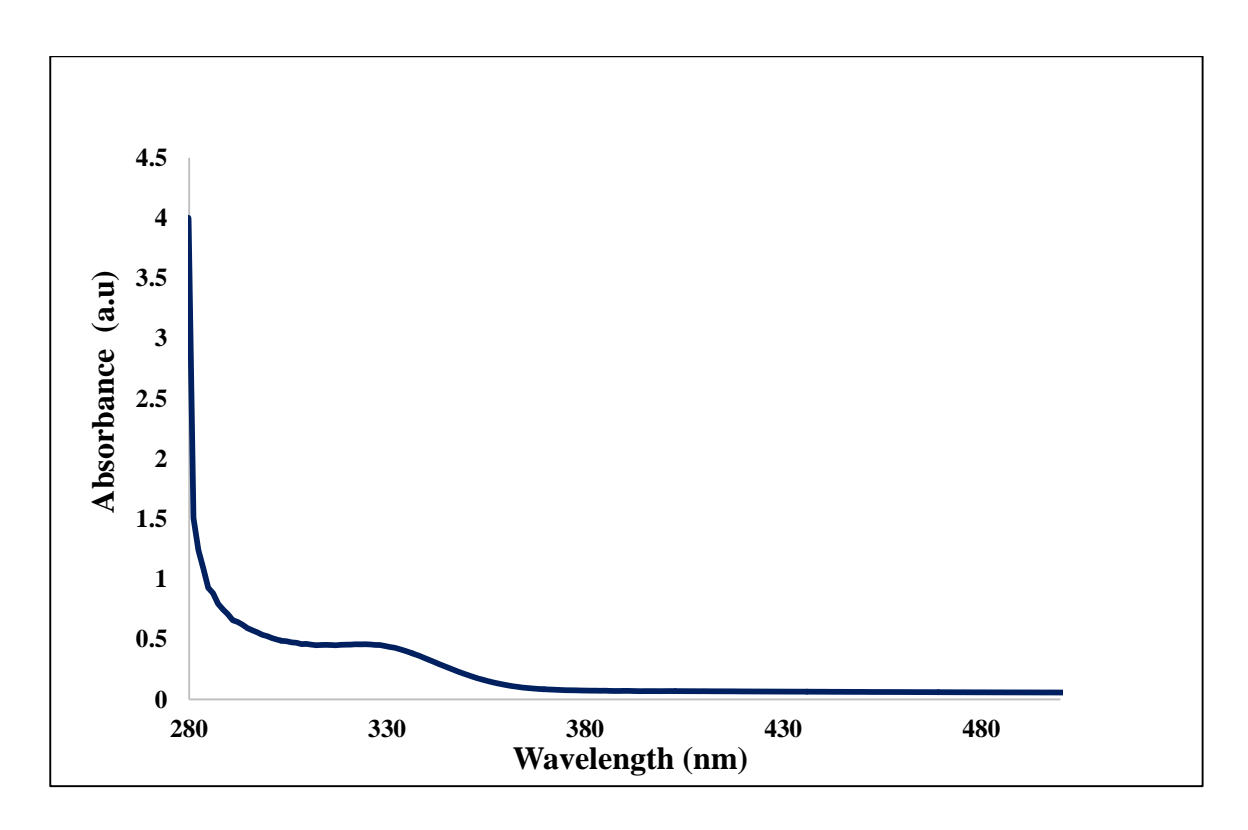


Fig. 4.11 UV- Vis Spectrum of  $[Fe(MTPMA)_2]Cl_3$ 

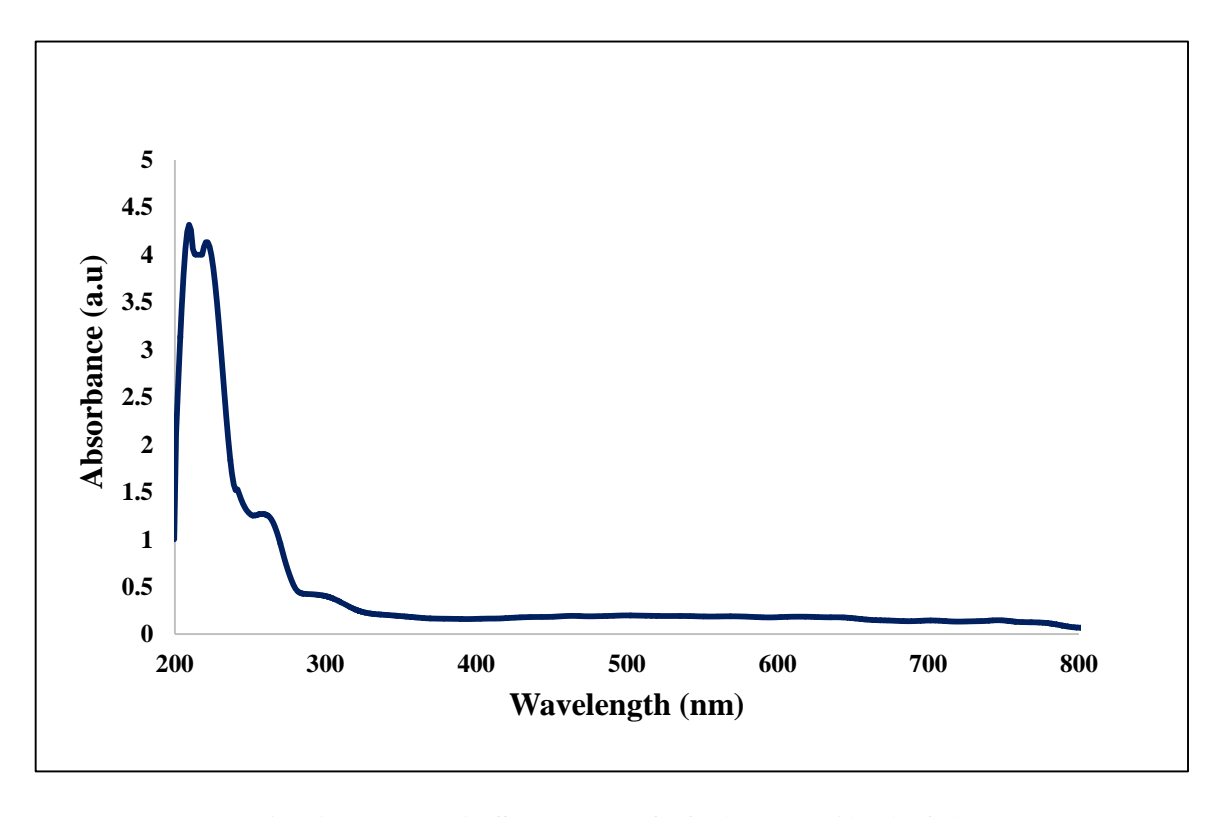


Fig. 4.12 UV- Vis Spectrum of [Co(MTPMA)<sub>2</sub>](NO<sub>3</sub>)<sub>2</sub>

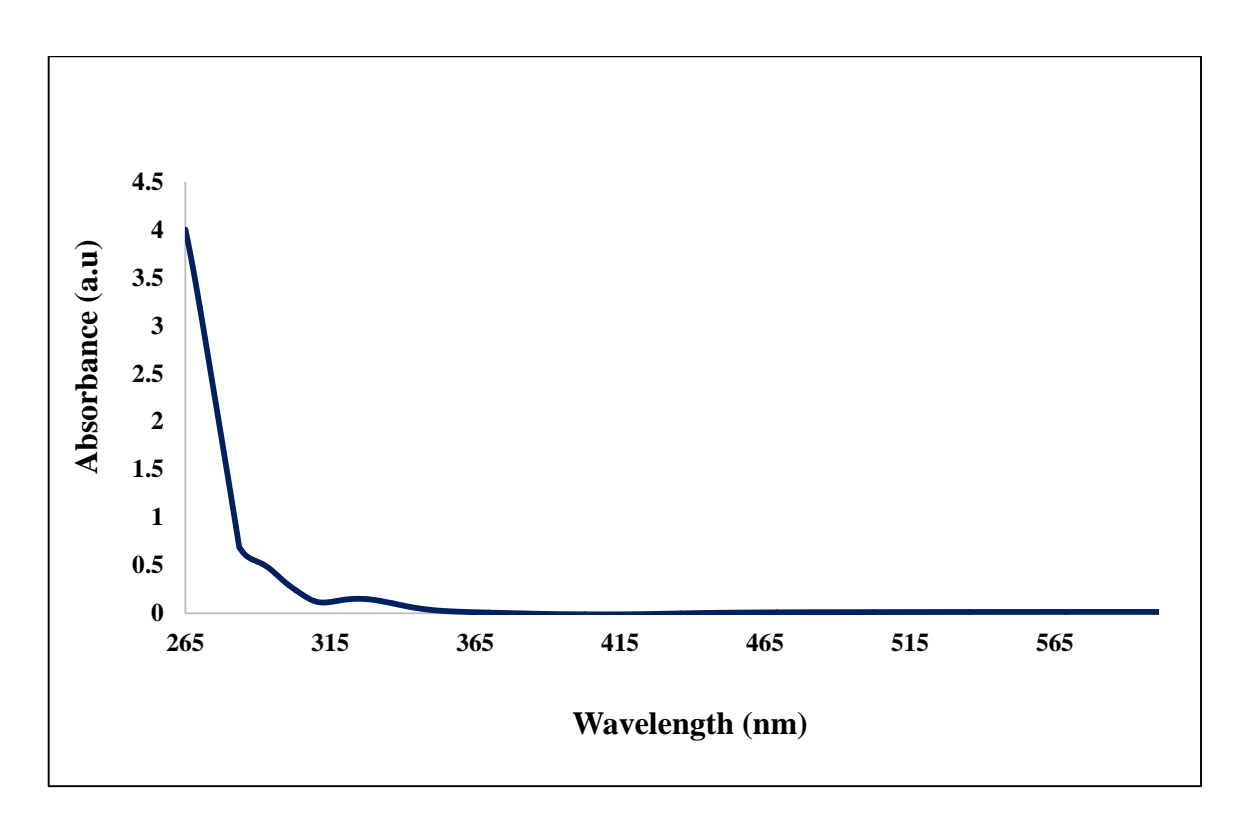


Fig. 4.13 UV- Vis Spectrum of [Ni(MTPMA)<sub>2</sub>]SO<sub>4</sub>

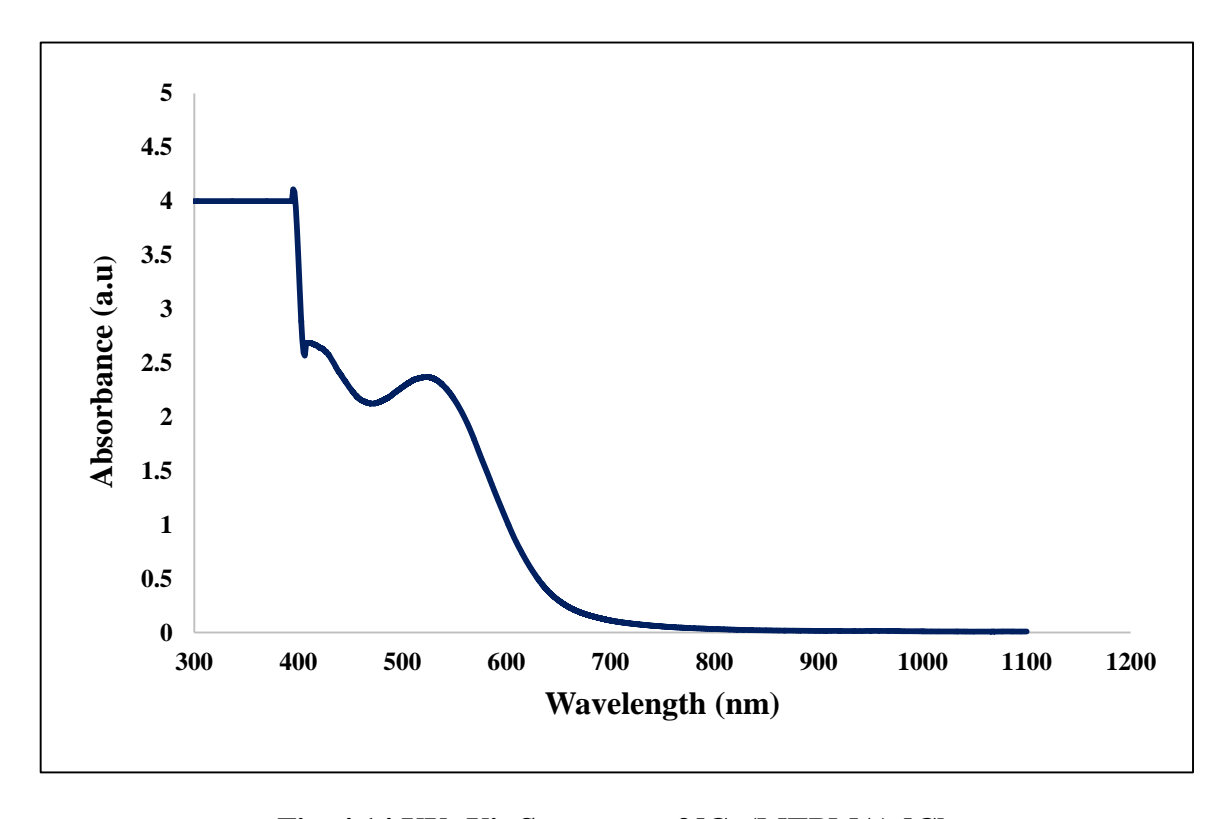


Fig. 4.14 UV- Vis Spectrum of [Cu(MTPMA)<sub>2</sub>]Cl<sub>2</sub>

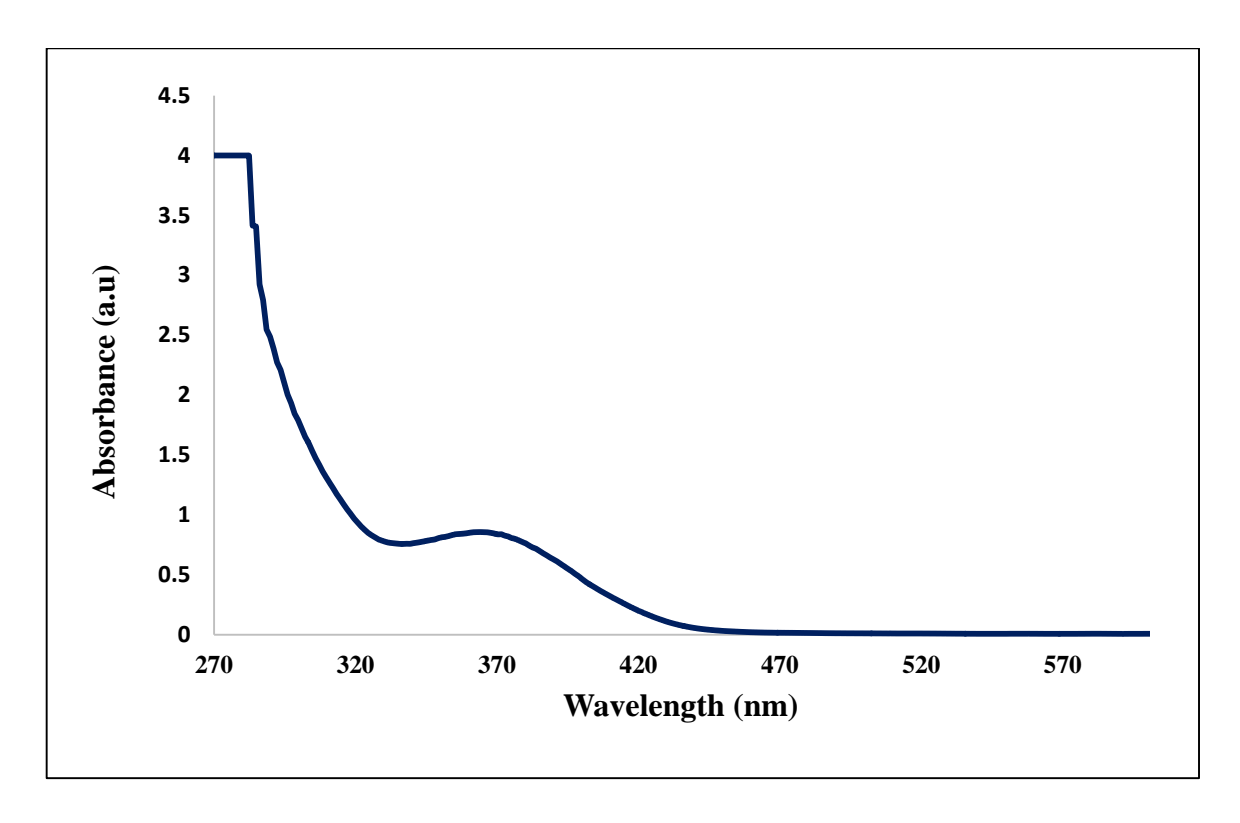


Fig. 4.15 UV- Vis Spectrum of [Zn(MTPMA)SO<sub>4</sub>]

## 4.4.6 Electron Paramagnetic Resonance Spectrum of [Cu(MTPMA)2]Cl2

The X band EPR spectrum of polycrystalline complex of  $Cu^{II}$  with MTPMA has been recorded at room temperature. The spectrum is shown in the **Fig.4.16** and Spin Hamiltonian parameters obtained are furnished in the **Table-4.7.**The EPR spectrum of the complex shows axial symmetry indicating distorted octahedral geometry. The  $g_{\parallel}$  and  $g_{\perp}$  values are 2.221 and 2.057 respectively .The g values of the complex follow the trend  $g_{\parallel}$  >  $g_{\perp}$ > $g_e$  suggesting that the unpaired electron predominantly lies in the d  $_x^2$ - $_y^2$  orbital at room temperature, as was evident from the value of the exchange interaction term G, estimated from the expression:  $G = (g_1 - 2.00277)/(g_{\perp} - 2.00277)$ . [20]

The local tetragonal axes are parallel or just slightly misaligned if G > 4.0. If G is less than 4.0, there is strong exchange coupling and the misalignment is noticeable. The observed exchange interaction parameter for the copper complex G > 4.0 suggests that the local tetragonal axes are aligned parallel or slightly misaligned and the unpaired electron is

present in the d  $x^2$  -  $y^2$  orbital. This result indicates that in the current complex, exchange coupling effects are not present.

Kivelson and Neidman have reported [21] that  $g_{\parallel}$  value for covalent environment is less than 2.3 and for ionic environment  $g_{\parallel}$  value is 2.4 or greater. Here, the  $g_{\parallel}$  value is slightly less than 2.3 indicating the covalent nature of the metal –ligand bonding in the complex.

Table-4.7: EPR Spectral data of [Cu(MTPMA)<sub>2</sub>]Cl<sub>2</sub>

Complex	$\mathbf{g}_{\parallel}$	g⊥	$\mathbf{g}_{\mathrm{av}}$	G	giso
[Cu(MTPMA) <sub>2</sub> ]Cl <sub>2</sub>	2.221	2.057	2.111	4.0202	-

Based on the above discussion, distorted octahedral geometry is assigned to copper (II) complex.

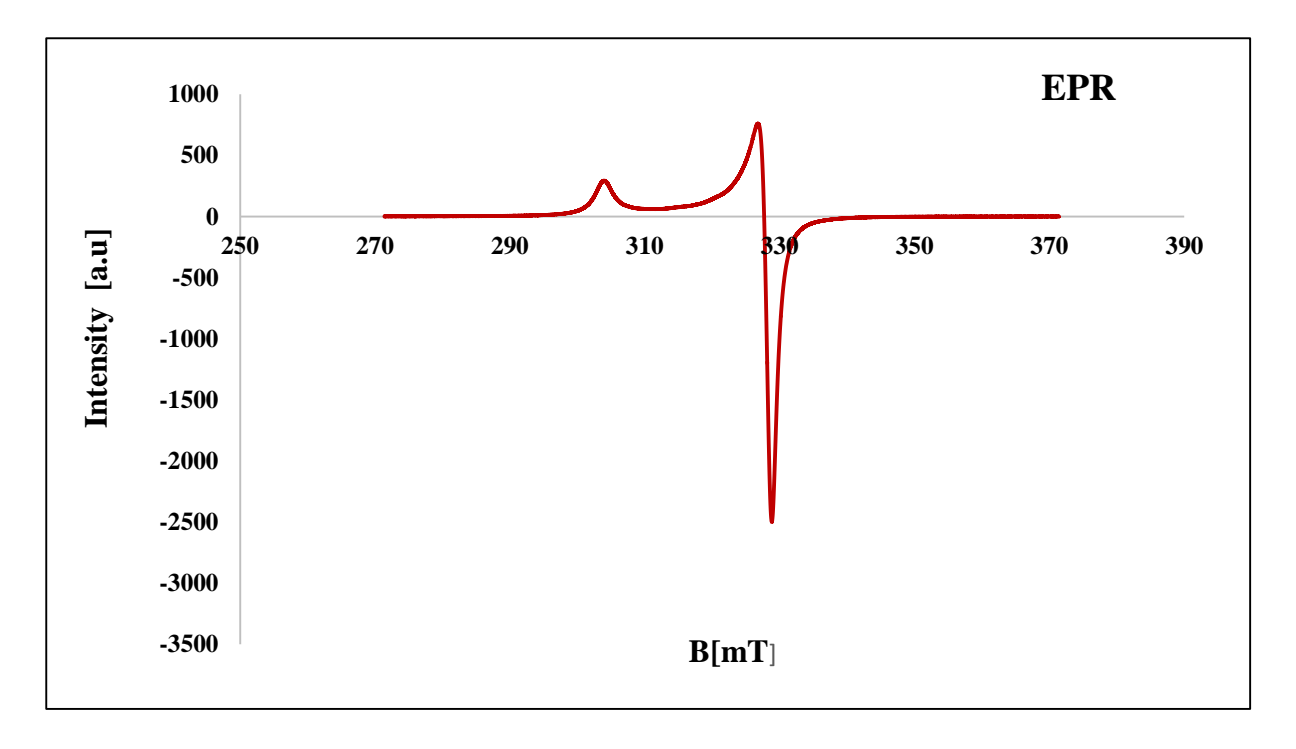


Fig.4.16 EPR Spectrum of [Cu(MTPMA)2]Cl2

## 4.4.7 LC-MS Spectrum of [Cu(MTPMA)<sub>2</sub>]Cl<sub>2</sub>

The LC-MS spectrum of copper complex is shown in Fig. 4.17. The copper complex ( $CuC_{26}H_{24}N_4S_2Cl_2$ ) with ligand shows the molecular ion peak at m/z =  $591(M)^+$ . The data confirms the stoichiometry of the metal complex as octahedral type.

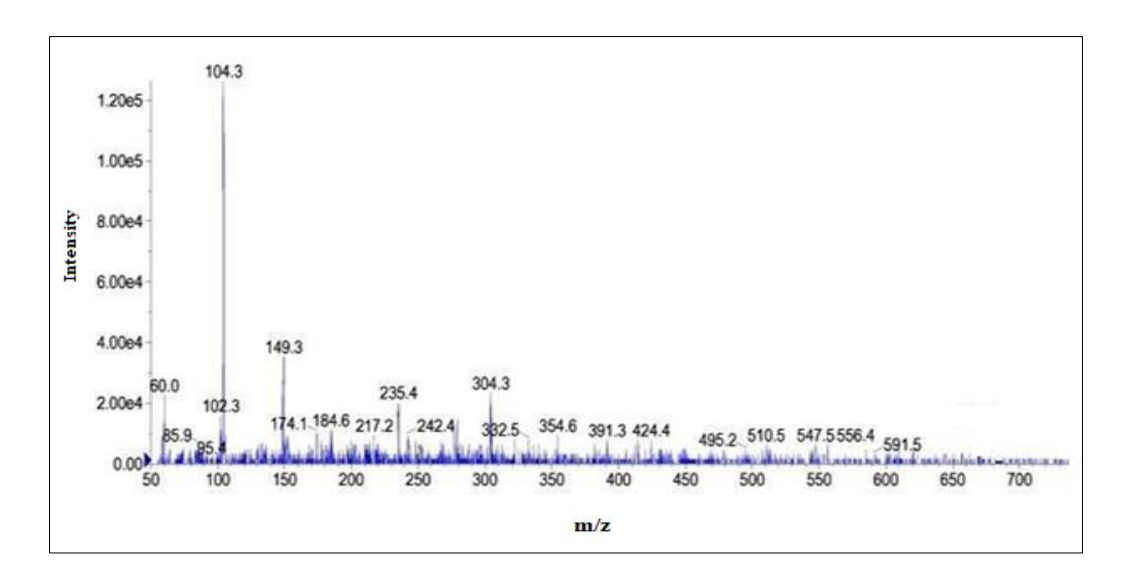


Fig.4.17 LC-MS Spectrum of [Cu(MTPMA)<sub>2</sub>]Cl<sub>2</sub>

## 4.4.8 Cyclic Voltammetry Studies

Electrochemical techniques are the most effective and convenient methods for studying redox systems mechanistically. The electrochemical properties of a chelating ring are highly dependent on its size, unsaturation distribution, and substitution pattern. Cyclic voltammetry studies of the synthesized complexes have been investigated in DMF (10<sup>-3</sup>mol<sup>-1</sup>) at the scan rate of 0.1 Vs<sup>-1</sup> in the potential range from + 2 V to -2 V. The redox potentials obtained are summarised in **Table-4.8** and peaks are shown in **Fig.4.18-4.20**.

The cyclic voltammogram of  $[Fe(MTPMA)_2]Cl_3$  complex in DMF solution measured at  $0.1Vs^{-1}$  registers a cathodic peak potential  $(E_{pc})$  value at -45.56 mV and corresponding anodic peak potential value  $(E_{pa})$  at 193.68 mV. These peak potential values suggest the reduction of  $Fe^{III}$  to  $Fe^{II}$ . The separation between the anodic and cathodic peak potential  $(\Delta E_p)$  is 239.24 mV, which indicates a quasi-reversible redox couple. The ratio of

current peaks  $I_{pa}/I_{pc}$  at  $0.1Vs^{-1}$  is -1.66. This value is less than 1 suggesting one electron transfer is followed by a chemical reaction. (ie EC mechanism is observed).

The cyclic voltammogram of  $[Co(MTPMA)_2](NO_3)_2$  complex in DMF solution measured at  $0.1Vs^{-1}$  records a cathodic peak potential  $(E_{pc})$  at -40.12 mV and corresponding anodic peak potential value  $(E_{pa})$  at 196.59 mV. These peak potentials suggest the reduction of  $Co^{II}$  to  $Co^{I}$ . The separation between the anodic and cathodic peak potential  $(\Delta E_p)$  is 236.71 mV, which indicates a quasi-reversible redox couple. The ratio of current peaks at  $0.1Vs^{-1}$  is -1.60. This value is less than 1 signifying the one electron transfer is followed by a chemical reaction. (ie EC mechanism is observed).[22]

The cyclic voltammogram of [Ni(MTPMA)<sub>2</sub>]SO<sub>4</sub> complex in DMF solution measured at  $0.1 \text{Vs}^{-1}$  registers a cathodic peak potential (E<sub>pc</sub>) value at -42.55 mV and corresponding anodic peak potential value (E<sub>pa</sub>) at 198.98 mV. These values suggest the reduction of Ni<sup>II</sup> to Ni<sup>I</sup>. The separation between the anodic and cathodic peak potential ( $\Delta E_p$ ) is 241.53 mV, which indicates a quasi-reversible redox couple. The ratio of current peaks at  $0.1 \text{Vs}^{-1}$  is -1.66. This value is less than 1 suggesting the one electron transfer is followed by a chemical reaction. (ie EC mechanism is observed).[23]

The cyclic voltammogram of  $[Cu(MTPMA)_2]Cl_2$  measured at 0.1 Vs<sup>-1</sup> scan rate features the reduction of  $Cu^{II}$  to  $Cu^{II}$  at cathodic peak potential of -42.56 mV. Reoxidation of  $Cu^{II}$  to  $Cu^{II}$  occurs at 203.96 mV at anodic peak potential upon scan reversal. The separation between the anodic and cathodic peak potentials  $\Delta Ep$  is 246.89mV, which indicates a quasi-reversible redox couple. Further, the current peak ratio at 0.1 Vs<sup>-1</sup> is -1.62. This value is less than 1 suggesting that one electron transfer is followed by a chemical reaction.[24]

The cyclic voltammogram of [Zn(MTPMA)SO<sub>4</sub>] complex in DMF solution measured at  $0.1 \text{Vs}^{-1}$  registers a cathodic peak potential ( $E_{pc}$ ) value at -30.66 mV and corresponding anodic peak potential value ( $E_{pa}$ ) at 200.27 mV. This peak potential suggest the reduction of  $Zn^{II}$  to  $Zn^{I}$ . The separation between the anodic and cathodic peak potential ( $\Delta E_{p}$ ) is 230.93 mV, which indicates a quasi- reversible redox couple. The ratio of current peaks at  $0.1 \text{Vs}^{-1}$  is -1.65. This value is less than 1 suggesting that one electron transfer is followed by a chemical reaction.(ie EC mechanism is observed).[25, 26]

Table- 4.8: Cyclic Voltammetric Data for MTPMA Metal Complexes in DMF solution at 298 K

Complex	E <sub>pc</sub> (mV)	E <sub>pa</sub> (mV	ΔE <sub>p</sub> (mV)	E <sub>1/2</sub> (mV)	I <sub>pc</sub> (µA)	I <sub>pa</sub> (μA)	I <sub>pa</sub> /I <sub>pc</sub>
[Fe(MTPMA) <sub>2</sub> ]Cl <sub>3</sub>	-45.56	193.68	239.24	74.06	-73.23	121.74	-1.66
[Co(MTPMA) <sub>2</sub> ](NO <sub>3</sub> ) <sub>2</sub>	-40.12	196.59	236.71	93.24	-73.71	118.16	-1.60
[Ni(MTPMA) <sub>2</sub> ]SO <sub>4</sub>	-42.55	198.98	241.53	93.22	-65.71	109.25	-1.66
[Cu(MTPMA) <sub>2</sub> ]Cl <sub>2</sub>	- 42.93	203.96	246.89	80.52	-69.38	113.72	-1.62
[Zn(MTPMA)SO <sub>4</sub> ]	-30.66	200.27	230.93	84.67	-59.66	98.6	-1.65

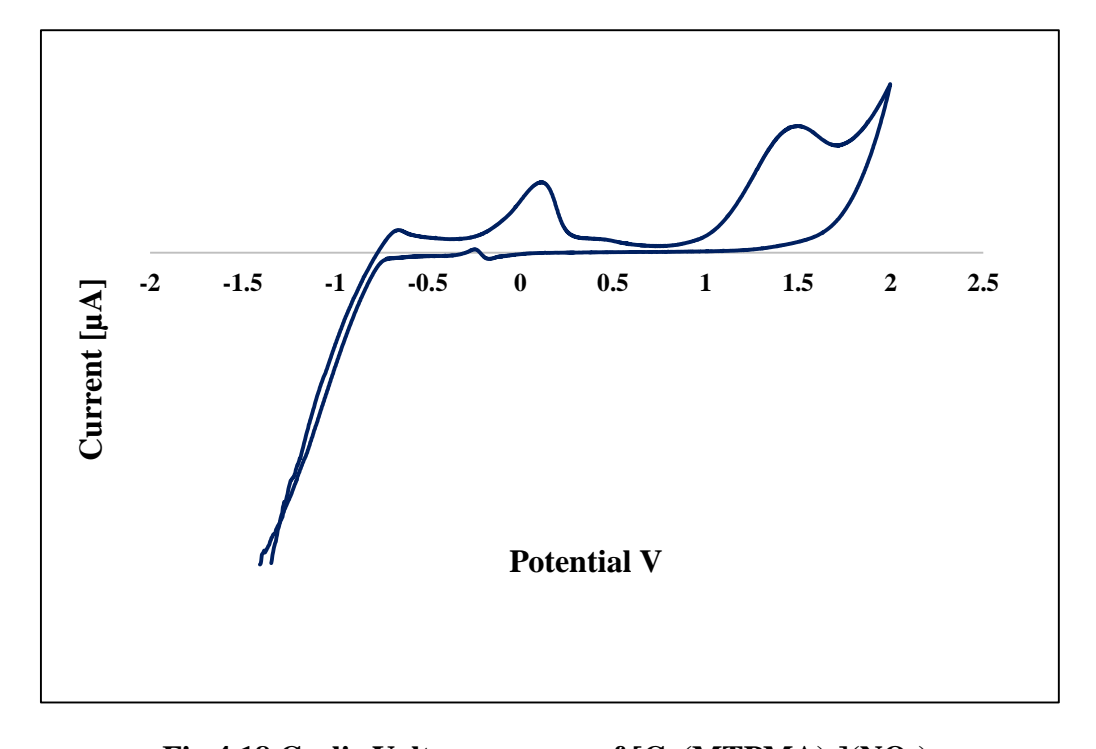
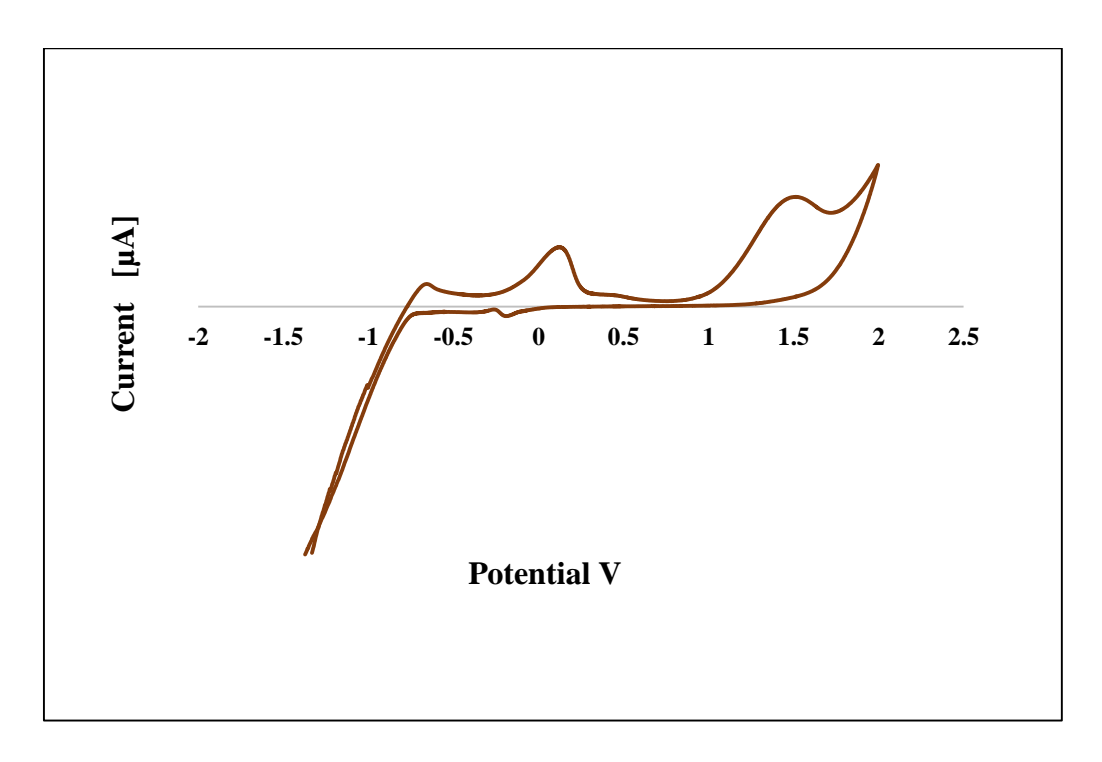


Fig.4.18 Cyclic Voltammogram of [Co(MTPMA)2](NO3)2



 $Fig. 4.19 \ Cyclic \ Voltammogram \ of \ [Cu(MTPMA)_2]Cl_2$ 

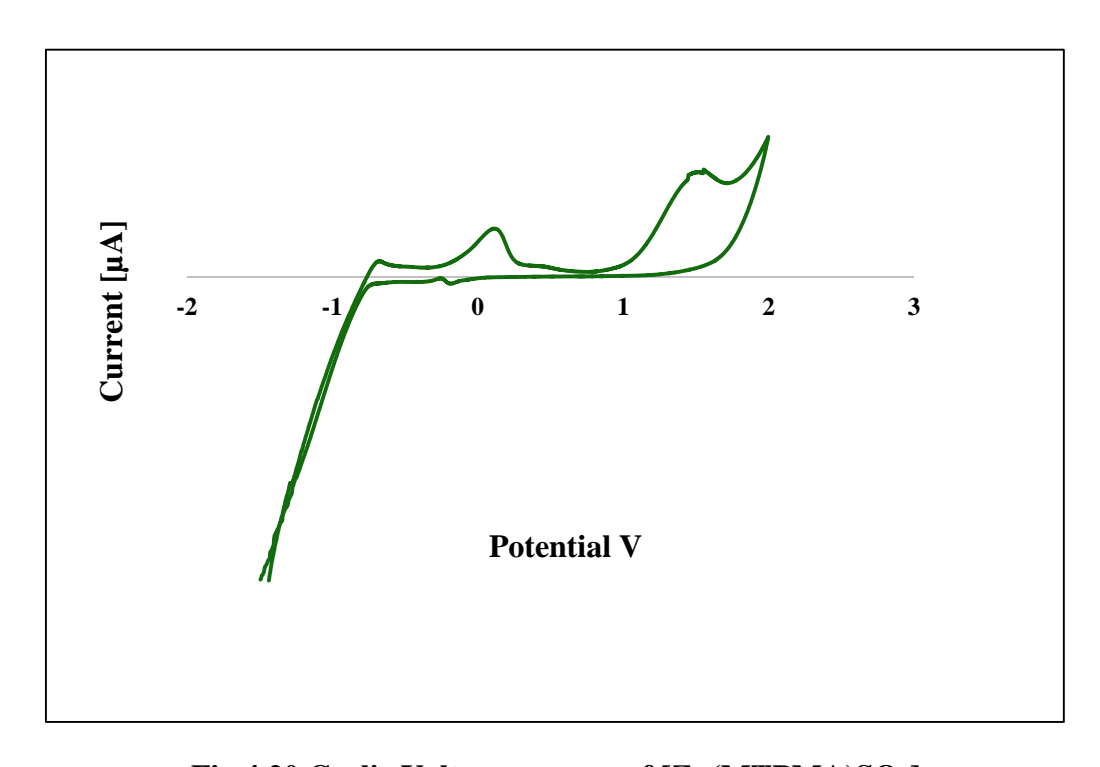


Fig.4.20 Cyclic Voltammogram of [Zn(MTPMA)SO<sub>4</sub>]

## **4.4.9** Thermal Decomposition Studies

The thermal data for the Schiff base metal complexes are furnished in **Fig.4.21-4.24**. by TG-DTG measurements were performed at temperatures ranging from room temperature to 850°C. The correlations between different decomposition steps of the compounds and the corresponding weight losses (**Table-4.9**) are discussed in terms of the proposed formulae of the compounds.

The thermal decomposition of Fe<sup>III</sup> complex proceeds with only one main degradation step. This step occurs within the temperature range 380-470°C with a mass loss of 88.72% (calculated mass loss: 90.99%), which is due to the complete loss of organic and anionic groups, leaving metal oxide as residue. [27]

The Co<sup>II</sup> complex with the molecular formula [Co(MTPMA)<sub>2</sub>](NO<sub>3</sub>)<sub>2</sub> is thermally decomposed in a single step. The estimated mass loss of 87.82% (calculated mass loss: 90.78%) within the temperature range 360–470°C may be attributed to the complete loss of organic and anionic groups, leaving metal oxide as residue.

The thermal decomposition of Ni<sup>II</sup> complex with molecular formula [Ni(MTPMA)<sub>2</sub>]SO<sub>4</sub> proceeds with only one degradation step. It occurs in the temperature range of 270-380°C with a mass loss of 82.31% (calculated mass loss: 90.41%) which is reasonably accounted for the complete loss of organic and anionic groups, leaving metal oxide as residue.

The Cu<sup>II</sup> complex with the molecular formula [Cu(MTPMA)<sub>2</sub>]Cl<sub>2</sub> is thermally decomposed in a single step. The estimated mass loss of 86.82% (calculated mass loss: 89.25%) within the temperature range 370-480°C may be attributed to the complete loss of organic and anionic groups, leaving metal oxide as residue.

Table- 4.9: Thermal Degradation Data of MTPMA Metal Complexes obtained from TG-DTG Curve

C1		Temperature		% of W	eight loss	% of ]	Residue		
Compound	Stage	Range (° C)	Assignments	Calc.	Expt.	Calc.	Expt.	Nature	
[Fe(MTPMA) <sub>2</sub> ]Cl <sub>3</sub>	I	380-470	Loss of Ligands and chloro groups	90.99	88.72	11.60	11.28	FeO	
[Co(MTPMA) <sub>2</sub> ](NO <sub>3</sub> ) <sub>2</sub>	I	390-500	Loss of Ligands and nitrate groups	90.78	87.82	11.71	12.8	СоО	
[Ni(MTPMA) <sub>2</sub> ]SO <sub>4</sub>	I	270-380	Loss of Ligands and sulphate groups	90.41	82.31	12.21	17.69	NiO	
[Cu(MTPMA) <sub>2</sub> ]Cl <sub>2</sub>	I	370-480	Loss of Ligands and chloro groups	89.25	86.82	13.45	13.18	CuO	
[Zn(MTPMA)SO <sub>4</sub> ]	I	280 -390	Loss of Ligands and sulphate groups	83.23	82.13	20.88	17.87	ZnO	

In case of  $Zn^{II}$  complex with the molecular formula [ $Zn(MTPMA)SO_4$ ], thermal decomposition occurs at 280-390°C with a mass loss of 82.13 % ( calculated mass : 83.23%)which is due to the decomposition of organic ligand and sulphate group, leaving metal oxide as residue.

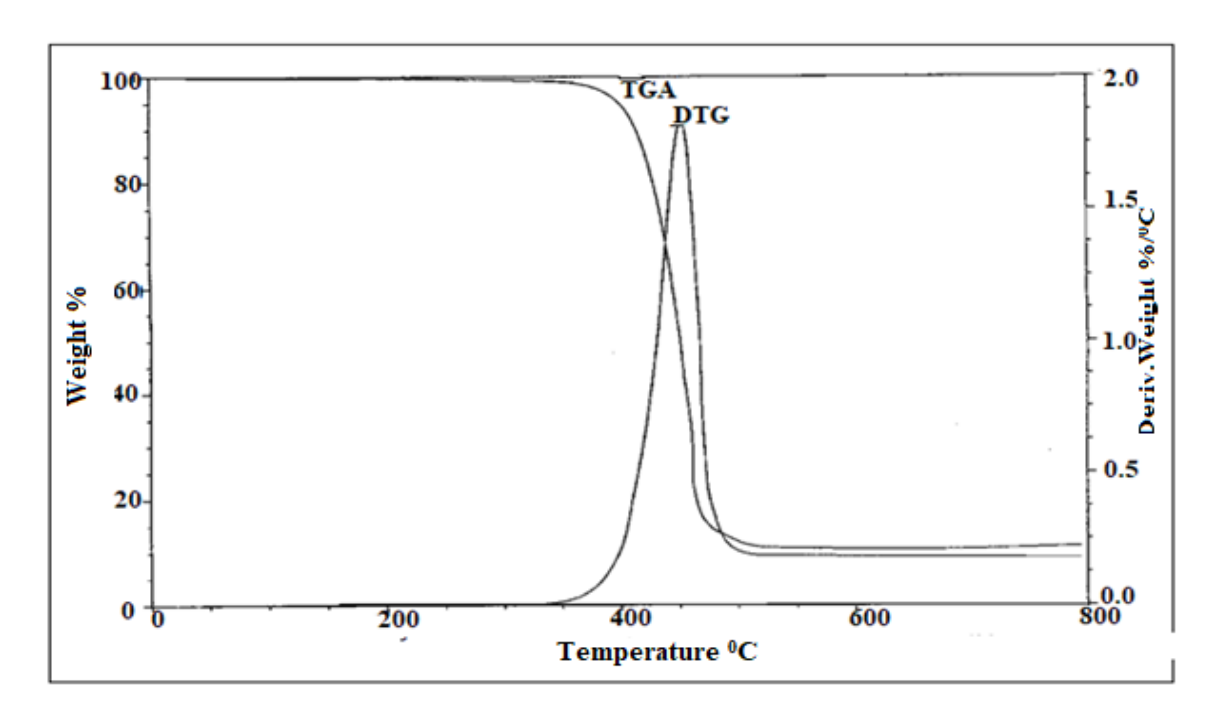


Fig.4.21 TG-DTG Curves of [Fe(MTPMA)<sub>2</sub>]Cl<sub>3</sub>

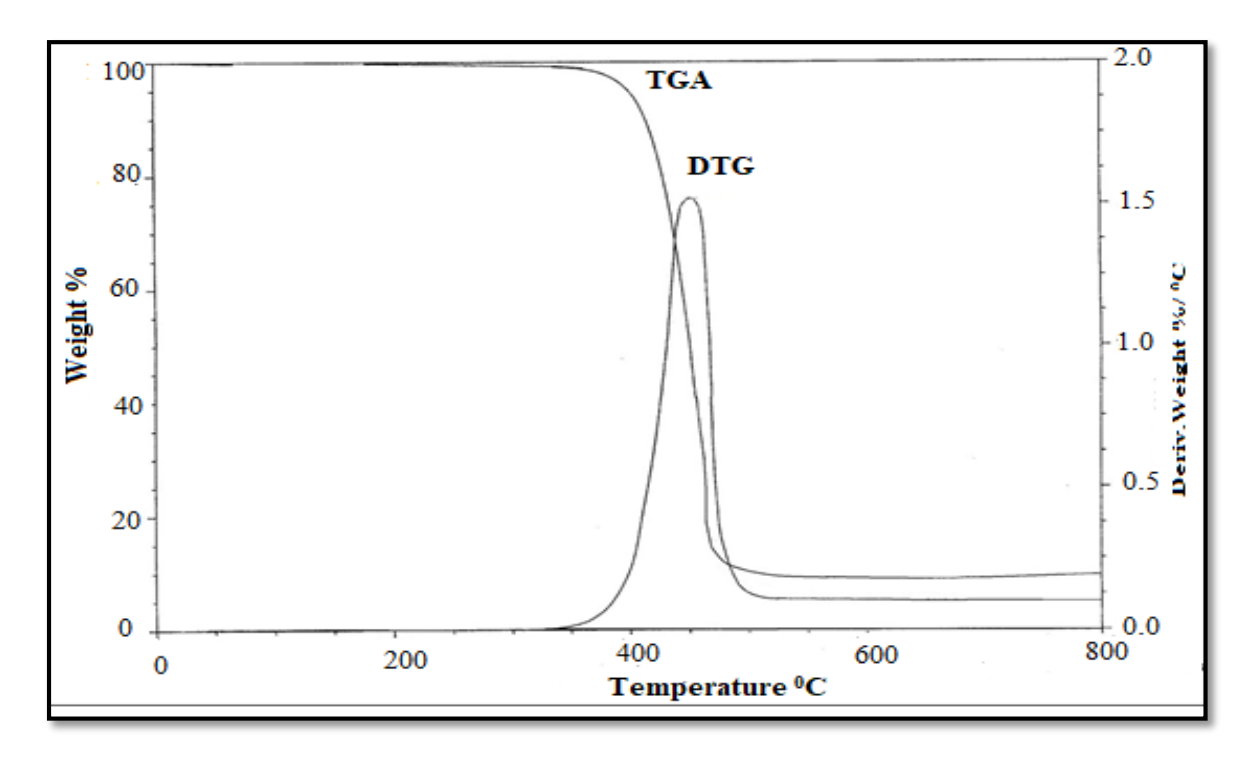


Fig.4.22 TG-DTG Curves of [Co(MTPMA)2](NO3)2

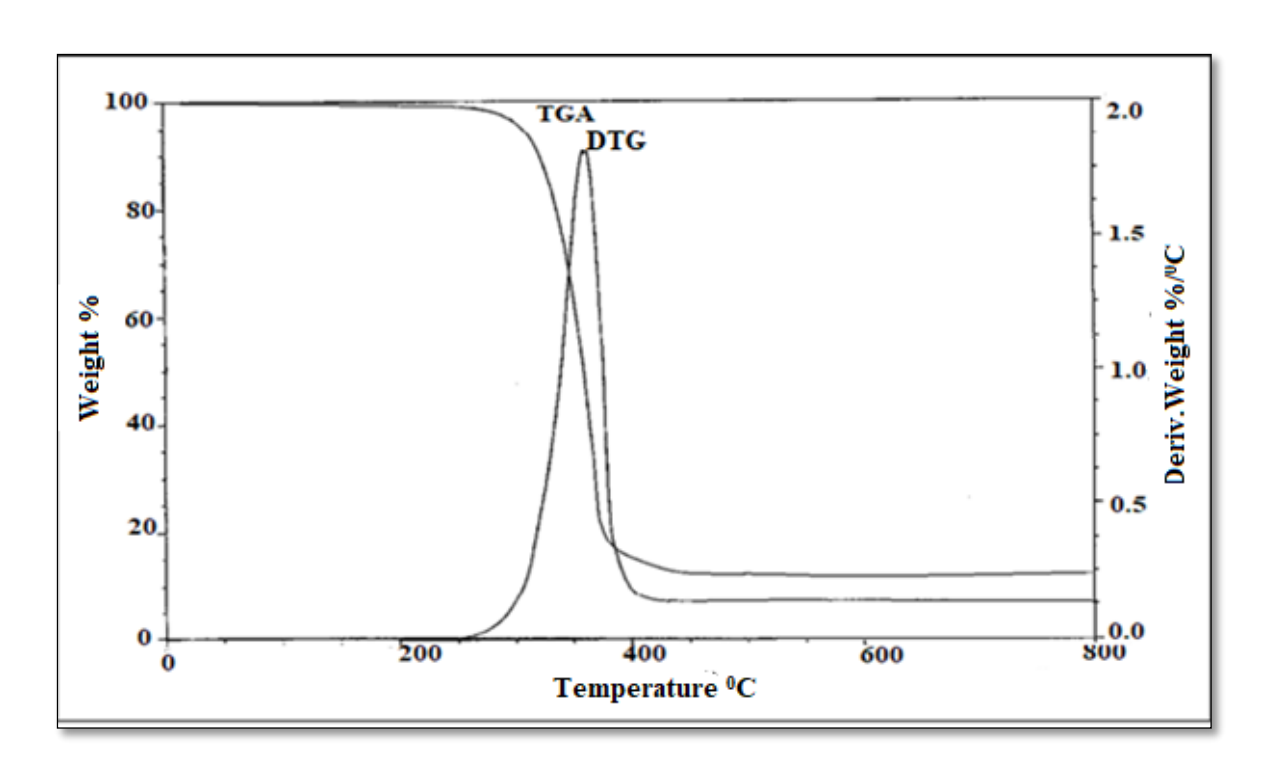


Fig.4.23 TG-DTG Curves of [Ni(MTPMA)2]SO<sub>4</sub>

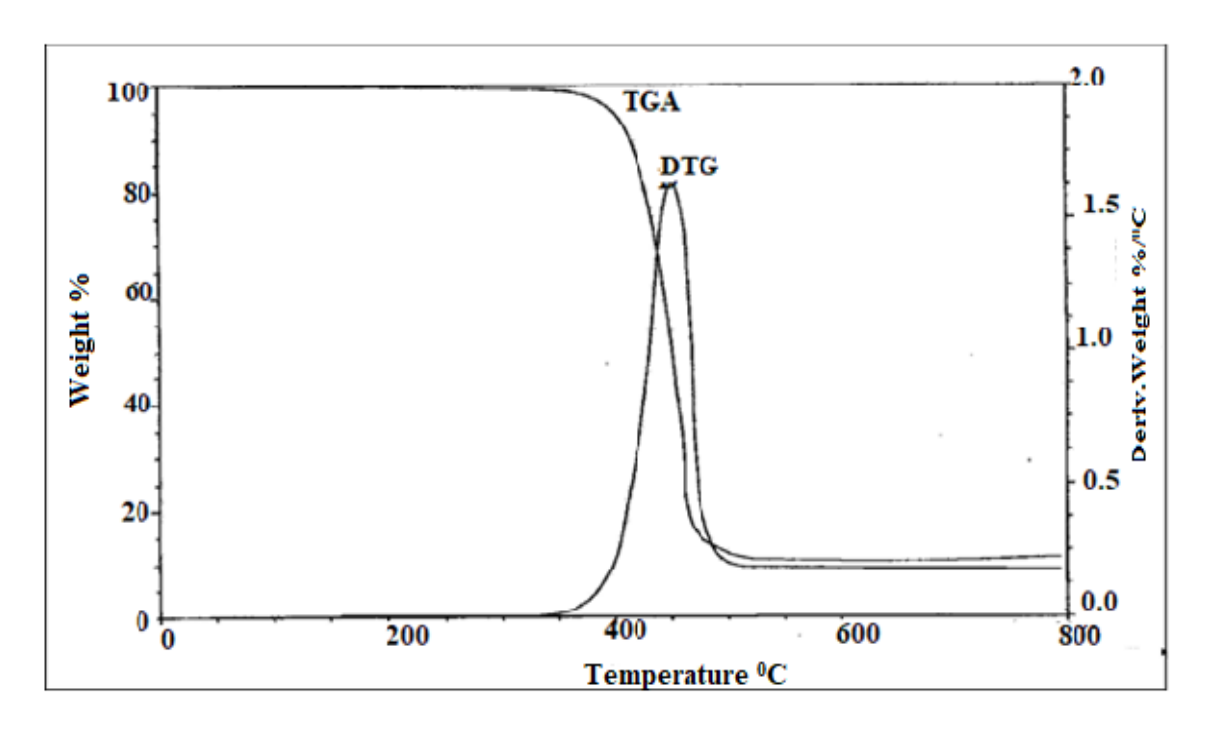


Fig.4.24 TG-DTG Curves of [Cu(MTPMA)<sub>2</sub>]Cl<sub>2</sub>

## 4.4.10 Unit Cell Parameters of Ligand MTPMA

The crystal structure analysis of ligand (E)-2-(methylthio)-N-(pyridin-2-ylmethylene)aniline was done by single crystal XRD method on a Bruker APEX-II CCD diffractometer equipped with graphite monochromated Mo K $\alpha$  radiation ( $\lambda$  = 0.71073 Å) and found to crystallize in monoclinic crystal system. The lattice parameters are a =24.51 Å, b=23.33 Å, c=17.75 Å,  $\alpha$ =90°,  $\beta$ =110° and  $\gamma$ =90° and volume = 9,517 A³ [28]. Since the grown crystal was found to be more distorted, further studies were restricted.

## 4.5 Biological Studies

## 4.5.1 Evaluation of Antimicrobial Activities of Synthesized Compounds

The *in vitro* antimicrobial activities of the compounds is tested against the bacteria, namely *B. subtilis*, *S. aureus*, *E. coli*, *P. aeruginosa*, and fungi such as *C. albicans* and *A. niger* by agar well diffusion method. By comparing the diameters of zones of inhibition obtained for the ligand and its complexes, it is inferred that the complexes exhibit higher antimicrobial activity than the free ligand.

The ligand MTPMA and its metal complexes have been screened against two Gram positive bacteria such as *B. subtilis* and *S. aureus* and two Gram negative bacteria such as *P. aeruginosa* and *E. coli* to study their antibacterial properties by agar well diffusion method using Muller Hinton Agar as nutrient and gentamicin as standard drug was employed. The inhibition zone based on zone size around the well is measured. As the concentration of the metal complex increases then the antimicrobial activity also increases. With reference to the standard drug (gentamicin), the ligand show lesser activity against *B. subtilis* and similar activity against *S. aureus* (100 µg/mL).

The results are shown in **Fig.4.25**. Iron (III) complex possesses highest activity against four bacterial species. It is followed by cobalt (II) and nickel (II) complexes whereas copper (II) and zinc (II) complexes show moderate activity compared to the ligand

(Fig.4.26). The iron(III) complex exhibits 45, 43, 48 and 46 mm zones of inhibition against *B. subtilis*, *S. aureus E. coli* and *P. aeruginosa* respectively where these values are greater than that of the ligand MTPMA as well as the gentamicin. [29] This is due to greater lipophilic nature of the complexes. The increased antibacterial activity is ascribed to either faster diffusion of metal complexes as a whole through the cell membrane or the combined activity impact of the metal and the ligand. On the basis of Overtone's concept [30-33] and Tweedy's chelation hypothesis [34], such increased activity of metal complexes can be explained. The polarity of the metal atom is considerably reduced during chelation due to ligand orbital overlap. Furthermore, p electron delocalization increases across the chelate ring, thereby enhancing the lipophilicity of the complex. [35] Metal complexes with antibacterial activity are believed to prevent bacteria from replication by inhibiting their active sites. [36] The results are presented in the **Table.4.10**.

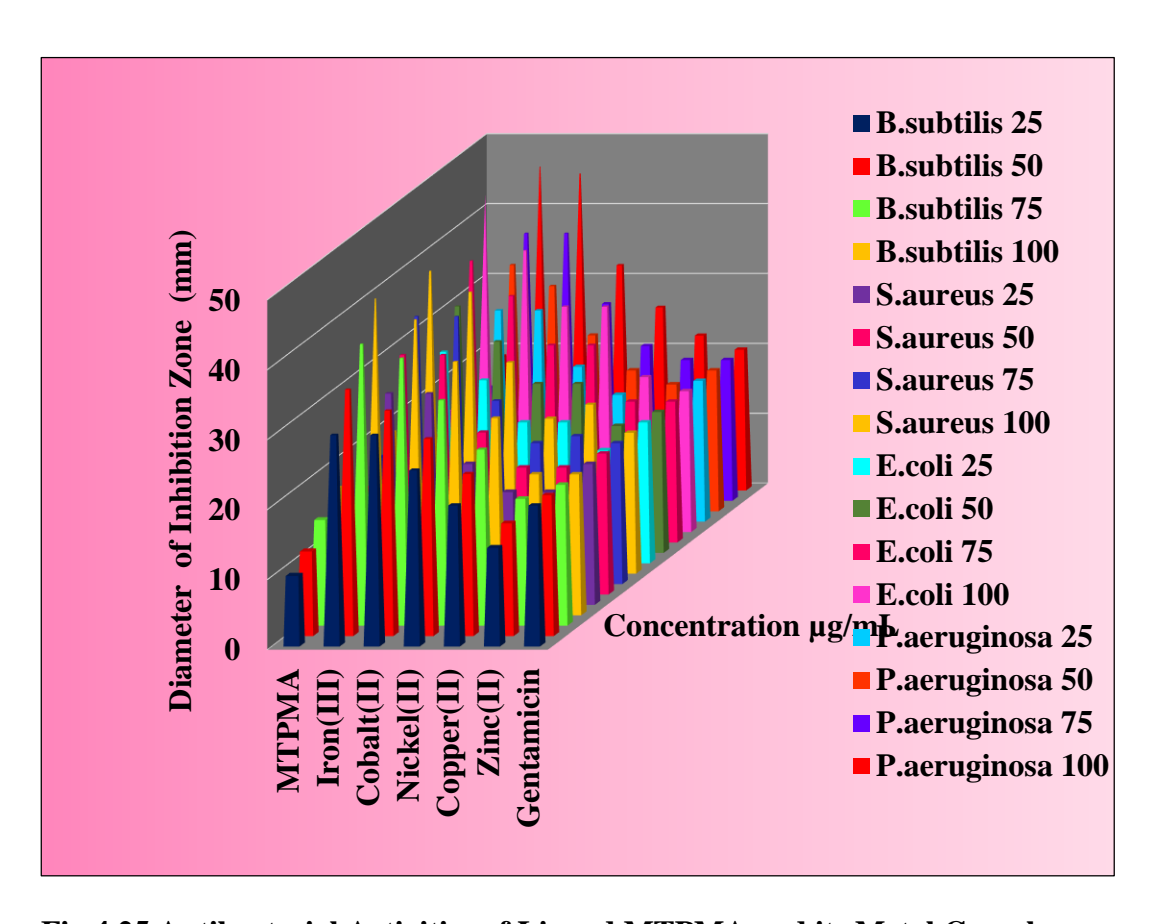


Fig.4.25 Antibacterial Activities of Ligand MTPMA and its Metal Complexes

**Table- 4.10: Antibacterial Activities of Ligand MTPMA and its Metal Complexes** 

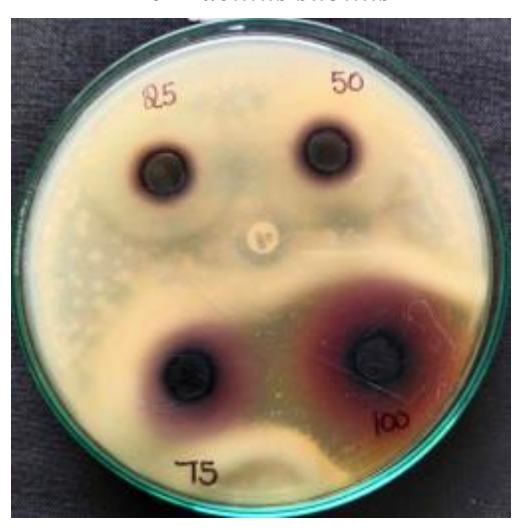
						Diameter of inhibition Zone (mm)										
Compound	B.subtilis				S.aureus			E.coli			P.aeruginosa					
	25 (μg/ mL)	50 (μg/ mL)	75 (μg/ mL)	100 (μg/ mL)	25 (μg/ mL)	50 (μg/ mL)	75 (μg/ mL)	100 (μg/ mL)	25 (µg/ mL)	50 (μg/ mL)	75 (μg/ mL)	100 (μg/ mL)	25 (μg/ mL)	50 (μg/ mL)	75 (μg/ mL)	100 (μg/ mL)
MTPMA	10	12	15	18	12	15	18	20	10	12	15	17	12	14	16	19
[Fe(MTPMA) <sub>2</sub> ]Cl <sub>3</sub>	30	35	40	45	30	34	38	43	30	35	40	48	30	35	38	46
[Co(MTPMA) <sub>2</sub> ](NO <sub>3</sub> ) <sub>2</sub>	30	32	38	42	30	34	38	40	26	30	35	40	30	32	38	45
[Ni(MTPMA) <sub>2</sub> ]SO <sub>4</sub>	25	28	32	36	20	23	26	30	20	24	28	32	22	25	28	32
[Cu(MTPMA) <sub>2</sub> ]Cl <sub>2</sub>	20	23	25	28	16	18	20	22	20	24	28	32	18	20	22	26
[Zn(MTPMA)SO <sub>4</sub> ]	14	16	18	20	16	18	21	24	16	18	20	22	14	18	20	22
Gentamicin	20	20	20	20	20	20	20	20	20	20	20	20	20	20	20	20



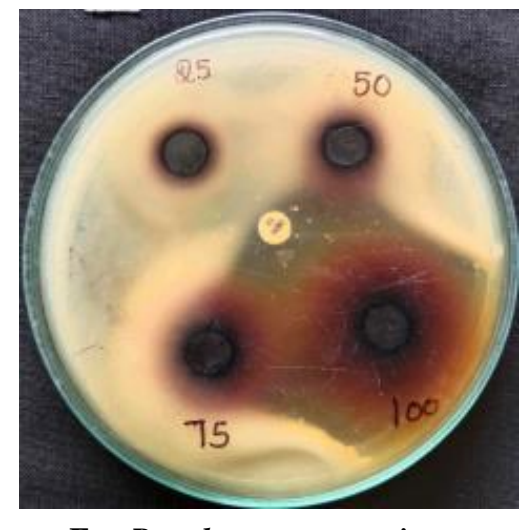
Fe- Bacillus subtilis



Fe - Staphylococcus aureus



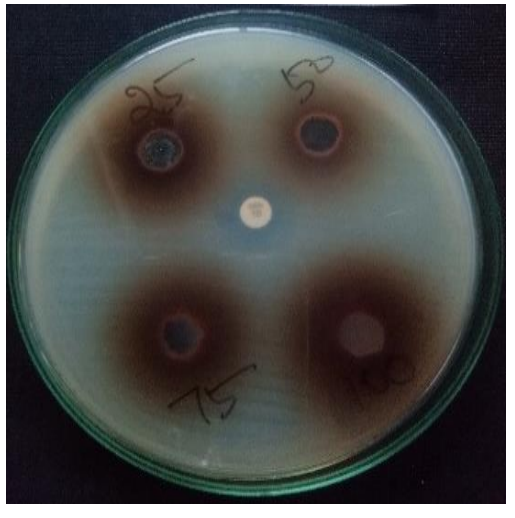
Fe - E. coli



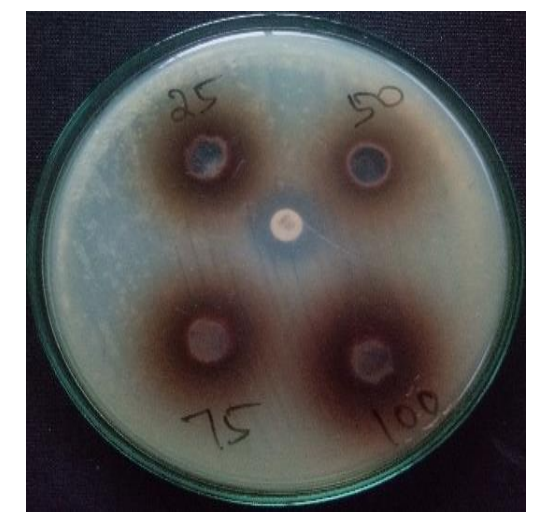
Fe - Pseudomonas aeruginosa



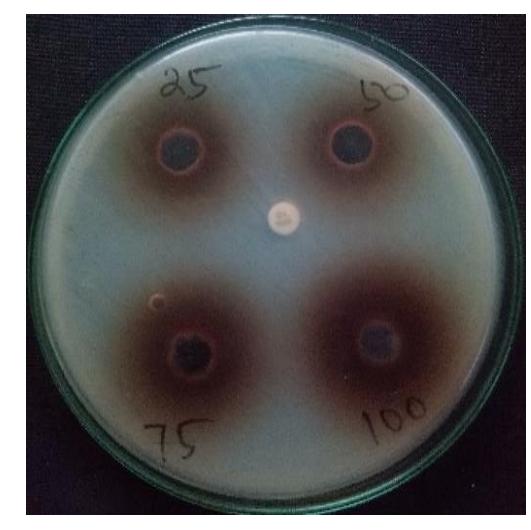
Co - Bacillus subtilis



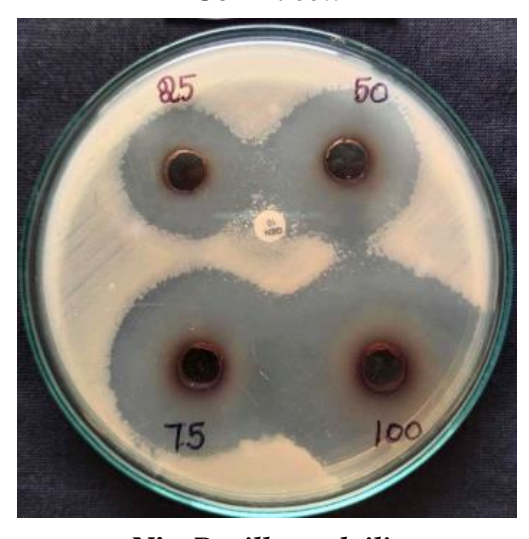
Co - Staphylococcus aureus



Co - E. coli



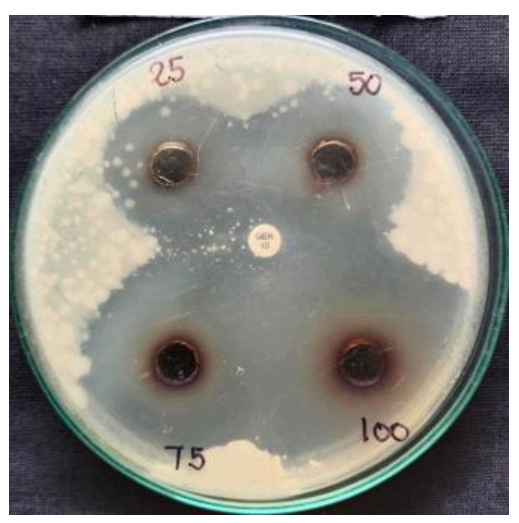
Co - Pseudomonas aeruginosa



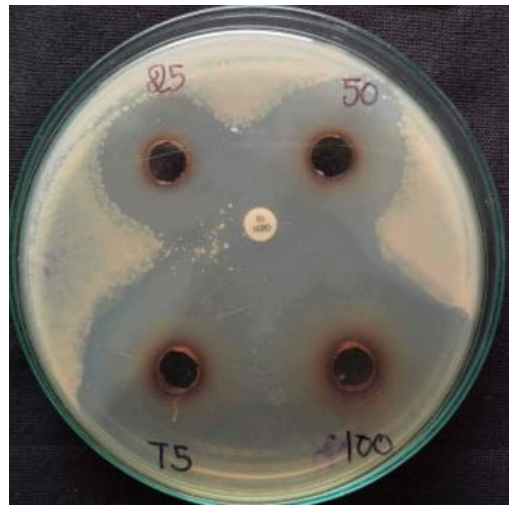
Ni - Bacillus subtilis



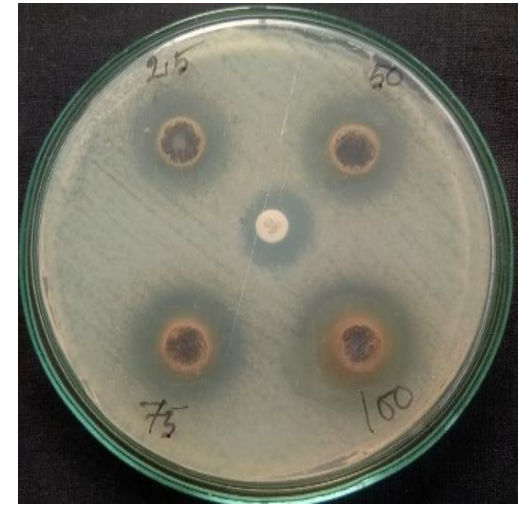
Ni - Staphylococcus aureus



Ni - E. coli



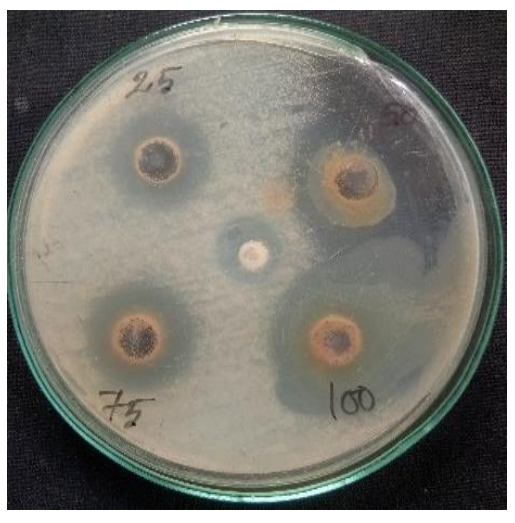
Ni - Pseudomonas aeruginosa



Cu - Bacillus subtilis



Cu - Staphylococcus aureus



Cu - E. coli



Cu - Pseudomonas aeruginosa

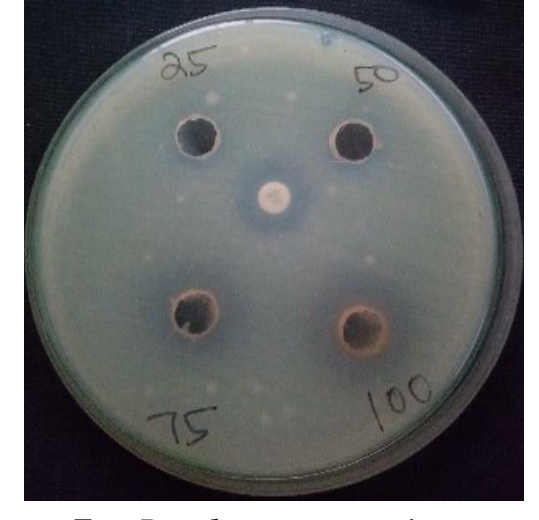


Zn - Bacillus subtilis



Zn - Staphylococcus aureus





Zn - E. coli

Zn - Pseudomonas aeruginosa

Fig.4.26 Diameters of Inhibition Zones of Complexes against Bacteria

The levels of *in vitro* antifungal activities of synthesized ligand MTPMA and the complexes are shown in the **Fig.4.27 and 4.28.** Activity has been studied against *C.albicans* and *A.niger* and compared with that of ketoconazole a standard drug. From the results it is clear that ligand has lesser activity against two species with reference to ketoconazole. Iron (III) complex is found to possess high activity towards *A.niger* whereas cobalt (II) complex also exhibits high activity towards *C.albicans* [37-39]. This shows that antifungal activity depends on nature of metal ion. The impermeability of the cell determines the variation in activity against different microorganisms. The passage of any lipid soluble substances is favoured by lipid membrane which surrounds the cell and leads to liposolubility, which is an essential factor influencing antifungal activity. The results are shown in the **Table-4.11.** 

Table- 4.11: Antifungal Activities of Ligand MTPMA and its Metal Complexes

Compound		Diameter of inhibition Zone (mm)						
		C.albi	cans			A.i	niger	
	25 (μg/mL)	50 (μg/mL)	75 (μg/mL)	100 (μg/mL)	25 (μg/mL)	50 (μg/mL)	75 (μg/mL)	100 (μg/mL)
MTPMA	12	14	17	19	11	14	16	18
[Fe(MTPMA) <sub>2</sub> ]Cl <sub>3</sub>	28	32	38	44	30	35	40	46
[Co(MTPMA) <sub>2</sub> ](NO <sub>3</sub> ) <sub>2</sub>	30	35	40	50	20	24	28	32
[Ni(MTPMA) <sub>2</sub> ]SO <sub>4</sub>	20	24	26	28	30	34	38	45
[Cu(MTPMA) <sub>2</sub> ]Cl <sub>2</sub>	20	22	25	27	25	28	32	26
[Zn(MTPMA)SO <sub>4</sub> ]	16	18	20	22	18	22	26	30
Ketoconazole	20	20	20	20	20	20	20	20

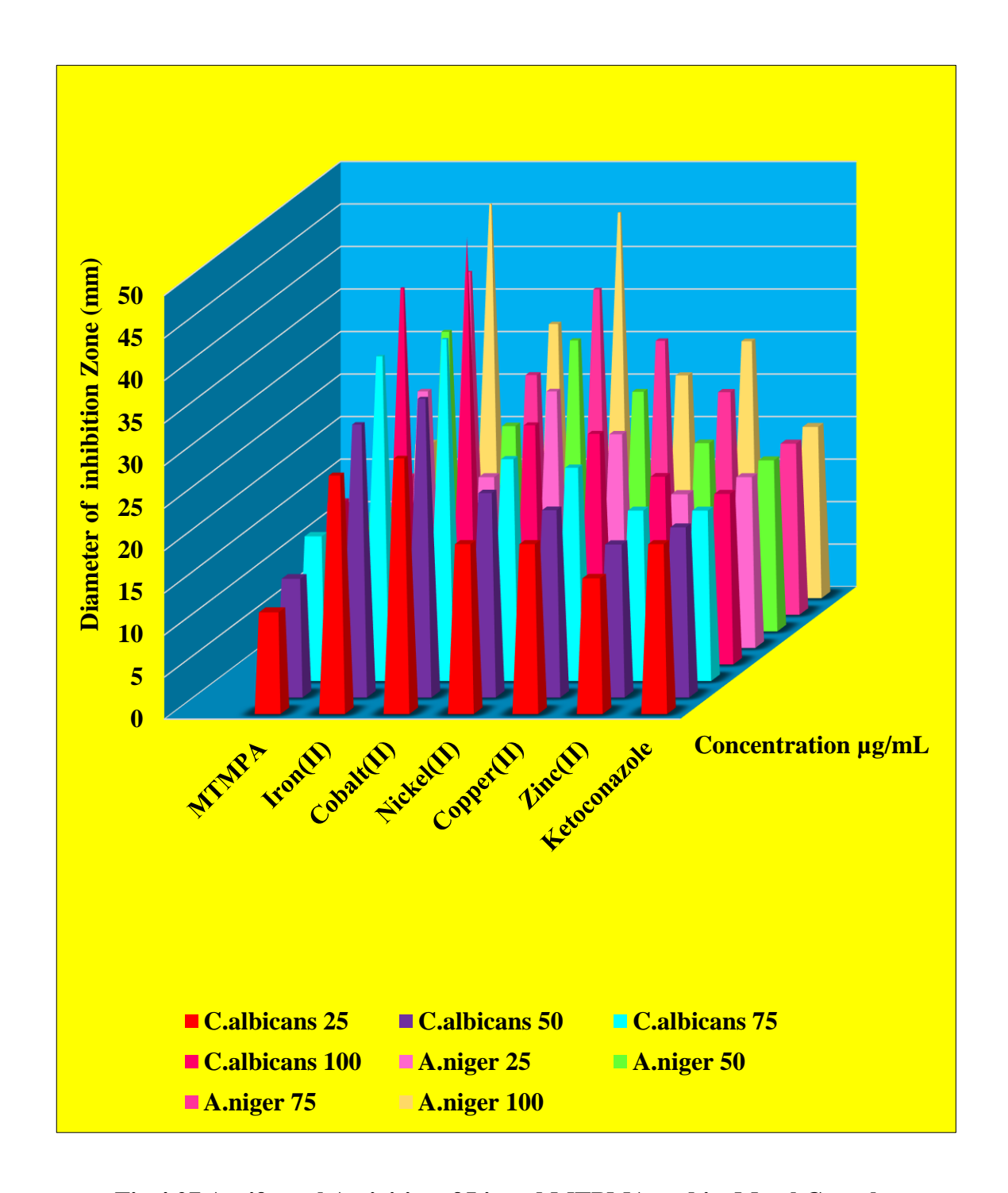
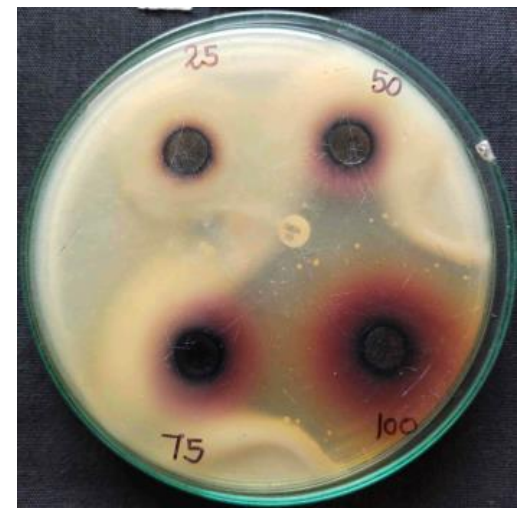
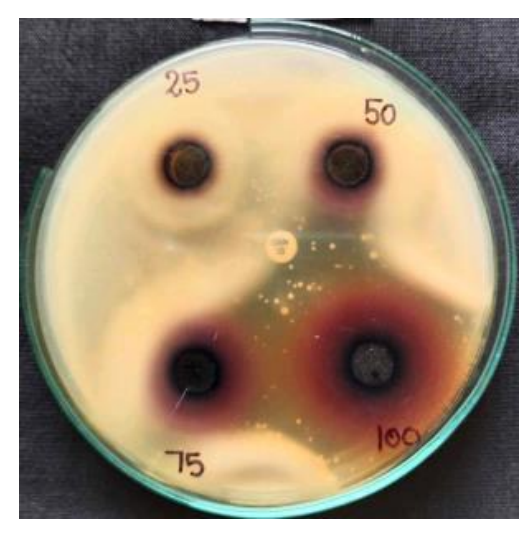


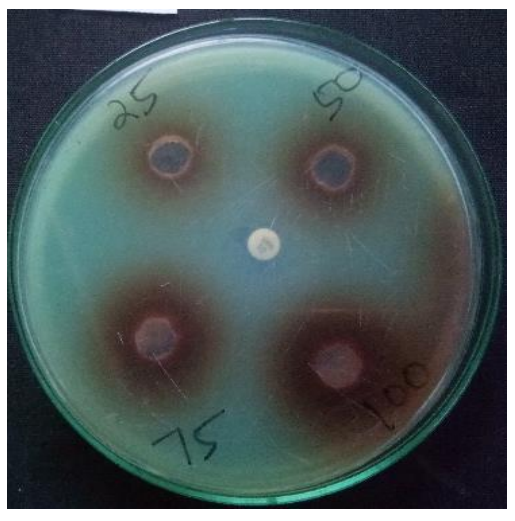
Fig.4.27 Antifungal Activities of Ligand MTPMA and its Metal Complexes



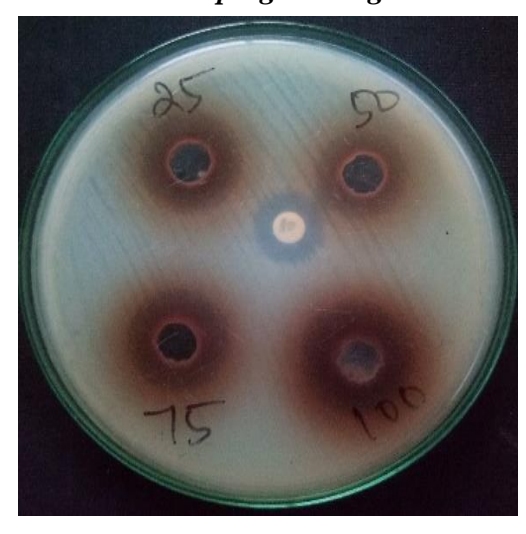
Fe - Candida albicans



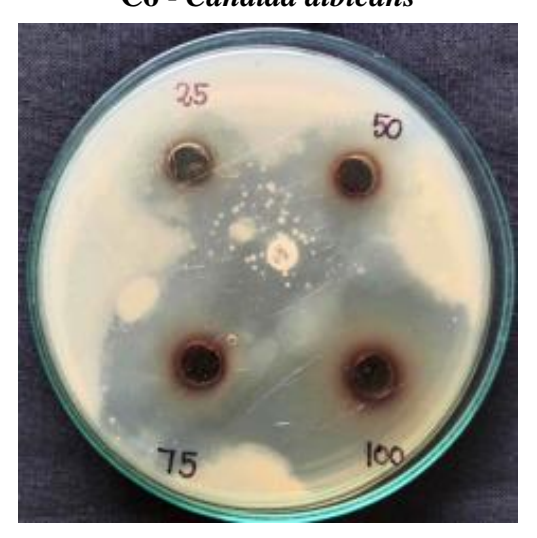
Fe - Aspergillus niger



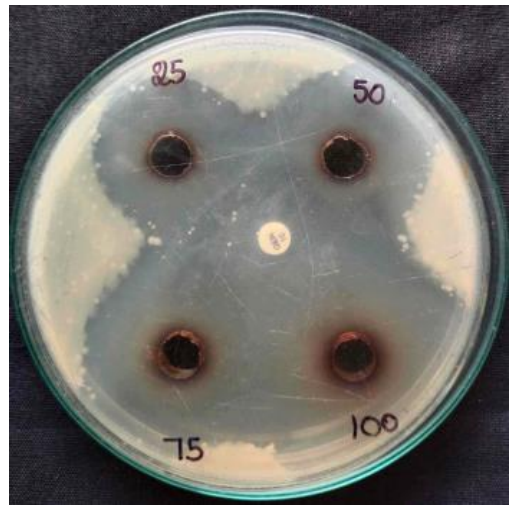
Co - Candida albicans



Co - Aspergillus niger



Ni - Candida albicans



Ni - Aspergillus niger

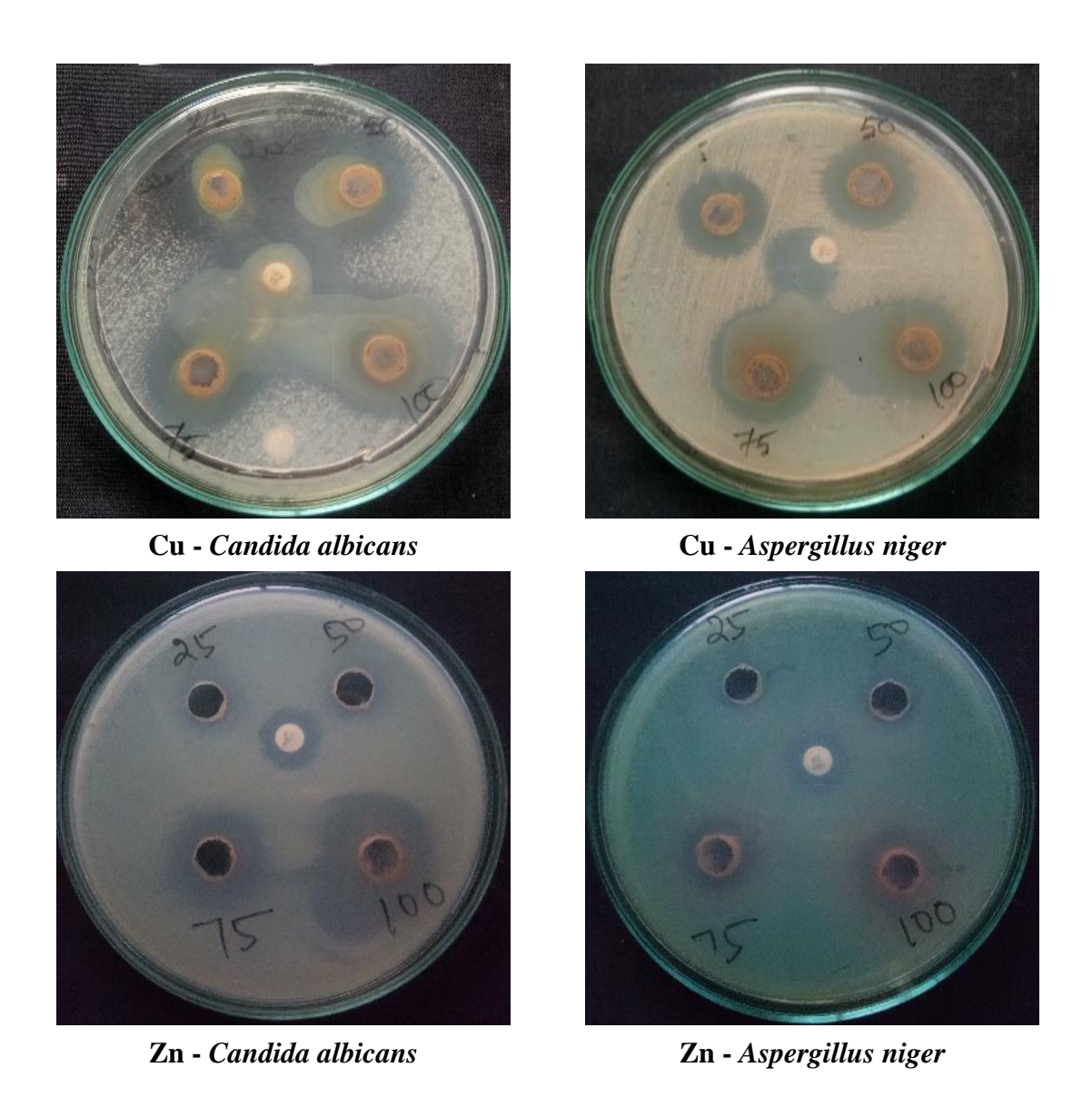


Fig.4.28 Diameters of Inhibition Zones of Complexes against Fungi

## 4.5.2 Evaluation of Antioxidant Activity (DPPH free radical scavenging Method)

The antioxidant activities of synthesized ligand MTPMA and its metal complexes are shown in the **Fig. 4.29.**The activities have been tested by DPPH assay. DPPH is a stable free radical that can accept an electron or hydrogen radical and get converted to a stable, diamagnetic molecule. DPPH has an odd electron and so has a strong absorption band at 517 nm. When this electron becomes paired off, the absorption decreases stoichiometrically with respect to the number of electrons or hydrogen atoms taken up .Such a decrease in absorbance, shows the increased scavenging activity of the test compound. This tendency

of decrease in absorption increases with increases in concentration of the test compound. The results shown in **Table-4.12** suggest that the metal complexes possess higher antioxidant activity than the ligand but lower activities when compared to that of ascorbic acid (vitamin C) as standard .The results show promise for further investigation to target oxidative damage disease. IC<sub>50</sub> values of the test compounds are shown in **Table-4.13** along with the correlation coefficient (R<sup>2</sup>) values. The lower the IC<sub>50</sub> value, the higher is the antioxidant activity. The Cu (II) complex possesses high antioxidant activity since its IC<sub>50</sub> values are low.[39]

The order can be given as L-Ascorbic acid >[Cu(MTPMA)<sub>2</sub>]Cl<sub>2</sub> >  $[Zn(MTPMA)SO_4] > [Ni(MTPMA)_2]SO_4 > [Fe(MTPMA)_2]Cl_3) > [Co(MTPMA)_2](NO_3)_2 > MTPMA with IC_{50} values as 0.431 > 1.719 > 2.126 > 2.967 > 4.237 > 16.80 > 215.44 ~\mu M.$ 

**Table-4.12: Antioxidant Activities of Ligand MTPMA and its Metal Complexes** 

Compound		% of Free Radical Scavenging					
	$5.0 \mu g/mL$	10μg/mL	15μg/mL	20μg/mL			
L-Ascorbic acid	49	52	59	64			
MTPMA	10	15	24	32			
[Fe(MTPMA) <sub>2</sub> ]Cl <sub>3</sub>	31	38	43	49			
[Co(MTPMA) <sub>2</sub> ](NO <sub>3</sub> ) <sub>2</sub>	13	21	36	42			
[Ni(MTPMA)2]SO4	35	45	48	51			
[Cu(MTPMA) <sub>2</sub> ]Cl <sub>2</sub>	27	36	41	48			
[Zn(MTPMA)SO <sub>4</sub> ]	29	40	44	47			

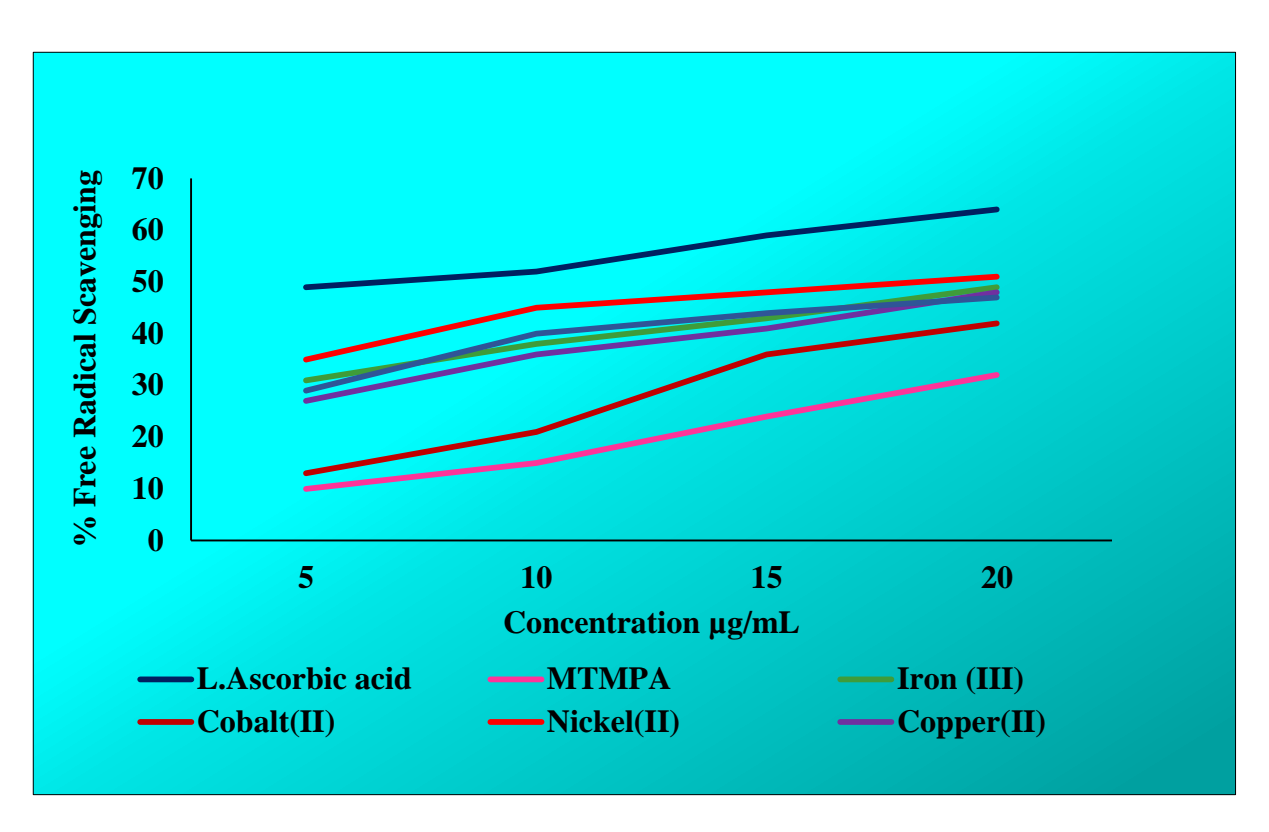


Fig.4.29 Free Radical Scavening Activities of Ligand MTPMA and its Metal Complexes

Table-4.13: IC50 ( $\mu M$ ) and R² values of Standard Drug, MTPMA and its Metal Complexes

Compound	IC <sub>50</sub> , (μM)	$\mathbb{R}^2$
L- Ascorbic acid	0.431	0.9797
MTPMA	215.44	0.9877
[Fe(MTPMA) <sub>2</sub> ]Cl <sub>3</sub>	4.237	0.9960
[Co(MTPMA) <sub>2</sub> ](NO <sub>3</sub> ) <sub>2</sub>	16.80	0.9742
[Ni(MPMA) <sub>2</sub> ]SO <sub>4</sub>	2.967	0.9571
[Cu(MPMA) <sub>2</sub> ]Cl <sub>2</sub>	1.719	0.9880
[Zn(MPMA)SO <sub>4</sub> ]	2.126	0.9043

## 4.5.3 Evaluation of Antidiabetic Activity

The inhibitory effect of Schiff base ligand MTPMA and its metal complexes on carbohydrate hydrolysing enzyme  $\alpha$ - amylase and  $\alpha$ - glucosidase has been studied. The results of antidiabetic activity are shown in the **Tables-4.14** and **4.15**. These enzyme inhibitors work by inhibiting the action of these enzymes and delaying carbohydrate digestion and preventing a rapid rise in blood glucose levels, particularly after meals. Therefore inhibition of these two enzymes is a promising strategy for diabetes management. Metal complexes are found to exhibit more inhibition efficiency than the ligand MTPMA and comparable or slightly less efficient than the standard drug acarbose. The inhibition efficiency levels are shown in **Fig.4.30** and **4.31**.

Cobalt (II) complex shows excellent inhibition efficiency against  $\alpha$ - amylase enzyme and copper (II) complex also exhibits high inhibition efficiency towards  $\alpha$ - glucosidase enzyme.[39]

The enhanced activity of cobalt (II) complex is due to the tendency of cobalt to lower the glycemic level and act as an effective agent for diabetes. The enhanced activity of copper (II) complex against diabetes is due to the tendency of copper to increase the tolerance of pancreatic β-cells against oxidative stress.[40]

The enhanced activity of zinc (II) complex is due to the fact that zinc has an insulin mimetic effect and protects against oxidative damage associated with the disease for the treatment of diabetes mellitus.[41]

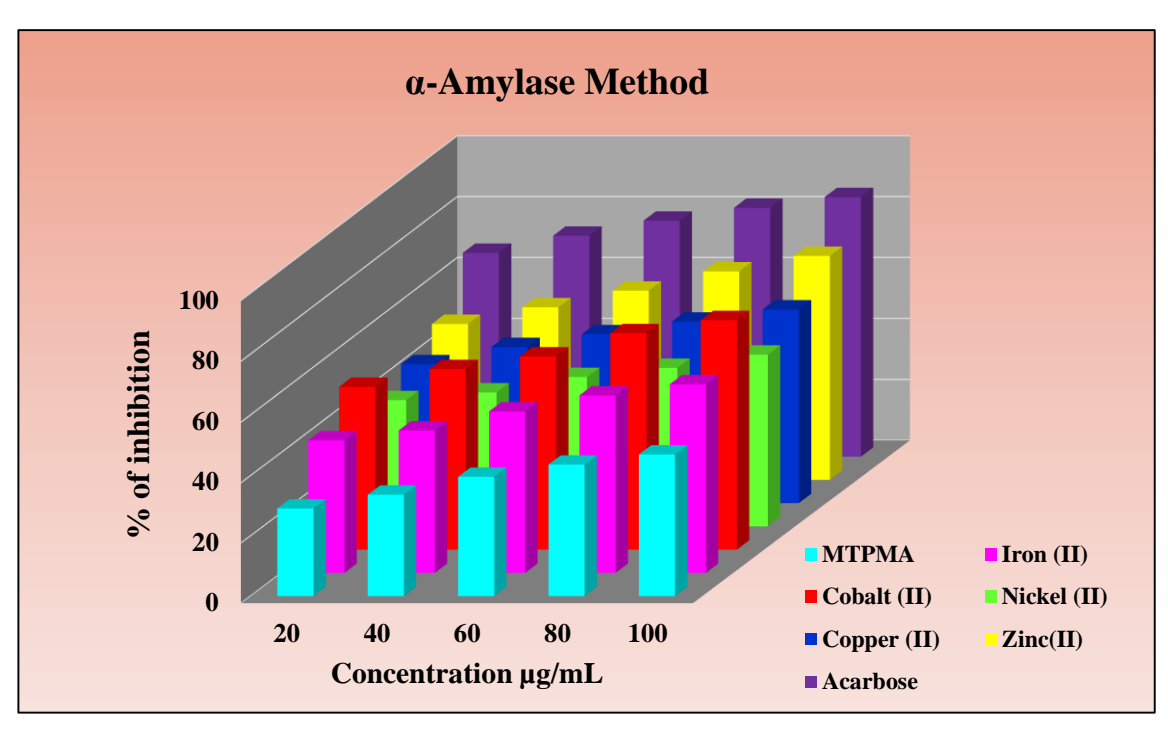


Fig.4.30 Antidiabetic Activities of Ligand MTPMA and its Metal Complexes Measured by  $\alpha$ -Amylase Method

Table- 4.14: Antidiabetic Activities of Ligand MTPMA and its Metal Complexes Measured by  $\alpha$ - Amylase Method

Compound	% of Inhibition						
	$20\mu g/mL$	40μg/mL	60μg/mL	80μg/mL	100μg/mL		
MTPMA	29.13	33.71	39.65	43.70	47.08		
[Fe(MTPMA) <sub>2</sub> ]Cl <sub>3</sub>	43.97	47.21	53.48	58.73	62.41		
[Co(MTPMA) <sub>2</sub> ](NO <sub>3</sub> ) <sub>2</sub>	53.82	59.66	63.82	71.44	75.73		
[Ni(MTPMA) <sub>2</sub> ]SO <sub>4</sub>	41.74	44.28	49.31	52.34	56.67		
[Cu(MTPMA) <sub>2</sub> ]Cl <sub>2</sub>	45.80	51.44	55.64	59.79	63.78		
[Zn(MTPMA)SO <sub>4</sub> ]	51.29	56.78	62.21	68.53	73.64		
Acarbose	66.90	72.53	77.46	81.69	85.21		

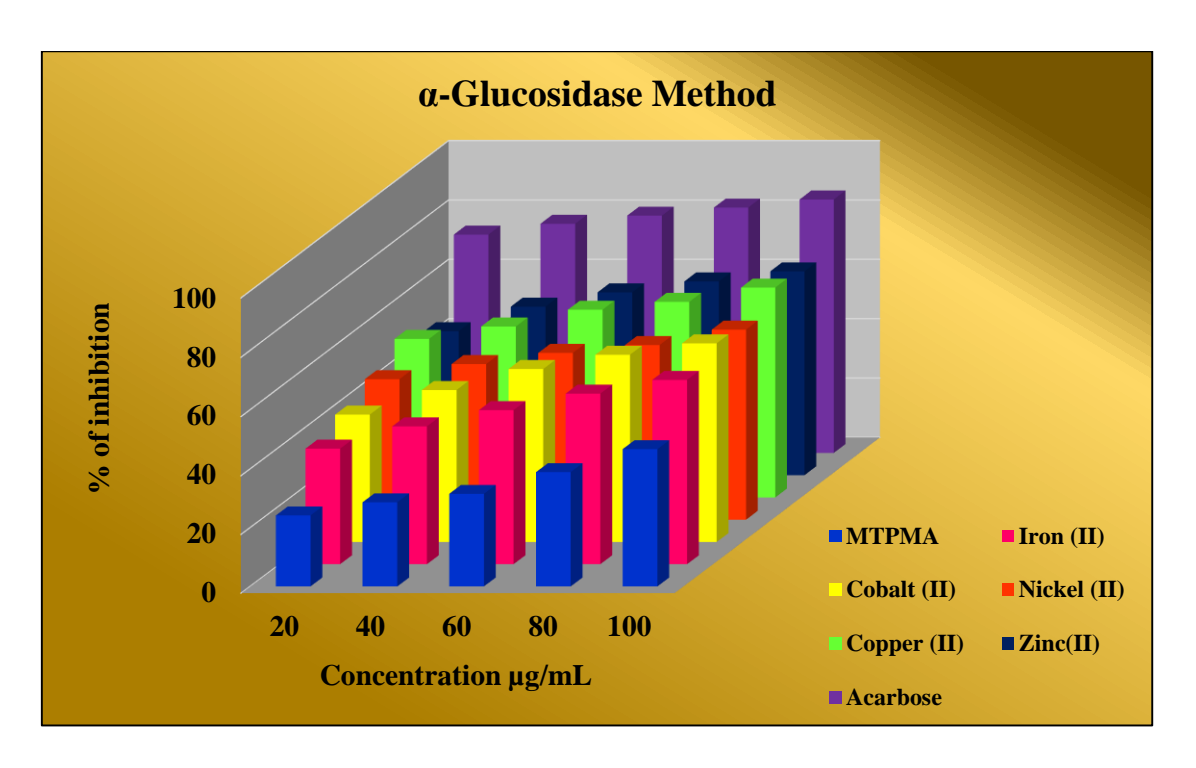


Fig.4.31 Antidiabetic Activities of Ligand MTPMA and its Metal Complexes Measured by  $\alpha$ - Glucosidase Method

Table- 4.15: Antidiabetic Activities of Ligand MTPMA and its Metal Complexes Measured by  $\alpha$ - Glucosidase Method

Compound	% of Inhibition						
	20μg/mL	40μg/mL	60μg/mL	80μg/mL	100μg/mL		
MTPMA	24.17	28.67	31.53	38.92	46.76		
[Fe(MTPMA) <sub>2</sub> ]Cl <sub>3</sub>	39.36	46.87	52.34	57.91	62.53		
[Co(MTPMA) <sub>2</sub> ](NO <sub>3</sub> ) <sub>2</sub>	43.27	51.54	58.63	63.42	67.28		
[Ni(MTPMA) <sub>2</sub> ]SO <sub>4</sub>	47.61	52.71	56.49	59.13	64.31		
[Cu(MTPMA) <sub>2</sub> ]Cl <sub>2</sub>	53.63	57.80	63.45	66.09	70.91		
[Zn(MTPMA)SO <sub>4</sub> ]	48.63	56.91	61.73	65.41	68.81		
Acarbose	73.63	77.27	80	82.72	85.45		

## 4.6 CONCLUSION

The new Schiff base complexes have been synthesized from pyridine -2carboxaldehyde and 2-(methylthio)aniline containing tridentate NNS – donor atoms. The Schiff base ligand MTPMA and its complexes are characterized by <sup>1</sup>H NMR, FT-IR, UV-Visible, EPR, Mass, cyclic voltammetry, thermal decomposition studies and are tested for antimicrobial, antioxidant and antidiabetic activities. Unit cell parameters obtained from X-ray diffraction measurements suggest that the ligand MTPMA crystallize with monoclinic crystal system. The association of the azomethine nitrogen atom of the ligand, sulphur atom of the thioether moiety and nitrogen atom of the carboxaldehyde with the metal ions has been inferred from IR spectra. The electronic absorption spectral data of the isolated complexes support the electronic transitions and geometry. EPR spectrum of copper complex suggest the octahedral geometry. The electrochemical study reveals that the metal ions undergo quasi-reversible redox reaction by one electron transfer process. The molar conductance measurements reveal that all the other complexes are electrolytic in nature except that of zinc. Antimicrobial, antioxidant and antidiabetic activities reveal that the metal complexes are more active than the Schiff base ligand which is in agreement with the fact that chelation of metals to the ligand enhances the biological activity of the complexes.

#### REFERENCES

- 1. A.Charles and K.Sivaraj, *Res. J. Life Sci.*, 2019, **5(2)**, 982-992.
- 2. S.Bal and S. S. Bal, Monatsh. Chem, 2015, **146(6)**, 903-912.
- 3 C.M.Liu, R.G.Xiong, Y.J.Liu and K.K.Cheung, *Polyhedron*, 1996, **15(24)**, 4565-4571.
- 4. O.A.Dar, S.A.Lone, M.A.Malik, M.Y.Wani, A.Ahmad and A.A.Hashmi, *Rsc Adv.*, 2019, **9**, 15151-15157.
- 5. R. Kumar, S.C.Sahoo and P.K.Nanda *Res. J. Chem. Environ.*, 2021, **25** (4), 96-103.
- 6. A. Charles, R. Krishnaveni, and K. Sivaraj, *Asian J. Chem.*, 2020, **32(12)**, 3012-3018.
- 7. X. Ran, L. Wang, Y. Lin, J.Hao and D. Cao, *Appl. Organomet. Chem.*, 2010, **24(10)**, 741-747.
- 8. V.R.Rajewar, M.K.Dharmale and S.R.Pingalkar, J. Pure App. Chem. Res., 2015, 4(2), 42-52.
- 9. X.L. Yang, G.Q. Zhong, and L.Wu. *J. Chem.*, 2013, 1-5.
- 10. B.K. Rai and Rachana Kumari, *Orient. J. Chem.*, 2013, **29**(3), 1163-1167.
- 11. A. Prakash, S. Kabir, M. Agrawal, R. Sharma and A. K.Gupta, *Int. J. Chemtech Res.*, 2014, **6(2)**, 1276-1280.
- 12. K. R. Surati and P. A. Sathe, *Med. Chem. Res.*, 2016, **25(12)**, 2742-2751.
- 13. M.H. Al-amery and T.Q.M. Al-Sahlanee, *Res. J. Chem. Environ.*, 2019, **23** (Special Issue I), 200-227.
- 14. K.C.Malhotra and K. Balakrishnan, J. Inorg. Nucl. Chem., 1977, 39(9), 1523-1525.
- 15. G. Narain and P.R.Shukla, J. Inst. Chem., 1985, **57**, 231-237.
- 16. J. N. Asegbeloyin, O. T. Ujam, E. C. Okafor, I. Babahan, E.P. Coban, A. Özmen, and H. Biyik, *Bioinorg. Chem. Appl.*, 2014, 1-11.
- 17. Kiran Singh, Preeti Siwach and Amit Sharma, *Asian J. Chem.*, 2020, **32 (12)**, 3157-3164.
- 18. R. S. Joseyphus and M. S. Nair, *Mycobiology*, 2008, **36(2)**, 93-98.

- 19. A. A. Olanrewaju, F. S. Fabiyi, R.Gupta and E.G. Kolawole, *J. Chem. Res.*, 2018, **3(5)**, 103-120.
- 20. G.Kumar, D.Kumar, S.Devi, R.Johari and C.P.Singh, *Eur. J. Med. Chem.*, 2010, **45**, 3056-3062.
- 21. D.Kivelson and R.J.Niedman, *Chem. Phys.*, 1961, **35**, 149.
- 22. A.Palanimurugan and A.Kulandaisamy, J. Organomet. Chem., 2018, 861, 263–274.
- 23. S.Kathiresan, S.Mugesh, J.Annaraj and M.Murugan, *NJC*, 2017, **41**(3), 1267-1283.
- 24. A.Jarrahpour, D.Khalili, E.De Clercq, C.Salmi and J.M.Brunel, *Molecules*, 2007, **12(8)**, 1720–1730.
- 25. N. Raman, C. Thangaraja, and S.Johnsonraja, *Cent. Eur. J. Chem.*, 2005, **3**(3), 537-555.
- 26. N.Maghraoui, D. Aggoun, B. Bouzerafa, H. Bezzi, Y.Ouennoughi, D.Lopez, M. F. Garcia, A. Ourari and M.S.Mubarak, *Arab. J. Chem.*, 2021, **14**, 103025-103028.
- 27. M. Rahangdale, G. Pethe, A. Yaul and A. Aswar. Res. J. Pharm Biological and Chem. Sci., 2011, 2(3), 341-348
- 28. A. Raja, V. Rajendran, P. Uma Maheshwari, R. Balamurugan, C.A. Kilner, M.A. Halcrow, M. Palaniandavar, *J. Inorg. Biochem.*, 2005, **99**, 1717-1732.
- 29. S. S. Tajudeen and G. Kannappan, *Ind J Adv Chem Sci.*, 2016, **4**(1), 40-48
- 30. M.J. Pelczar Jr, E.C.S. Chan and N.R. Krieg, 'Microbiology', 5<sup>th</sup> Edn., 1988, Mcgraw-Hill, New Delhi
- 31. Y. Anjaneyalu and R.P. Rao, *Synth. React. Inorg. Met.-Org. Chem.*, 1986, **16(2)**, 257 –272
- 32. L. Mishra and V.K. Singh, *Indian J. Chem.*, 1993, **32A**, 446-449
- 33. J.G. Hersfall, *Bot. Rev.*, 1945, **11(7)**, 357-397.
- 34. S. Belaid, A. Landreau, S. Djebbar, O. Benali-Baitich, G. Bouet and J.P. Bouchara, *J. Inorg. Biochem.*, 2008, **102(1)**, 63-69.
- 35. N.Nahid, A.Shat and S. Dhyani, *J Coord Chem.*, 2009, **62(18)**, 3003-3011.
- 36. N. Dharmaraj, P. Viswnathanmurthi and K. Natarajan, *Transtion Met. Chem.*, 2001, **26**, 105-109.

- 37. B. K.Singh, A. Prakash, H. K.Rajour, N. Bhojak and D. Adhikari, *Spectrochim Acta A :Mol Biomol Spectrosc.*, 2010, **76(3-4)**, 376-383.
- 38. M. Mesbah, T.Douadi, F.Sahli, S. Issaadi and S. Boukazoula and S.Chaffaa, *J.Mol. Struct.*, 2018, **1151**, 41-48.
- 39. S.S. Shah, D.Shah, I. Khan, S. Ahmad, U. Ali and A. Ur Rahman, *Biointerface Res. Appl. Chem.*, 2020, **10(6)**, 6936-6963.
- 40. S. Santha Lakshmi, K. Geetha, M Gayathri and G. Shanmugam, *J. Chem. Sci.*, 2016, **128(7)**, 1095-1102
- 41. A.Sudha, S.Arulmozhi and S.J.Askar Ali, Asian J. Chem., 2020. 32(9), 2187-2194.

# Synthesis, Characterisation, Antimicrobial, Antioxidant And Antidiabetic Activities of (Z)-N-(1H-indol-3-yl)methylene-2-(methylthio)aniline and its Metal Complexes

#### 5.1 Introduction

Schiff bases are an important class of organic ligands that coordinate to metal ions via azomethine nitrogen, are derived from a primary amines and carbonyl compounds. The C=N linkage in azomethine derivatives is essential for their biological activity, and they are reported to possess remarkable antibacterial, antifungal, anticancer and antimalarial activities [1-2] .Compared to aliphatic aldehydes, aromatic aldehydes form very stable Schiff bases because Schiff bases derived from aliphatic aldehydes readily polymerize. Schiff bases are generally bi, tri and tetra dentate chelating ligands and form very stable complexes with transition metal ions. In recent years, there has been enhanced interest in the synthesis and characterization of transition metal complexes containing Schiff bases as ligands due to their importance as catalysts in many reactions [3-6]. The complexes of Schiff bases with metals like Co<sup>II</sup>, Cu<sup>II</sup> and Zn<sup>II</sup> ions have played a major role in the growth of coordination chemistry. These complexes have evoked considerable curiosity due to their DNA binding and cleavage properties under physiological conditions [7-9]. It is reported that Schiff base derivatives of indole-3-carboxaldehyde with different L-amino acids as well as with aminophenol are found to be very stable, when labelled with <sup>99m</sup>Tc it also becomes radioactive in nature, which is further used for visualizing the tumors and also for the rapid clearance of the tumor. In addition, Schiff base derivatives of indole -3-carboxaldehyde also help in proper circulation of blood by clearing the blocks in the blood vessels [10]. Cobalt and nickel complexes are found to have wide application in disease management program. This increased the number of attempts to synthesis these complexes with superior potency and lesser toxicity than the existing drugs [11]. Here we report the synthesis, characterization, antimicrobial and antidiabetic activities of complexes of Fe<sup>III</sup>, Co<sup>II</sup>, Ni<sup>II</sup>,

 $Cu^{II}$  and  $Zn^{II}$  with Schiff base ligand (IMMA) derived from indole- 3- carboxaldehyde and 2-(methylthio)aniline..

## 5.2 Synthesis of (Z)-N-(1H-indol-3-yl)methylene-2-(methylthio)aniline IMMA

Schiff base IMMA was prepared by adding indole-3-carboxaldehyde (0.145 g 1 mmol) dissolved in absolute ethanol (20mL) slowly to a constantly stirred solution of 2-(methylthio)aniline (0.139 g 1 mmol) in 20mL of ethanol and this content was refluxed for 2 hours and then transferred into a beaker containing ice. Pale yellow crystals separated out. They were filtered, washed with ethanol and dried in a desiccator over anhydrous CaCl<sub>2</sub>.

# 5.3 Synthesis of Metal Complexes of IMMA

The ethanolic solution of corresponding salt [iron chloride hexahydrate, cobalt nitrate hexahydrate, nickel sulphate heptahydrate, copper chloride dihydrate and zinc sulphate hexa hydrate] was slowly mixed to a hot stirring ethanolic solution of (Z)-N-(1H-indol-3-yl)methylene-2-(methylthio)aniline in 1:2 (M:L) molar ratio. The reaction mixture was refluxed for 3 h, then allowed to cool and by slow evaporation coloured precipitates were formed. These precipitates were filtered, washed with cold ethanol and dried in a desiccator over anhydrous calcium chloride.

#### **5.4** Results and Discussion

#### **5.4.1** Elemental Composition

The Schiff base IMMA was obtained as a pale yellow solid and it was soluble in common organic solvents. Metal complexes of Schiff base IMMA are found to be solids, non-hygroscopic, stable at room temperature and are soluble in DMF and DMSO but sparingly soluble in common organic solvents. The analytical data and physical properties of the IMMA and its complexes are furnished in **Table-5.1**. The complexes gave satisfactory analytical data which indicate that all the complexes are in 1:2 metal to ligand ratio. The schematic diagram for the synthesis of Schiff base IMMA and metal complexes are shown in **Fig.5.1**.

**Table-5.1: Analytical Data and Physical Properties of the Ligand IMMA and its Metal Complexes** 

Compound	Empirical formula	Colour		M. Wt.	.mol·1 Point _	Elemental Analysis found (Cal) (%)					
			(%)	ginor	°С	С	Н	N	S	Cl	Metal
IMMA	$C_{16}H_{14}N_2S_1$	Pale Yellow	85	266.34	190	72.14 (72.19)	5.29 (5.30)	10.51 (10.57)	12.03 (12.05)	-	-
[Fe(IMMA) <sub>2</sub> (H <sub>2</sub> O) <sub>2</sub> ]Cl <sub>3</sub>	FeC <sub>32</sub> H <sub>32</sub> N <sub>4</sub> S <sub>2</sub> O <sub>2</sub> Cl <sub>3</sub>	Red Brown	70	730.92	>250	52.58 (52.57)	4.41 (4.39)	7.66 (7.69)	8.77 (8.75)	14.55 (14.52)	7.64 (7.61)
[Co(MPMA) <sub>2</sub> (H <sub>2</sub> O) <sub>2</sub> ](NO <sub>3</sub> ) <sub>2</sub>	CoC <sub>32</sub> H <sub>32</sub> N <sub>6</sub> S <sub>2</sub> O <sub>8</sub>	Light Brown	75	751.61	>250	51.13 (51.03)	4.29 (4.19)	11.18 (11.16)	8.53 (8.52)	-	7.84 (7.81)
[Ni(IMMA) <sub>2</sub> ]SO <sub>4</sub>	NiC <sub>32</sub> H <sub>28</sub> N <sub>4</sub> S <sub>3</sub> O <sub>4</sub>	Light Green	65	687.45	>250	55.90 (55.87)	4.10 (4.08)	8.14 (8.19)	13.99 (13.95)	-	8.53 (8.51)
[Cu(IMMA) <sub>2</sub> (H <sub>2</sub> O) <sub>2</sub> ]Cl <sub>2</sub>	CuC <sub>32</sub> H <sub>32</sub> N <sub>4</sub> S <sub>2</sub> O <sub>2</sub> Cl <sub>2</sub>	Dark Green	85	703.27	>250	54.64 (54.61)	4.58 (4.51)	7.96 (7.92)	9.11 (9.13)	10.09 (10.13)	9.03 (9.02)
[Zn(IMMA) <sub>2</sub> ]SO <sub>4</sub>	ZnC <sub>32</sub> H <sub>28</sub> N <sub>4</sub> S <sub>3</sub> O <sub>4</sub>	Dirty White	85	694.14	>250	55.36 (55.40)	4.06 (4.08)	8.07 (7.99)	13.85 (13.82)	-	9.41 (9.39)

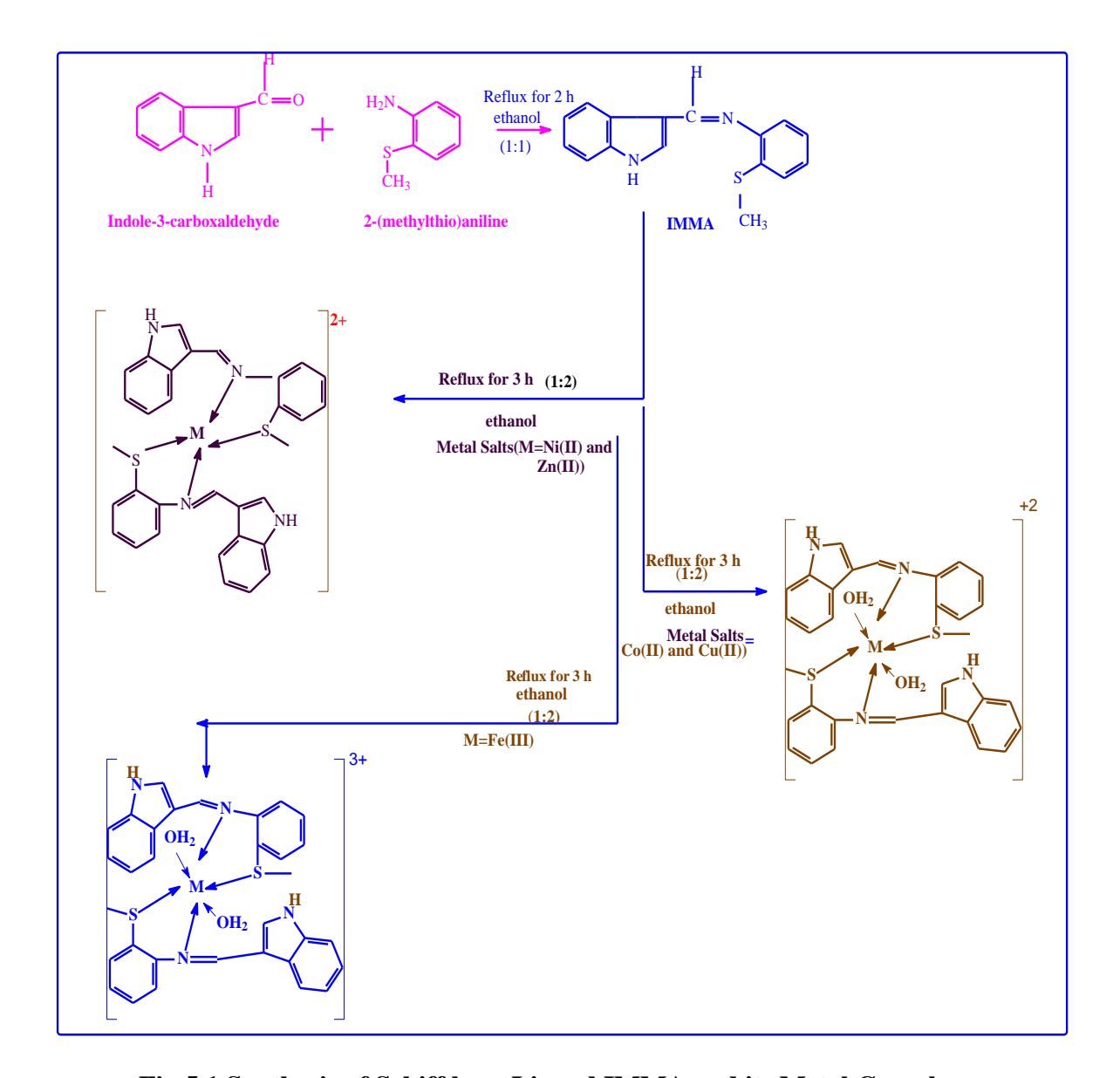


Fig.5.1 Synthesis of Schiff base Ligand IMMA and its Metal Complexes

# 5.4.2 Molar Conductivity

The molar conductance values obtained for the complexes in DMF at the concentration 10<sup>-3</sup> M are presented in **Table-5.2**.

The data presented in Table-5.2 indicate that all the complexes are in 1:2 metalligand ratio and also suggest that all complexes are electrolytic in nature since their values lie in the range of 69 -184 ohm<sup>-1</sup> cm<sup>2</sup> mole<sup>-1</sup>. It also suggest that anions are present outside the coordination sphere.[12]

**Table-5.2: Molar Conductance Values of the IMMA Metal Complexes** 

S.No	Compound	Molar Conductance Ω <sup>-1</sup> cm <sup>2</sup> mol <sup>-1</sup>
1.	[Fe(IMMA) <sub>2</sub> (H <sub>2</sub> O) <sub>2</sub> ]Cl <sub>3</sub>	184
2.	[Co(IMMA) <sub>2</sub> (H <sub>2</sub> O) <sub>2</sub> ](NO <sub>3</sub> ) <sub>2</sub>	146
3.	[Ni(IMMA) <sub>2</sub> ]SO <sub>4</sub>	76.5
4.	[Cu(IMMA) <sub>2</sub> (H <sub>2</sub> O) <sub>2</sub> ]Cl <sub>2</sub>	155
5.	[Zn(IMMA) <sub>2</sub> ]SO <sub>4</sub>	69

# 5.4.3 <sup>1</sup>H-NMR Spectra

In the  $^1$ H NMR spectrum of the Schiff base ligand IMMA shown in **Fig.5.2** there is a sharp singlet peak at  $\partial$  8.7 ppm assignable to azomethine proton (-HC=N) whereas a multiplet observed at  $\partial$  7.1- 8.2 ppm is due to aromatic protons of indole moiety and 2-(methylthio)aniline. A singlet found at  $\partial$  2.5 ppm corresponds to -CH<sub>3</sub> protons. However, azomethine proton undergoes deshielding upon coordination as observed in  $^1$ H NMR spectrum of Zn complex (**Fig.5.3**) and appears at 9.0 ppm confirming the coordination through azomethine nitrogen. The multiplet corresponding to aromatic ring protons appears in the region 7.1–8.7 ppm and are slightly shifted downfield, indicating the involvement of sulphur atom of aromatic ring in coordination. A sharp singlet peak at  $\partial$  10ppm is attributed to -NH protons of indole ring. Thus, a comparison of signals due to the ligand and the complex, it is confirmed that the condensation of indole -3-carboxaldehyde with 2-(methylthio)aniline resulted in the formation of (*Z*)-*N*-(1*H*-indol-3-yl)methylene-2-(methylthio)aniline and also coordination of Zn metal to Schiff base [13]. The  $^1$ H NMR signals of the ligand IMMA and Zn complex are listed in the **Tables-5.3 and 5.4.** 

Table-5.3: <sup>1</sup>H NMR Spectral Data of the Ligand IMMA

S. No.	Signal Position (ppm)	Relative No. Of Protons	Multiplicity	Inference
1.	9.9	1H	Singlet	Free –NH (Indole Ring)
2.	8.7	1H	Singlet	-HC=N (Azomethine proton)
3.	7.1-8.2	9Н	Multiplet	Ar-CH
4.	2.5	3Н	Singlet	-CH <sub>3</sub>

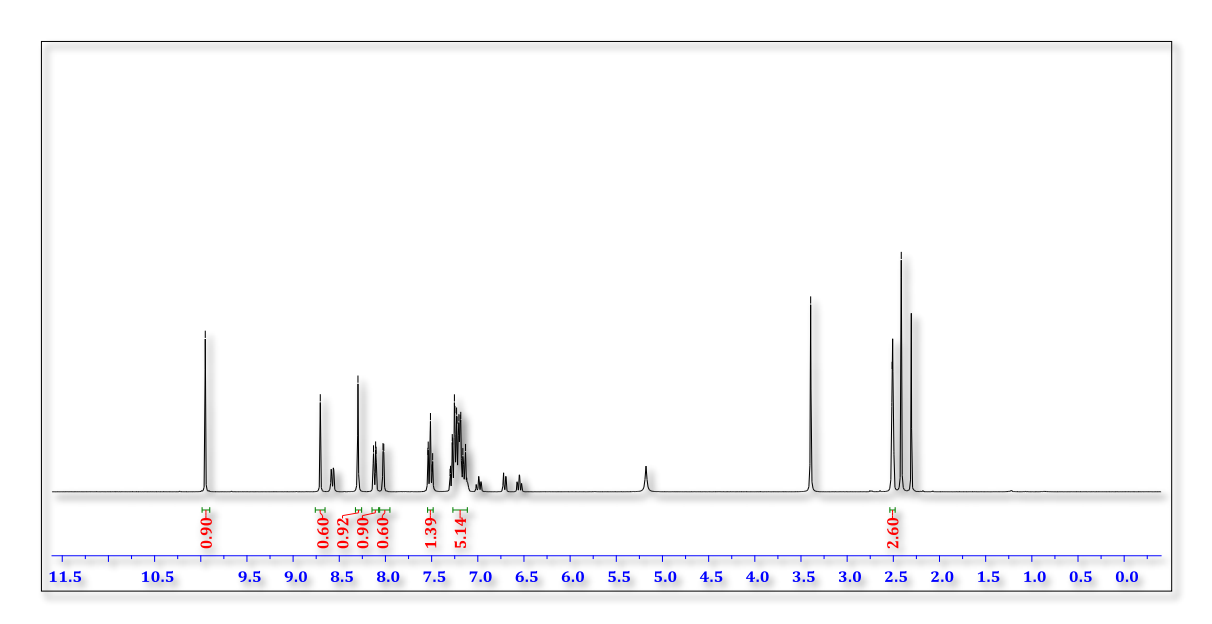


Fig.5.2  $^{1}$ H NMR Spectrum of Schiff Base Ligand IMMA

Table-5.4: <sup>1</sup>H NMR Spectral Data of the [Zn(IMMA)<sub>2</sub>]SO<sub>4</sub>

S.No.	Signal Position (ppm)	Relative No. of Protons	Multiplicity	Inference
1.	10	2Н	Singlet	Free –NH (Indole Ring)
2.	9.0	2Н	Singlet	-HC=N (Azomethine protons)
3.	7.1-8.7	18H	Multiplet	Ar-CH
4.	2.4	6Н	Singlet	-CH <sub>3</sub>

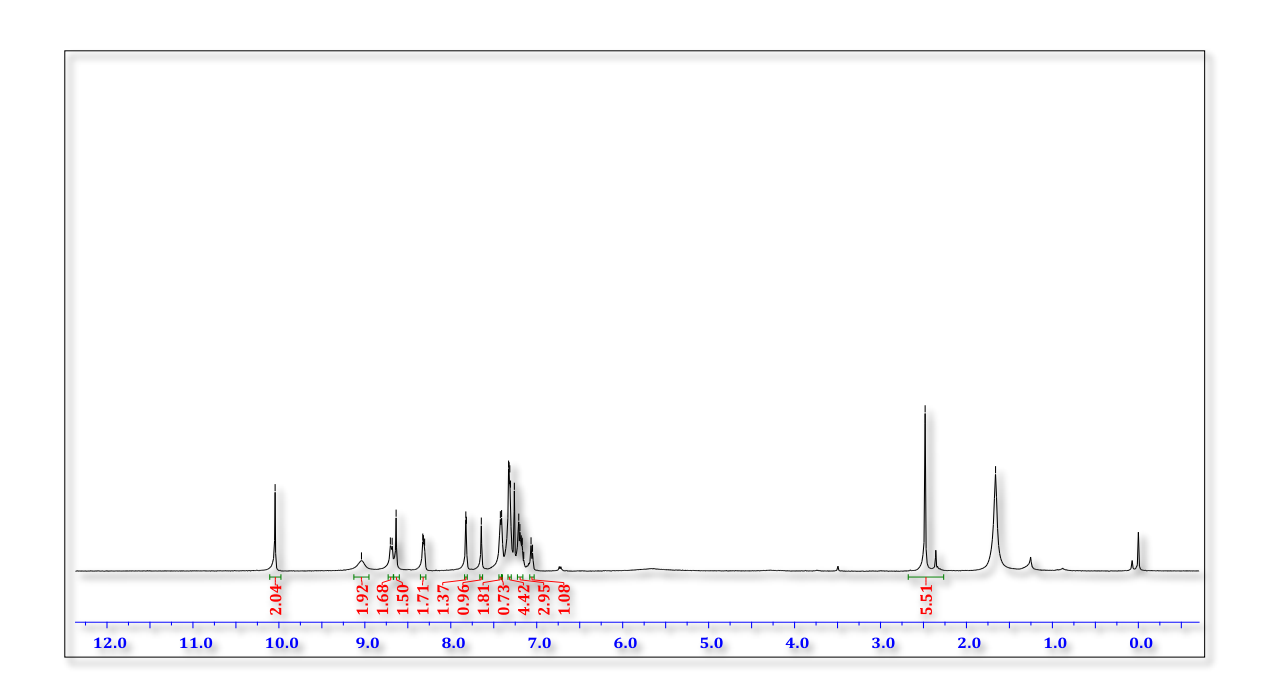


Fig.5.3 <sup>1</sup>H NMR Spectrum of [Zn(IMMA)<sub>2</sub>]SO<sub>4</sub>

# 5.4.4 FT-IR Spectra

The spectra in **Fig.5.4-5.9** show typical bands of ligand and complexes. There are some noteworthy changes in the spectra of the metal complexes from that of the ligand as expected. The sharp peak at  $1634~\rm cm^{-1}$  is the characteristic band for azomethine  $\dot{\upsilon}_{(CH=N)}$  group of the ligand The formation of CH=N linkage is also supported by the absence of a bands at  $1735 \rm cm^{-1}$  and  $3420 \rm cm^{-1}$  which are characteristics stretching frequencies of free carbonyl group of aldehyde and amino group of aniline respectively present in the starting materials [14] .

The azomethine band of the ligand is now shifted to lower frequencies ranging from 1577-1634 cm<sup>-1</sup> indicating that this group takes part in complexation with the metal. This is due to an increase of bond order on complexation, which in turn reduces the electron density of azomethine nitrogen atom and thus results in a shift in the frequency of C=N band. The bands in the region 1333 - 1386 cm<sup>-1</sup> are due to C-N stretching vibrations. Band at 780 cm<sup>-1</sup> in the spectra of ligand corresponds to C-S stretching vibration. This band is shifted

to lower frequencies (725-757 cm<sup>-1</sup>) in the spectra of all complexes indicating the involvement of sulphur atom in coordination. In the low frequency region (Far IR region), new bands are observed for the complexes. The bands at 422 - 427 cm<sup>-1</sup> and 606 - 639 cm<sup>-1</sup> are due to metal-nitrogen and metal-sulphur stretching vibrations and they were not seen in the spectrum of the free ligand. The band in the frequency region 1500 cm<sup>-1</sup> is due to C=C of aromatic skeleton [15].

From the above observations, it is clear that the metal ions are coordinated to the Schiff base ligand IMMA through sulphur atom and azomethine nitrogen. However, the bands at 3307, 3391 and 3380 cm<sup>-1</sup> in the spectra of iron (III), cobalt(II) and copper (II) complexes respectively are due coordination of water molecules. The IR spectral data of the ligand IMMA and metal complexes are summarized in the **Table-5.5**.

Table-5.5: Selected FT-IR Absorption Frequencies (cm<sup>-1</sup>) of the Ligand IMMA and its Metal Complexes

Compound	V CH=N	V C=N	V C-S	V M-N	V M-S	V (O-H) H2O
IMMA	1634	1333	780			
[Fe(IMMA) <sub>2</sub> (H <sub>2</sub> O) <sub>2</sub> ]Cl <sub>3</sub>	1604	1359	725	423	606	3380
[Co(IMMA) <sub>2</sub> (H <sub>2</sub> O) <sub>2</sub> ](NO <sub>3</sub> ) <sub>2</sub>	1607	1383	734	423	639	3391
[Ni(IMMA) <sub>2</sub> ]SO <sub>4</sub>	1604	1360	734	422	605	
[Cu(IMMA) <sub>2)</sub> (H <sub>2</sub> O) <sub>2</sub> ]Cl <sub>2</sub>	1577	1386	757	427	639	3307
[Zn(IMMA) <sub>2</sub> ]SO <sub>4</sub>	1604	1359	735	423	607	

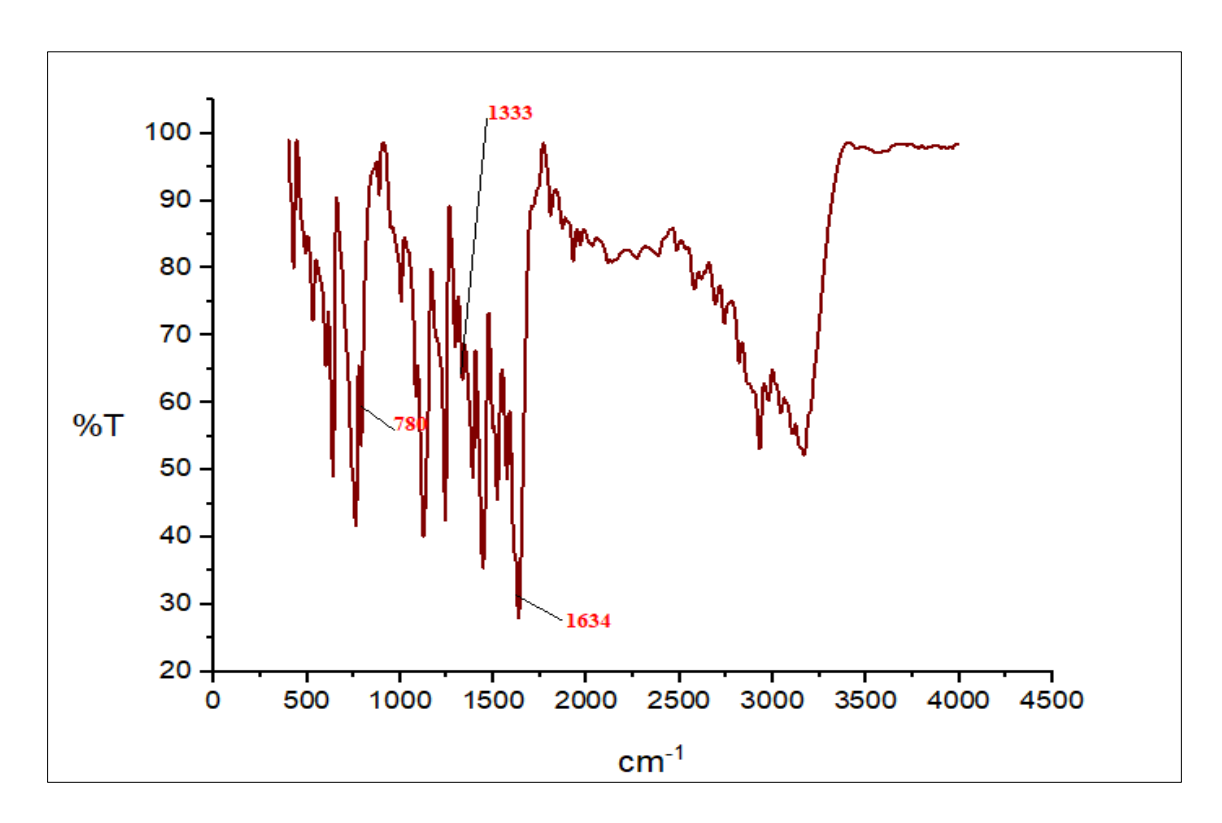


Fig. 5.4 FT-IR Spectrum of Schiff Base IMMA

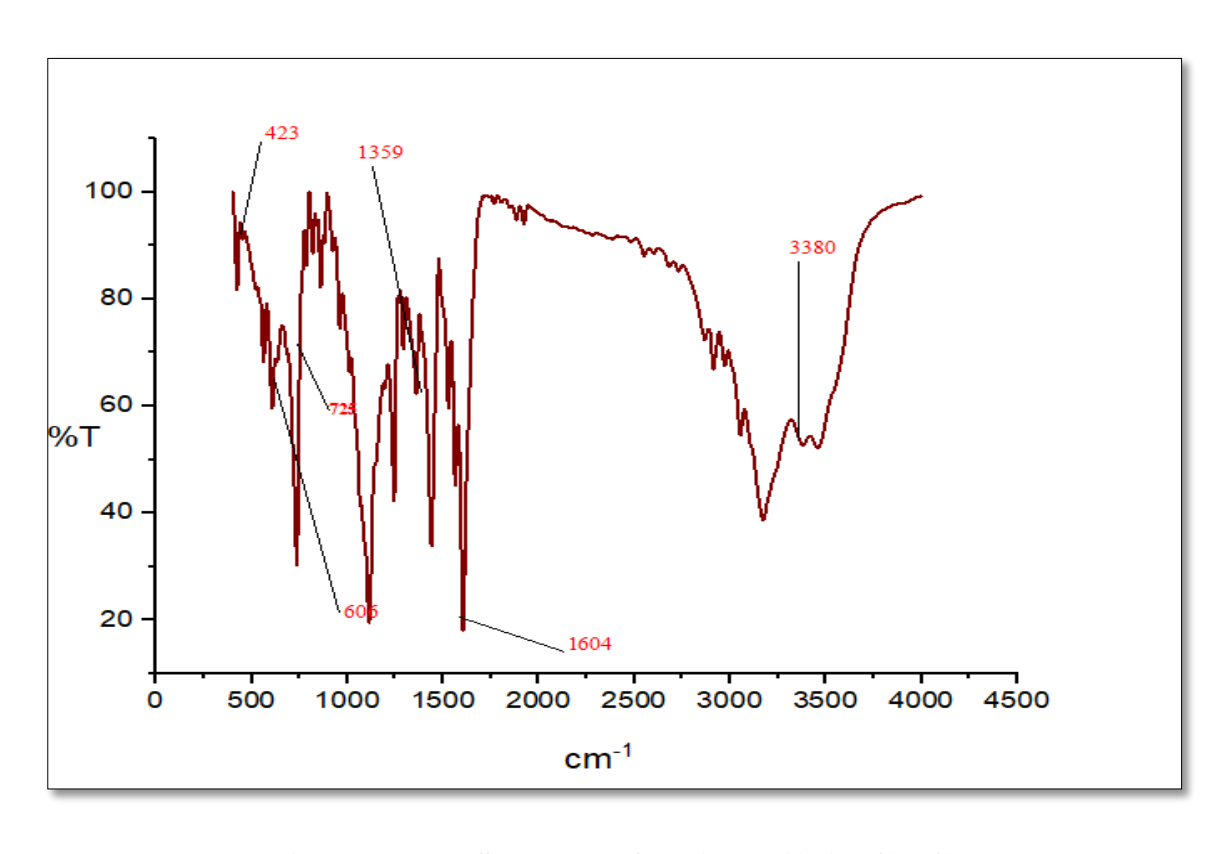


Fig. 5.5 FT-IR Spectrum of [Fe(IMMA) $_2$ (H $_2$ O) $_2$ ]Cl $_3$ 

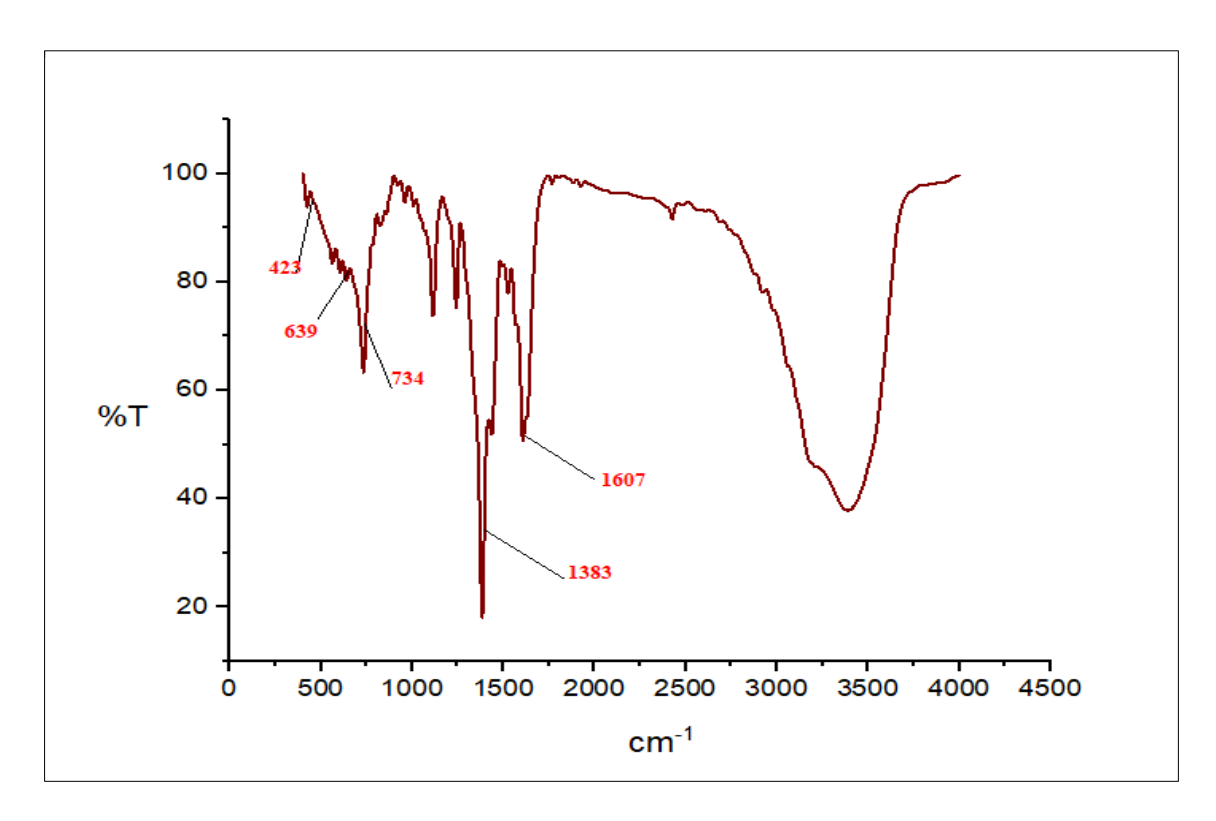


Fig. 5.6 FT-IR Spectrum of [Co(IMMA)2(H2O)2](NO3)2

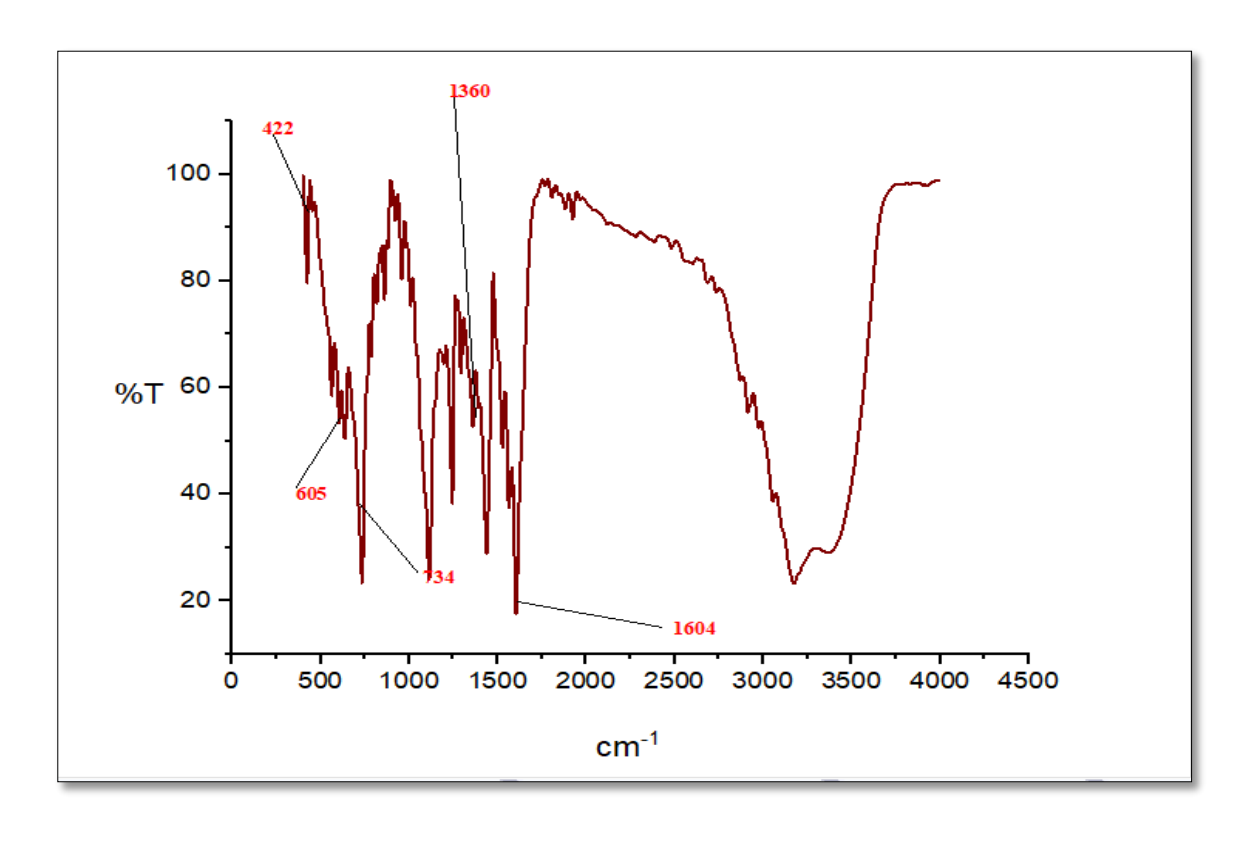


Fig. 5.7 FT-IR Spectrum of [Ni(IMMA)<sub>2</sub>]SO<sub>4</sub>

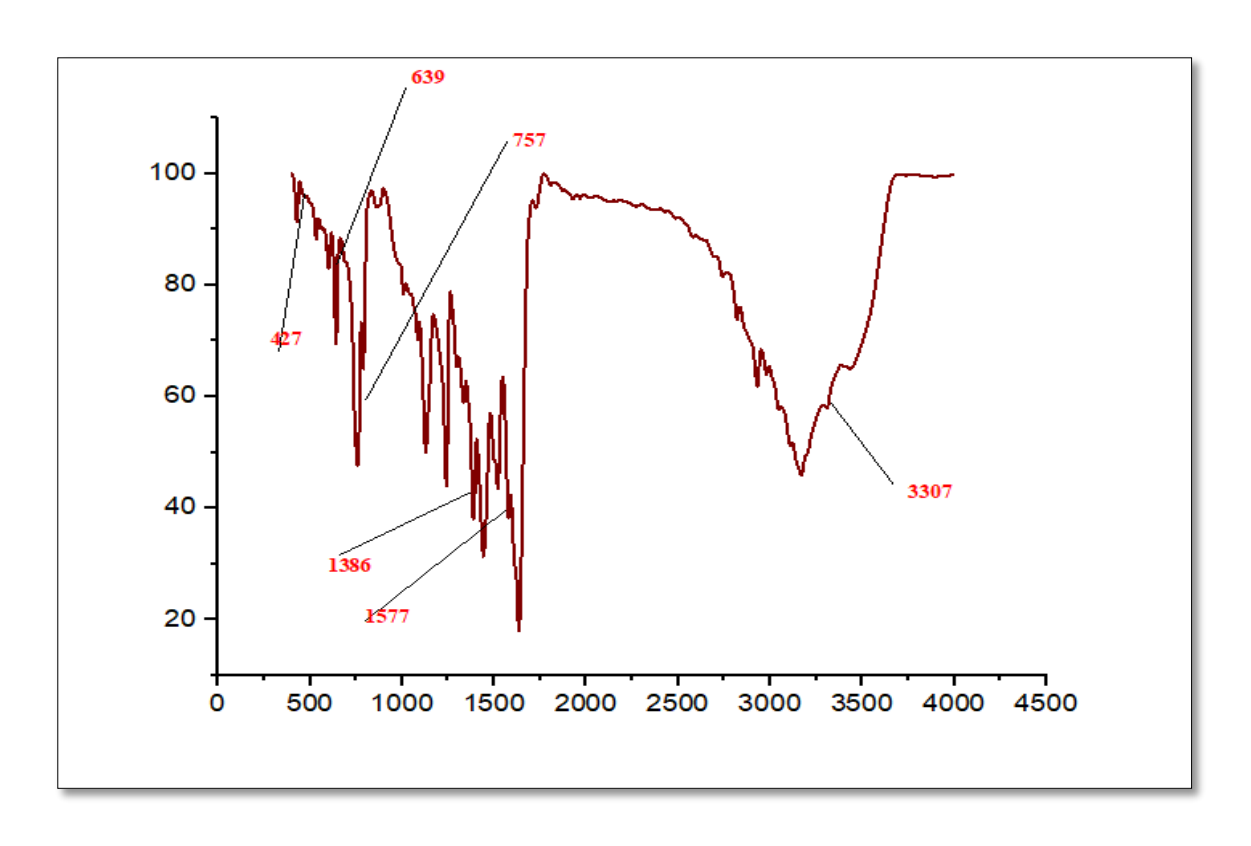


Fig. 5.8 FT-IR Spectrum of  $[Cu(IMMA)_2)(H_2O)_2]Cl_2$ 

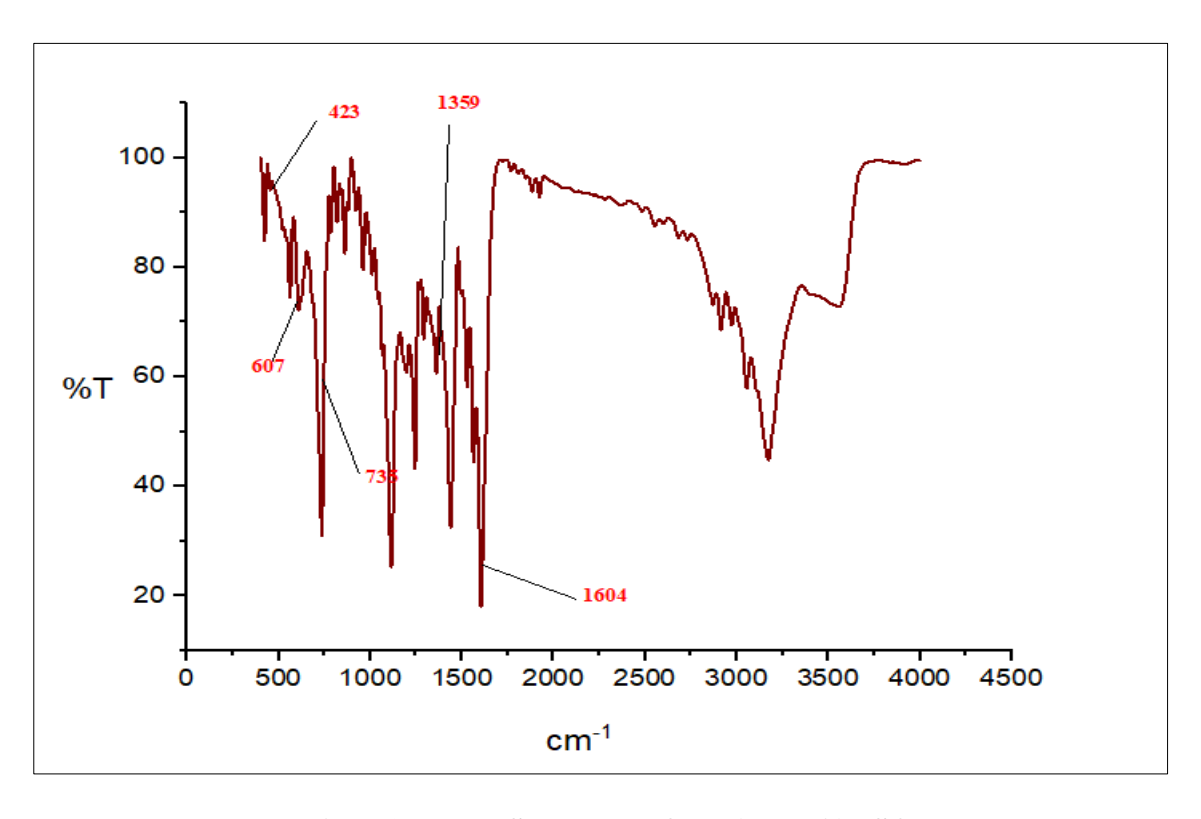


Fig. 5.9 FT-IR Spectrum of [Zn(IMMA)<sub>2</sub>]SO<sub>4</sub>

## 5.4.5 UV- Visible Spectra and Magnetic Moment

The electronic spectra of the Schiff base ligand IMMA and its complexes in DMSO are recorded in the range 200 -1000 nm. The electronic spectra of the ligand IMMA and its complexes in DMSO ( $10^{-3}$ mol<sup>-1</sup>) are furnished in **Fig. 5.10-5.15**. The absorption region, band maxima and their probable assignments are given in **Table-5.6**. The values of magnetic moments of all the metal ions in the complexes are also given in the same table. The ligand shows two bands at 38, 470 cm<sup>-1</sup> and 27, 843 cm<sup>-1</sup> which are attributed to  $\pi \to \pi^*$  and  $n \to \pi^*$  electronic transitions respectively. In the spectra of the complexes, these bands are shifted to lower wavelengths indicating the coordination of the ligand to the metal ion and they also show d-d transitions of the metal d-orbitals in the visible region [16].

The Fe<sup>III</sup> complex belongs to the  $d^5$  system. In the low spin, octahedral Fe<sup>III</sup> complex, the ground state for Fe<sup>III</sup> is  ${}^2T_{2g}$ . The electronic spectra of Fe<sup>III</sup> complex showed band at the 24, 691 cm<sup>-1</sup> which is due to charge transfer assigned to sulphur-metal and nitrogen- metal LMCT transitions.

The electronic spectrum of Co<sup>II</sup> complex has two bands at 14, 637 cm<sup>-1</sup> and 29, 686 cm<sup>-1</sup> which are attributed to d-d transition and charge transfer transitions assigned to sulphur-metal and nitrogen-metal LMCT transitions respectively. These are characteristic of octahedral geometry [17] around cobalt (II) in the complex. The magnetic moment of the cobalt (II) complex is 4.76 BM which corresponds to three unpaired electrons on cobalt (II) ion.

In the electronic spectrum of  $Ni^{II}$  complex, the band appearing at 24,691 cm<sup>-1</sup> is attributed to the transition  ${}^{1}A_{1} \rightarrow {}^{1}E$  which is consistent with the square planar geometry [18].

In the spectrum of copper (II) complex, the broad band appearing at 15,336 cm $^{-1}$  is attributed to d-d transition. The Cu $^{II}$  is d $^{9}$  system, due to unsymmetrical Eg orbital, low spin

distorted octahedral complex is expected. A high intensity charge transfer band is seen at 22,680 cm<sup>-1</sup> and its broadness is due to symmetry forbidden combination of sulphur to metal and nitrogen to metal LMCT transitions. These bands confirm the geometry around Cu<sup>II</sup> ion to be distorted octahedral. The observed magnetic moment of Cu<sup>II</sup> complex is 1.73 BM which confirms the octahedral structure of this monomeric complex. [19, 20]

The electronic spectrum of Zn<sup>II</sup> complex does not possess adsorption band due to d-d transition. The bands observed at 37,828 cm<sup>-1</sup> and 29,797 cm<sup>-1</sup> are due to  $\pi \to \pi^*$  and  $n \to \pi^*$  absorptions [21, 22].

**Table- 5.6: Electronic Spectral Data of the Ligand IMMA and its Metal Complexes** 

Compound	Wavelength λ <sub>max</sub> (nm)	Wave number v (cm <sup>-1</sup> )	Assignment	Geometry and Magnetic Moment	
D (D (A)	259	38, 610	$\pi - \pi^*$		
IMMA	359	27, 855	$n-\pi^*$		
[Fe(IMMA) <sub>2</sub> (H <sub>2</sub> O) <sub>2</sub> ]Cl <sub>3</sub>	405	24, 691	LMCT	Octahedral 1.91 BM	
	683	14, 641	d-d transition	Octahedral	
$[\text{Co}(\text{IMMA})_2(\text{H}_2\text{O})_2](\text{NO}_3)_2$	336	29, 761	LMCT	4.76 BM	
[Ni(IMMA) <sub>2</sub> ]SO <sub>4</sub>	402	24, 875	$^{1}A_{1}\rightarrow {}^{1}E$	Square planar Diamagnetic	
	652	15, 337	d-d transition	Distorted	
$[Cu(IMMA)_{2)}(H_2O)_2]Cl_2$	440	22, 727	LMCT	Octahedral 1.73 BM	
[Zn(IMMA) <sub>2</sub> ]SO <sub>4</sub>	264	37, 878	π-π*	Tetrahedral	
[Zii\tiviivii 1/2]504	335	29, 850	n-π <sup>*</sup>	Diamagnetic	

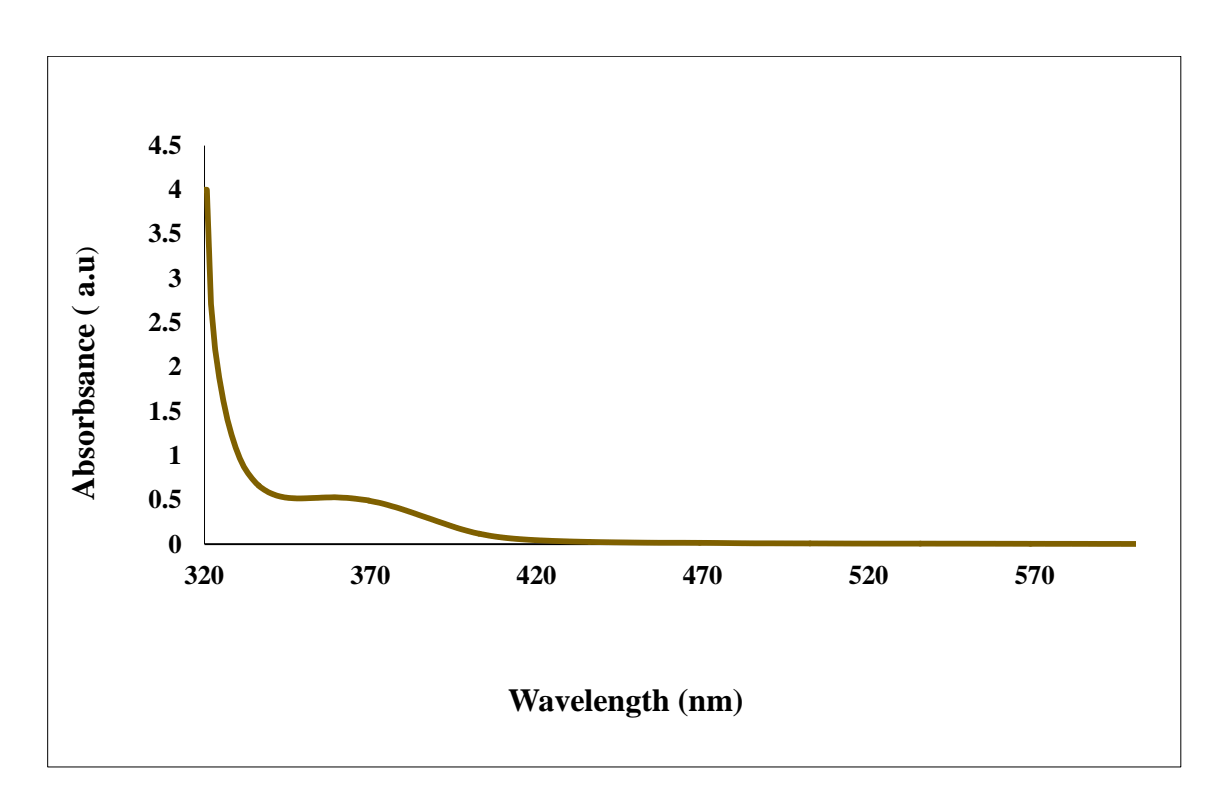
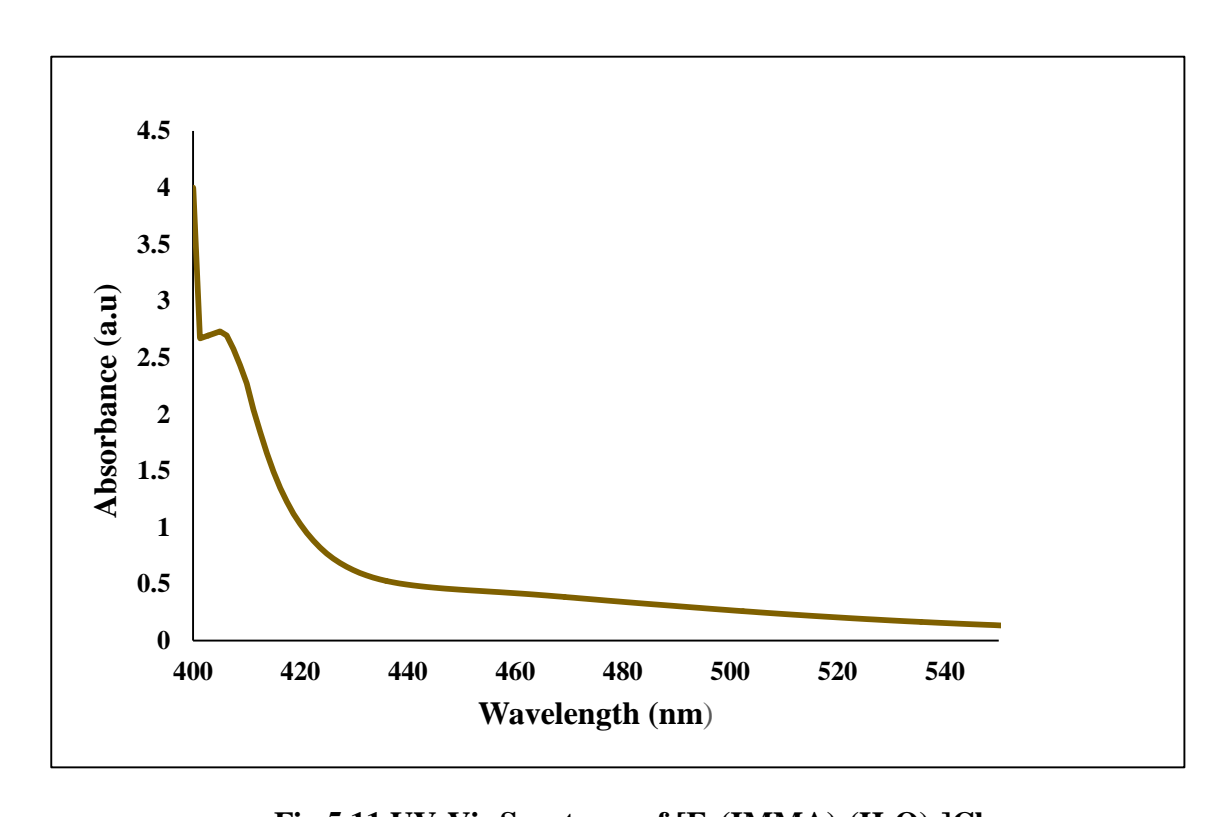


Fig. 5.10 UV-Vis Spectrum of Schiff Base IMMA



 $Fig. 5.11\ UV-Vis\ Spectrum\ of\ [Fe(IMMA)_2(H_2O)_2]Cl_3$ 

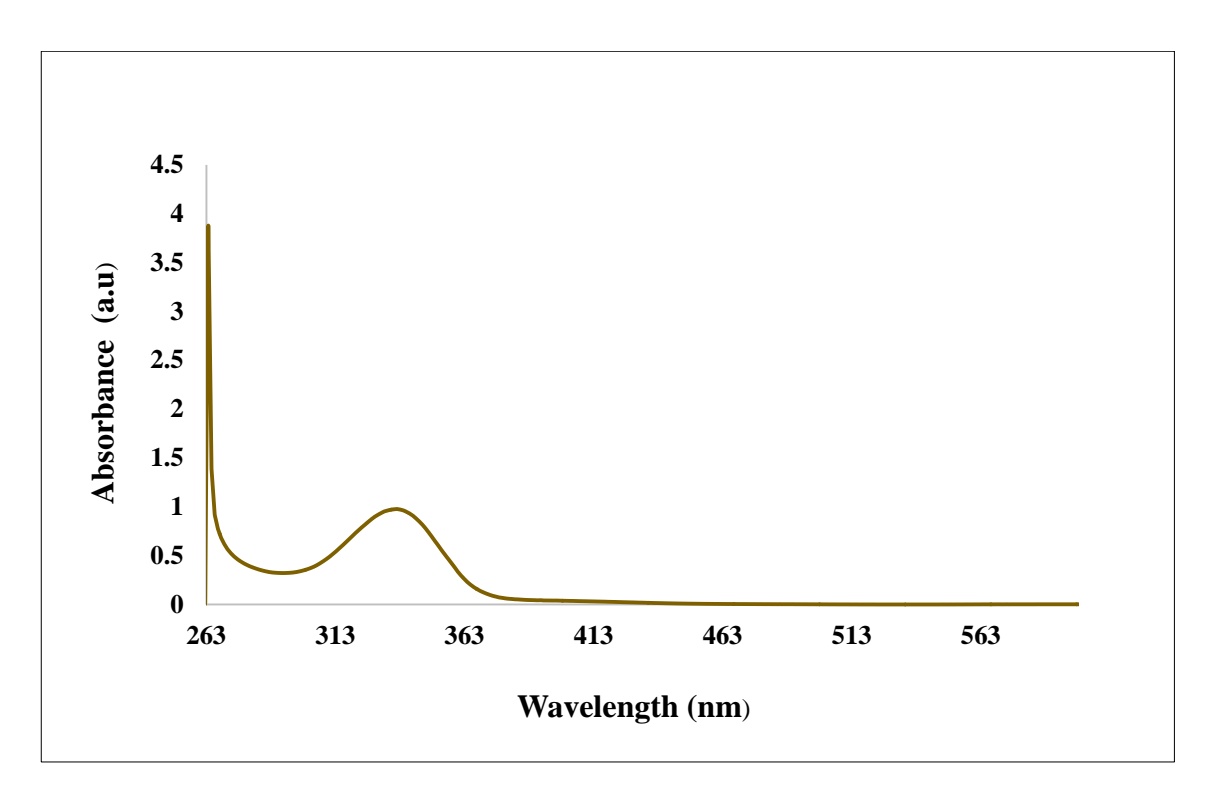


Fig. 5.12 UV-Vis Spectrum of [Co(IMMA)2(H2O)2](NO3)2

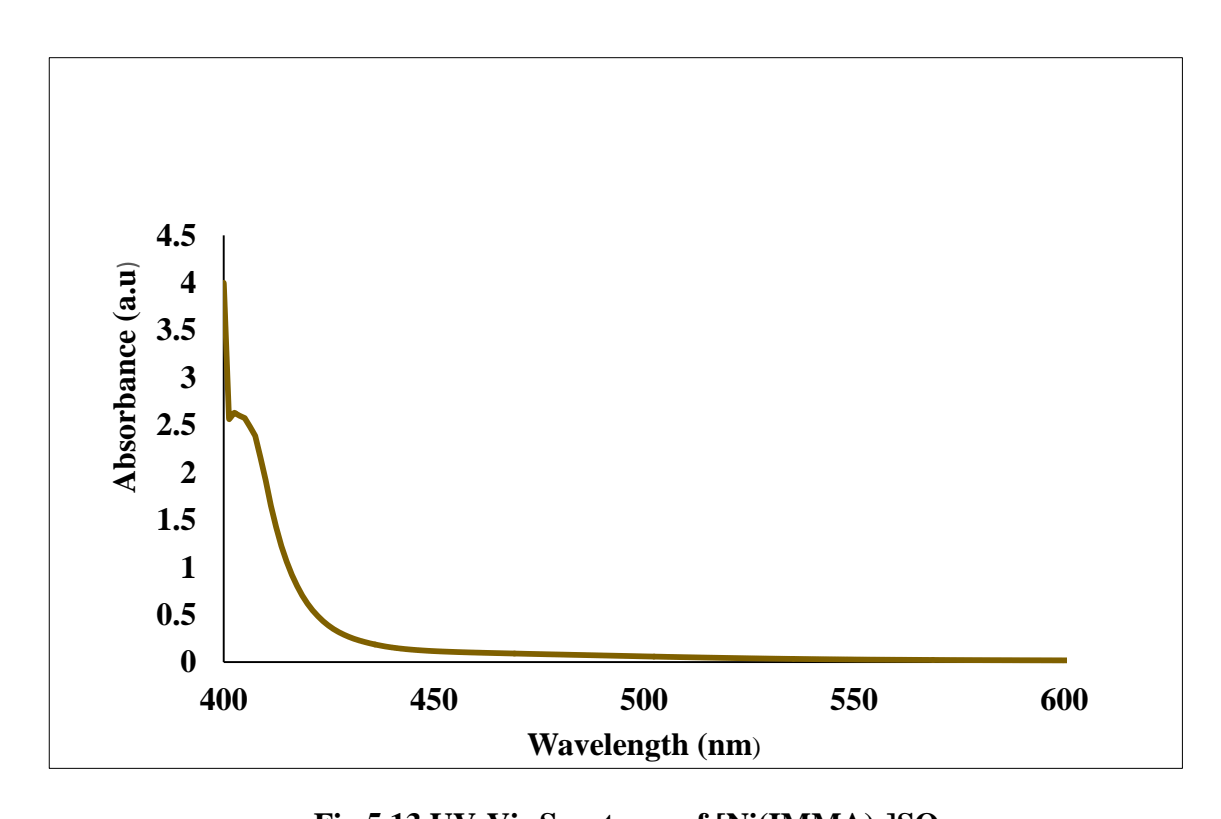


Fig.5.13 UV-Vis Spectrum of [Ni(IMMA)2]SO4

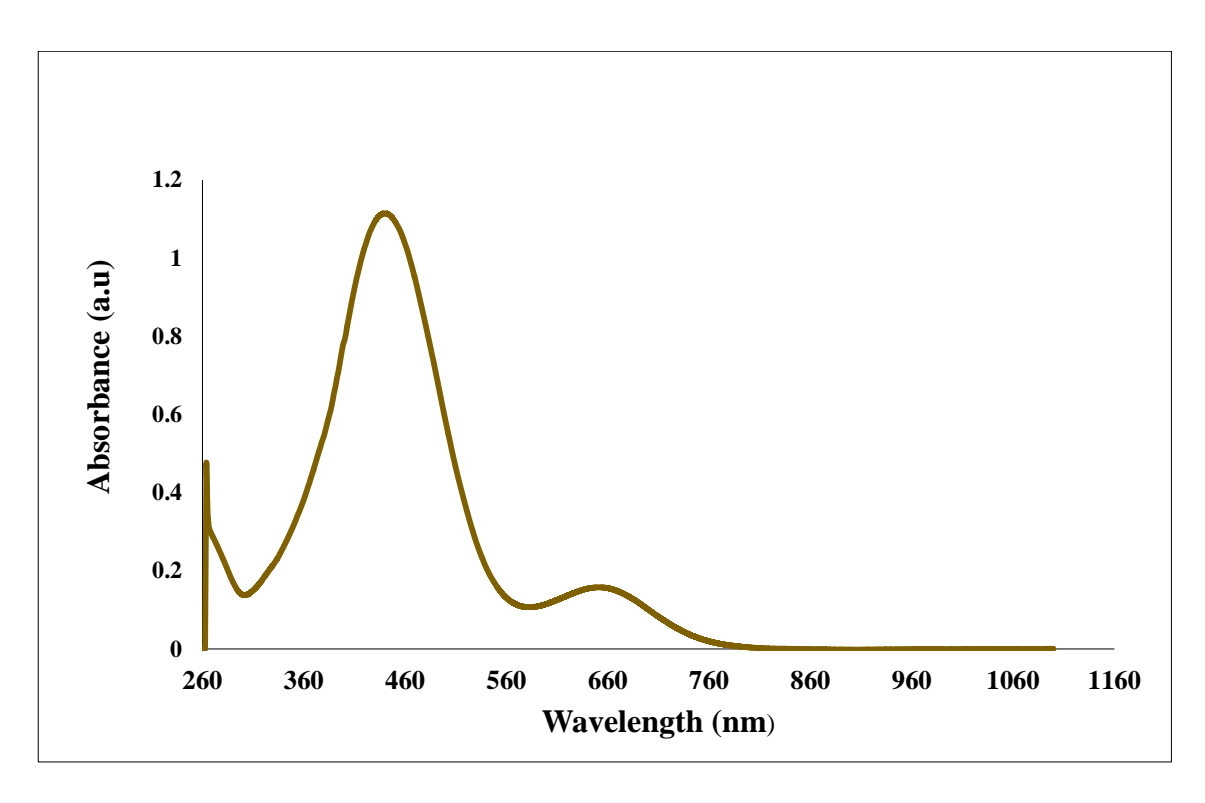


Fig.5.14 UV-Vis Spectrum of [Cu(IMMA)2)(H2O)2]Cl2

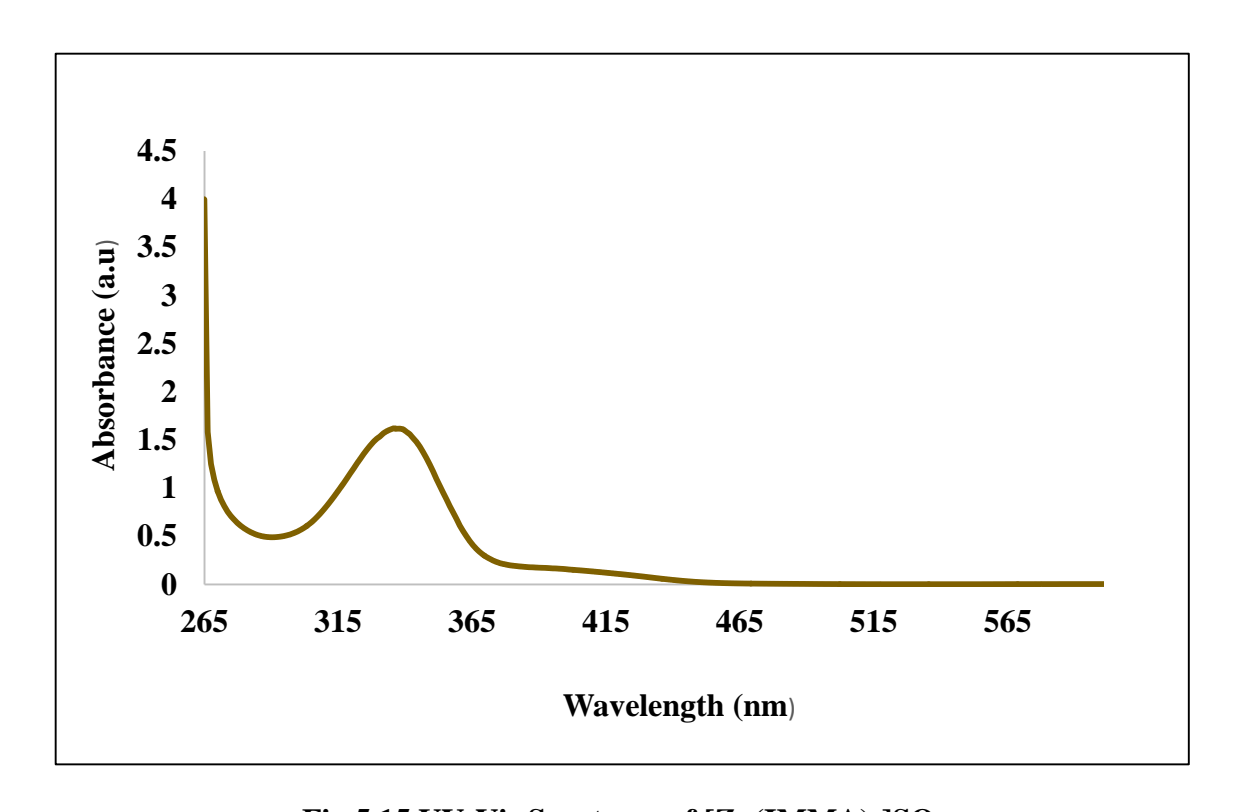


Fig.5.15 UV-Vis Spectrum of [Zn(IMMA)2]SO4

## 5.4.6 Electron Paramagnetic Resonance Spectrum of [Cu(IMMA)2)(H2O)2]Cl2

The EPR spectrum of the metal complexes provide information that are important in understanding the environment of metal ion in complexes such as the geometry, nature of the ligating sites from the Schiff base to metal and the degree of covalency of the metalligand bonds.

The X band EPR spectrum of the copper (II) complex is shown in **Fig.5.16** was recorded at room temperature in solid state under the frequency of 9.452 GHz and the centre line is at 325 mT. The copper(II) complex shows one intense absorption band in the high field region and is found to be isotropic due to the tumbling motion of the molecules. The  $g_{iso}$  value of the copper (II) complex derived from (*Z*)-*N*-(1*H*-indol-3-yl)methylene-2-(methylthio)aniline is 2.07 which is slightly higher than g value of free electron (2.0023), indicating the covalent nature of the metal-ligand bonds and confirms the presence of one unpaired electron in the  $d_{x^2-y^2}$  orbital of the Cu<sup>II</sup> ion.[23].

The magnetic moment of 1.73 BM for the copper complex indicates the presence of one unpaired electron, showing the complex to be mononuclear in nature. The electronic spectra, magnetic moment value and the relative isotropic g parameter indicate octahedral geometry around Cu<sup>2+</sup> metal ion in the complex. [24]

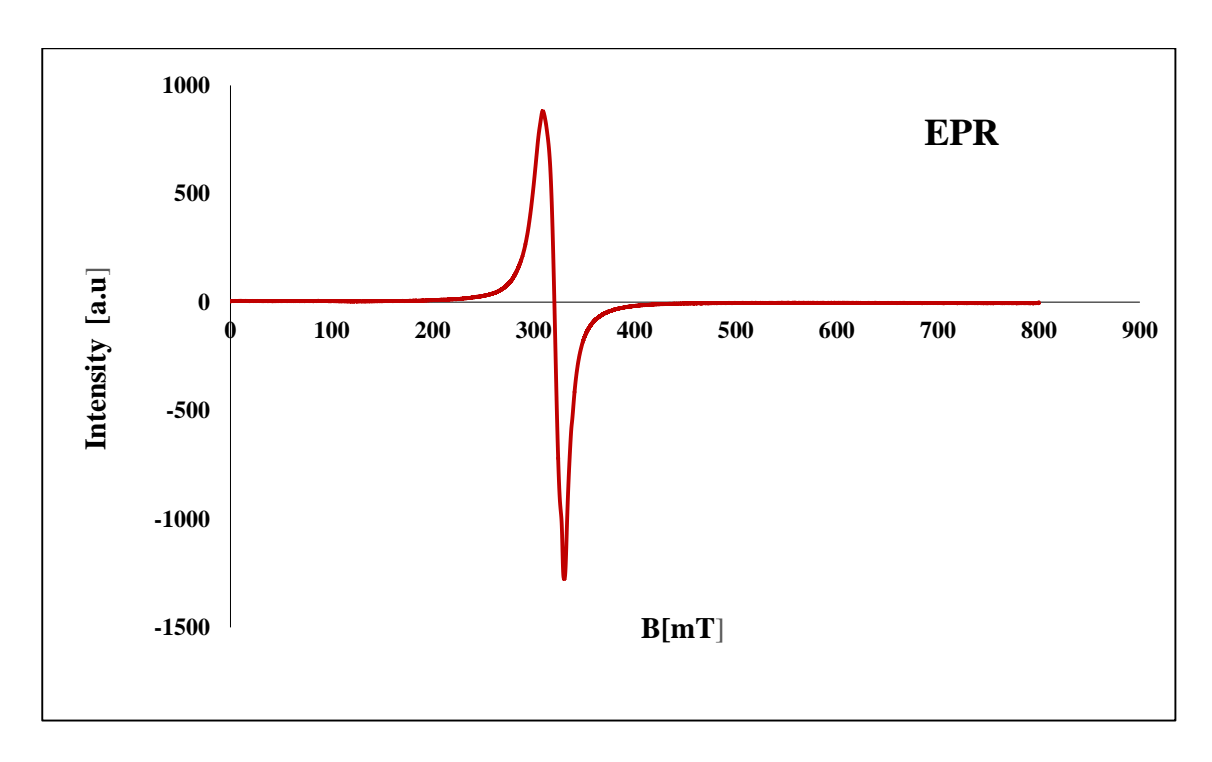


Fig.5.16 EPR Spectrum of [Cu(IMMA)2)(H2O)2]Cl2

# 5.4.7 LC-MS Spectrum of [Zn(IMMA)<sub>2</sub>]SO<sub>4</sub>

The LC-MS spectrum of zinc complex is shown in **Fig. 5.17.** The zinc complex  $(ZnC_{32}H_{28}N_4S_3O_4)$  with ligand shows the molecular ion peak at m/z=692  $(M-2)^+$ . The data confirms the stoichiometry of the metal complex as tetrahedral type.

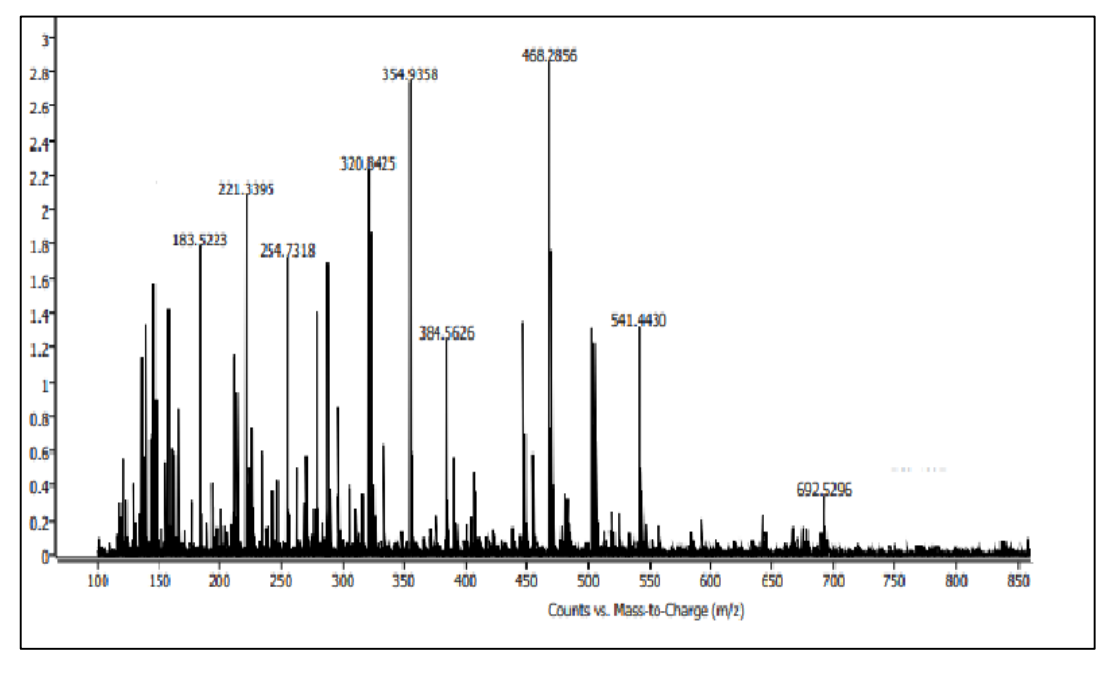


Fig.5.17 LC-MS Spectrum of [Zn(IMMA)2]SO4

## **5.4.8** Cyclic Voltammetry Studies

Cyclic voltammograms of the synthesized complexes are shown in **Fig.5.18-5.22**. The redox potentials obtained are provided in **Table-5.7**.

The cyclic voltammogram of  $[Fe(IMMA)_2(H_2O)_2]Cl_3$  complex in DMF solution measured at  $0.1Vs^{-1}$  registers a cathodic peak potential  $(E_{pc})$  value at -687 mV and corresponding anodic peak potential value  $(E_{pa})$  at -494 mV. These peak potential values suggest the reduction of  $Fe^{III}$  to  $Fe^{II}$ . The separation between the anodic and cathodic peak potential  $(\Delta E_p)$  is 193 mV. This indicates a quasi- reversible redox couple. The ratio of current peaks  $(I_{pa}/I_{pc})$  at  $0.1Vs^{-1}$  is 0.41. This value is less than one suggesting one electron transfer is followed by a chemical reaction. (ie EC mechanism is observed).[25]

The cyclic voltammogram of  $[Co(IMMA)_2(H_2O)_2](NO_3)_2$  complex in DMF solution measured at  $0.1Vs^{-1}$  registers a cathodic peak potential  $(E_{pc})$  value at -744 mV and corresponding anodic peak potential value  $(E_{pa})$  at -564 mV. These peak potential values suggest the reduction of  $Co^{II}$  to  $Co^{I}$ . The separation between the anodic and cathodic peak potential  $(\Delta E_p)$  is 180 mV. This indicates a quasi- reversible redox couple. The ratio of current peaks at  $0.1Vs^{-1}$  is 0.5. This value is less than one suggesting one electron transfer is followed by a chemical reaction. (ie EC mechanism is observed).

The cyclic voltammogram of [Ni(IMMA)<sub>2</sub>]SO<sub>4</sub> complex in DMF solution measured at  $0.1Vs^{-1}$  registers a cathodic peak potential ( $E_{pc}$ ) value at -779 mV and corresponding anodic peak potential value ( $E_{pa}$ ) at -590 mV. These peak potential values suggest the reduction of Ni<sup>II</sup> to Ni<sup>I</sup>. The separation between the anodic and cathodic peak potential ( $\Delta E_p$ ) is 189 mV. This indicates a quasi- reversible redox couple. The ratio of current peaks at  $0.1Vs^{-1}$  is 0.66. This value is less than one suggesting one electron transfer is followed by a chemical reaction. (ie EC mechanism is observed).

The cyclic voltammogram of  $[Cu(IMMA)_2(H_2O)_2]Cl_2$  complex in DMF solution measured at  $0.1Vs^{-1}$  registers a cathodic peak potential  $(E_{pc})$  value at -665 mV and corresponding anodic peak potential value  $(E_{pa})$  at -322 mV. These peak potentials suggest the reduction of  $Cu^{II}$  to  $Cu^{I}$ . The separation between the anodic and cathodic peak potential  $(\Delta E_p)$  is 343 mV. This indicates a quasi- reversible redox couple. The ratio of current peaks  $(I_{pa}/I_{pc})$  at  $0.1Vs^{-1}$  is 0.29. This value is less than one suggesting one electron transfer is followed by a chemical reaction. (ie EC mechanism is observed).[26]

The cyclic voltammogram of [Zn(IMMA)<sub>2</sub>]SO<sub>4</sub> complex in DMF solution measured at  $0.1 \text{Vs}^{-1}$  registers a cathodic peak potential ( $E_{pc}$ ) value at -568 mV and corresponding anodic peak potential value ( $E_{pa}$ ) at -335 mV. These values suggest a  $Zn^{II}/Zn^{I}$  redox couple. The separation between the anodic and cathodic peak potential ( $\Delta E_{p}$ ) is 233 mV. This indicates a quasi- reversible redox couple. The ratio of current peaks at  $0.1 \text{Vs}^{-1}$  is 0.92. This value is less than one suggesting one electron transfer is followed by a chemical reaction. (i.e EC mechanism is observed).

Table-5.7: Cyclic Voltammetric Data for IMMA Metals Complexes in DMF solution at 298 K.

Compound	E <sub>pc</sub> (mV)	E <sub>pa</sub> (mV)	ΔE <sub>p</sub> (mV)	E <sub>1/2</sub> (mV)	I <sub>pc</sub> (µA)	I <sub>pa</sub> (µA)	I <sub>pa</sub> /I <sub>pc</sub>
[Fe(IMMA) <sub>2</sub> (H <sub>2</sub> O) <sub>2</sub> ]Cl <sub>3</sub>	-687	-494	193	-590.5	17.61	7.37	0.41
[Co(IMMA) <sub>2</sub> (H <sub>2</sub> O) <sub>2</sub> ](NO <sub>3</sub> ) <sub>2</sub>	-744	-564	180	-654	12.40	6.3	0.5
[Ni(IMMA) <sub>2</sub> ]SO <sub>4</sub>	-779	-590	189	-684.5	12.01	8.00	0.66
[Cu(IMMA) <sub>2</sub> (H <sub>2</sub> O) <sub>2</sub> ]Cl <sub>2</sub>	-665	-322	343	-493.5	28.40	8.33	0.29
[Zn(IMMA) <sub>2</sub> ]SO <sub>4</sub>	-568	-335	233	-451.5	14.2	13.2	0.92

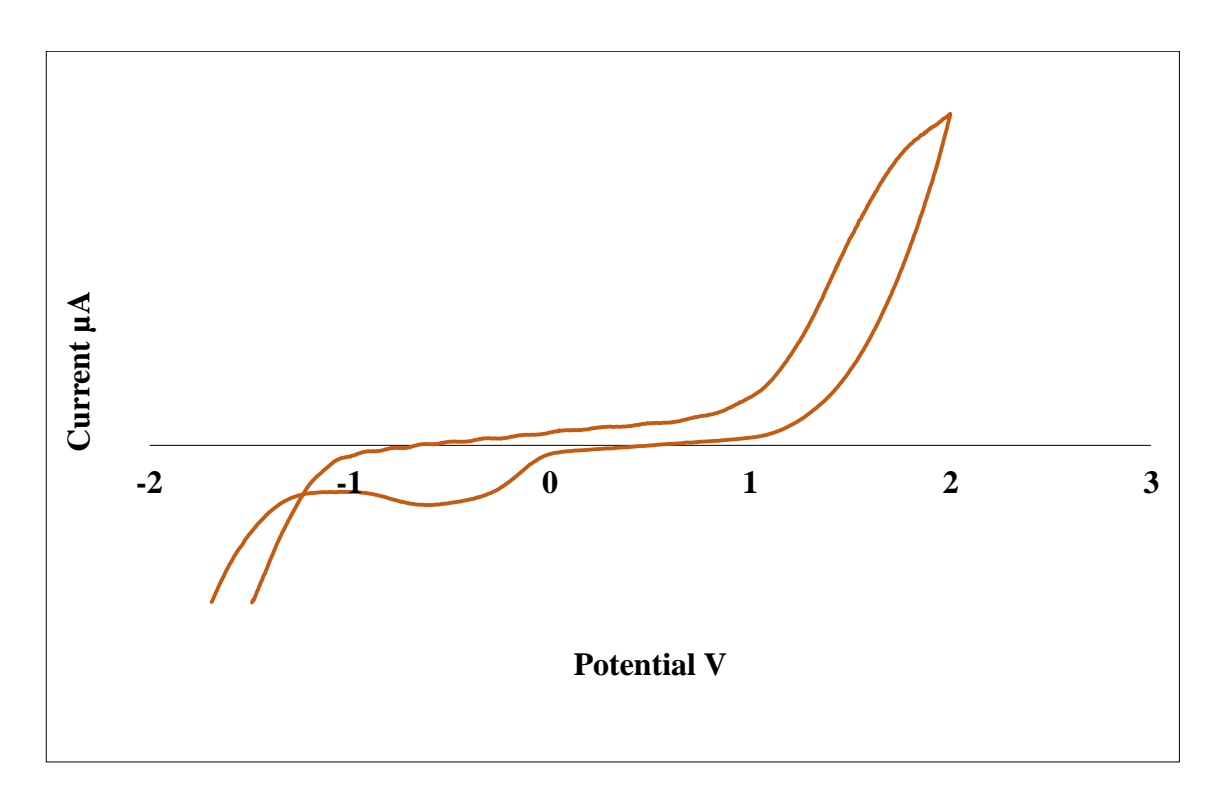
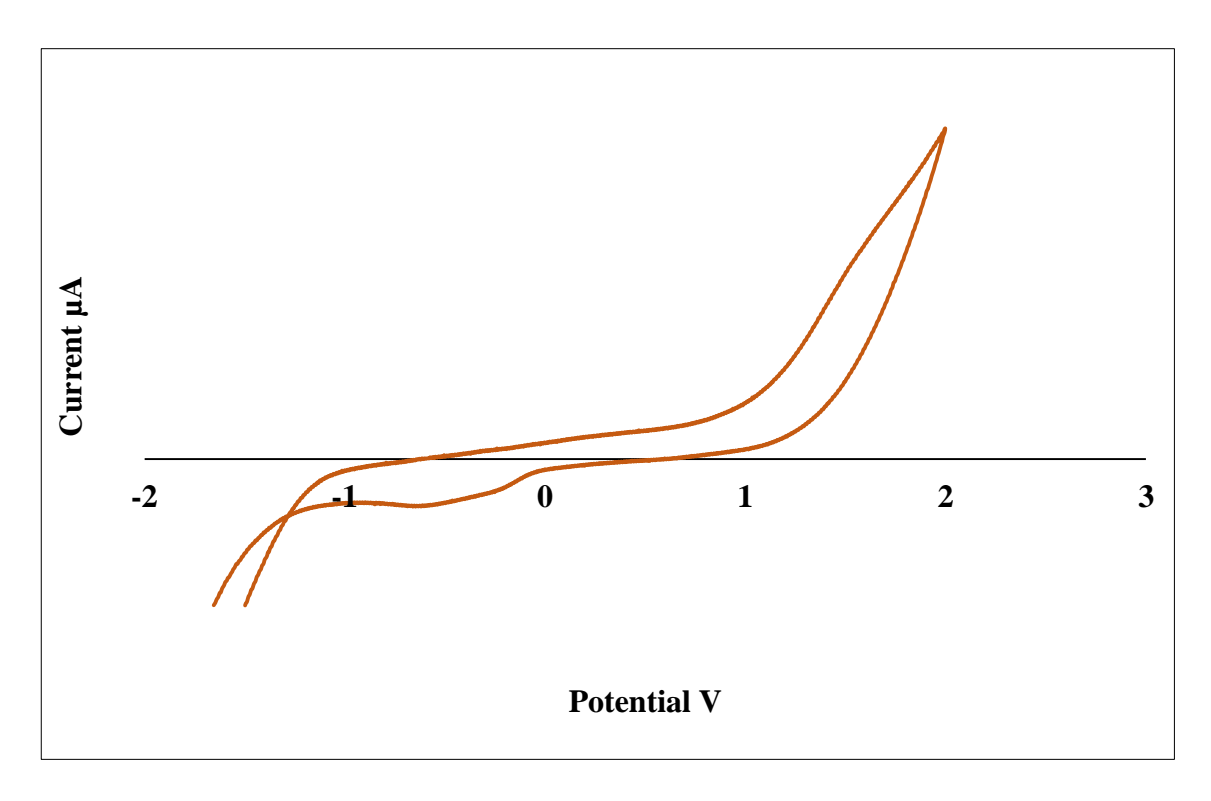


Fig.5.18 Cyclic Voltammogram of [Fe(IMMA)<sub>2</sub>(H<sub>2</sub>O)<sub>2</sub>]Cl<sub>3</sub>



 $Fig. 5.19 \ Cyclic \ Voltammogram \ of \ [Co(IMMA)_2(H_2O)_2](NO_3)_2$ 

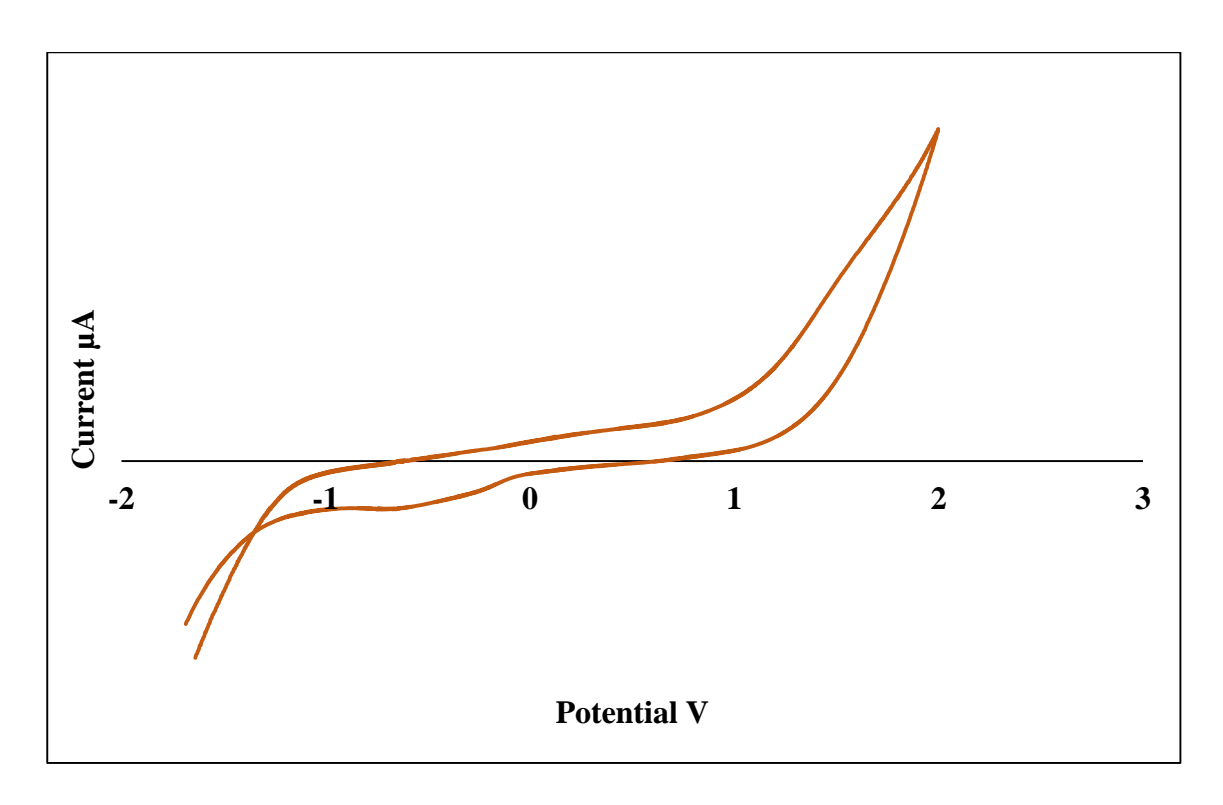
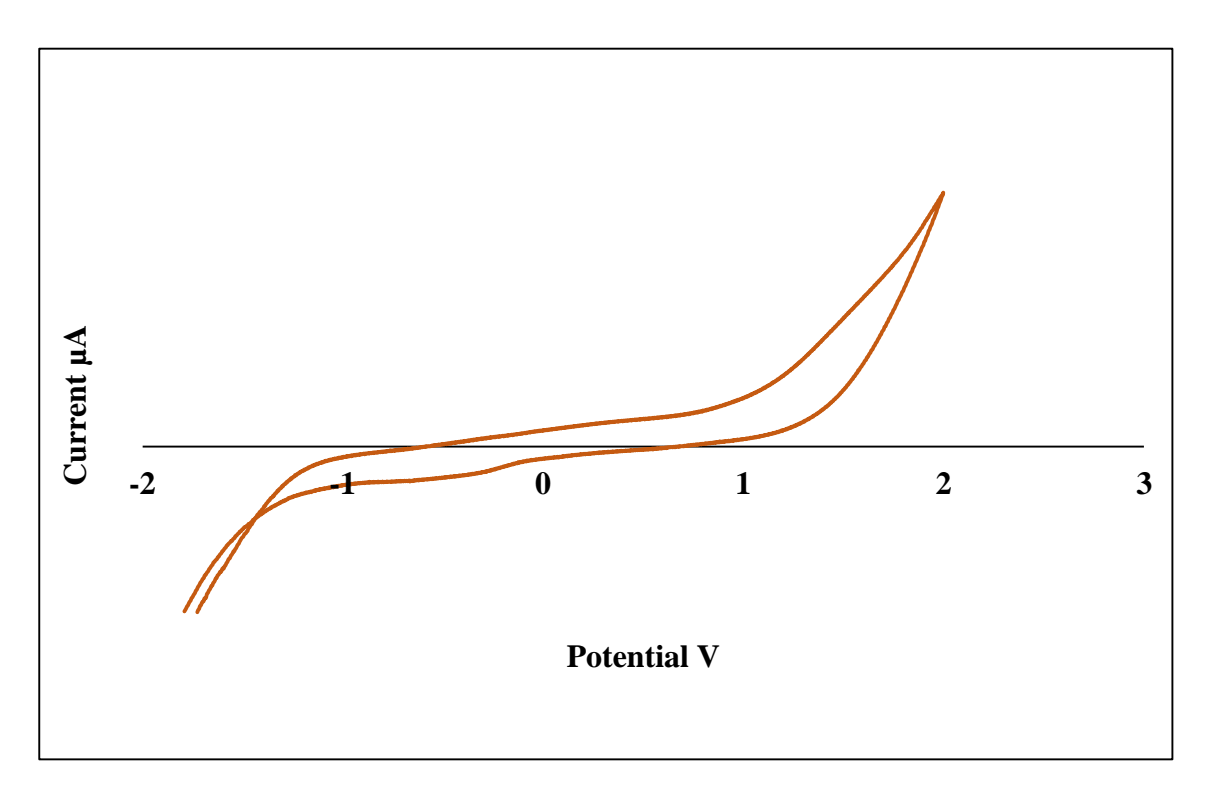


Fig.5.20 Cyclic Voltammogram of [Ni(IMMA)2]SO4



 $Fig. 5.21\ Cyclic\ Voltammogram\ of\ [Cu(IMMA)_2(H_2O)_2]Cl_2$ 

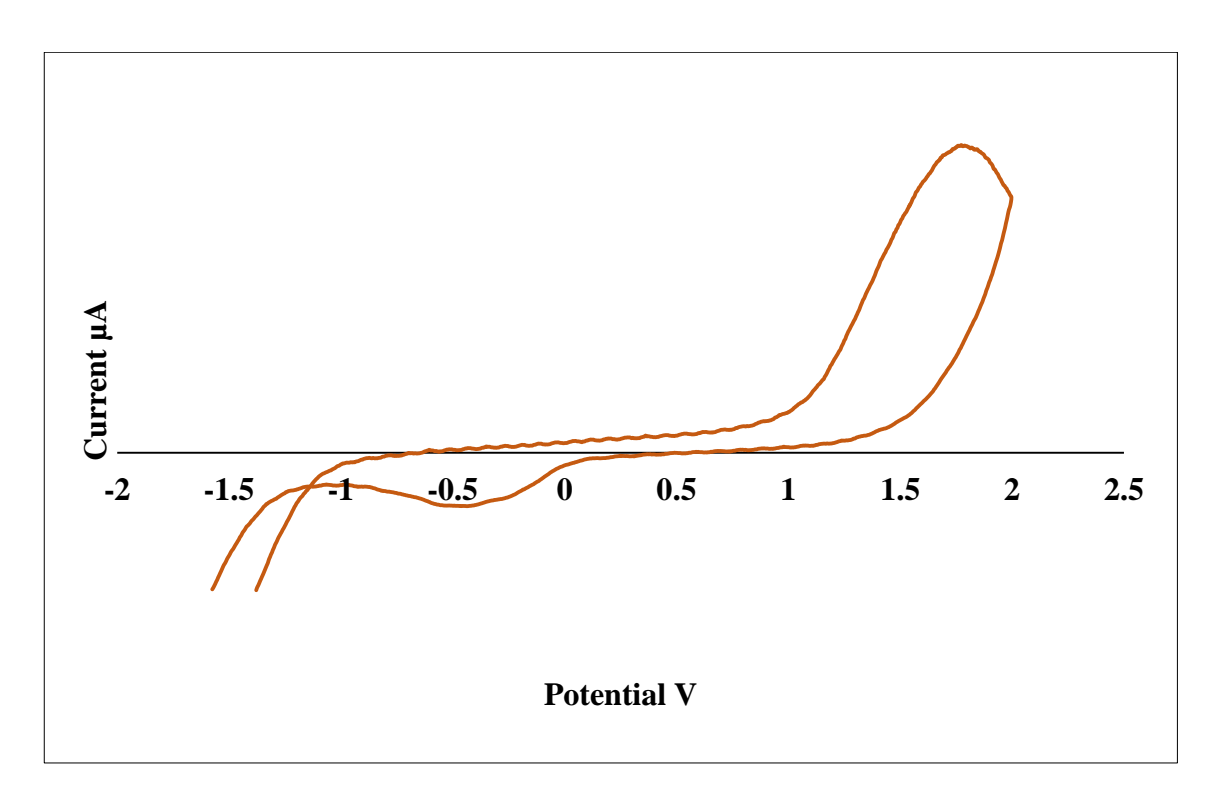


Fig.5.22 Cyclic Voltammogram of [Zn(IMMA)2]SO4

## **5.4.9** Thermal Decomposition Studies

Thermo gravimetry plays a significant role in the study of thermal stabilities of metal complexes. It also gives the information whether the water molecules are present inside or outside of the coordination sphere of the metal ion. The simultaneous TG and DSC patterns of all the metal complexes are shown in the **Fig.5.23 - 5.27**. Heating rate is controlled suitably at 20° C min<sup>-1</sup> under nitrogen atmosphere using alumina as reference compound. The correlation between different decomposition steps of the compounds and the corresponding weight losses (**Table-5.8**) are discussed in terms of the proposed formula of the compounds.

The thermal decomposition data obtained for iron (III) complex are provided in Table 5.8 and the TG-DSC curves are shown in Fig.5.23. There is a DSC peak centered at 50°C. This peak indicates the elimination of adsorbed water. Another DSC peak centered at 128 °C is due to removal of coordinated water molecules. The observed mass loss due to

removal of bound water is about 6.0% (expected 5.0%). The anhydrous complex formed due to loss of water exists in the temperature range 130-225 °C. The decomposition of the anhydrous complex occurs in the temperature range 225-375 °C and it is indicated by the DSC peak found at 250 °C. The horizontal portion of the TG curve at the range 375-500 °C may indicate the existence of an intermediate [Fe(IMMA)]Cl<sub>3</sub>. The DSC peak centered at 513°C shows the decomposition of it to form FeCl<sub>3</sub> which is the final residue. The observed mass of FeCl<sub>3</sub> is 20.7% of the original sample, while the expected mass of FeCl<sub>3</sub> is 22.0%.

The TG-DSC curves obtained for the cobalt (II) complex is shown in Fig.5.24. The DSC peak found at 96.33 °C is due to removal of coordinated water. The mass loss due to coordinated water is approximately 4.8 %. The DSC peak centered at 250°C is suggestive of the onset of decomposition of the anhydrous complex, where both the organic molecules and nitrato groups are removed to form the final residue Co<sub>3</sub>O<sub>4</sub>. The found mass of the final residue is 32.5% and calculated mass is 32.06%. [28]

The recorded thermogram of the nickel (II) complex is shown in Fig.5.25 and the thermal data are given in Table.5.8. The DSC peak centered at 72.7 °C and the mass loss upto that temperature corresponds to elimination of adsorbed water. Other DSC peaks found at 186.4 °C and 340 °C represent the decomposition through elimination of the organic ligand IMMA to form the final residue NiSO<sub>4</sub>. The expected mass of the final residue is 36.95% while the observed value is 37.11%.

Table- 5.8 Stepwise Thermal Degradation Data of Metal Complexes obtained from TG-DSC Curve

		Temperature			% Weight loss	
Compound	Stages	Range ( <sup>0</sup> C)	Assignments	Nature of Residue	Calc	Expt
	I	50	Loss of adsorbed water molecules			
[Fe(IMMA) <sub>2</sub> (H <sub>2</sub> O) <sub>2</sub> ]Cl <sub>3</sub>	II	128	Loss of two coordinated water molecules	FeCl <sub>3</sub>	22.0	20.7
	III	225-375	Decomposition of anhydrous complex	rec13		20.7
	IV	513	Decomposition of intermediate complex			
[Co(MPMA) <sub>2</sub> (H <sub>2</sub> O) <sub>2</sub> ](NO <sub>3</sub> ) <sub>2</sub>	I	96	Loss of coordinated water molecules	C <sub>2</sub> O	32.06	22.5
	II	250	Decomposition of anhydrous complex	Co <sub>3</sub> O <sub>4</sub>		32.5
INI:(IMMA) 100	I	73	Loss of adsorbed water molecules	Nigo	26.05	37.11
[Ni(IMMA) <sub>2</sub> ]SO <sub>4</sub>	II	186-340	Elimination of organic ligand	NiSO <sub>4</sub>	36.95	37.11
[Cu(IMMA) <sub>2</sub> )(H <sub>2</sub> O) <sub>2</sub> ]Cl <sub>2</sub>	I	110-187	Loss of two coordinated water molecules	[Cw/DADAAACL]	<i>57</i> 01	57.01
	II	441	Elimination of one organic ligand	[Cu(IMMA)Cl <sub>2</sub> ]	57.01	57.91
7 (0.04) 100	I	80	Loss of adsorbed water molecules			
Zn(IMMA) <sub>2</sub> ]SO <sub>4</sub>	II	199	Elimination of one organic ligand ZnSO <sub>4</sub>		-	-
	III	441	Decomposition of intermediate complex			

The TG-DSC curves obtained for the copper (II) complex is shown in Fig.5.26 and the thermal decomposition data obtained are furnished in Table.5.8. The DSC peaks centered at 110 °C and 187.4 °C are attributed to the successive loss of two water molecules. The DSC peak seen at 441.1 °C may be due to loss of one IMMA ligand so as to form [Cu(IMMA)Cl<sub>2</sub>]. This intermediate complex is very stable and is found as a residue at the temperature of 850 °C. The observed mass of the final residue namely [Cu(IMMA)Cl<sub>2</sub>] is 57.91% while its expected mass is 57.01%.

The TG-DSC curves obtained for the zinc (II) complex is shown in Fig.5.27 and the thermal decomposition data obtained are furnished in Table 5.8. The DSC peak centered at 79.95 °C is attributed to adsorbed water molecules. The dry water free complex mass may be 10% less than the mass of the sample taken. The anhydrous complex undergoes decomposition and removal of one molecule of the organic ligand to form an intermediate [Zn(IMMA)SO<sub>4</sub>]. This decomposition process is indicated by the DSC peak centered at 199 °C. The intermediate on further programmed heat undergoes gradual mass loss to produce a final residue of ZnSO<sub>4</sub>. The expected and the observed masses of the final residue do not agree, it may be because of the contamination of ZnSO<sub>4</sub> with [Zn(IMMA)SO<sub>4</sub>].

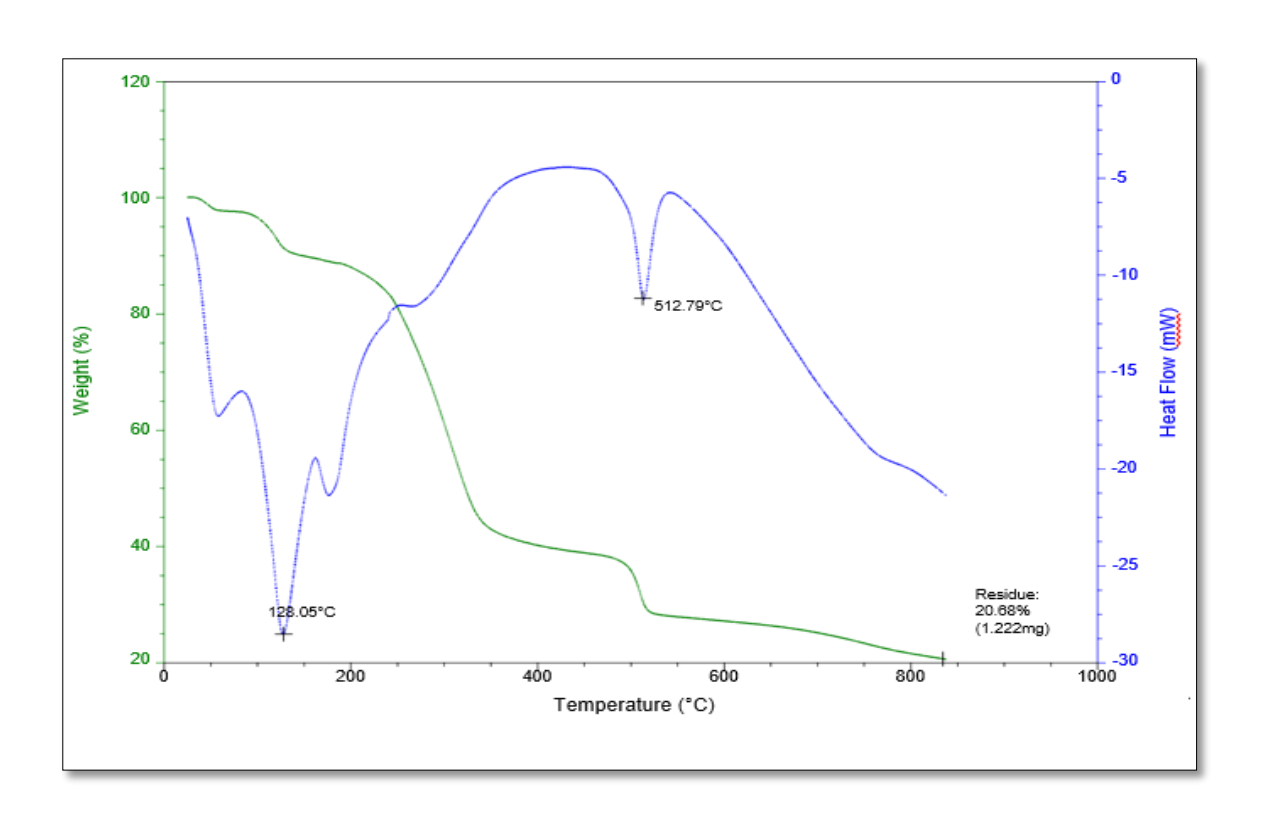


Fig.5.23 TG-DSC Curves of [Fe(IMMA)<sub>2</sub>(H<sub>2</sub>O)<sub>2</sub>]Cl<sub>3</sub>

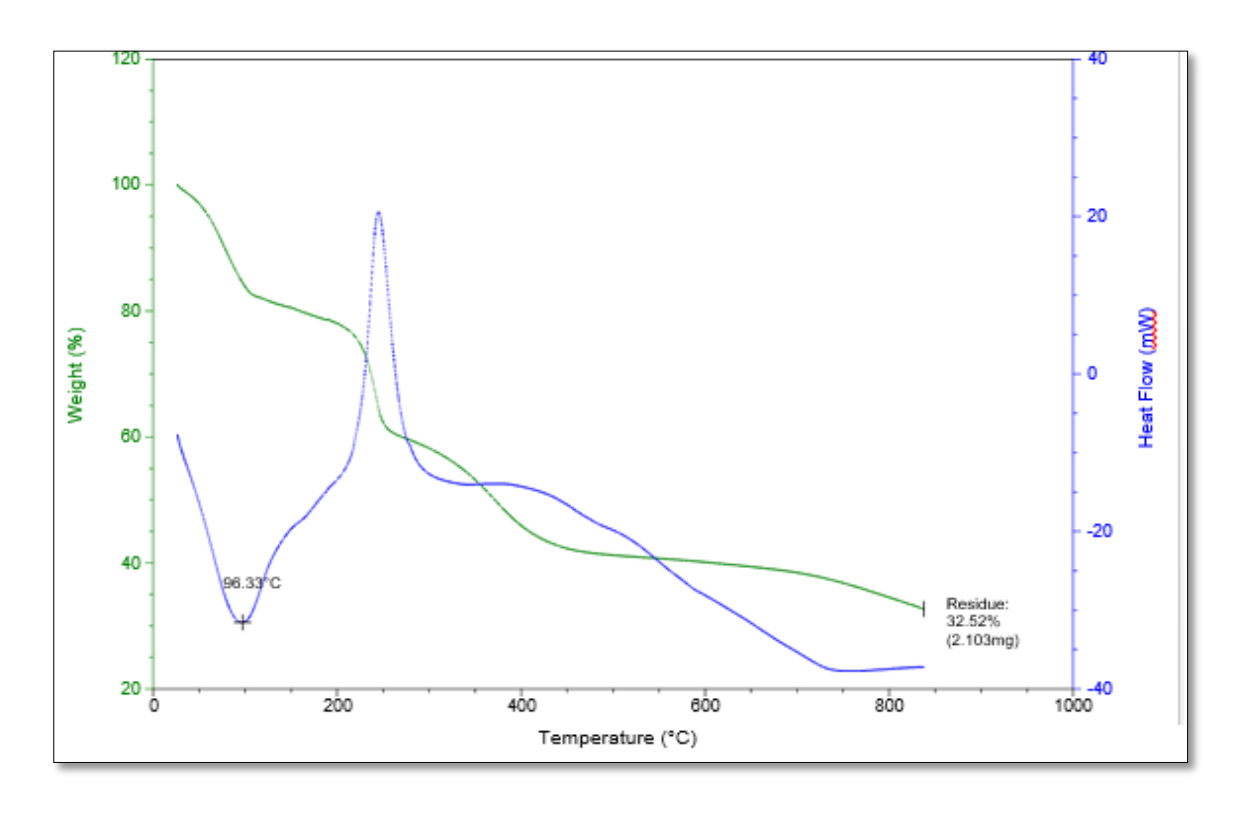


Fig.5.24 TG-DSC Curves of [Co(IMMA)<sub>2</sub>(H<sub>2</sub>O)<sub>2</sub>](NO<sub>3</sub>)<sub>2</sub>

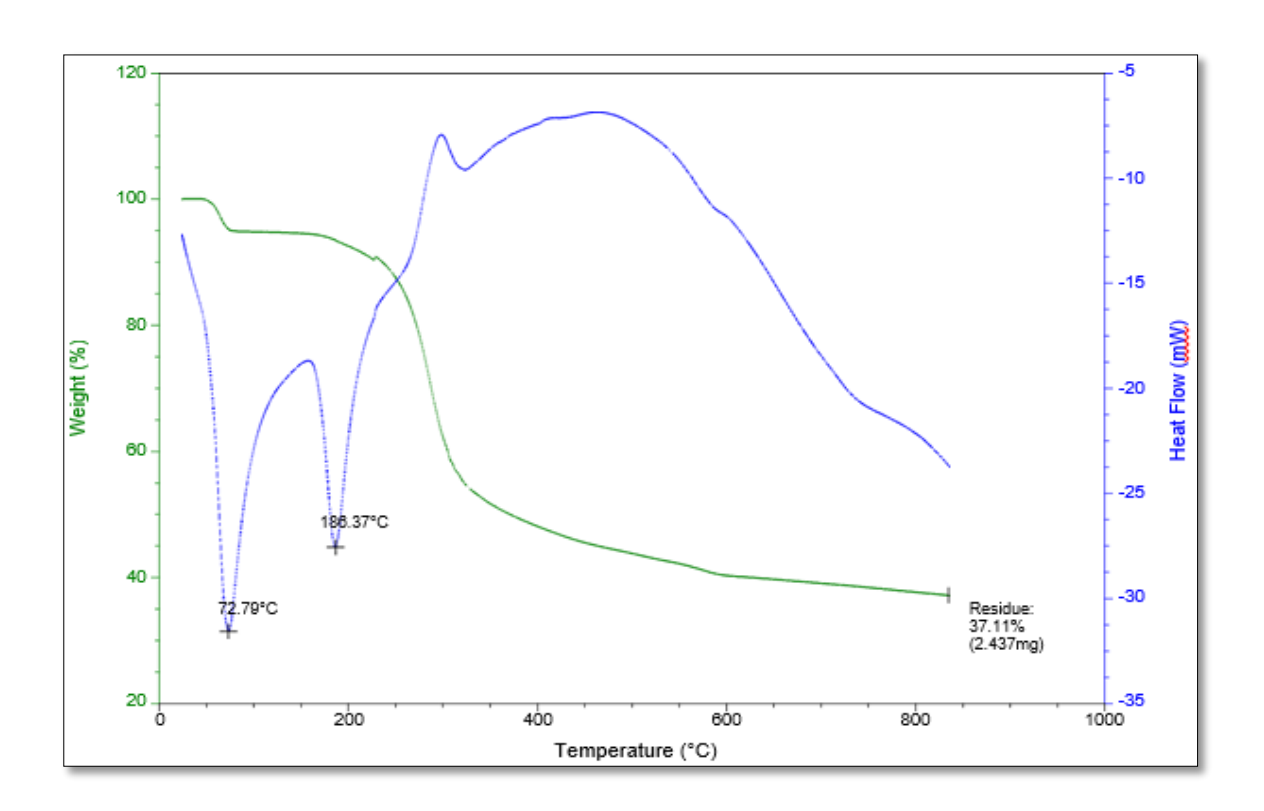


Fig.5.25 TG-DSC Curves of [Ni(IMMA)<sub>2</sub>]SO<sub>4</sub>

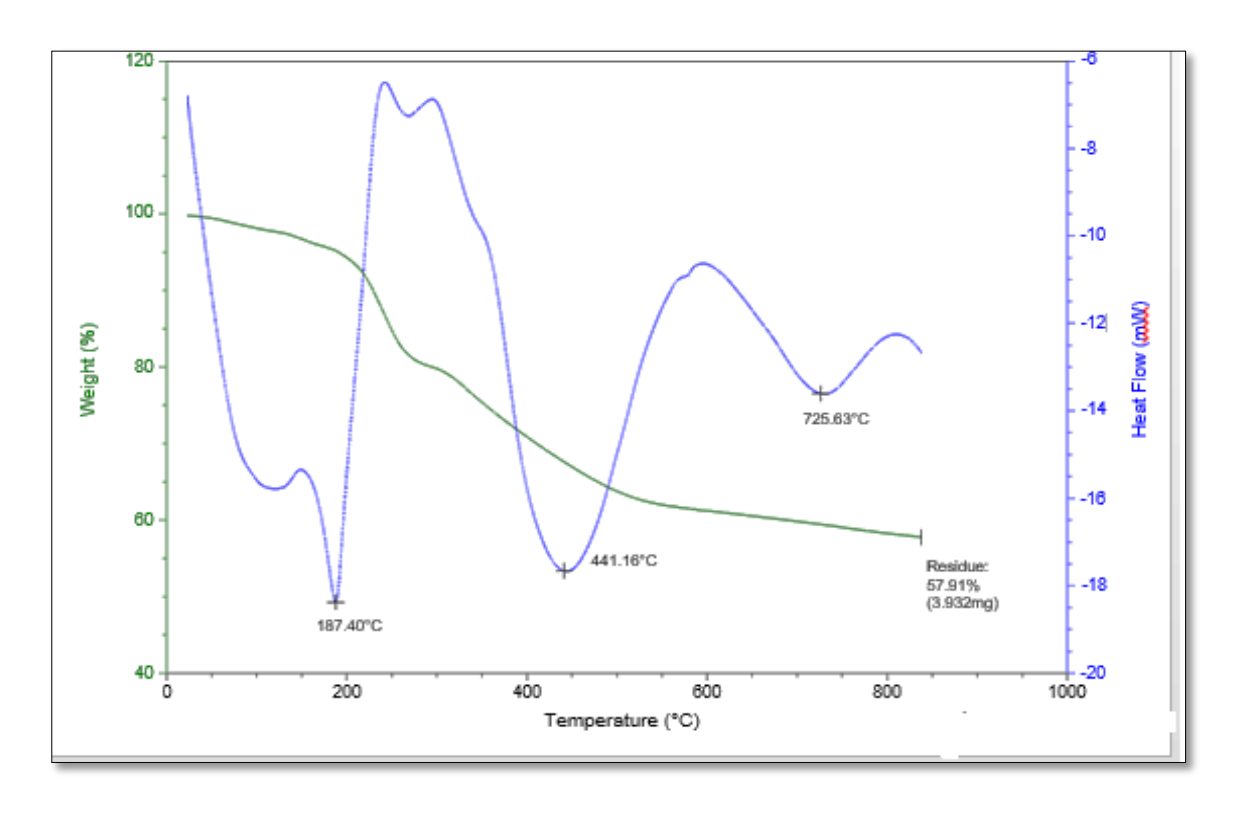


Fig.5.26 TG-DSC Curves of  $[Cu(IMMA)_2(H_2O)_2]Cl_2$ 

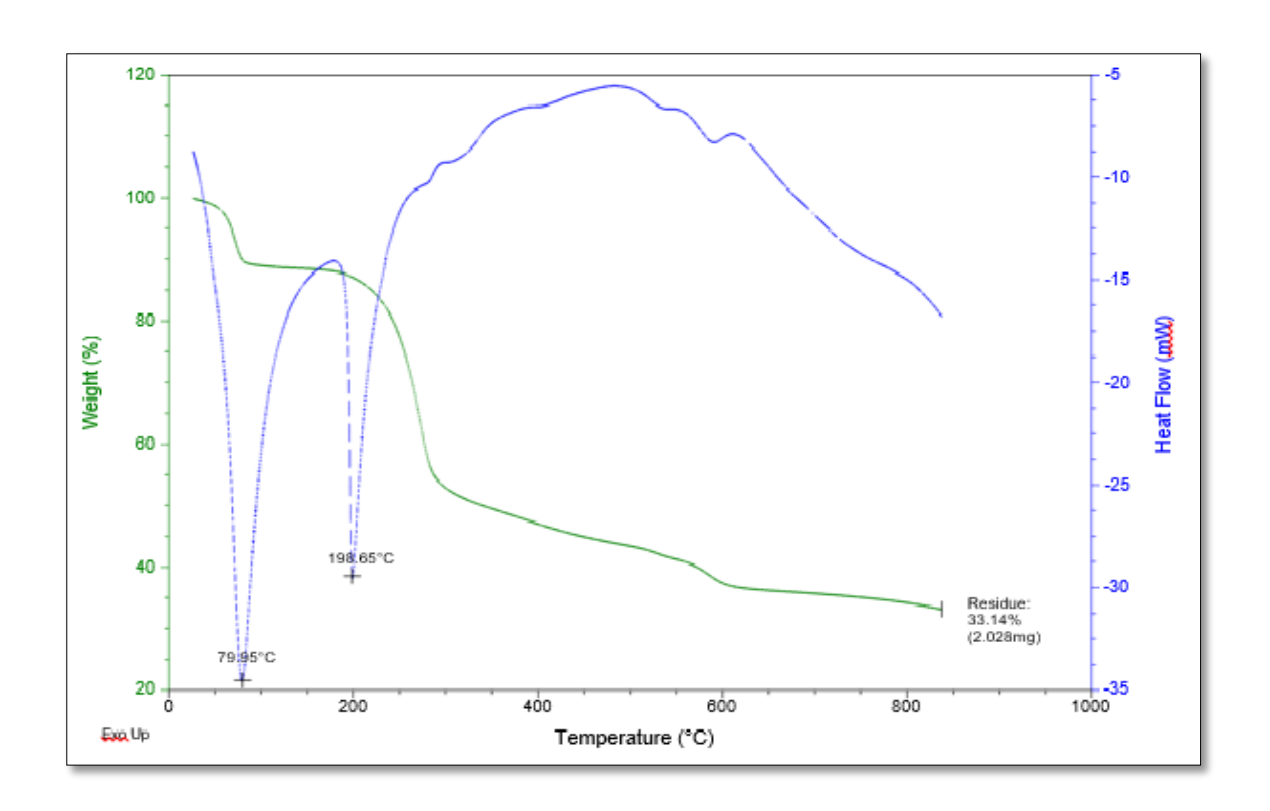


Fig.5.27 TG-DSC Curves of [Zn(IMMA)2]SO4

## 5.5 Biological Studies

## 5.5.1 Evaluation of Antimicrobial Activities of Synthesized Compounds

The *in vitro* antimicrobial activities of the compounds are screened against the bacteria, *B. subtilis*, *S. aureus*, *E. coli*, *P. aeruginosa* and fungi such as *C. albicans and A. niger* by agar well diffusion method. By comparing the diameters of zones of inhibition obtained for the ligand and its complexes, it inferred that the complexes exhibit higher antimicrobial activity than the free ligand. The results of antibacterial and antifungal screening are given in **Tables-5.9** and **5.10**.

The results represent cobalt (II) complex possess highest activity against bacterial species followed by zinc (II), copper (II) complexes which shows moderate activity compared to the ligand. The cobalt (II) complex exhibited 28, 32, 28 and 30 mm zones of inhibition against *B.subtilis*, *S.aureus*, *P.aeruginosa* and *E.coli* respectively where these

values are greater than the values obtained for the ligand MPMA as well as the control gentamicin. The values lead to an interesting observation that the formation of azomethine -CH=N group by the condensation of the aldehyde and the amine -NH<sub>2</sub> of the 2-(methylthio)aniline could be a crucial step in determining the microbial activity. Azomethine nitrogen which is the most basic centre in the Schiff base moiety contributes a key role, and could be an active centre in the whole molecule.[30-35] The results are shown in the **Fig.5.28** and **5.29**.

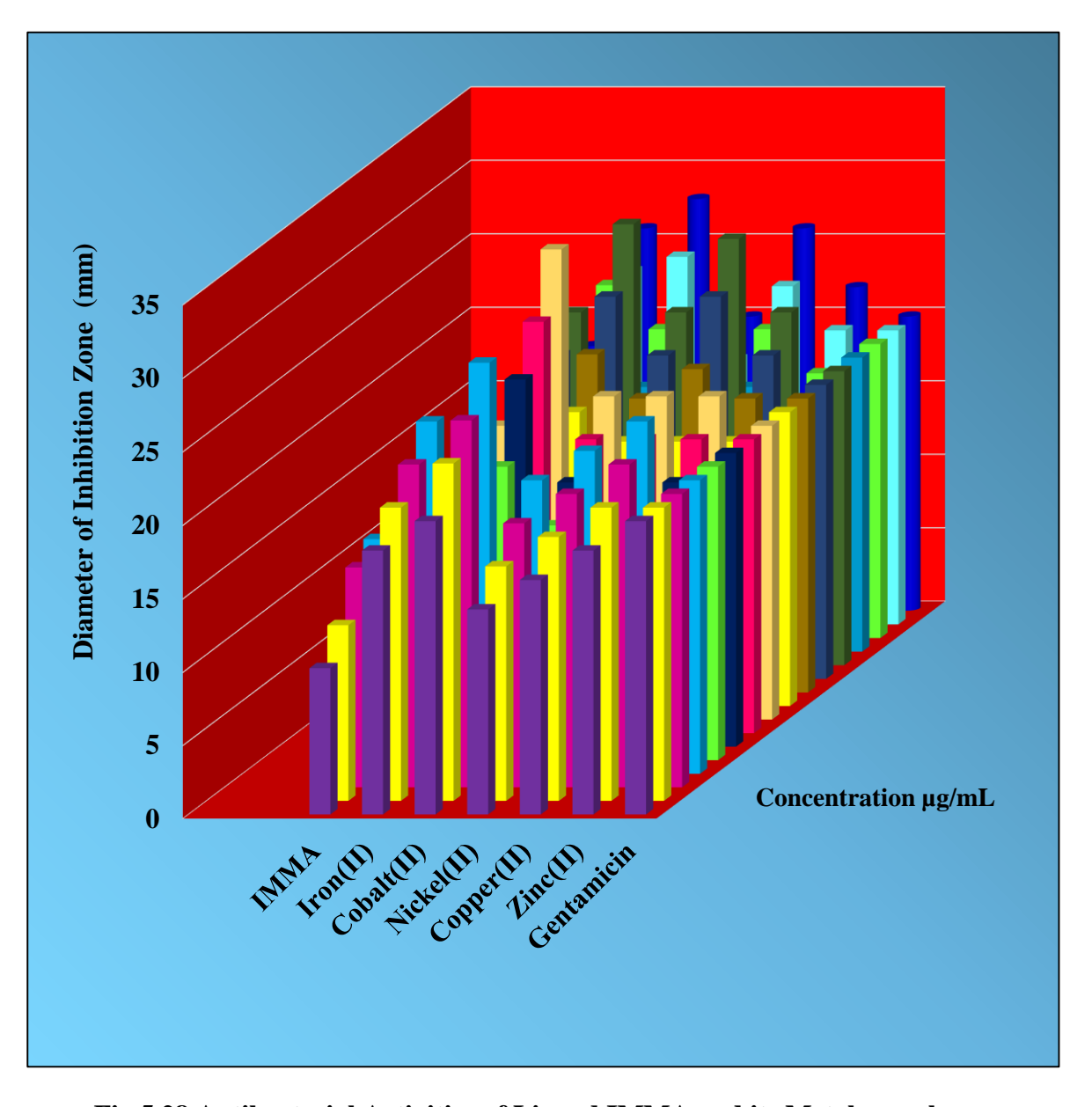


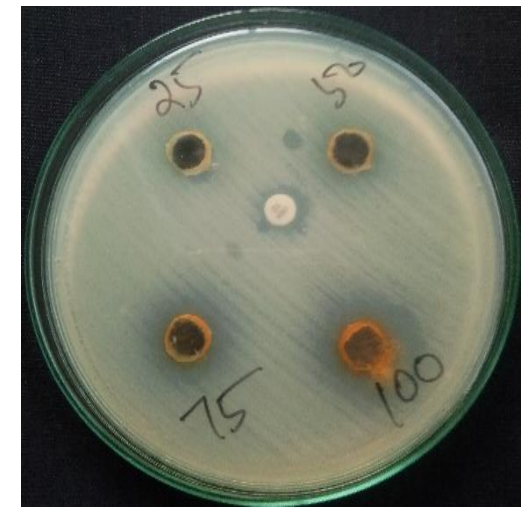
Fig.5.28 Antibacterial Activities of Ligand IMMA and its Metal complexes

Table- 5.9: Antibacterial Activities of Ligand IMMA and its Metal Complexes

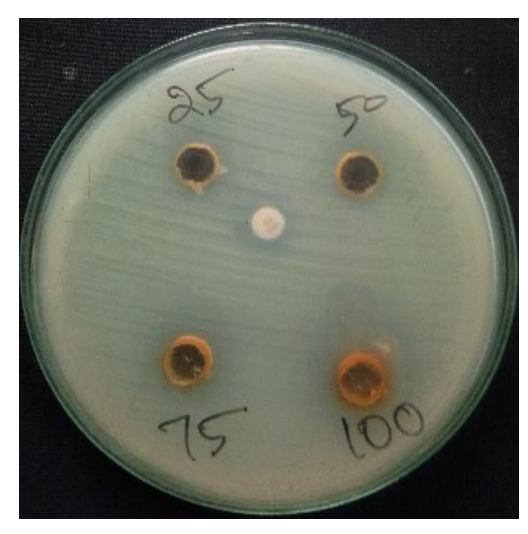
Compound		Diameter of inhibition Zone (mm)														
		B.su	btilis			S.au	reus			E.c	oli			P.aeru	ginosa	
	25 (µg/mL)	50 (µg/mL)	75 (µg/mL)	100 (µg/mL)	25 (µg/mL)	50 (µg/mL)	75 (µg/mL)	100 (µg/mL)	25 (µg/mL)	50 (µg/mL)	75 (µg/mL)	100 (µg/mL)	25 (µg/mL)	50 (µg/mL)	75 (µg/mL)	100 (µg/mL)
IMMA	10	12	15	16	10	12	14	16	10	13	15	18	11	13	15	18
[Fe(IMMA) <sub>2</sub> (H <sub>2</sub> O) <sub>2</sub> ] Cl <sub>3</sub>	18	20	22	24	14	18	18	20	18	22	22	24	20	24	24	26
[Co(MPMA) <sub>2</sub> (H <sub>2</sub> O) <sub>2</sub> ](NO <sub>3</sub> ) <sub>2</sub>	20	23	25	28	20	25	28	32	20	23	26	30	18	21	25	28
[Ni(IMMA) <sub>2</sub> ]SO <sub>4</sub>	14	16	18	20	16	18	20	22	18	20	22	24	14	16	18	20
[Cu(IMMA) <sub>2)</sub> (H <sub>2</sub> O) <sub>2</sub> ]Cl <sub>2</sub>	16	18	20	22	16	18	20	22	18	22	26	29	18	21	23	26
[Zn(IMMA) <sub>2</sub> ]SO <sub>4</sub>	18	20	22	24	16	18	20	22	18	20	22	24	16	18	20	22
Gentamicin	20	20	20	20	20	20	20	20	20	20	20	20	20	20	20	20

**Table- 5.10: Antifungal Activities of Ligand IMMA and its Metal Complexes** 

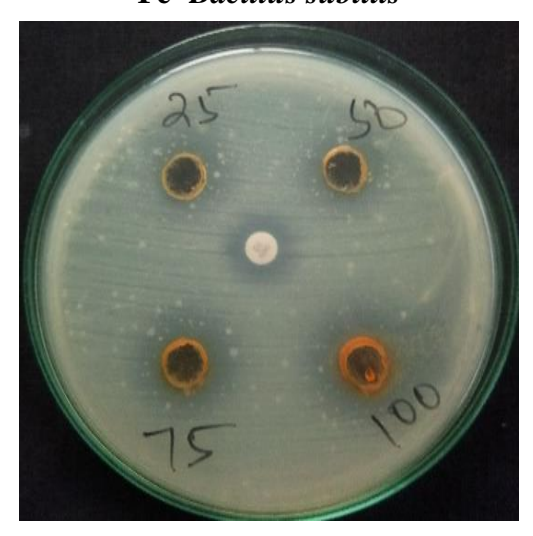
		Diameter of inhibition Zone (mm)								
Compound		C.albicans				A.niger				
	25 (μg/mL)	50 (μg/mL)	75 (μg/mL)	100 (μg/mL)	25 (μg/mL)	50 (μg/mL)	75 (μg/mL)	100 (μg/mL)		
IMMA	13	14	16	18	12	14	17	19		
[Fe(IMMA) <sub>2</sub> (H <sub>2</sub> O) <sub>2</sub> ]Cl <sub>3</sub>	14	18	18	20	20	24	24	26		
[Co(MPMA) <sub>2</sub> (H <sub>2</sub> O) <sub>2</sub> ](NO <sub>3</sub> ) <sub>2</sub>	18	20	22	24	20	23	25	28		
[Ni(IMMA) <sub>2</sub> ]SO <sub>4</sub>	16	18	20	22	14	18	20	22		
[Cu(IMMA) <sub>2)</sub> (H <sub>2</sub> O) <sub>2</sub> ]Cl <sub>2</sub>	16	18	20	22	14	16	18	20		
[Zn(IMMA) <sub>2</sub> ]SO <sub>4</sub>	20	22	24	26	16	18	20	22		
Ketoconazole	20	20	20	20	20	20	20	20		



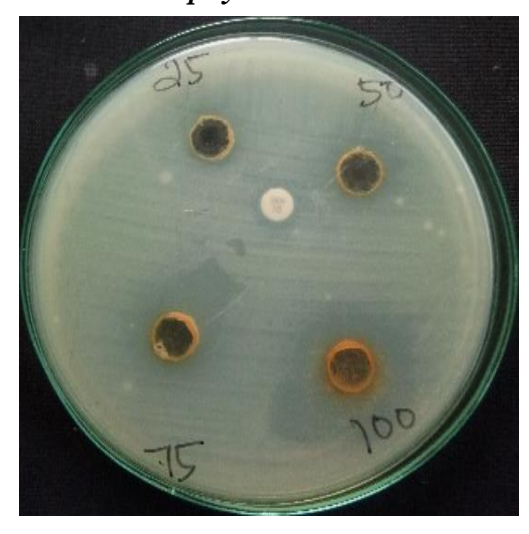
Fe- Bacillus subtilis



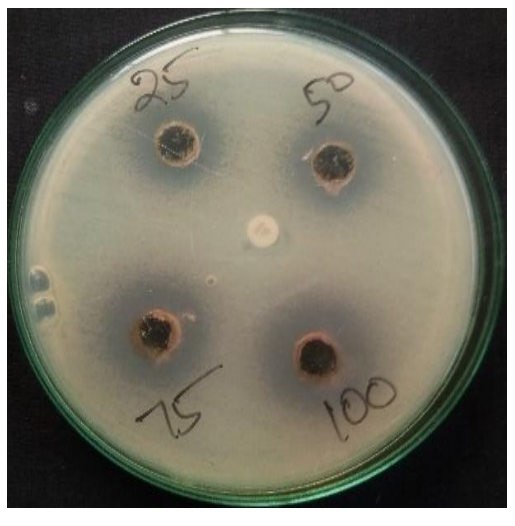
Fe - Staphylococcus aureus



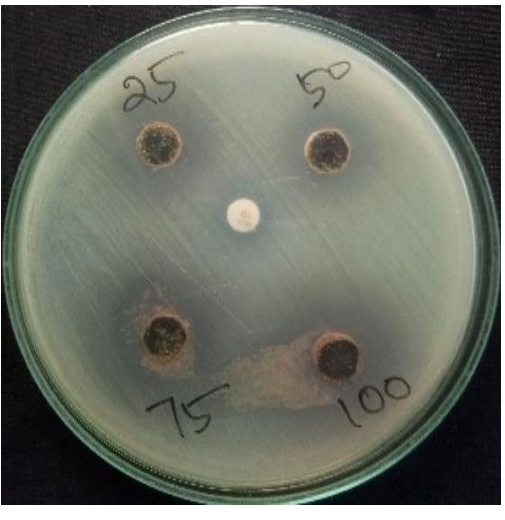
Fe - E. coli



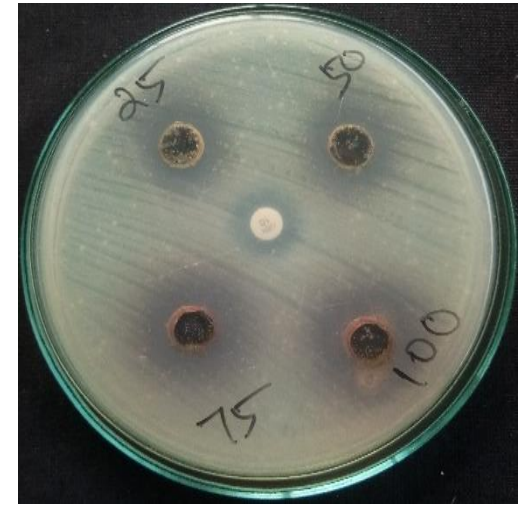
Fe - Pseudomonas aeruginosa



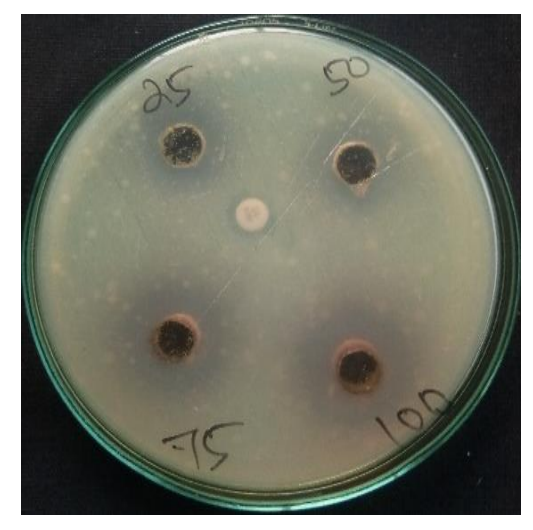
Co - Bacillus subtilis



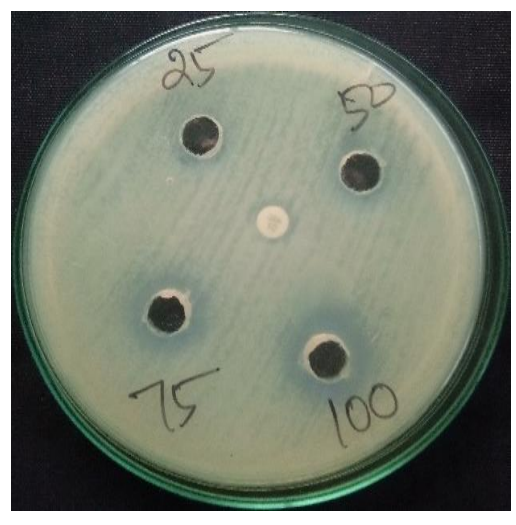
Co - Staphylococcus aureus



Co - E. coli



Co - Pseudomonas aeruginosa



Ni - Bacillus subtilis



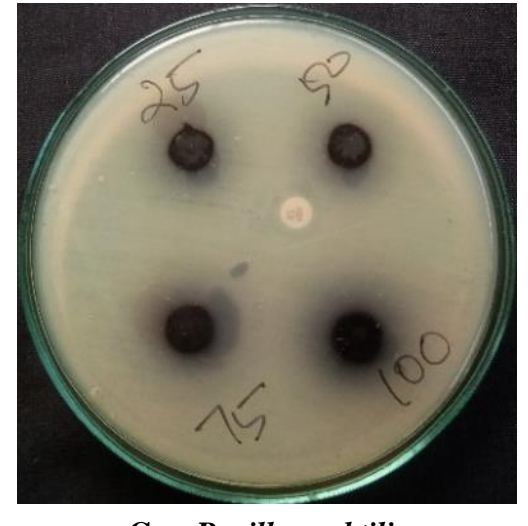
Ni - Staphylococcus aureus



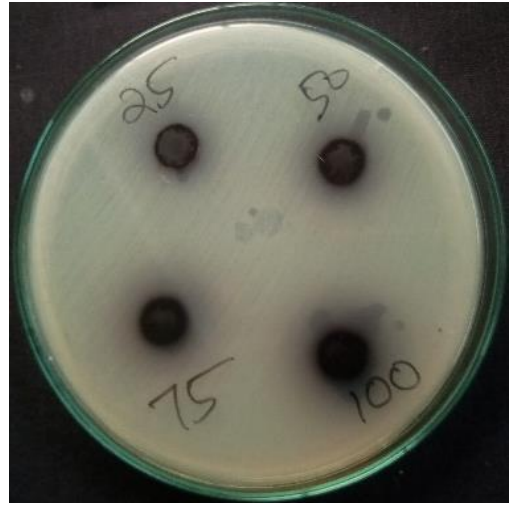
Ni - E. coli



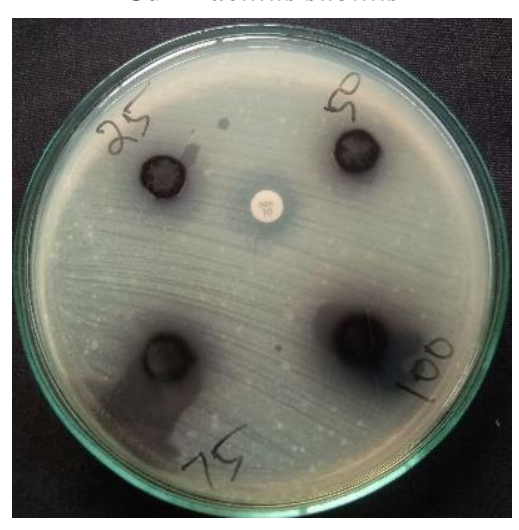
Ni - Pseudomonas aeruginosa



Cu - Bacillus subtilis



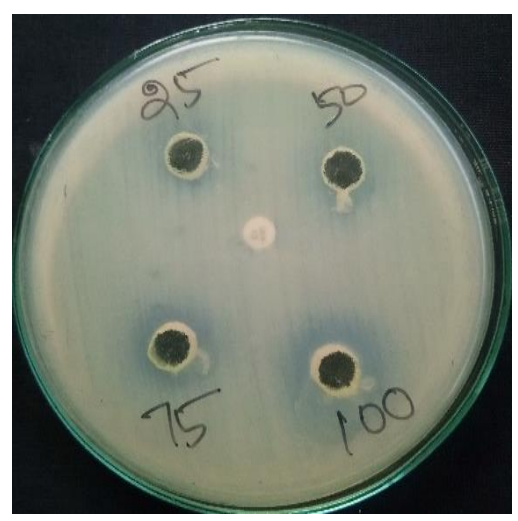
Cu - Staphylococcus aureus



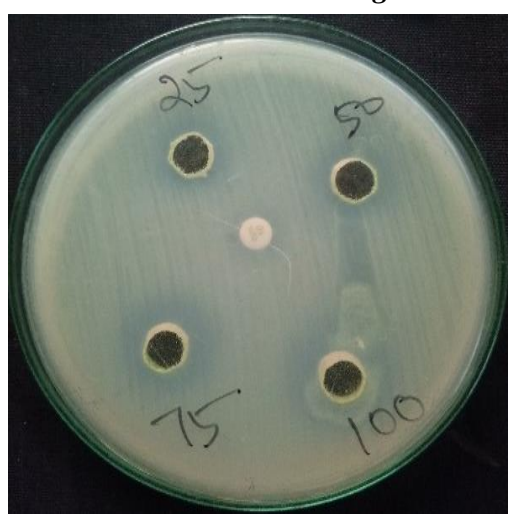
Cu - E. coli



Cu - Pseudomonas aeruginosa

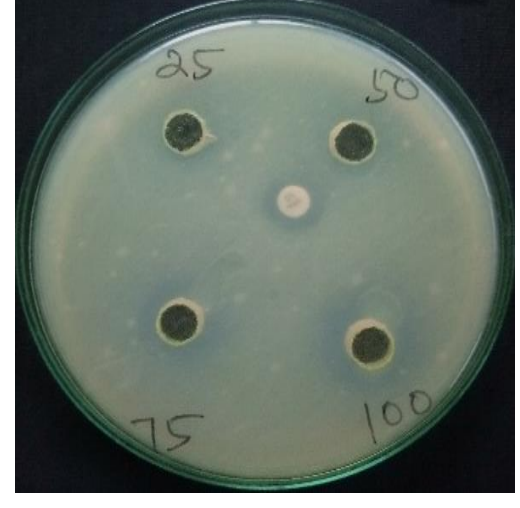


Zn - Bacillus subtilis



Zn - Staphylococcus aureus





Zn - E. coli

Zn - Pseudomonas aeruginosa

Fig. 5.29 Diameters of Inhibition Zones of Complexes against Bacteria

The *in vitro* antifungal activities of synthesized ligand IMMA and the complexes are screened against, *C.albicans* and *A.niger* by agar well diffusion method using potato dextrose agar as nutrient and ketoconazole as control .Zinc (II) complex is found to possess high activity towards *C.albicans* whereas cobalt (II) complex exhibits high activity towards *A.niger* [36]. The results are exposed in **Fig.5.30** and **5.31**.

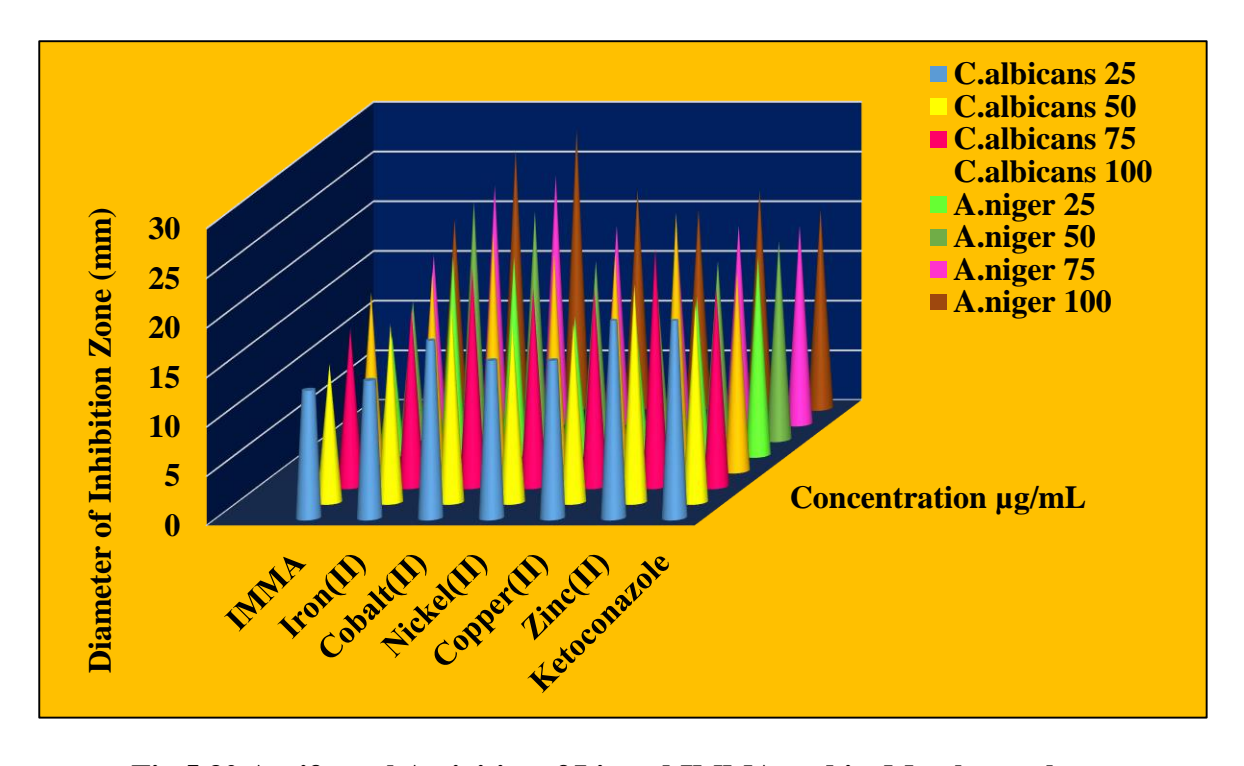
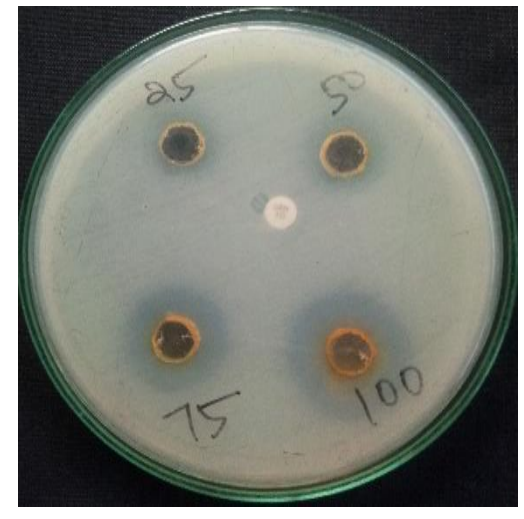


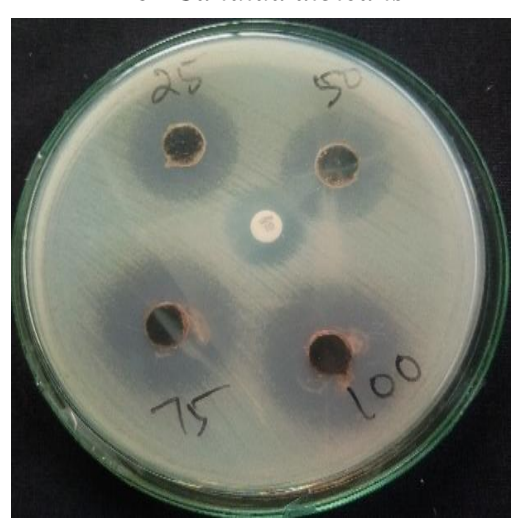
Fig.5.30 Antifungal Activities of Ligand IMMA and its Metal complexes



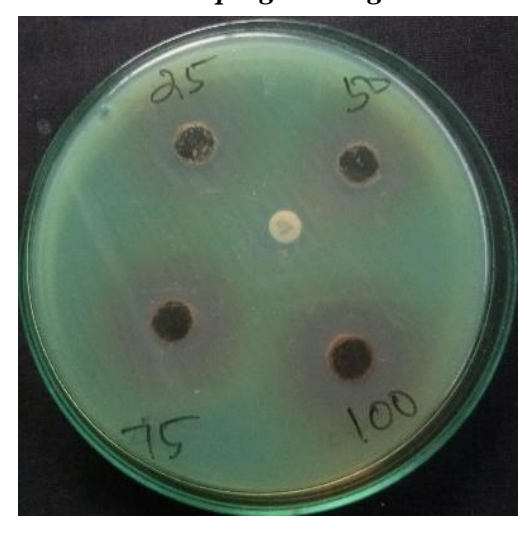
Fe - Candida albicans



Fe - Aspergillus niger



Co - Candida albicans



Co - Aspergillus niger



Ni - Candida albicans



Ni - Aspergillus niger

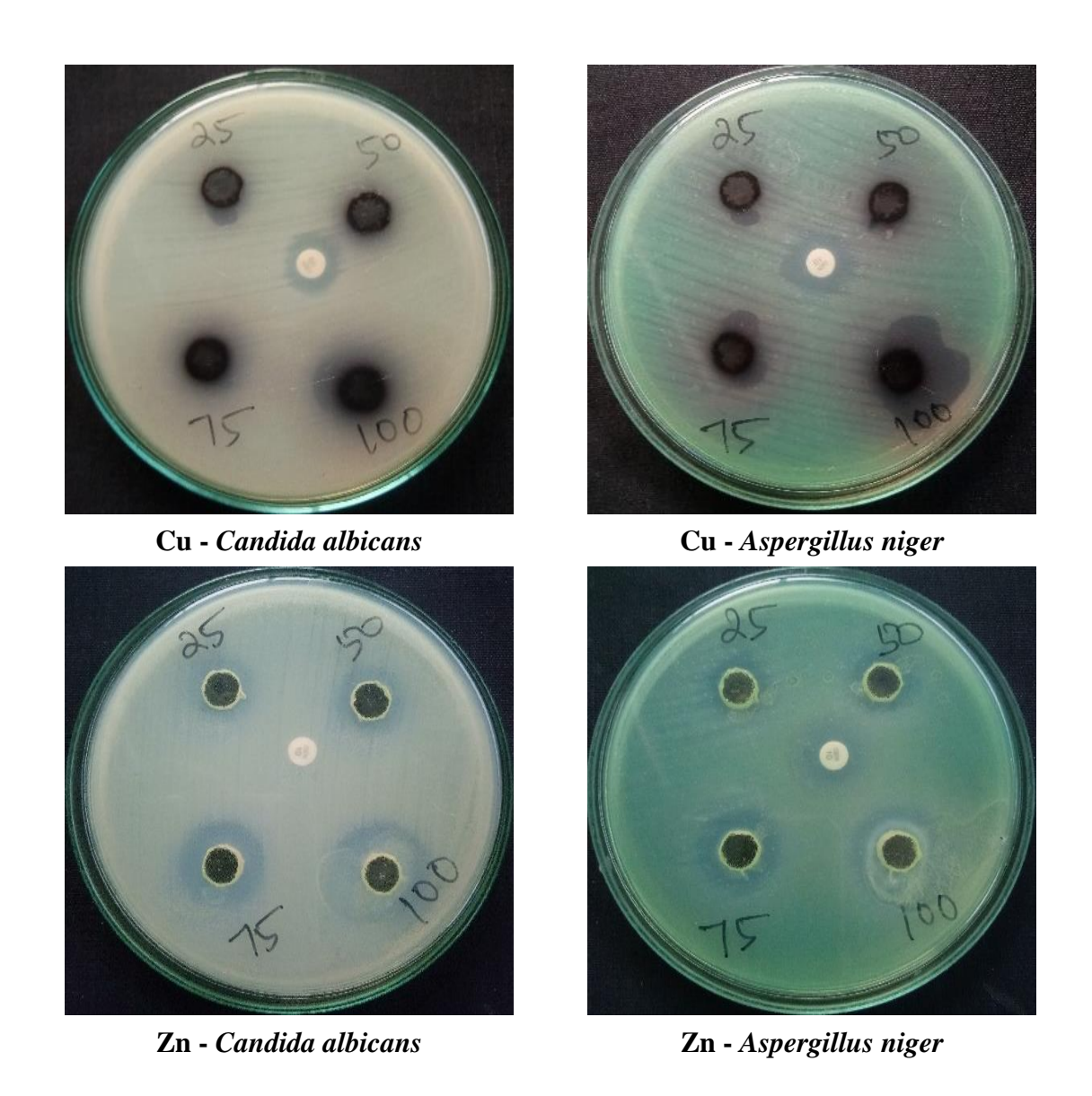


Fig.5.31 Diameters of Inhibition Zones of complexes against Fungi

## **5.5.2** Evaluation of Antioxidant Activities (DPPH free radical scavenging Method)

The antioxidant assay is carried out using different concentrations of Schiff base ligand IMMA and its metal complexes (Fig.5.32) on the basis of the free radical scavenging effect of the stable DPPH radical, while ascorbic acid (vitamin C), is used as standard. DPPH is a stable free radical that can receive an electron or a hydrogen radical to form a stable diamagnetic molecule. DPPH has an odd electron and so has a strong absorption band at 517 nm. When this electron becomes paired off, the absorption decreases stoichiometrically with respect to the number of electrons or hydrogen atoms taken up .Such decrease in absorbance shows increase in the scavenging activities of the compounds. This tendency of decrease in absorption, increases with increase in concentration of the test compounds. The observed results are shown in **Table-5.11**. They suggest that the DPPH scavenging activities of Schiff base metal complexes are significantly higher than that of free ligand (IMMA), indicating that these complexes are much better/stronger free radical scavengers and better antioxidants than IMMA but lower when compared to ascorbic acid (vitamin C) as standard. IC<sub>50</sub> values of the tested compounds are shown in **Table-5.12** along with the correlation coefficient (R<sup>2</sup>) values. The amount of antioxidant necessary to reduce DPPH concentration by 50% is a commonly used parameter to measure antioxidant activity and is referred to as IC<sub>50</sub>. The lower the IC<sub>50</sub> value, the higher is the antioxidant activity. The Fe (III) complex possess high antioxidant activity since its IC<sub>50</sub> value is low and shows promise for further investigation to target oxidative damage disease[37, 38].

The order can be given as L-Ascorbic acid >  $Fe^{III}$  >  $Cu^{II}$  >  $Cu^{II}$  >  $Ni^{II}$  >  $Ni^{II}$  > IMMA with  $IC_{50}$  values as  $0.431 > 5.62 > 11.88 > 24.54 > 954 > 3019 > 4570 <math>\mu$ M. The oxidizing potentials of the samples are associated with the existence of compounds to exert action by breaking the free radical chain via hydrogen atom donation. As a result, the findings of this study suggest that the produced compounds could be used to treat oxidative stress-related disorders.

Table-5.11: Antioxidant Activities of Ligand IMMA and its Metal Complexes

Compound	% of Free Radical Scavenging					
	5.0 μg/mL	10 μg/mL	15 μg/mL	20 μg/mL		
LAscorbic acid	49	52	59	64		
IMMA	8	13	22	30		
[Fe(IMMA) <sub>2</sub> (H <sub>2</sub> O) <sub>2</sub> ]Cl <sub>3</sub>	35	46	51	57		
[Co(IMMA) <sub>2</sub> (H <sub>2</sub> O) <sub>2</sub> ](NO <sub>3</sub> ) <sub>2</sub>	13	20	32	40		
[Ni(IMMA) <sub>2</sub> ]SO <sub>4</sub>	9	14	25	34		
[Cu(IMMA) <sub>2)</sub> (H <sub>2</sub> O) <sub>2</sub> ]Cl <sub>2</sub>	11	22	29	37		
[Zn(IMMA) <sub>2</sub> ]SO <sub>4</sub>	9	21	31	42		

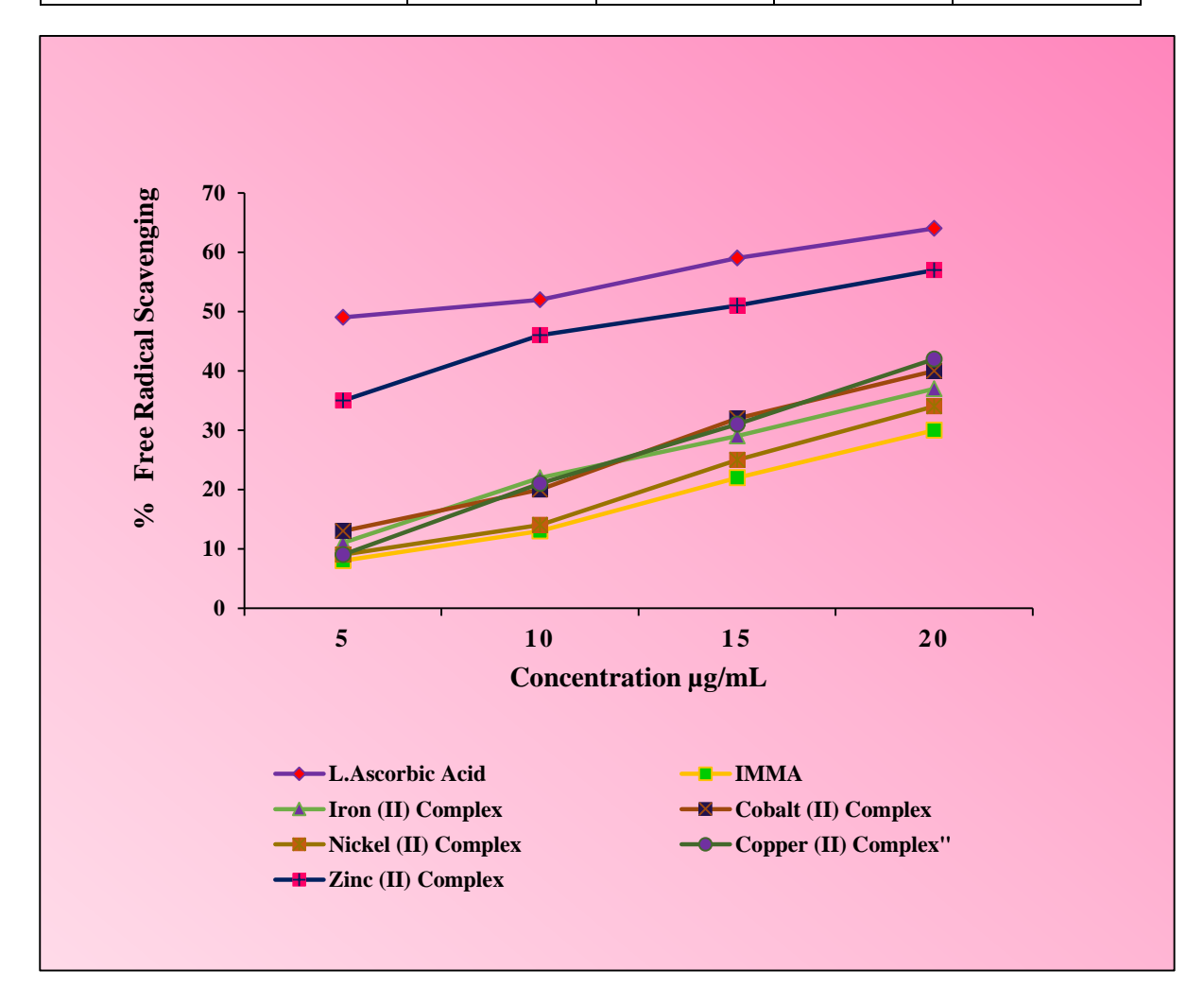


Fig.5.32 Free Radical Scavening Activities of Ligand IMMA and its Metal Complexes

Table-5.12: ICs0  $(\mu M)$  and R<sup>2</sup> values of Standard Drug, Ligand IMMA and its Metal Complexes

Compound	IC50, (μM)	$\mathbb{R}^2$
L. Ascorbic Acid	0.431	0.9797
IMMA	4570	0.9877
[Fe(IMMA) <sub>2</sub> (H <sub>2</sub> O) <sub>2</sub> ]Cl <sub>3</sub>	5.62	0.9666
[Co(IMMA) <sub>2</sub> (H <sub>2</sub> O) <sub>2</sub> ](NO <sub>3</sub> ) <sub>2</sub>	11.88	0.9902
[Ni(IMMA) <sub>2</sub> ]SO <sub>4</sub>	3019	0.9809
[Cu(IMMA) <sub>2</sub> )(H <sub>2</sub> O) <sub>2</sub> ]Cl <sub>2</sub>	7.626	0.9904
[Zn(IMMA) <sub>2</sub> ]SO <sub>4</sub>	954	0.9988

## **5.5.3** Evaluation of Antidiabetic Activity

The inhibitory effects of Schiff base ligand IMMA and its metal complexes on carbohydrate hydrolysing enzyme  $\alpha$ -amylase and  $\alpha$ -glucosidase have been studied. The results of antidiabetic activities are shown in Tables-5.13 and 5.14. These enzyme inhibitors work by inhibiting the action of these enzymes and delaying carbohydrate digestion, preventing a rapid rise in blood glucose levels, particularly after meals. Therefore inhibition of these two enzymes is a promising strategy for diabetes management. Metal complexes are found to exhibit more inhibition efficiency than the ligand IMMA and comparable or slightly less efficiency than the standard drug acarbose. (Fig.5.33 and Fig.5.34)

Zinc (II) complex shows excellent inhibition efficiency against  $\alpha$ - amylase enzyme and  $\alpha$ - glucosidase enzyme. Next to zinc, cobalt (II) complex shows a high inhibition towards  $\alpha$ - amylase enzyme and copper (II) complex exhibits high inhibition efficiency towards  $\alpha$ - glucosidase enzyme.[39]

The enhanced activity of zinc (II) complex is due to the fact that zinc has an insulin mimetic effect and protects against oxidative damage associated with the disease for the treatment of diabetes mellitus.[40]

Zinc is a natural component of insulin, a substance that regulates sugar metabolism in all living things and is found in hundreds of zinc enzymes and thousands of protein domains. Zinc complexes, in addition to vanadium complexes, have been presented as additional options for treating type 2 diabetes. Zinc and diabetes interact at various places throughout cellular metabolism. Zinc appears to work similarly to insulin in promoting glucose absorption by adipose tissue. Zinc deficiency causes a reduction in glucose absorption by adipose tissue.

Zinc has crucial physiological and pharmacological activities. Diabetes is caused by hyperzincuria and poor zinc absorption in the intestine. In addition, higher zinc intake has been linked to a decreased occurrence of type 2 diabetes in women [41].

Table-5.13: Antidiabetic Activities of Ligand IMMA and its Metal Complexes Measured by α- Amylase Method

Compound	% of Inhibition						
	$20\mu g/mL$	40μg/mL	60μg/mL	80μg/mL	100μg/mL		
IMMA	28.41	35.84	41.19	48.36	53.62		
[Fe(IMMA) <sub>2</sub> (H <sub>2</sub> O) <sub>2</sub> ]Cl <sub>3</sub>	54.92	59.85	66.19	72.53	77.46		
$ [\text{Co}(\text{IMMA})_2(\text{H}_2\text{O})_2](\text{NO}_3)_2 $	55.82	59.67	66.28	73.46	77.82		
[Ni(IMMA) <sub>2</sub> ]SO <sub>4</sub>	38.73	43.66	47.18	51.40	56.33		
[Cu(IMMA) <sub>2)</sub> (H <sub>2</sub> O) <sub>2</sub> ]Cl <sub>2</sub>	50.70	54.22	57.74	61.97	64.78		
[Zn(IMMA) <sub>2</sub> ]SO <sub>4</sub>	57.74	61.26	67.60	73.23	78.87		
Acarbose	66.90	72.53	77.46	81.69	85.21		

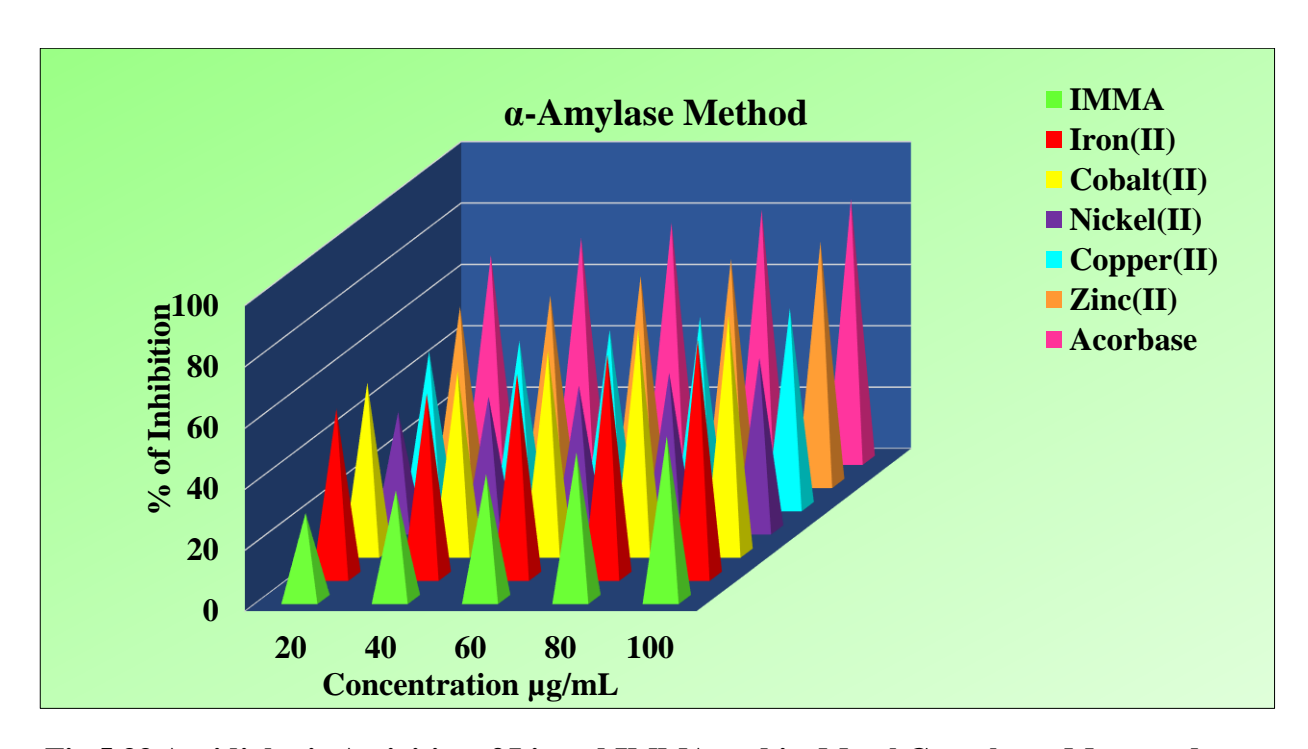


Fig.5.33 Antidiabetic Activities of Ligand IMMA and its Metal Complexes Measured by  $\alpha$ -Amylase Method

Table-5.14: Antidiabetic Activities of Ligand IMMA and its Metal Complexes Measured by  $\alpha$ - Glucosidase Method

Compound		% of Inhibition						
	20μg/mL	40μg/mL	60μg/mL	80μg/mL	100μg/mL			
IMMA	23.87	29.71	34.61	39.09	44.28			
[Fe(IMMA) <sub>2</sub> (H <sub>2</sub> O) <sub>2</sub> ]Cl <sub>3</sub>	48.18	59.09	65.45	72.72	75.45			
[Co(IMMA) <sub>2</sub> (H <sub>2</sub> O) <sub>2</sub> ](NO <sub>3</sub> ) <sub>2</sub>	47.27	55.45	60.90	65.45	73.63			
[Ni(IMMA) <sub>2</sub> ]SO <sub>4</sub>	30.90	36.36	41.81	58.45	62.67			
[Cu(IMMA) <sub>2)</sub> (H <sub>2</sub> O) <sub>2</sub> ]Cl <sub>2</sub>	56.36	60.90	64.54	69.09	70.90			
[Zn(IMMA) <sub>2</sub> ]SO <sub>4</sub>	52.72	60.90	70.90	73.63	78.18			
Acarbose	73.63	77.27	80.0	82.72	85.45			

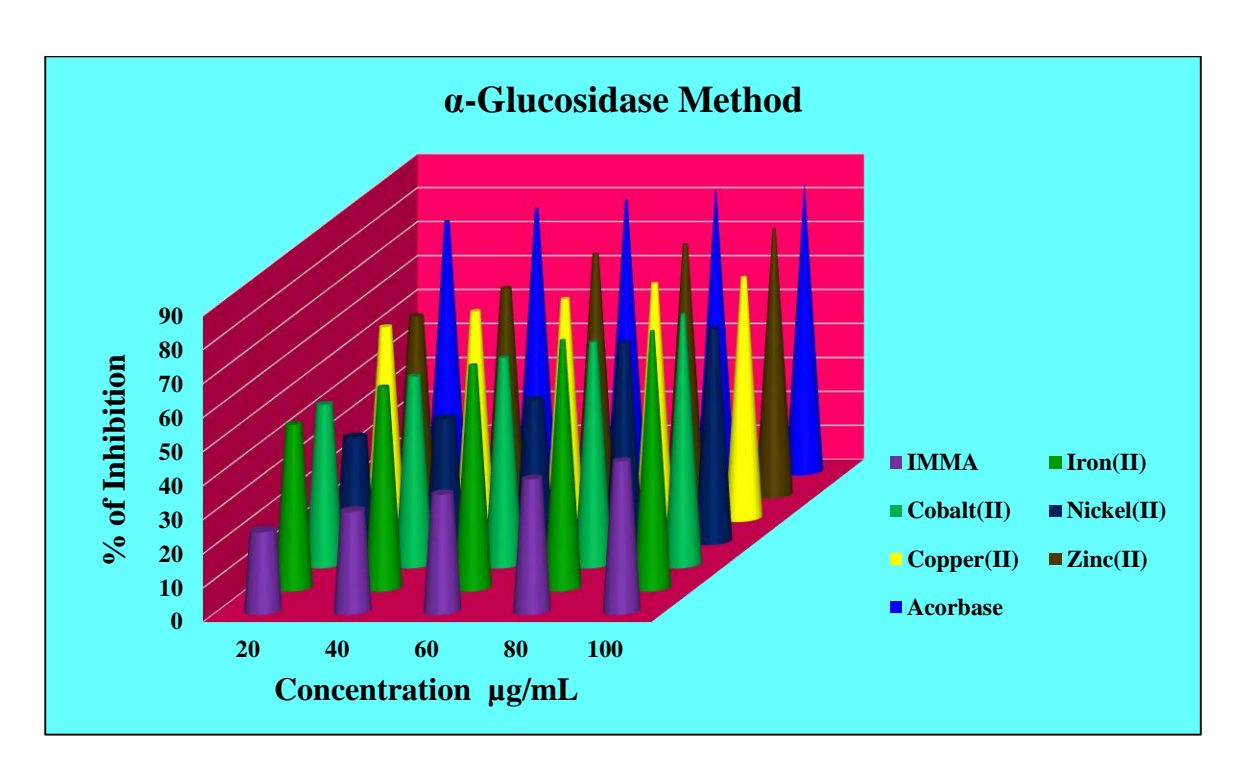


Fig. 5.34 Antidiabetic Activities of Ligand IMMA and its Metal Complexes Measured by  $\alpha$ -Glucosidase Method

#### 5.6 Conclusion

The new Schiff base ligand IMMA derived from indole-3-carboxaldehyde and 2-(methylthio)aniline and its Fe<sup>III</sup>, Co<sup>II</sup>, Ni<sup>II</sup>, Cu<sup>II</sup> and Zn<sup>II</sup> metal complexes were synthesized and characterized by different physico - chemical techniques such as molar conductance, elemental analysis, nuclear magnetic resonance (<sup>1</sup>HNMR) spectroscopy, Fourier transform infrared spectroscopy(FT-IR), ultraviolet-visible spectroscopy, magnetic susceptibility, electron paramagnetic resonance spectroscopy, TG-DSC analysis and electrochemical studies. The spectral studies revealed that the ligand was bidendate and co-ordinated to the metal through azomethine nitrogen atom, sulphur atom of thio ether moiety, forming octahedral complexes with Cu<sup>2+</sup>, Co<sup>2+</sup>, Fe<sup>3+</sup>, square planar geometry with Ni<sup>2+</sup>and tetrahedral geometry with Zn<sup>2+</sup> ions. Molar conductance measurements, elemental analyses and magnetic susceptibility indicated that above mentioned complexes were formed in 1:2 metal ligand ratio. The electrochemical studies revealed that the metal ions undergo quasi reversible redox reactions by one electron transfer processes. The bio-efficacy levels of the

Schiff base and its metal complexes have been studied against the growth of microbes in vitro to evaluate their antimicrobial potentials and it was found that metal complexes were more active than the Schiff base ligand which is in agreement with the fact that chelation of metals to the ligand enhances the biological activity of the complexes. The antioxidant activity levels of the ligand and the metal complexes have also been studied and concluded that iron (III) complex has high antioxidant activity. The antidiabetic activity levels of the ligand and metal complexes were screened against  $\alpha$ -amylase enzyme and  $\alpha$ -glucosidase enzyme and compared with that of the standard drug acarbose. From the result, it was identified that zinc (II) complex has high inhibition activity against both the enzymes.

#### REFERENCES

- 1. S.K Bharti, S. K. Patel, G. Nath, R. Tilak and S.K. Singh, *Transit. Met. Chem.*, 2010, **35(8)**, 917-925.
- 2. A.K. Gautam, A. Kumar, K. Sharma and B. K. Rai, *Orient. J. Chem.*, 2016, **32(2)**, 1249-1254.
- 3. S.Arulmurugan, Helen P. Kavitha and B.R.Venkatraman, *Rasayan J.Chem.*, 2010, **3(3)**, 385-410.
- 4. M.J. Jisha and C.Isac Sobanaraj, *Asian J. Research Chem.*, 2017, **10(6)**, 765-770.
- 5. S.S. Tajudeen and G Kannappan, *Indian J. Adv. Chem. Sci.*, 2016, **4**(1) 40-48.
- 6. E. Horozic, J. Suljagic and M. Suljkanovic, Am. J. Org. Chem., 2019, 9(1), 9-13.
- 7. Z.H.Chohan, A.Munawar and C. T.Supuran, *Met. Based Drugs*, 2001, **8(3)**, 137-143.
- 8. Z.H.Chohan, H.Pervez, A.Rauf, A.Scozzafava and C.T. Supuran, *J. Enzyme Inhib.Med.Chem.*, 2002, **17(2)**, 117-122.
- 9. A.Xavier and N.Srividhya, *IOSR-JAC*, 2014, **7(11)**, 06-15.
- 10. D. Sinha, A.K. Tewari, S. Singh, G. Shukla, P. Mishra, H.Chandra, A. K. Mishra, *Eur. J. Med. Chem.*, 2008, **43(1)**, 160-165.
- 11. H. Venkatasubramanian, S.Sha, S. Hemalatha and D. Easwaramoorthy, *Rasayan J. Chem.*, 2019, 12(4), 2005-2010.
- 12. E.Yousif, A. Majeed, Khulood Al-Sammarrae, Naida Salih, Jumat Salimon, and Bashar Abdullah, *Arab. J. Chem.*, 2013, **10**, S1639-S1644.
- 13. N. K. Chaudhary and P. Mishra, *Bioinorg. Chem. Appl.*, 2017, 1-13.
- 14. Md. Saddam Hussain, A.S.M.E.Shaheed, Md.Nuruzzaman Khan, Md. Abdul Mannan, M.M.Haque, C.M.Zakaria, Ranjan K Mohapatra and Md.Kudrat-E-Zahan, *J. Chem. Biol. Phys.Sci.*, 2018, **8(4)**, 654-668.
- 15. H.N.Aliyu and R.S.Zayyan, *Int. J. Curr. Microbiol. App. Sci.*, 2014, **3**, 445-452.
- 16. M.S. El-Shahawi, M.S. Al-Jahdali, A. S. Bashammakh, A.A. Al-Sibaai and H.M. Nassef, *Spectrochim. Acta A Mol. Biomol. Spectrosc.*, 2013, **113**, 459-465.

- 17. L.S.Kumar, K. S. Prasad and H.D. Revanasiddappa, *Eur. J. Chem.*, 2011, **2(3)**, 394-403.
- 18. V.Kuchtanin, L. Klescíkova, M. Soral, R. Fischer, Z.Ruzickova, E. Rakovsky and P.Segl'a *Polyhedron*, 2016, **117**, 90-96.
- 19. V. K. Gaikwad and U. M Yadav, Sch. Res. J. Interdiscip. Stud., 2016, **3(24)** 2225-2234.
- 20. B.K.Rai, P. Sinha, V.Singh, S.N.Vidhyarthi and A.Pandey, *Orient. J. Chem.*, 2014, 30(3), 1429-1433.
- 21. A.M. Anusuya, B.S. Krishna, S.B. Benaka Prasad, K. Yogesh Kumar, R. Raveesha and M.K.Prashanth, *Asian J. Chem.*, 2021, **33(10)** 2519-2524.
- 22. N. Nanjundan, R.Narayanasamy, S. Geib, K. Velmurugan, R. Nandhakumar, M.D. Balakumaran and P.T. Kalaichelvan, *Polyhedron*, 2016, **110**, 203-220.
- 23. M.A. Neelakantana, F. Rusalraj, J. Dharmarajaa, S. Johnsonraja, T. Jeyakumar and M. S. Pillai, *Spectrochim. Acta A: Mol. Biomol. Spectrosc.*, 2008, **71(4)**, 1599–1609.
- 24. C. Spinu and A. Kriza, *Acta Chim. Slov.*, 2000 **47(2)**, 179-185.
- 25. M.Rajasekar, S.Sreedaran, R. Prabu, V. Narayanan, R. Jegadeesh, N. Raaman and A. Kalilur Rahiman, *J. Coord. Chem.*, 2010, *63*(1), 136-146.
- 26. A. Kumar, V. K.Vashistha, P.Tevatia, and R. Singh, *Spectrochim. Acta A: Mol. Biomol. Spectrosc.*, 2017, **176**, 123-133.
- 27. G. Indiradevi, N. P. Pranamya and M. Ali Hassan, *World J. Pharm. Life Sci.*, **2019**, **5**(**5**), 71-76.
- R. Reshma, R. S. Joseyphus, A. Dasan and L. John, *J. Coord. Chem*, 2019, 72 (19–21), 3326–3337.
- 29. E.S. Aazam, A.F. EL Husseiny and H.M. Al-Amri, *Arab. J. Chem*, 2012, **5**(1), 45-53.
- 30. S.Rafique, M. Idrees, A. Nasim, H.Akbar, A. Athar *Biotechnol. Mol. Biol. Rev.*, 2010, **5(2)**, 38-45.
- 31. S Kumar, D.N. Dhar and P.N. Saxena, J. Sci. Ind. Res., 2009, **68**, 181-187.

- 32. N. Raman, J Dhaveethu Raja and A. Sakthivel, *J. Chem. Sci.*, 2007, **119(4)**, 303-310.
- 33. E. Ispir, *Dyes Pigm.* 2009, **82(1)**, 13-19.
- 34. M.Gülcan, M.Sönmez and I. Berber, *Turk. J. Chem.*, 2012, **36(1)**, 189-200.
- 35. J.Saranya, S. Jone Kirubavathy, S.Chitra, A. Zarrouk, K.Kalpana, K. Lavanya and B. Ravikiran, *Arab. J. Sci. Eng.*, 2020, **45(6)**, 4683-4695.
- 36. H.S. Elshafie, S.A. Sadeek, I. Camele and A.A.Mohamed, *Int. J. Mol. Sci.*, 2 2022, 23(4), 2110-2128.
- 37. P. Gull, M.A Malik, O.A.Dar and A. A. Hashmi *J. Mol. Struct.*, 2017, **1134**, 734-741.
- 38. S.Slassi, M. Aarjane and A. Amine, J. Iran. Chem. Soc., 2022, 1-9.
- 39. H.R. Afzal, N. Khan, K. Sultana, A. Mobashar, A. Lareb, A.Khan, A.Gull, H. Afzaal, M.T. Khan, M.Rizwan and M. Imran, *ACS Omega*, 2021, **6(6)**, 4470–4479.
- 40. R.Miyazaki, H. Yasui and Y. Yoshikawa, *Open J. Inorg. Chem.*, 2016, **6(2)**, 114-124.
- 41. S.P. Pawar, T.J. Patil and R.S Bendre, *Asian Journal of Research in Chemistry*, 2018, **11(1)**, 8-14.

# **Applications of Schiff Bases as Corrosion Inhibitors and Dye Adsorbents**

#### 6.1 Schiff Bases as Corrosion Inhibitors

#### 6.1.1 Introduction

Corrosion is a process of gradual deterioration or eating away of a metal from its surface due to the unwanted chemical or electrochemical reaction of metals with its environment. Corrosion of materials is considered to be the worst technical problem faced by all the industries. This is the most crucial process that is adversely affecting the properties of materials in contact with. In industry, mild steel finds wide application for mechanical and structural purposes. Because of its good mechanical properties and relatively low cost, it is widely utilised as a fabrication material in the chemical and petrochemical sectors as well as a type of structural engineering material, used in tonnages in offshore engineering, refining pipelines and mining constructions. HCl and sulphuric acid solutions are commonly employed for the pre-treatment of mild steel components such as pickling, acid cleaning and oil well oxidizing. But in acidic medium mild steel corrodes mainly due to the dissolution of the cementite phase Fe<sub>3</sub>C which is generally found in steel.

Corrosion of iron or mild steel also takes place due to the rust formed on the surface of iron or low alloyed steel when exposed to humid air or water at room temperature. It also occurs at metal surfaces in the presence of oxygen and moisture involving two electrochemical reactions: oxidation at anode side and reduction at cathode side. Inspite of extraordinary development in the corrosion science and technology the process of corrosion remains a foremost obstacle for industries all over the world. By adopting suitable methods

corrosion can be controlled but it accounts for additional expenditure and economic losses. [1, 2]

The use of inhibitors is one of the most practical methods for prevention of corrosion. Corrosion inhibitors are used to minimise the rate of corrosive attacks caused by the aggressiveness of the acid solution. Schiff bases already have corrosion inhibition properties against acid on metals due to the presence of electron cloud on the aromatic ring or the electronegative atom such as nitrogen, oxygen and sulphur in a relatively long chain. Compounds play a role due to the presence of functional groups such as CHO, N=N, ROH, molecular area and molecular weight of the inhibitor molecule. An interesting application of Schiff base as a corrosion inhibitor is due to their ability to form a monolayer on the surface which is to be protected. This inhibiting efficiency of the Schiff bases was found to be higher than their constituent carbonyls and amines. Many authors have related the strong inhibition efficiency of the Schiff base to the presence of an occupied  $\pi^*$  orbitals in the Schiff base molecule which allows electron back donation from metal d orbitals and thereby stabilize the existing metal-inhibitor bond which is not possible with the constituent molecules. Many studies have reported that azomethine linkage in Schiff base are responsible for the special ability to prevent corrosion or slow down the corrosion. [3, 6]

There are two types of modes of adsorption of the anticorrosive molecule. Chemical adsorption process in which co-ordinate type bond is formed by transfer of charge or sharing of charge from organic molecules to low energy vacant d orbitals of the metal surface . Physical adsorption involves electrostatic interaction between electrically charged metal surface and charged inhibitor molecules. The inhibitor molecule should have centres capable of forming bonds with metal surface by electron, in such cases metal surface acts as an electrophile and inhibiting molecule acts as a nucleophile or Lewis base. Nucleophilic centre such as oxygen, nitrogen and sulphur have lone pairs of electrons which are easily

available for sharing. With the benzene rings, the inhibitors form multi-absorption sites, thus allowing stable mono layer formation. Hence the adsorbed Schiff base may hide and protect the metal surface from the corrosive environment in acid solutions.

#### **6.1.2** Result and Discussion

The present study has been carried out to measure the corrosion inhibition performances of various Schiff bases derived from heterocyclic aldehydes and 2-(methylthio)aniline towards the corrosion of mild steel in HCl medium at different concentrations by weight loss measurement, adsorption isotherm and thermodynamic calculations.

## **6.1.2.1** Weight Loss Measurement

Weight loss data of mild steel in 10% HCl in the absence and presence of various concentrations of corrosion inhibitors are given in the **Tables-6.1-6.4.** 

Tables-6.1- 6.4 represent the variations of inhibition efficiency of the synthesized Schiff base inhibitors 1-3 in 10% HCl for mild steel over a wide range of concentrations (500, 1000, 1500, 2000 ppm). It is found that the inhibition efficiency increases by increasing the inhibitor concentration towards corrosion process. The inhibition is maximum at 2000ppm for all the synthesized Schiff bases 1-3 in 10% HCl. This indicates that increase of inhibition efficiency by increasing the concentration of the target. The inhibition process is affected by the adsorption of inhibitor molecules on to the steel surface. The process of adsorption is governed by the chemical structure of the inhibitors and their response towards the environment. It is governed by the following factors.

- 1. Electrostatic attraction between the charge inhibitor and metal surface.
- 2. Interaction between metal and d electrons of the inhibitor or uncharged moieties in the inhibitor molecules and the metal surface.[7, 8]

Table-6.1: Corrosion Parameters from Weight Loss Measurement in 10%HCl Solution containing 500ppm Schiff base Ligands

Compound	Immersion Time (min)	Weight Loss (g)	Inhibition Efficiency(%)	Corrosion Rate(mmpy)	Surface coverage (θ)
Blank	30	3.836		63.42	
Schiff Base 1	30	0.181	95.28	2.992	0.9528
Schiff Base 2	30	0.077	97.99	1.272	0.9799
Schiff Base 3	30	0.159	95.85	2.628	0.9585

Table-6.2: Corrosion Parameters from Weight Loss Measurement in 10%HCl solution containing 1000 ppm Schiff base Ligands

Compound	Immersion Time (min)	Weight Loss (g)	Inhibition Efficiency(%)	Corrosion Rate(mmpy)	Surface coverage (θ)
Blank	30	3.940		65.13	
Schiff Base 1	30	0.153	96.11	2.529	0.9611
Schiff Base 2	30	0.041	98.96	0.677	0.9895
Schiff Base 3	30	0.102	97.41	1.686	0.9741

Table-6.3: Corrosion Parameters from Weight Loss Measurement in 10%HCl solution containing 1500 ppm Schiff base Ligands

Compound	Immersion Time (min)	Weight Loss (g)	Inhibition Efficiency(%)	Corrosion Rate(mmpy)	Surface coverage (θ)
Blank	30	3.943		65.186	
Schiff Base 1	30	0.131	96.67	2.165	0.9667
Schiff Base 2	30	0.017	99.56	0.281	0.9956
Schiff Base 3	30	0.089	97.74	1.471	0.9774

Table-6.4: Corrosion Parameters from Weight Loss Measurement in 10%HCl solution containing 2000ppm Schiff base Ligands

Compound	Immersion Time (min)	Weight Loss (g)	Inhibition Efficiency(%)	Corrosion Rate(mmpy)	Surface coverage (θ)
Blank	30	3.953		65.35	
Schiff Base 1	30	0.097	97.55	1.603	0.9755
Schiff Base 2	30	0.012	99.69	0.198	0.9969
Schiff Base 3	30	0.065	98.35	1.074	0.9835

## **6.1.2.2** Molecular Structure and Inhibitor Properties

The chemical structures of the synthesized inhibitors comprise unsaturation sites, heteroatoms like sulphur, nitrogen (aromatic rings and heterocyclic rings) and azomethine linkages.

The conjugation in the aromatic rings like pyrrole, pyridine and indole interacts with the metal surface forming a strong adsorption bond. Azomethine linkage in presence of acidic medium gets protonated and gets adsorbed to the negative species formed during the dissolution of mild steel. [FeCl<sup>-</sup>]. Presence of heteroatom like sulphur in the inhibitors leads to the formation of  $d\pi$ - $d\pi$  bond resulting from overlap of 3d electrons from iron atom to the 3d vacant orbital of the sulphur atom which may favour the adsorption of the inhibitor on the metal surface.[9-12]

Based on the above parameters, Schiff base 2 (MTPMA) from pyridine-2-carboxaldehyde is found to have higher inhibition efficiency from 97 to 99. This is due to high basicity of pyridine ring and tridenticity nature i.e. presence of two nitrogen and one sulphur hetero atoms whereas Schiff base 3(IMMA) from indole-3-carboxaldehyde falls the next due to fused ring system which is found to have high configurational electron density

and bonding characteristics. Comparatively Schiff base 1 (MPMA) from pyrrole-2-carboxaldehyde have least inhibition ability due to less basic five-membered ring.

#### 6.1.2.3 Adsorption Isotherm and Thermodynamics Calculation

Adsorption isotherm is used to examine the interaction between the inhibitor and the mild steel surface. The degree of surface coverage  $(\theta)$  for each inhibitor at various concentrations is calculated using the equation.

$$\theta = C_T^* - C_T / C_T^*$$

where  $C_T^*$  and  $C_T$  are the weight losses of steel in the absence and in the presence of inhibitor respectively.

The surface coverage values  $(\theta)$  are tested graphically by fitting into a suitable adsorption isotherm. **Table-6.5** presents the relation between  $C/\theta$  and C. The linear relationship of  $C/\theta$  Vs C shown in the **Fig.6.1** suggests that the adsorptions of Schiff bases 1-3 on the mild steel obey Langmuir adsorption isotherm. This isotherm can be given as

$$C/\theta = 1/k_{ad} + C$$

where kad is the adsorption-desorption equilibrium constant

C is the concentration of the inhibitor.

Table-6.5: Relation between C/θ and C

Compound		(	C/0	
Compound	500ppm	1000ppm	1500ppm	2000ppm
Schiff Base 1	524.76	1040.47	1551.67	2050.44
Schiff Base 2	510.25	1010.50	1506.62	2006.21
Schiff Base 3	521.64	1026.58	1534.68	2033.55

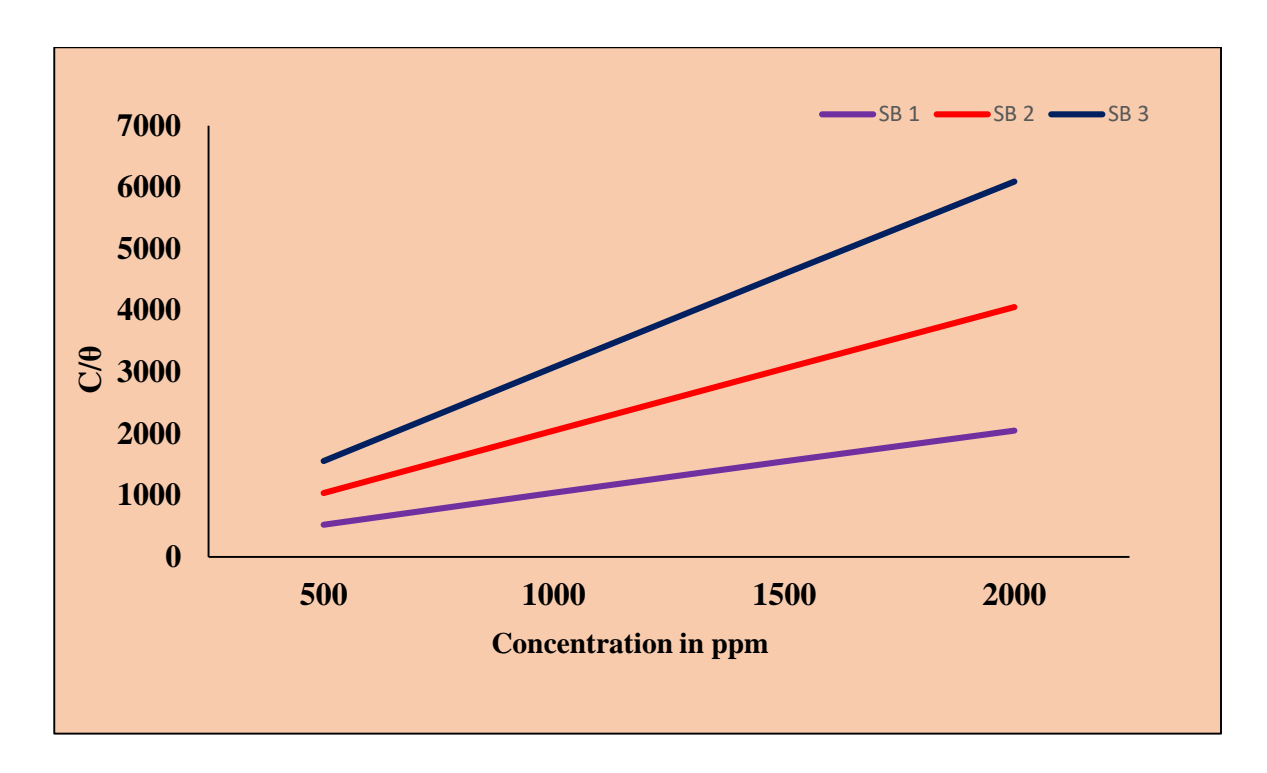


Fig.6.1 Linear relationship between  $C/\theta$  and C

Strong regression correlations ( $R^2$  =0.9999, 1, 1) of the Langmuir adsorption isotherms for the Schiff bases 1-3 are observed. This isotherm assumes that adsorption of molecules on the adsorbent is monolayer. The values of  $k_{ad}$  calculated for Langmuir adsorption isotherms for Schiff bases 1-3 are 19.775, 12.401 and 18.163 respectively. The value of  $k_{ad}$  is related to  $\Delta G^o_{ad}$  i.e. standard free energy of absorption by the following equation.[13-15]

$$\Delta G^{o}_{ad} = -(RTln55.5k)$$

where R is the gas constant, T is the absolute temperature. The constant 55.5 is the molar concentration of water in solution and expressed in mol L<sup>-1</sup>. **Table- 6.6** shows the calculated  $\Delta G^{o}_{ad}$  and  $K_{ad}$  values of Schiff bases 1-3.

Table-6.6: Relation between  $\Delta G^{o}_{ad}$  and  $K_{ad}$  Values of Schiff Bases 1-3

Compound	Slope	Kad	$\mathbb{R}^2$	$\Delta \mathbf{G^o}_{\mathbf{ad}}$
Schiff Base 1	1.0176	19.755	0.9999	-19.38
Schiff Base 2	0.9968	12.401	1	-18.090
Schiff Base 3	1.0088	18.163	1	-19.146

The negative values of  $\Delta G^o_{ad}$  indicate the spontaneous adsorption of Schiff base inhibitors on the mild steel surface .The values of  $\Delta G^o_{ad}$  around -20 KJ mol<sup>-1</sup> are consistent with physisorption, that is, electrostatic attraction between the charged inhibitor and metal surface and those around -40 KJ mol<sup>-1</sup> indicate chemisorption, that is complete transfer of charge from organic molecules to metal surface. The  $\Delta G^o_{ad}$  values of Schiff bases 1-3 are around -20 KJ mol<sup>-1</sup> indicating that there exist physisorption only between organic molecules and mild steel surface.[16-18]

#### **6.1.2.4 SEM: Scanning Electron Microscope**

The mild steel samples are analysed by SEM after immersion in 10% HCl with and without Schiff bases 1-3 for 30 minutes. The polished mild steel surface is smooth without pits and cracks. When the mild steel surface is exposed to 10% HCl without inhibitor, the surface gets highly damaged due to aggressive action of acid solution, that is, high iron dissolution rate is found in acid solution and so the sample plate consists of more number of pits and cracks. But, when the mild steel surface is exposed to optimum concentrations of Schiff bases 1-3 (MPMA, MTPMA and IMMA) there is a formation of stable protective layer on the steel surface. This suppresses the charge and mass transfer by acting as a barrier. [19]

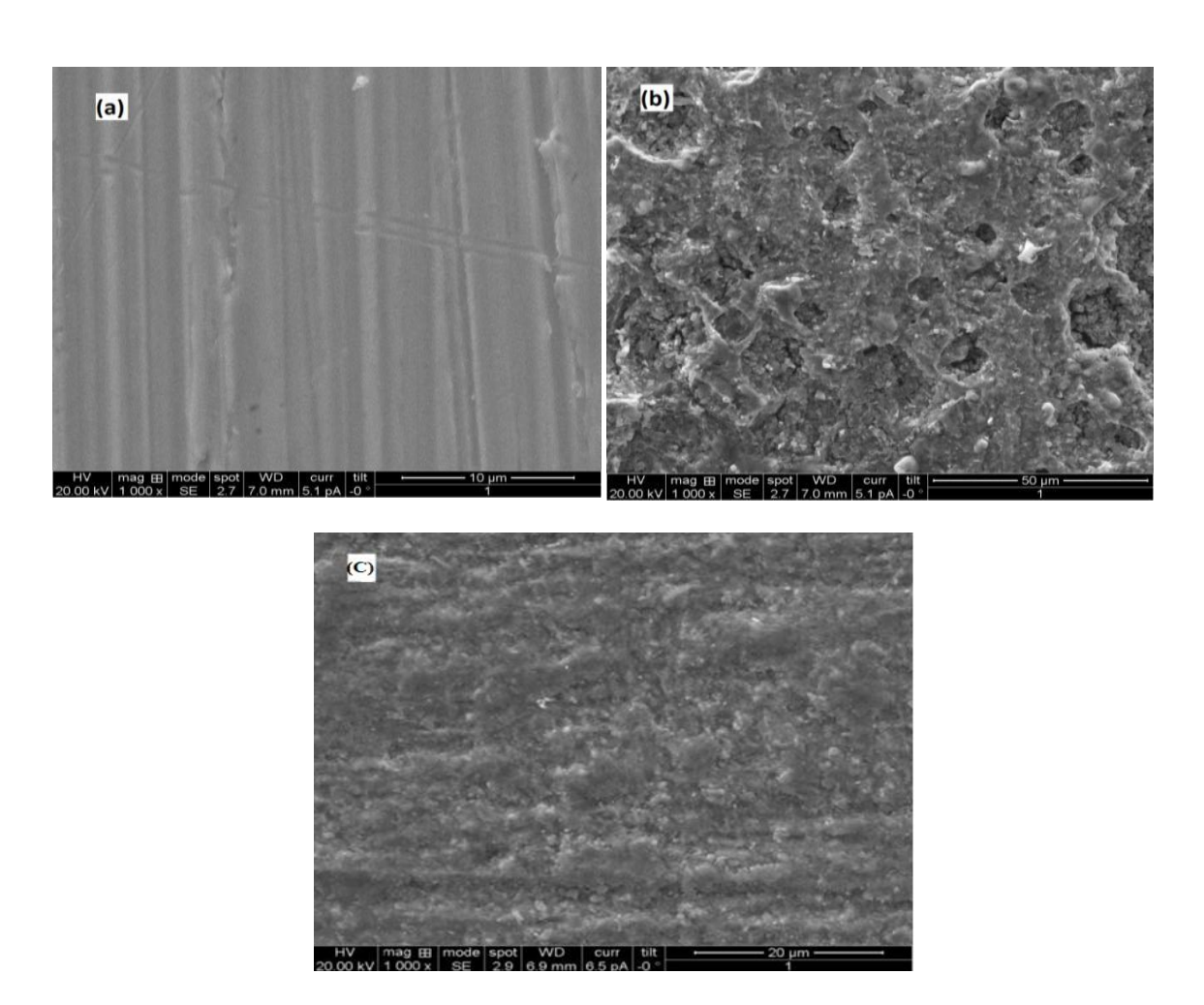


Fig. 6.2: SEM images of (a) Polished Mild Steel Surface (b) Mild Steel in 10% HCl (c) Mild Steel in 10% HCl with 500 ppm MTPMA

### 6.1.3 Conclusion

In the present work, the corrosion inhibiting activities of Schiff bases MPMA, MTPMA and IMMA were evaluated in 10% HCl using weight loss method and adsorption isotherms. All the studied Schiff bases (1-3) showed excellent inhibiting activities and acted as a mixed type inhibitors for mild steel corrosion in 10% HCl acid solution. Among all the tested compounds, the Schiff base 2 (MTPMA) showed highest corrosion inhibition efficiency. The adsorption of Schiff bases on mild steel obey Langmuir adsorption isotherm . The negative  $\Delta G^o_{ad}$  values indicate the spontaneity of the adsorption. Increase in inhibitor concentration increases the inhibiting potency.

## **6.2** Dye Adsorbent Properties of Schiff Bases

#### **6.2.1** Introduction

Effluents from various industries such as textile, printing, paper, plastics and leather contain synthetic dyes stuffs as pollutants. These dyes were found to be toxic due to the presence of aromatic rings in the structure. They are also non-biodegradable, carcinogenic and mutagenic for both human and aquatic life. The presence of these coloured dye substance disturb the aquatic ecosystem by preventing the penetration of light and heat into the water which in turn affects the photosynthesis of phytoplankton. Synthetic dye such as malachite green is an organic compound which is used as antimicrobial agent in aquaculture. It is also used as biological strain for microscopic analysis, but when tested with rat it causes a dose related increase in liver DNA adducts along with lung adenomas. It also gets retained in the fish muscle for longer time and finally enters into human food chain. [20, 21]

For water treatment many conventional methods such as reverse osmosis, ion exchange method, lime coagulation and oxidation were employed initially. But due to high energy consumption and expenses, these methods have been restricted. Removal of malachite green from waste water can be achieved by physical, chemical and biological process. [22] But these process generate huge amount of toxic sludge which are ineffective at low concentration of dye. Therefore it is very essential to develop a new innovative and low cost processes by which dye molecules can be removed. Adsorption method is one of the most widely used method for removal of dye from aqueous medium due to low cost, ease of operation and high efficiency .[23, 24]

In continuation of our work on the synthesis and structural studies of Schiff bases and its metal complexes, we report here the adsorption studies of Schiff bases 1-3 against cationic dye "malachite green" in aqueous solution. Schiff base 1 (MPMA) was derived from condensing pyrrole-2-carboxaldehyde and 2-(methylthio)aniline. Schiff base 2

(MTPMA) was derived from condensing pyridine-2-carboxaldehyde and 2-(methylthio)aniline whereas Schiff base 3 (IMMA) was derived from condensing indole-3-carboxaldehyde and 2-(methylthio)aniline.

#### **6.2.2** Result and Discussion

## **6.2.2.1 Batch Adsorption Experiments**

#### **6.2.2.1.a** Effect of Contact Time

To determine equilibrium time for maximum uptake of adsorption process, the adsorption of malachite green using three Schiff bases derived from 2-(methylthio)aniline and heterocyclic aldehydes are studied as a function of contact time with initial dye concentration of 50 ppm, adsorbent dose is 0.1 g, volume of the dye solution is 20 mL, at temperature of  $25 \pm 2^{\circ}$ C and agitation speed is 200 rpm with pH = 8. The result shows an increase in the removal of dye with time and at 60 minute attains equilibrium. This effect is due to the fact that amount of dye uptake is a function of time. Thus in the present malachite green sorption studies, 60 minutes is chosen as the contact time required for attaining equilibrium. [25, 26]

**Fig. 6.3** shows that Schiff base 3 (IMMA) is found to have increased capacity of removing malachite green from aqueous solution than Schiff base 2 (MTPMA) which is found to have more activity than Schiff base 1 (MPMA). This is due to electrostatic interaction and hydrogen bonds between active groups of malachite green and Schiff bases such as azomethine linkage, thio group and  $N^+$  (CH<sub>3</sub>)<sub>2</sub> and also may be due to  $\pi$ - $\pi$  interaction of aromatic phenyl rings of malachite green and Schiff bases .[27]

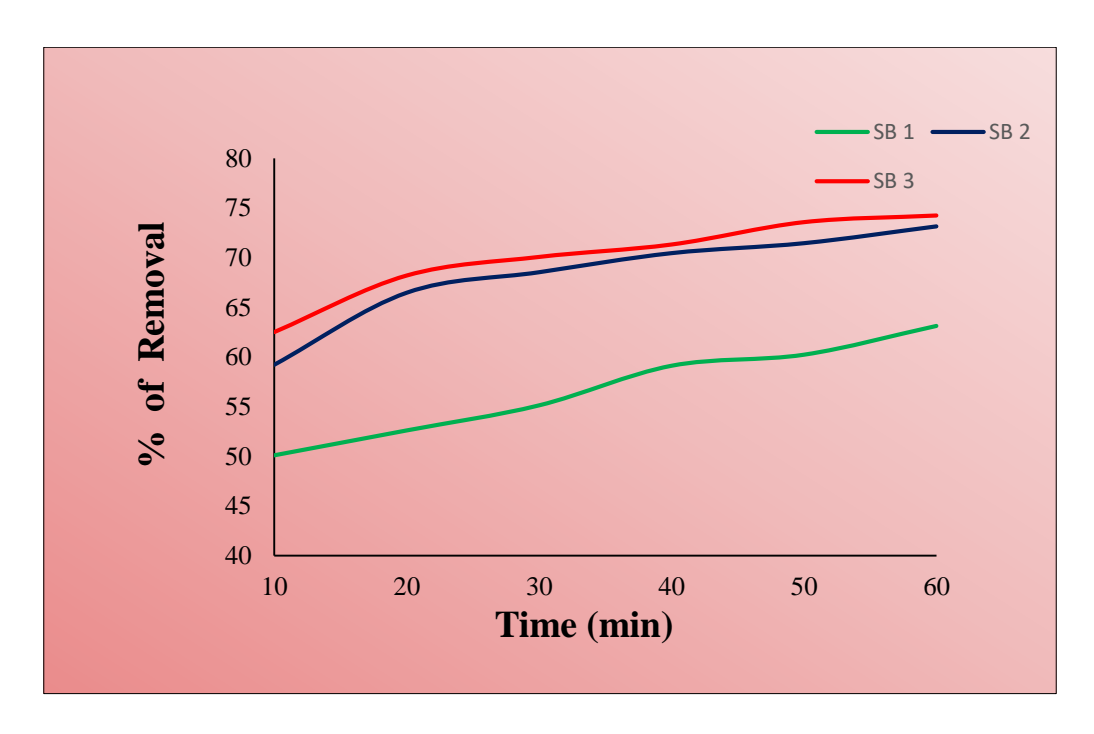


Fig. 6.3 Effect of Contact time on the adsorption of malachite green by the Schiff bases 1-3

### **6.2.2.1.** b Effect of Initial Dye Concentration

The effect of initial malachite green concentration on removal is shown in the **Fig.6.4**. The percentages of removal of malachite green by Schiff bases 1-3 are found to be reduced as the initial concentration of the dye is increased at the fixed adsorbent dosage say 0.1 g. Furthermore there is a linear relationship between removing capacities of the Schiff bases and the concentrations of dye. This shows that initial dye concentration plays a vital role in the adsorption tendency of malachite green on Schiff bases.

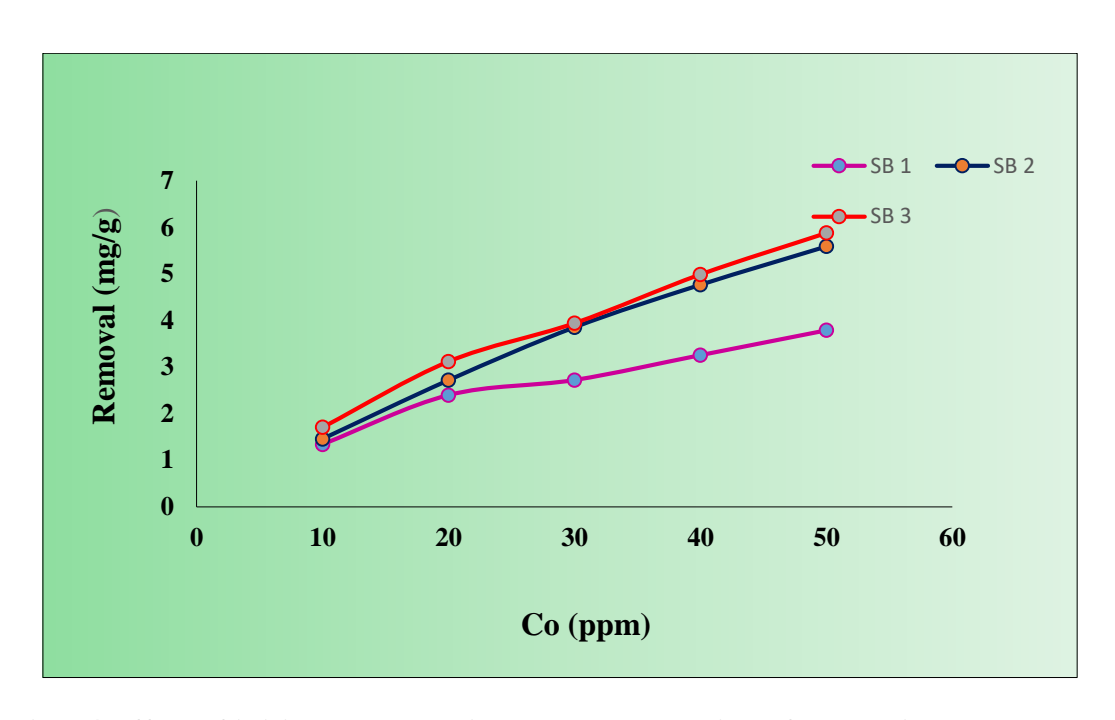


Fig.6.4 Effect of initial concentration on the adsorption of malachite green by the Schiff bases 1-3

Even though, the amount of the dye adsorbed increases with increase in the concentration of dye solution, the percentage of removal is found to be decreased. This is due to the fact that at higher concentration, there is an electrostatic repulsion between dye molecules which results in competition between dye molecules for the limited active centres in the adsorbent surface. [28] **Tables- 6.7- 6.9** show the effect of initial concentration on the adsorption of the malachite green by Schiff bases 1-3.

Table-6.7: Effect of initial concentration on the adsorption of the malachite green by Schiff base 1 (MPMA)

Concentration of Malachite green (Co) mg/L	Ce (mg/L)	Percentage of Removal	qe (mg/g)	Ce/qe	Log Ce	Log qe
10	3.2984	67.01	1.3402	2.4609	0.5183	0.1272
20	8.0105	59.94	2.3979	3.3406	0.9037	0.3798
30	16.3874	45.37	2.7225	6.0192	1.2145	0.4349
40	23.7172	40.70	3.2566	7.2828	1.3751	0.5127
50	31.0471	37.90	3.7900	8.1918	1.4920	0.5786

Table-6.8: Effect of initial concentration on the adsorption of the malachite green by Schiff base 2 (MTPMA)

Concentration of Malachite green (Co) mg/L	Ce (mg/L)	Percentage of Removal	qe (mg/g)	Ce/qe	Log Ce	Log qe
10	2.7160	72.84	1.4560	1.8643	0.4339	0.1631
20	6.4190	67.90	2.7162	2.3630	0.8075	0.4339
30	10.7400	64.20	3.8521	2.7881	1.0310	0.5856
40	15.0617	62.34	4.9877	3.0192	1.1771	0.6979
50	20.6171	58.77	5.8771	3.5080	1.3142	0.7691

Table-6.9: Effect of initial concentration on the adsorption of the malachite green by Schiff base 3 (IMMA)

Concentration of Malachite green (Co) mg/L	Ce (mg/L)	Percentage of Removal	qe (mg/g)	Ce/qe	Log Ce	Log qe
10	1.4705	85.29	1.7059	0.8620	0.1674	0.2317
20	4.4117	77.94	3.1176	1.4150	0.6446	0.4938
30	10.2941	65.68	3.9412	2.6118	1.0125	0.5956
40	16.1763	59.56	4.7648	3.3948	1.2088	0.6780
50	22.0582	55.88	5.5884	3.9471	1.3435	0.7472

### **6.2.2.2** Adsorption Isotherm Models

In the adsorption process, the equilibrium data explains how the adsorbate molecules interact with the absorbent molecules after reaching equilibrium. This provides an easy understanding of the nature of interaction.

The assumptions of Langmuir isotherm are monolayer formation of adsorbate molecules on the surface of the absorbent molecules having finite number of active sites of

uniform distribution and energies of adsorption. On the other hand, Freundlich isotherm postulates heterogeneous nature of the adsorbent surface, reversible process and multilayer adsorption.

#### **6.2.2.2.** a Langmuir Isotherm

A straight line with slope  $1/q_m$  and an intercept of  $1/q_m$ .K is obtained from a plot between  $C_e/q_e$  and  $C_e$ . **Fig. 6.5-6.7** illustrate Langmuir linear plot is obtained for adsorption of malachite green at different initial ion concentrations using the prepared Schiff bases 1-3 as adsorbents. The experimental data for the adsorption of malachite green on the Schiff bases 1-3 are well fitted into the Langmuir isotherm model and is confirmed by calculated correlation coefficient ( $R^2$ ) values. These values are higher than 0.96 and they indicate a good mathematical fit.[29, 30] From slope and intercept,  $q_m$  and K, the Langmuir parameters for malachite green removal are calculated and tabulated in the **Table-6.10**. According to Langmuir isotherm, the largest monolayer capacity of Schiff base 3 (IMMA) is found to be 6.55 mg/g and for Schiff base 2 (MTPMA) it is 11.35 mg/g. The reason for increased monolayer capacity of Schiff base 2 may be due to higher basicity of pyridine ring. But being monocyclic it can remove only 72% of dye whereas Schiff base 3 contains fused aromatic ring system, conjugated  $\pi$  system and free hydrogen atom which are responsible for maximum adsorption of malachite green from aqueous solution.

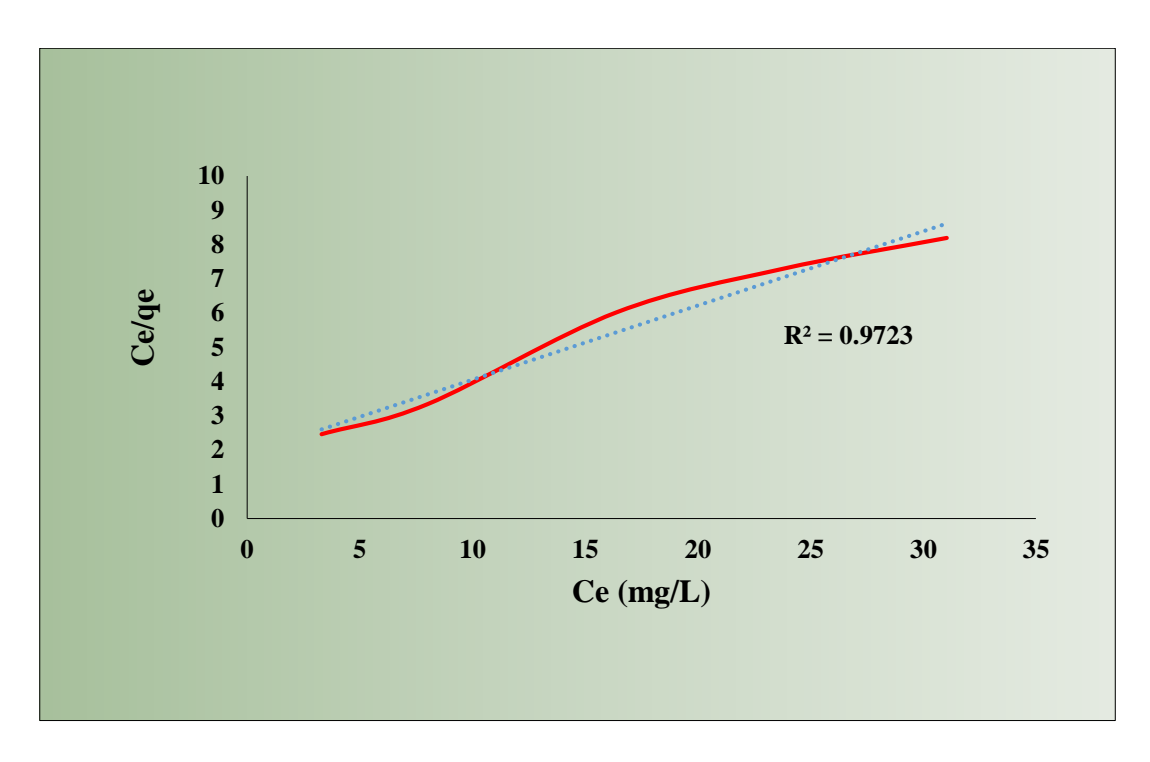


Fig.6.5 Langmuir Adsorption Isotherm of MPMA

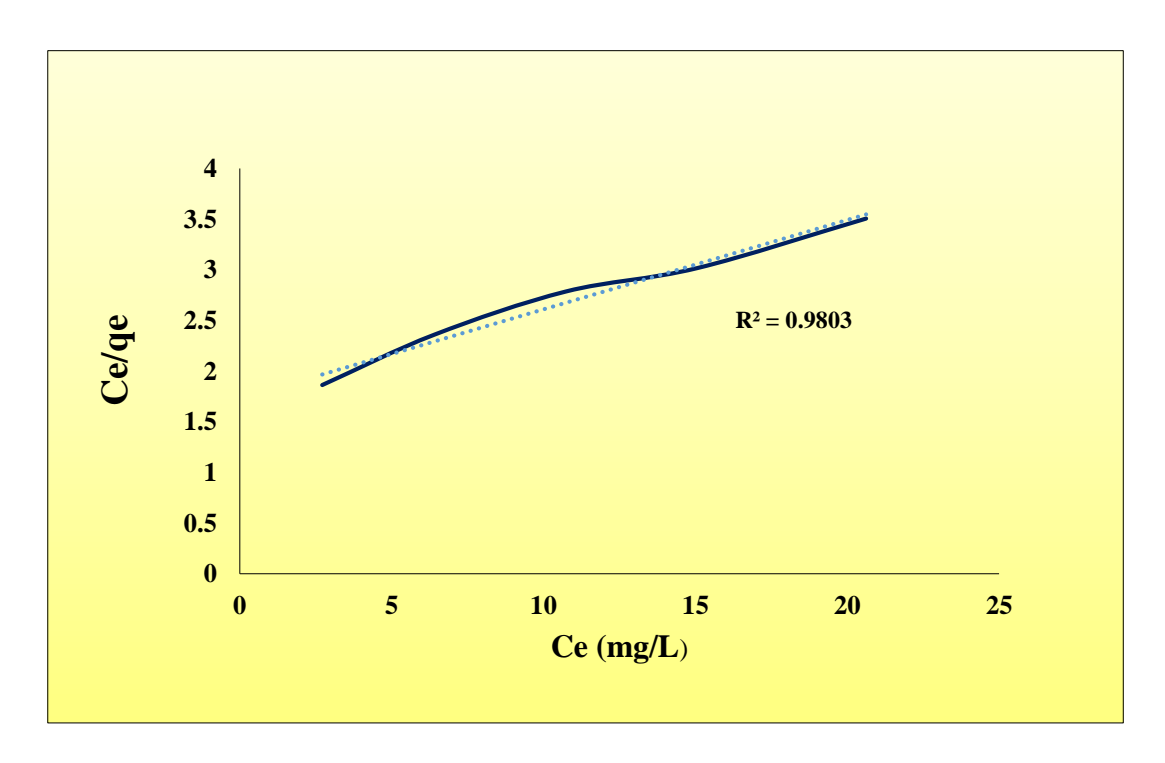


Fig.6.6 Langmuir Adsorption Isotherm of MTPMA

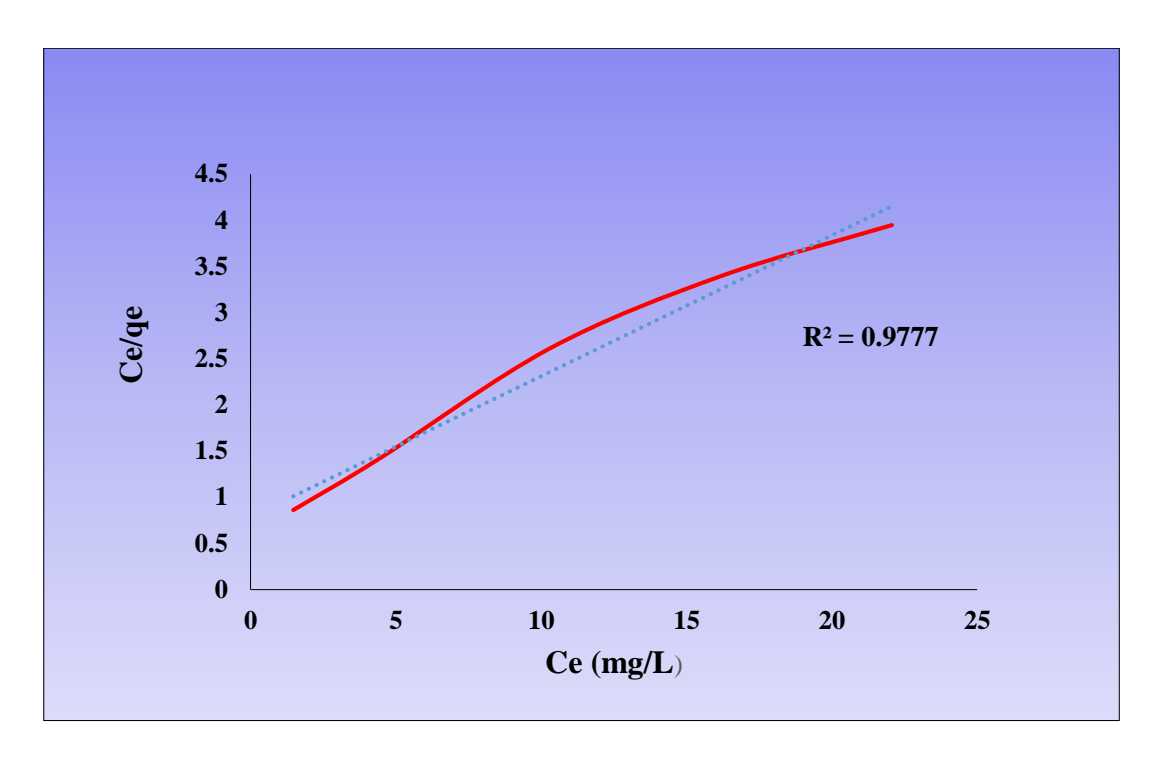


Fig.6.7 Langmuir Adsorption Isotherm of IMMA

Table - 6.10: Langmuir sorption parameters for malachite green adsorption using SB 1-3 adsorbents

Compound	qm (mg/g)	K (L/mg)	$\mathbb{R}^2$
MPMA	4.61	0.5294	0.9723
МТРМА	11.35	0.57	0.9803
IMMA	6.55	1.27	0.9777

#### 6.2.2.2. b Freundlich Isotherm

Based on linear regression approach, the results of malachite green sorption using three Schiff bases 1-3 are shown in **Fig. 6.8- 6.10.** They are examined to get the model parameters such as 1/n and  $K_f$  of Freundlich isotherm. Accordingly, the correlation coefficients  $R^2$  values confirm that the adsorption of malachite green molecules by the Schiff bases 1-3 obeys Freundlich isotherm. The adsorption favourability and degree of

heterogeneity of the surfaces of adsorbents are quantified by the magnitude of 1/n. When 1/n is less than 1, it indicates favourable adsorption which leads to increase in adsorption capacity. So that new active sites will be formed. Hence, as shown in **Table-6.11** all the Schiff bases 1-3 were found to have 1/n value less than 1 suggesting heterogeneity on the adsorbent surface .[31-34]

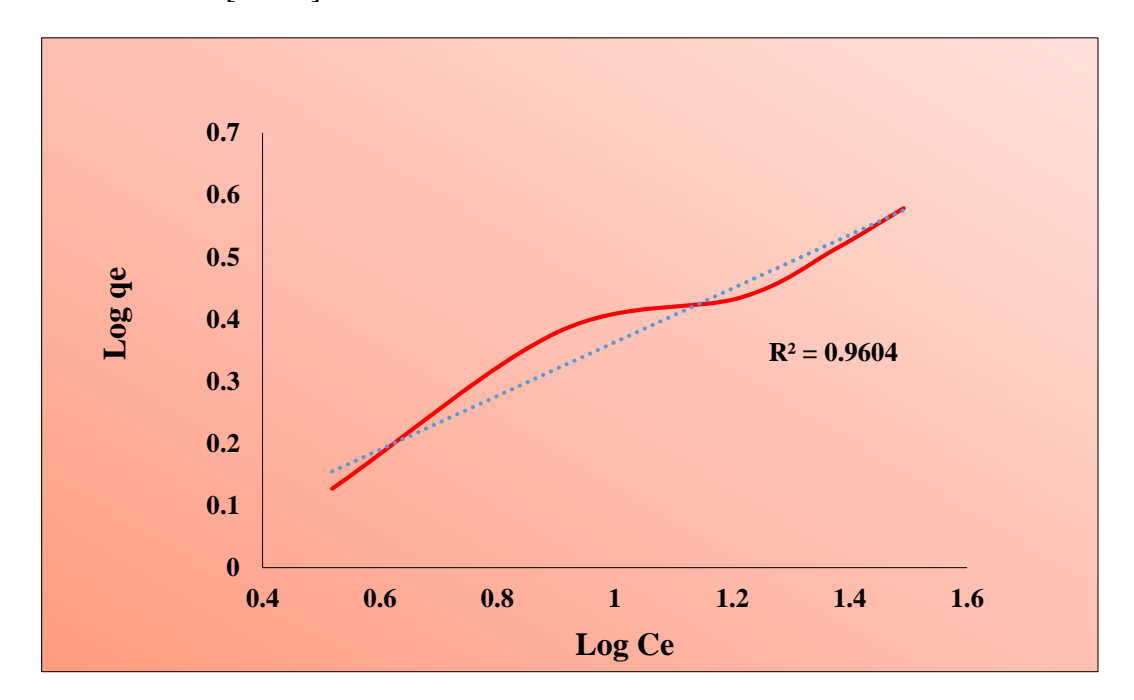


Fig.6.8 Freundlich Adsorption Isotherm of MPMA

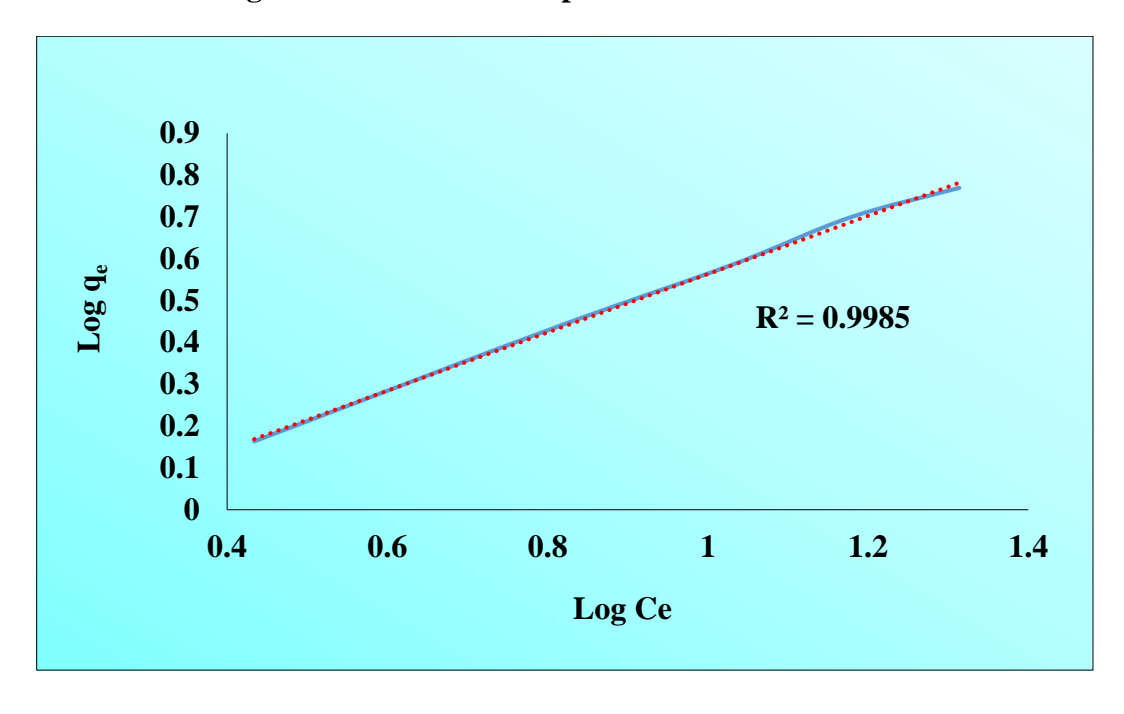


Fig.6.9 Freundlich Adsorption Isotherm of MTPMA

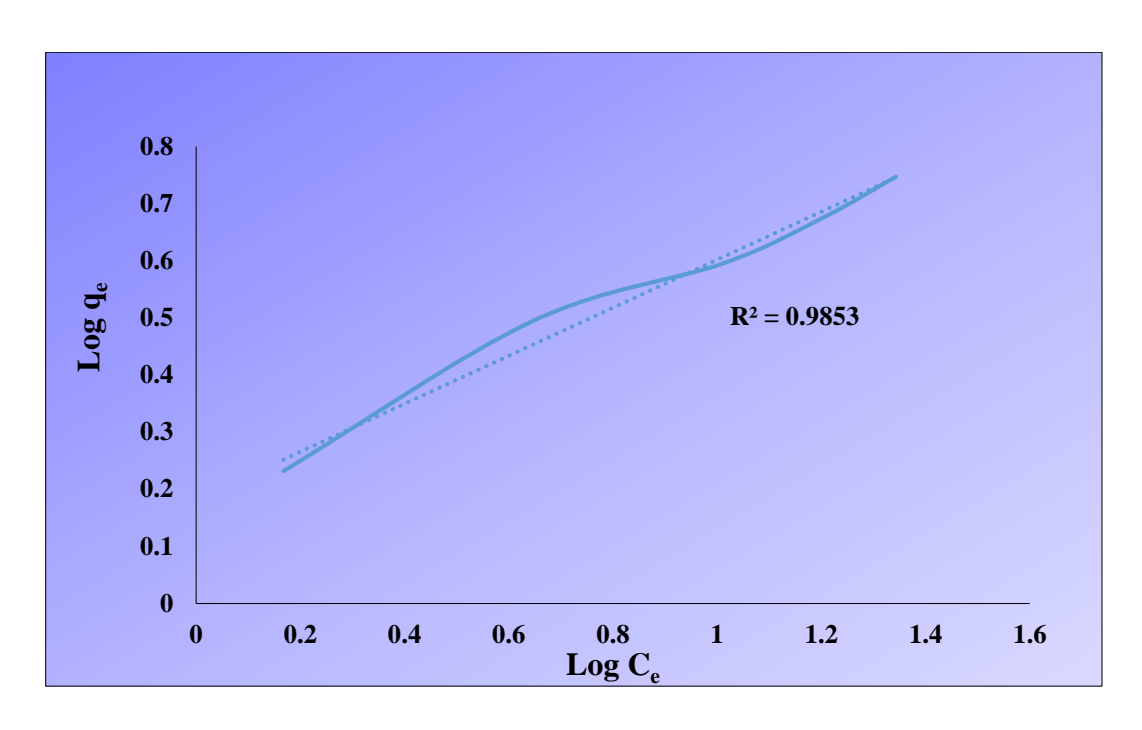


Fig.6.10 Freundlich Adsorption Isotherm of IMMA

Table-6.11: Freundlich sorption parameters for malachite green adsorption using SB 1-3 adsorbents

Compound	Kf	n	$\mathbb{R}^2$
MPMA	0.8531	2.314	0.9604
MTPMA	0.734	1.434	0.9985
IMMA	1.519	2.380	0.9853

#### 6.2.3 Conclusion

Three newly prepared Schiff bases MPMA, MTPMA and IMMA have been used for the adsorption of malachite green from aqueous solutions . The results show an increase in the adsorption process with time and attains equilibrium at 60 minutes. Amount of approximately 85 % of malachite green dye is adsorbed by the Schiff base 3 from 50 mg/litre within 60 minutes at pH=8. By comparing the Langmuir parameters of three Schiff bases 1-3, it is observed that Schiff base 3 has  $q_m$  =6.55 and K=1.27 which suggest that it has more active sites due to the presence of fused ring system and hetero atoms with lone pairs of electrons and free hydrogen atom, therefore Schiff base 3 shows maximum adsorption of malachite green from aqueous solution.

#### REFERENCES

- 1. M. N. Desai, M. B. Desai, C. B. Shah and S. M. Desai, *Corros. Sci.*, 1986, **26(10)**, 827—837.
- 2. A. A. Ghani, H. Bahron, M.K. Harun and K. Kassim, *Adv Mat Res*, 2012, **554**, 425-429.
- 3. S. Issaadi, T. Douadi, A. Zouaoui, S. Chafaa, M.A. Khan and G.Bouet, *Corros. Sci*, 2011, **53(4)**, 1484-1488.
- 4. S.A. Soliman, M.S. Metwally, S.R. Selim, M.A. Bedair and M.A. Abbas, *J. Ind. Eng. Chem*, 2014, **20**(6), 4311-4320.
- 5. M.Finsgar and J. Jackson, *Corros Sci.*, 2014, **86**, 17-41.
- 6. N. Zulfareen, K. Kannan, T. Venugopal, and S. Gnanavel, *Arab. J. Chem.*, 2015, **9(1)**, 121-135.
- 7. H. Ju, Z.P. Kai and Y. Li, *Corros. Sci.*, 2008, **50**(3), 865–871.
- 8. R. K. Upadhyay and S. P. Mathur, *E-J. Chem*, 2007, **4** (**3**), 408-414.
- 9. S. Benabid, T. Douadi, S. Issaadi, C. Penverne, and S. Chafaa, *Measurement*, 2017, **99**, 53-63.
- 10. S. Thirugnanaselvi, S. Kuttirani and A. R. Emelda, *Trans. Nonferrous Met. Soc. China*, 2014, **24(6)**, 1969–1977.
- 11. C. Verma, M.A. Quraishi, A. Alfantazi and K. Y. Rhee, *Int. J. Biol. Macromol*, 2021, **184**, 135-143.
- 12. D. Bouknana, B.Hammouti, M.Messali, A. Aouniti, and M.Sbaa, *Port. Electro chim. Acta*, 2014, **32(1)**, 1-19.
- 13. M. T. Muniandy, A. A. Rahim, H. Osman, A. M. Shah, S. Yahya and P. B. Raja, *Surf. Rev. Lett.*, 2011, **8** (3 & 4), 127-133.
- 14. F.Tezcan, G. Yerlikaya, A. Mahmood and G. Kardaş, *J. Mol. Liq.*, 2018, **269**, 398-406.
- 15. D.S.Chauhan, M.J.Mazumder, M.A.Quraish, K.R.Ansari and R.K.Suleiman, *Int. J. Biol. Macromol.*, 2020, **158**, 231-243.
- 16. K.R. Ansari, D.S.Chauhan, M.A. Quraishi, M.A. Mazumder and A. Singh, *Int. J. Biol. Macromol*, 2020, **144**, 305-315.

- 17. R. Menaka and S. Subhashini, *Polym. Int.*, 2017, **66** (**3**), 349-358.
- 18. I. Ahamad, C. Gupta, R. Prasad and M. A. Quraishi, *J. Appl. Electrochem.*, 2010, **40(12)**, 2171–2183,
- 19. S.Junaedi, A. A. Al-Amiery, A. Kadihum, A.A.H. Kadihum and A. B. Mohamad, *Int. J. Mol. Sci.* **14(6)**, 11915-11928.
- 20. B.Yuan, L.G.Qiu, H.Z Su, C.L. Cao and J.H.Jiang, *Int. J. Biol. Macromol.*, 2015, **82**, 1-6.
- 21. S. Chatterjee, D.S. Lee, M.W. Lee and S.H.Woo, *Bioresour Techno*, 2009, **100**(11), 2803-2809.
- 22. C.Huang, H.Liao, X.Ma, M.Xiao, X.Liu, S.Gong, X. Shu and X. Zhou, *Chem. Phys. Lett*, 2021, **780**, 1-6.
- 23. Y. Jiang, B.Liu, J. Xu, K. Pan, H. Hou, J. Hu and J. Yang, *Carbohydr. Polym*, 2018, **182** (15) 106–114.
- 24. M.Sanati, A. Dehno Khalaji, A.Mokhtari and M. Keyvanfard, *Prog. Chem. Biochem. Res* 2021, **4(3)**, 319-330.
- 25. E.M. El-Sayed, T.M. Tamer, A.M. Omer and M.S.M. Eldin, *Desalination Water Treat*, 2016, **57(47)**, 22632-22645.
- 26. R. Hassan, H. Arida, M. Montasser, and N. A. Latif, *J. Chem*, 2013, 1-10.
- 27. A.S. Manchaiah and V. Badalamoole, *Water Environ J*, 2019, **34(3)**, 364-373.
- 28. G. R. Bardajee, Z. Hooshyar and F. E. Shahidi, *Int. J. Environ. Sci. Technol*, 2015, **12(5)**, 1737–1748.
- 29. F. Alakhras, H. Ouachtak, E. Alhajria, R. Rehman, G. Al-Mazaidehd, I. Anastopoulos and E. C. Lima, *Sep Sci Technol*, 2022, **57(4)**, 542-554.
- 30. K. K. Al-Zboon, B.M. Al-smadi and S. Al-Khawaldh, *Water Air Soil Pollut*, 2016, **227(7)**, 1-22.
- 31. M. Landarani, M. A. Chamjangali and B.Bahramian, *Water Air Soil Pollut*, 2020, **231(10)**, 1-17.
- 32. M.V.Subbaiah and D.S. Kim, *Ecotoxicol. Environ. Saf*, 2016, **128**, 109-117.
- 33. Y.Tan, Y. Kang, W. Wang, X. Lu, B. Wang, Q. Zhang, C. Cui S. Cui, S. Jiao, G. Pang and S. Feng, *Appl. Surf. Sci*, 2021, **569**, 150970-150983.
- 34. S. M. Ibrahim, H. M. Hassanin and M.M. Abdelrazek, *Water Sci. Technol*, 2020, **81**(3), 421-435.

# **Summary and Conclusion**

This thesis embodies the results of research on some new Schiff bases and their complexes with Fe<sup>III</sup> Co<sup>II</sup>, Ni <sup>II</sup>, Cu<sup>II</sup> and Zn<sup>II</sup> ions. They were synthesized and subjected to studies on structural elucidation, redox properties, thermal stability, antimicrobial, antioxidant, antidiabetic, anticorrosion and dye adsorbent properties.

Chapter 1 deals with the general introduction of coordination compounds, Schiff base ligands, their types and their biological importance. It discusses the metallo-elements in biological systems and coordination chemistry of metallic elements. It also includes the literature review on the Schiff base metal complexes. The scope and objectives of the current work is given indicating the choice and importance of the work reported in the thesis. Synthesis and characterization of transition metal complexes containing the Schiff bases MPMA, MTPMA and IMMA were purposed to be carried out. The structural features of the complexes with metal ions Fe<sup>III</sup> Co<sup>II</sup>, Ni <sup>II</sup>, Cu<sup>II</sup> and Zn<sup>II</sup> are to be determined by molar conductance, chemical and elemental analyses, magnetic susceptibility and spectral analysis. Certain biological applications and industrial applications of the synthesized compounds are to be studied.

Chapter 2 describes the various physicochemical and analytical methods used for the characterization and structural elucidation of ligands and their metal complexes. The methods employed are :

- ❖ CHNS elemental analyser
- Chemical analysis for metal and anion contents
- ❖ <sup>1</sup>H-NMR spectroscopy

- Infrared spectroscopy
- ❖ UV- visible spectrophotometry
- ❖ Magnetic susceptibility measurements by Gouy method
- Electron paramagnetic resonance spectroscopy
- Mass spectroscopy
- Cyclic voltammetry studies
- Thermal decomposition studies
- ❖ X-ray Diffraction Measurements

The evaluation of antimicrobial activities of the ligands and their metal complexes against human pathogenic microbes by agar disc diffusion method has been described. The procedures for antioxidant studies by DPPH assay and antidiabetic studies against carbohydrate hydrolysing enzymes are also outlined. The procedures to study corrosion inhibition properties and dye adsorbent properties against malachite green by the synthesized compounds are also described in this chapter.

Chapter 3 deals with the synthesis of a new Schiff base 2-(methylsulfanyl)–N–(1H-pyrrol-2-ylmethylidene)aniline MPMA derived from pyrrole-2-carboxaldehyde and 2-(methylthio)aniline and its Fe<sup>III</sup>, Co<sup>II</sup>, Ni<sup>II</sup>, Cu<sup>II</sup> and Zn <sup>II</sup> metal complexes. Characterization of synthesized ligand and complexes by microanalytical, magnetic and spectral studies is outlined. The molar conductivity values suggest that all the complexes are electrolytes. The metal to ligand molar ratio is found to be 1:2. Physico-chemical studies prove that the Schiff base coordinates to metal ions through azomethine nitrogen and sulphur atom of thioether moiety and that the ligand behaves as a bidentate ligand. In the light of above discussion, an octahedral geometry is proposed for iron (III), cobalt (II) and copper (II) complexes and square planar geometry for nickel (II) and tetrahedral stereochemistry for zinc (II)

complexes. Cyclic voltammograms of all the complexes show a well-defined quasireversible redox peak corresponding to a simple one electron transfer process. The Schiff
base and its complexes have been tested *in vitro* for their antibacterial activities against two
Gram positive and two Gram negative bacteria. *In vitro* evaluation of antifungal activities
has been carried out against *Candida albicans* and *Aspergillus niger*. All the compounds
showed positive inhibition against these organisms and the Schiff base complexes are found
to have more potent biocidal activity than the corresponding ligand. Free radical scavenging
activities of all the synthesized compounds have been tested against DPPH• (2, 2-diphenyl1-picrylhydrazyl). Among the prepared compounds, copper (II) complex was found to
possess highest free radical scavenging activity. Antidiabetic activities of all the compounds
have been tested *in vitro* against  $\alpha$ -amylase and  $\alpha$ -glucosidase enzymes. Cobalt (II) complex
showed excellent inhibition efficiency against  $\alpha$ -amylase and copper (II) complex showed
excellent inhibition efficiency against  $\alpha$ -glucosidase.

Chapter 4 deals with the synthesis, characterisation and biological studies of a new Schiff base MTPMA derived from pyridine-2-carboxaldehyde and 2-(methylthio)aniline and its Fe<sup>III</sup>, Co<sup>II</sup>, Ni<sup>II</sup>, Cu<sup>II</sup> and Zn <sup>II</sup> metal complexes. Interpretation of the data obtained from microanalytical, magnetic and spectral studies, confirms that the Schiff base is a tridentate ligand which coordinates the metal ions through nitrogen atom of pyridine ring, nitrogen atom of imine group and sulphur atom of thioether moiety. Except zinc(II) complex all other complexes were electrolytes. The metal to ligand molar ratio is found to be 1:2 for all complexes except that of zinc, which is in 1:1 ratio. In the light of above data, an octahedral geometry is purposed to all the complexes except that of zinc, which is found to have tetrahedral geometry. Cyclic voltammograms of all the complexes show a well-defined quasi-reversible redox peak corresponding to a simple one electron transfer process.

The Schiff base and its complexes have been screened *in vitro* for their antibacterial activities against two Gram positive and two Gram negative bacteria. *In vitro* antifungal activity evaluation has been carried out against *Candida albicans* and *Aspergillus niger*. All the compounds show positive inhibition against these organisms and the Schiff base complexes are found to have more potent biocidal activity than the corresponding ligand. Free radical scavenging activities of all the synthesized compounds have been tested against DPPH• (2,2-diphenyl-1-picrylhydrazyl). There is a linear relationship between concentration of the compounds and the antioxidant activity. Among the synthesized compounds, copper (II) complex was found to possess highest free radical scavenging activity. Antidiabetic activities of all the compounds have been tested *in vitro* against  $\alpha$ -amylase and  $\alpha$ -glucosidase enzymes. Cobalt (II) complex showed excellent inhibition efficiency against  $\alpha$ -glucosidase.

Synthesis, characterisation and biological studies on a new Schiff base (IMMA) derived from indole-3-carboxaldehyde and 2-(methylthio)aniline and its metal complexes are outlined in Chapter 5. The synthesized ligand and complexes have been characterised by elemental analyses, molar conductivities, <sup>1</sup>H NMR, FT-IR, UV-Vis, EPR, mass spectra and TG studies. The molar conductivity values suggest that all the complexes are electrolytes. The metal to ligand molar ratio is found to be 1:2. Physico-chemical studies confirm that the Schiff base coordinates to metal ions through azomethine nitrogen and sulphur atom of thioether moiety and behaves as a bidentate ligand. An octahedral geometry is proposed for iron (III), cobalt (II) and copper (II) complexes whereas square planar for nickel (II) and tetrahedral for zinc (II) complexes. Cyclic voltammograms of all the complexes show a well-defined quasi-reversible redox peak corresponding to a simple one

electron transfer process. The Schiff base and its complexes have been screened *in vitro* for their antibacterial activities against two Gram positive and two Gram negative bacteria. *In vitro* antifungal activity evaluation has been carried out against *Candida albicans* and *Aspergillus niger*. All the compounds show positive inhibition against these organisms and the Schiff base complexes are found to have more potent biocidal activity than the corresponding ligand. Free radical scavenging activities of all the synthesized compounds have been tested against DPPH• (2,2-diphenyl-1-picrylhydrazyl). Iron (III) complex was found to possess highest antioxidant activity. Antidiabetic activities of all the compounds have been tested *in vitro* against  $\alpha$ -amylase and  $\alpha$ -glucosidase enzymes. Zinc (II) complex was found to have highest inhibition efficiency against both enzymes.

Chapter 6 deals with the corrosion inhibition properties and dye adsorbent properties of Schiff base ligands. Corrosion inhibiting activities of Schiff bases MPMA, MTPMA and IMMA have been evaluated in 10% HCl using weight loss method and adsorption isotherms. All the studied Schiff bases show excellent inhibiting activity by acting as mixed type inhibitors for mild steel corrosion in 10% HCl acid solution. Among all the tested compounds, the MTPMA shows highest corrosion inhibition efficiency than others. The adsorption of Schiff bases on mild steel obey Langmuir adsorption isotherm. The negative  $\Delta G^0_{ad}$  values indicate the spontaneity of the adsorption. Increase in inhibitor concentration increases the inhibiting potency.

Three newly prepared Schiff bases MPMA, MTPMA and IMMA have been used as adsorbents for the adsorption and removal of malachite green from aqueous solutions. The results show an increase in adsorption with time and equilibrium is attained in 60 minutes. An amount of approximately 85 % of malachite green dye is adsorbed by the IMMA from 50 mg/litre within 60 minutes at pH=8. By comparing the Langmuir parameters of three

Schiff bases MPMA, MTPMA and IMMA, it is observed that IMMA has  $q_m$  =6.55 and K=1.27 which suggest that it has more active sites than the others due to the presence of fused ring system and hetero atoms with lone pairs of electrons and free hydrogen atom, therefore IMMA shows maximum adsorption of malachite green from aqueous solutions.

# **Future Plan**

In future it is planned to study the catalytic activities and crystal structure of the prepared complexes and also to extend the work by using rare earth metals for the synthesis of complexes.

# **List of Publications**

#### Paper published in International Journals

- 1. **A. Sharmila,** P. Thamizhini and K. Lakshmi Prabha, Study on Synthesis, Spectral Characterization and Antimicrobial Activity of Bidendate Schiff Base Transition Metal Complexes, *Rasayan Journal of Chemistry*, **14**(1), **653-658**, **(2021).Print ISSN: 0974- 1496** [Group-A of UGC-CARE List (Scopus indexed)].
- 2. **A. Sharmila,** P. Thamizhini and K. Lakshmi Prabha, Synthesis, Spectral and Biological Studies on Transition Metal Complexes of (Z)-2-(methylthio)-N-(pyridin-2-ylmethylene)aniline, *Rasayan Journal of Chemistry*, **Special issue**, **180-187**, (2021), **Print ISSN: 0974-1496**. [Group-A of UGC-CARE List (Scopus indexed)].
- 3. P. Thamizhini, A. Sharmila and K. Lakshmi Prabha, Synthesis and spectral analysis of Schiff base of mixed ligand copper(II) complexes, *Rasayan Journal of Chemistry*, 14(1), 288-294, (2021) Print ISSN: 0974-1496[Group-A of UGC-CARE List (Scopus indexed)].
- 4. P. Thamizhini, A. Sharmila and K. Lakshmi Prabha, DNA binding and DNA cleavage Activity of Mixed Ligand Copper(II) complexes of 2-(methylsulfanyl)-N-(1H-pyrrole-2-ylmethylidne)aniline, *Research Journal of Chemistry and Environment*, 25(10), 49-60, (2021). Print ISSN: 0972-0626[Group-A of UGC-CARE List (Scopus indexed)].

# **List of Papers Presented in International Conferences**

- Presented a paper entitled "Synthesis ,Spectral Analysis and Antimicrobial studies on Transition Metal Complexes derived from Bidentate Schiff Base", International Conference on Smart Materials Chemistry "(CHEMSAT-21"), Department of Chemistry, St. Joseph's College (Autonomous), Tiruchirappalli, 29<sup>th</sup> -31<sup>th</sup> July 2021.
- Presented a paper entitled "Spectral and Biological Studies on Transition Metal Complexes of 2-(methylsulfanyl)—N-(1H-pyrrol-2- ylmethylidene)aniline" International Conference on Chemical Research for Sustainable Development (ICCRSD-2021), Department of Chemistry, SRM Institute of Science and Technology, Chennai, 24<sup>th</sup> and 25<sup>th</sup> September 2021.